

Kite Power for an Electric Pickup Truck Final Report

AE3200: Design Synthesis Exercise

This page was intentionally left blank

Kite Power for an Electric Pickup Truck

Final Report

by

DSE Group 15

Student Name	Student Number
Thom Wennink	4381688
Robbin van der Voort	4672356
Joris de Lint	4844807
Kasper Masure	4861086
Winter Oostwoud	4876008
Julie Paddeu	4997522
Mathieu Van der Straeten	5008832
Camille Derie	5009197
Coen Mingelen	5050871
Ole Grootes	5070759

Tutor: Dr.-Ing. Roland Schmehl
Coaches: Dr.ir. Erik-Jan van Kampen
Lubin Huo
DSE Project Duration: April 19, 2022 - June 23, 2022
Final Report Due Date: June 21, 2022
Faculty: Faculty of Aerospace Engineering, TU Delft

Cover: KITE-E system
Style: TU Delft Report Style, with modifications by Daan Zwaneveld

Acknowledgements

“There’s only one earth.
And there’s no spare.”

Wubbo Ockels

First, we would like to express our deepest gratitude towards our principle tutor and coaches, Roland Schmehl, Erik-Jan van Kampen and Lubin Huo, for their invaluable advice and support during our design synthesis exercise (DSE). Without their profound knowledge and feedback throughout every design step in this DSE, the realisation of our design would not have been possible.

We would like to extend our sincere thanks to the OSSC, and the teaching assistants by a larger extent, for the organisation of this project. Not only have they provided additional guidance, their valuable advice and contributions have also significantly extended our project management and systems engineering capabilities.

Especially helpful to us during this project was Kitepower. More specifically, we would like to thank Joep Breuer, Kitepower’s CTO, for his treasured support, feedback and project involvement. Without him, we would not have had the opportunity to obtain direct expert feedback from his experted employees nor to have gained an on-site Kitepower experience.

We would also like to express our special thanks to Uri Cayón Domingo for allowing us to use his aerodynamic kite simulation program. His work, involvement and technical suggestions enabled us to perform a detailed aerodynamic analysis and verification/validation process.

We very much appreciate David Aberdeen for providing us access to the commercial SurfPlan version. Due to the provided licence, we were able to visualise our established kite design.

We would like to acknowledge Rudo Enserink for expanding our knowledge about future kite production technologies and widening our horizon.

Lastly, we would like to thank external companies and experts for their co-operation. Without them, we would not have obtained the required information and expertise for the completion of this project’s analyses.

*DSE Group 15
Delft, June 2022*

Executive Overview

Mission Need

The transportation industry is transitioning to a carbon-neutral sector. With electric-powered vehicles emerging as an attractive solution, energy suppliers are facing new challenges. Airborne wind energy (AWE) is a promising solution for electrical power generation, since it is a natural resource-based technology ready to be implemented in movable small volume applications. By doing so, energy-autarkic systems can be created and operated in remote off-grid areas, and as electric generators in crisis regions. This inspired the generation of the general Mission Need Statement (MNS) for this project: ***"Provide an energy-autarkic solution for an electric pickup truck operating in a remote environment."*** [1]

Mission Objective

The mission need statement led to the definition of the mission objective through the Project Objective Statement (POS): ***"Design, with 10 students within 10 weeks, an airborne wind energy system with a cost and mass budget of €45,000.- and 500 kg, that can be fitted to the Rivian R1T for self-charging and is to be used as a mobile renewable power plant."*** [1]

Market Analysis

The first step in product design is to explore potential market gaps. A market exploration showed that the system fits both within the electric pickup truck market and the mobile energy generation market. Since no systems currently exist that combines the electric pickup truck and mobile energy generation markets, new opportunities for a market intrusion are found. A strengths, weaknesses, opportunities & threats (SWOT) analysis concluded that the mobile airborne wind energy system (MAWES) provides an opening into a niche market, enabling unlimited range to electric pickup trucks, while being energy-autarkic as the main strength and market opportunity. On the other hand, the high environmental dependency and niche target market were determined to be the main weakness and threat.

Next, three main operational regions were established, which are related to their respective fields of application. Firstly, the system can be used by well-off adventurers, in North-America and Patagonia. Secondly, the system provides a way to deliver energy in disaster struck regions, such as the Caribbean. Lastly, the system can be used for peace missions, for example in the Middle East. The market analysis concluded with an estimated demand of 2550 units for the Kite Integrated in Truck Electrical Energy (KITE-E) system.

Furthermore, airborne regulations were investigated, concluding that the AWES is categorised as a specific unmanned aerial system. From this categorisation it also followed that a specific operations risk assessment (SORA) needs to be performed in order to obtain a European operational licence. Finally, the system operator should possess an A1/A3 and an A3 drone pilot licence.

Trade-Off Study Summary

Before performing a detailed design option trade-off for different subsystems, non-feasible, non-concepts, and future concepts were discarded. The trade-off was performed by judging design options on a scale from 0 to 5, based on seven weighted requirements. The criteria were complexity, cost, mass, performance, reliability, sustainability, and volume. The weights of these requirements were dependent on the specific subsystem requirements and characteristics. From the trade-off, the converged design concept followed:

- **Airborne system:** A single supported leading edge inflatable kite is the chosen design.
- **Control system:** For control system actuation, a suspended cable robot was chosen. The airborne control system will be powered by a separate on-board wind turbine. The control sensing system was determined to use an ultrasonic wind sensor for the wind measurements, a Global Positioning System (GPS) with barometer for the relative position measurements, and a magnetometer together with accelerometers and gyroscopes for the attitude and acceleration measurements. The sensors will be placed on the airborne control system and ground station. Communication and telemetry is performed by an external Wi-Fi system.
- **Launching and landing system:** For launching, a general flat laying approach was chosen. For landing, the reel-in method to the side of the wind-window was determined to be the best option.
- **Tether system:** A Dyneema SK78 non-conductive tether will be used for the tether and bridle system.
- **Ground system:** The airborne system will be stored in the truck bed and the gear tunnel of the truck. For anchoring, a handbrake should be sufficient to remain stationary during operations.

- **Power generation system:** A direct current (DC) motor-generator will be used for the reel-in/-out of the tether connected to the kite. This decision was however revisited during the detailed design.
- **Short term energy storage system:** For the short term energy storage system, which provides energy during reel-in and powers the ground control, a supercapacitor will be used.

Operations

The operational procedure has been designed such that all operations can be performed by one person, assisted by an automated system. Five main phases were determined. In the pre-flight phase, the pickup truck needs to be parked at a ground angle of maximum 2° . The Rivian R1T contains the sensors to measure these angles. Launching equipment needs to be placed on the ground, approximately 15 m from the truck and loaded with material from the launching area, to prepare the anchoring point for the kite. All airborne subsystems then need to be connected to each other, and the kite needs to be attached to the magnetic clamps of the launching equipment before it is inflated. The kite is positioned with the trailing edge pointing into the wind. The tether is tensioned before inflating the kite, such that the trailing edge is pushed down on the ground. This means that the rear bridle lines need to be fully retracted, which is accommodated by the KCU. The inflation of the kite is done with the built-in compressor of the Rivian R1T.

After KCU sensor checks have been performed, the operator will slowly drive the pickup truck to about a minimum distance of 40 meters from the kite. If sufficient wind is not present for launching, the truck can be placed further from the kite so more tether length can be used to reel in the kite to create a higher apparent wind speed.

To begin launching, the operator gives a signal to the control system to begin the automated launching procedure. Now a sequence of separate steps are executed, beginning with disconnecting the magnetic clamp from the leading edge. Then, KCU reels out the depower tape and the main tether is reeled in till the kite is standing straight on its trailing edge. Now, if the wind is sufficiently high enough, the kite catches the full wind, and if there is sufficient wind the kite will fly up. If the wind is not high enough, a winch launch is performed. The tether will then be reeled in, increasing the apparent wind speed and thus letting the kite take to the air. Now that the kite is safely in the air, the tether can be reeled out. When the tether is not double winded around the drum any more, the power generation of the system can start.

The in-air phase consists of the pumping cycles to generate electricity by flying a figure-eight manoeuvre. After the kite reaches its minimum operational altitude of 165 m, as visible in Figure 1, pumping cycles are used for power generation. The design cyclic power output should be equal to 20 kW. During the figure-eight manoeuvres, the tether unrolls from the drum, which is connected to a generator, resulting in the generation of electrical energy until a maximum altitude of 290 m is reached. A part of this energy is stored to be used during the reel-in phase. The energy is used to pull the kite back in, from the maximum operational height to the minimum operational height, to start a new pumping cycle. The operational window of the kite spans 180° behind the pickup truck in the horizontal plane. This constraint prevents the tether from hitting the truck's cabin. If the wind turns 50° in one direction, the kite has to be landed to enable the operator to relocate the truck.

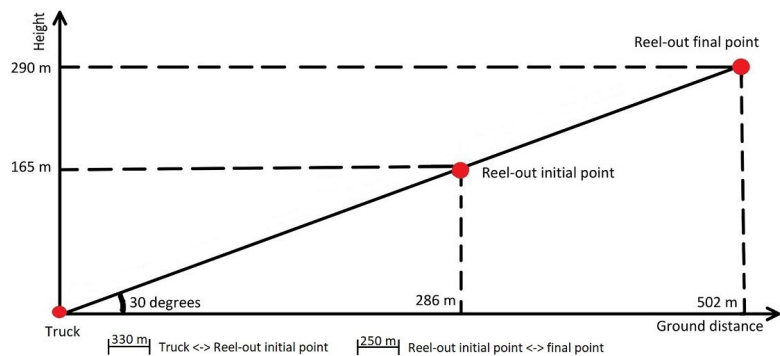


Figure 1: Operational envelope during the reel-out phase.

The landing procedure is started by reeling in to a minimum distance, where the kite can still be controlled by the Kite Control Unit (KCU). At that moment, the side of wind window landing approach will start. This landing is performed by bringing the kite to one of the sides of the wind window. From that position, the kite can be depowered and landed safely. The kite can then be laid on the ground by one person. If operation of the kite is not necessary anymore, the post-flight operations can be performed.

Post flight, the airborne subsystem elements are disconnected. The tether is rolled completely onto the drum and a cover is put over the entire system. The last post-flight operation step is storing the kite. The kite can be completely deflated by using the compressor of the Rivian R1T as a vacuum pump. The kite will be folded from the wing tips to the middle to keep the structural integrity of the kite intact. The folded kite can be put in a bag and stored in the gear tunnel of the truck.

To ensure continuous operations, proper maintenance of the system is important. Small failures and errors can have big consequences and can lead to system failure. Maintenance friendly design methods were introduced, and a predictive maintenance strategy has been created. Maintenance procedures have been designed for each subsystem.

Design Procedure

Design is an integral part of product and system development. A well-organised and streamlined design process is therefore a necessity to ensure a detailed and consistent design. The design procedure was described in depth in Chapter 9. The main functionalities, risks, and requirements that drive the design were taken into account throughout the entire design process.

As identified in Section 6.2, the main functionalities of the system during operations lie within the launching (F.3.3.2), landing (F.3.5.2), control (F.3.4.2), electricity generation (F.3.4.3) and utilisation (F.3.4.4). These were thus the main functions for which the system was designed. The main requirements driving the design, coming from Chapter 2, were the following:

- **AWE-CON-CO-01:** The total cost per airborne wind energy system shall be below €45,000-
- **AWE-CON-DES-01:** The preliminary design shall fit within the truck bed of the Rivian R1T.
- **AWE-CON-DES-02:** The preliminary design shall not exceed 500 kg.
- **AWE-CON-SAF-01:** The pickup truck shall remain static under the specified operational loads.
- **AWE-TEC-PG-03:** The power generation system shall have a nominal power output of 20 kW.
- **AWE-TEC-CS-04:** The control system shall provide fully automated pumping cycles.
- **AWE-TEC-OPS-01:** The launching and landing of the airborne system shall be a task for maximally one person.

The design procedure was a concurrent process, with many iterative and interdependent design elements of the system. To have a complete overview of the way in which elements of the total system influence each other with respect to design, an N2 chart was made. This chart was used in the design process itself, and aids in giving an overview of all interdependencies and iterative design elements. Before initiating the design procedure, all subsystems, their characteristics and the methods of analysis were determined. Methods of verification and validation were determined as well. Verification and validation has been performed throughout the design. For the actual design, subsystems were parallelly analysed, designed, and integrated. Using the N2 chart, the determination and calculation methods of the system element characteristics were fully integrated with each other, to enable a full design optimisation. This iteration was verified and validated as well, ensuring a consistent preliminary design.

Main Power Generation System Characteristics

One of the central requirements is that the KITE-E system should have an electrical output power of 20 kW. In order to find how the system can satisfy this requirement, an analysis of the power cycle is performed, based on the Luchsinger model [2]. This model is based on the assumption that the traction force is equal to the lift produced by the kite. Combining this force with reeling factors, which define the tether velocity relative to the wind speed, the average power generated over a cycle can be calculated. The model was put into a python script, which takes the aerodynamic performance of the system, the required electrical output power as an input, and a regular design wind speed at an operating altitude of 165-290 m. It then returns the required projected area of the kite, the optimal tether speeds during the reel-in and reel-out phase, as well as the corresponding traction forces. From this, also the power generated during reel-out and required during reel-in can be found. However, the traction force during reel-out was found to be too high, as the requirement for a static ground station would be violated. Therefore, a higher reel-out speed had to be used, to lower this tether force, but keep the same output power. For this reel-out speed, a new optimal reel-in speed was determined. As those speeds were not optimal anymore, the new power cycle implied a larger projected area of the kite to meet the requirement. This analysis resulted in a required projected area of 15.19 m², which was found in an iterative way, as the aerodynamic coefficients had to be adjusted for this area. Furthermore, it was found that reel-out would happen at a speed of 41% of the wind speed, with a traction force of 10.41 kN, and the reel-in at 180% of the wind speed, with a traction force of 0.50 kN. This leads to reel-out mechanical power generated of 42.62 kW, which multiplied with the reel-out efficiency, gives a reel-out electrical power of 27.79 kW for the DC generator, and a reel-in mechanical power needed of 9.03 kW for the alternating current (AC) motor, which divided by the reel-in efficiency leads to a reel-in electrical power of 14.14 kW. The design power cycle will last for 72 seconds, from which 58 seconds are used by the reel-out phase.

Figure 2 shows how the output power changes for a range of wind speeds. It can be seen that at the design wind speed of 10 m/s, the output power of 20 kW is reached. However, to also get the full potential out of the power of the wind at higher wind speeds, the generator limit is only reached at 14 m/s. This is the point where the tether can not be reeled out any faster, and the kite should either be depowered, or the elevation angle should be increased.

Using all these power cycle parameters, the power system components could be sized. Those are all off-the-shelf components, available on the market. Figure 3, shows the electrical block diagram of the system. This explains how all the components are connected and work together.

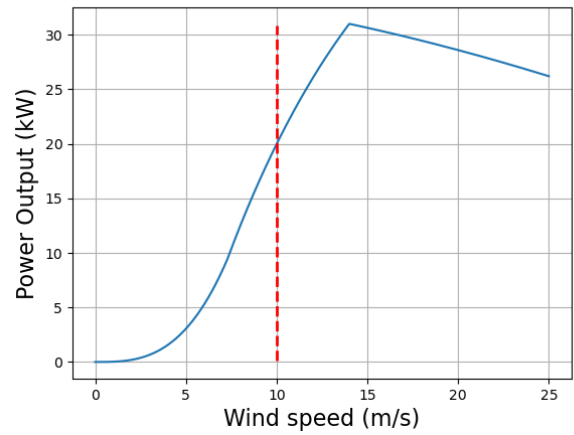


Figure 2: Output power for a range of wind speeds.

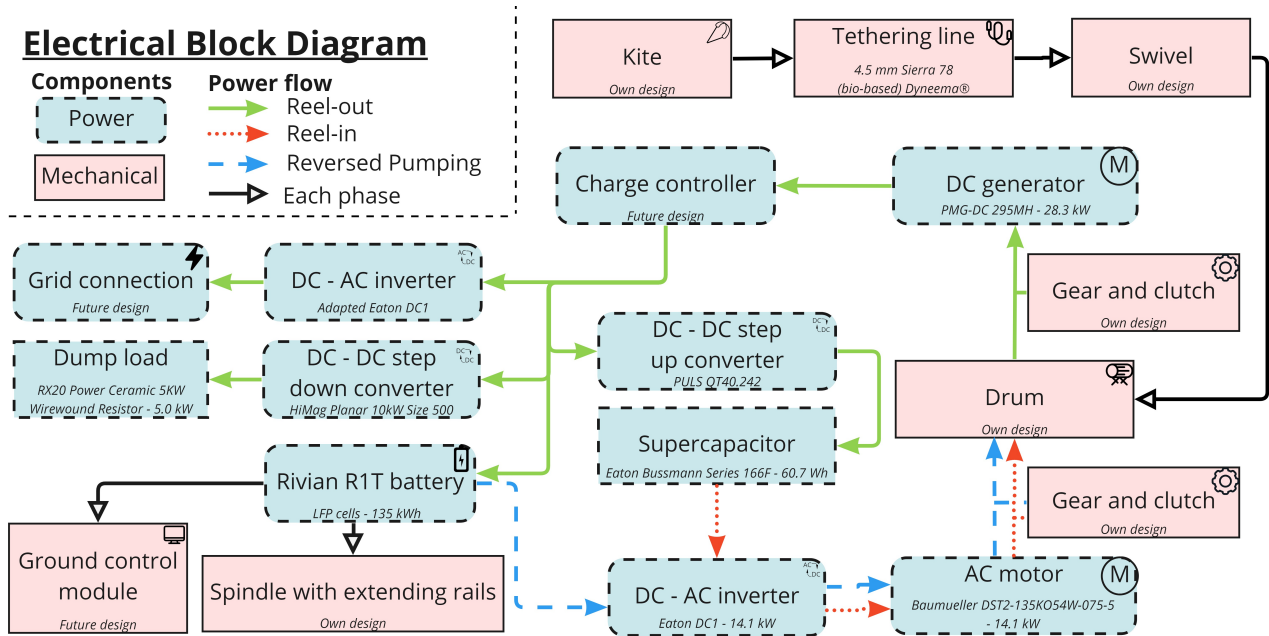


Figure 3: Electrical block diagram of the KITE-E power system

Aerodynamic Analysis

The kite’s airfoil was decided to consist of a traditional leading edge inflatable (LEI) tube with a single foil. This decision resulted from a trade-off between five feasible airfoil concepts that were assessed on performance, weight, complexity, application knowledge and operational practicality.

Following the airfoil choice, research was conducted into the aerodynamic performance influence of different planform parameters. The KITE-E’s design was decided to have a 0.4 taper ratio projected planform with a straight trailing edge and a half-ellipsoid leading edge, with an ellipse ratio ($\beta_{ellipse}$) of 0.33. The kite’s front view was decided to have a semi-ellipsoid outline with $\beta_{ellipse} = 0.5$. Similar to the Kitepower V3 kite, KITE-E’s kite has a flat aspect ratio (AR) of 5. Based on the previously mentioned aspects, the mean aerodynamic chord (MAC), wingspan (b) and tip and root chords were determined. An overview of the kite’s geometric characteristics is shown in Table 1, with a geometry visualisation in Figure 4 and Figure 5.

Table 1: Kite design layout parameters summary. In this table, the subscript (proj) relates to the projected planform, whereas the subscript (flat) relates to the flat planform.

Parameter	A _{proj}	b _{proj}	A _{flat}	b _{flat}	AR _{proj}	AR _{flat}	MAC	λ	c _t	c _r	Front $\beta_{ellipse}$	Top $\beta_{ellipse}$
Value	15.19 m ²	7.92 m	19.32 m ²	9.59 m	5.00	4.13	1.92 m	0.4	0.88 m	2.20 m	0.50	0.33

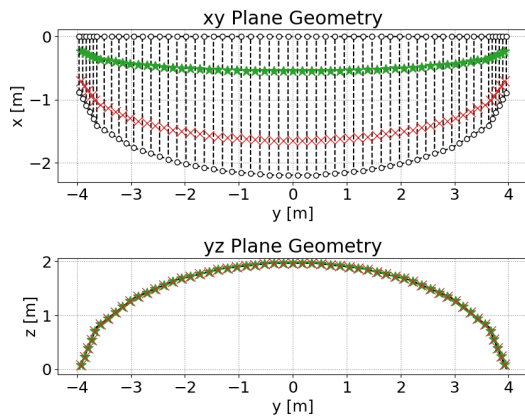


Figure 4: 15.19 m² LEI kite xy- and yz-plane geometries.



Figure 5: SurfPlan KITE-E 3D kite view.

For the aerodynamic performance modelling, a vortex step method (VSM) was used. This model has known limitations, of which these five were considered to be the most important ones: viscous effects are not accurately modelled, flat wake assumption, no aeroelasticity effect modelling, post-stall uncertainty, and assumptions about tether, bridle and KCU drag. Implementations of these limitations on KITE-E's design were discussed in the verification and validation.

The kite geometry analysis, using a vortex step method (VSM) code, resulted in a constant thickness over mean aerodynamic chord ratio (t/MAC) of 8%. Similarly, an optimal camber of 8% was found for this planform design. This final kite configuration was then simulated to determine its main aerodynamic performance parameters. Finally, a 0° twist was considered for the design simplicity.

Tether, bridle and KCU drag additions were estimated based on literature obtained estimations. The tether drag was calculated based on a specific formula [3] and the KCU drag was assumed to be 10% of the combined kite and tether system drag. Implementing these drag estimations into the VSM code and running the analysis led to the establishment of the aerodynamic characteristic polars, as displayed with detailed values by Table 2 and shown as graphs by Figure 6.

Table 2: Summarising table for the 15.19 m² kite system's aerodynamic performance characteristics.

Parameter	Angle of attack (α) range	C_L	C_D	C_L/C_D	C_L^3/C_D^2
Reel-out	8° to 15°	1.07	0.15	7.14	56
Reel-in	-1° to 3°	0.15	0.1	1.41	2.72

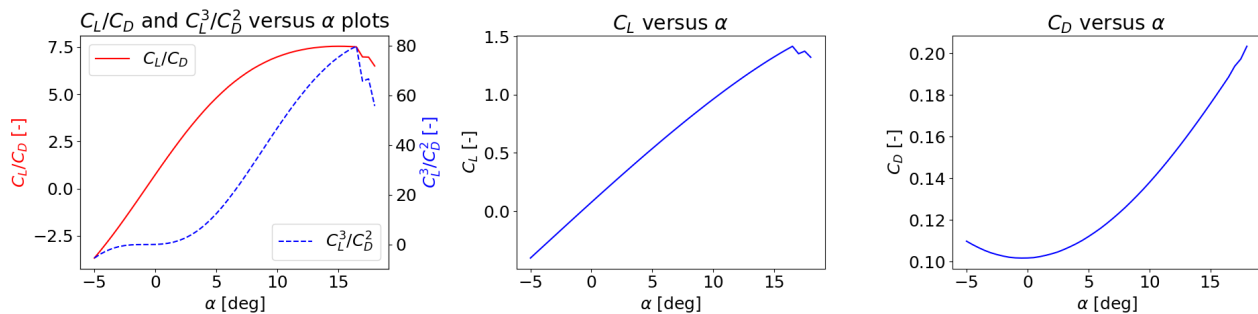


Figure 6: Aerodynamic polars for the 15.19 m² projected area kite system. ($N_{split} = 5$, Segments = 12, #Points = 10⁶)

Structures and Materials Characteristics

The system has multiple components, of which the dimensions and materials were determined. Firstly, the diameter of the Sierra 78 (bio-based) Dyneema® tether was determined to be 4.5 mm, including a safety factor of 2 on the design load. Splicing of the rope is discussed, to explain how the system will be put together after damage, using a Twelve-Strand Class II Smooth Eye Splice with whipping. For the determination of the tether dimensions, the fatigue characteristics of the tether are most important. Especially fatigue bending plays a large role in the design process, since this is the critical fatigue characteristic. The creep and fatigue bending lifetimes are calculated and the Safe Service Life (SSL) of the tether is determined to be 2526 flight hours (FH), since fatigue bending is the limiting fatigue characteristic. The maximum operational altitude is 290 m. With an elevation angle of 30°, the required length is 580 m. A 30% safety factor is added to the operational range, which ranges from 165 m to 290 m, resulting in 75 m extra tether. This results in a total tether length of 655 m.

The diameter of the leading edge is equal to a t/MAC of 8%, since this is ideal for the aerodynamic performance. This results in a diameter of 0.1606 m, with a leading edge pressure of 9 psi. The ideal strut configuration is determined to be a 6 strut kite, to allow for attachments between the two centre struts.

The bridle configuration was designed based on similar kite systems and a static load analysis. Based on the performed static load analysis, the force in each of the bridle was determined. This was used to determine the diameter of each bridle, including a safety factor of 2. However, due to the fact that the bridle configuration was divided in three levels, as shown in Figure 7, and the bridle diameter of each level is the same, to incorporate changes in load due to the movement in the kite, some bridles were overdesigned. Resulting in a diameter of 3 mm for level 1 and 2, and a diameter of 2 mm for level 3. The material used for the bridle lines is the same as is used for the tether, Sierra 78 (bio-based) Dyneema®. Based on this material, the identified bridle diameters, and the length of the bridle lines, the mass of the bridle system was found to be 0.145 kg.

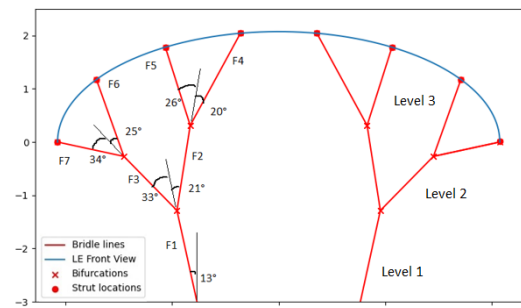


Figure 7: Bridle configuration, with identified angles at the bifurcations.

The kite material selected for both the airframe and the kite is ALUULA. This relatively new ultra-high molecular weight polyethylene (UHMWPE) composite outperforms the commonly used Dacron, both in weight and strength. Furthermore, ALUULA is 100% recyclable. An ALUULA airframe has half the weight of an identical airframe made of Dacron, and is stronger. The kite mass was extrapolated, using a 5 strut kite with an ALUULA airframe, to make an approximation. An approximation is necessary, since the mass of the valves and reinforcements can not accurately be determined. This approximation resulted in a total kite mass of 4.81 kg.

Ground Station Characteristics

The anchoring of the ground station must prevent the truck from sliding and tilting over when the kite system is active. This is vital for the safety of the product users. It was calculated that the car would only start to move on hard-packed snow. Furthermore, tilting of the pickup truck is to be prevented, as this would create a hazardous situation. After analysis, it was concluded that the pickup truck is not expected to tilt over the transverse axis. Lastly, dynamic loading is an important loading for the anchoring system. If the applied dynamic loads have a similar frequency as the car response, unwanted resonance can occur. This can lead to unpleasant bouncing of the car or even damage.

The natural frequency of the damping of the R1T was estimated at a range of 1.5 - 2.5 Hz. As this natural frequency is significantly higher than the oscillations caused by reel in and reel out, it is expected that no resonance will occur and that no additional modifications to the pickup truck will be necessary.

For optimal volume use, the tether will be double wound on the drum. The outer layer is completely reeled-out during the starting phase, before the operational altitude is reached. The tether is wound on the drum with a 0.5 mm spacing to avoid damage due to the tether rubbing against itself during winding. To limit the weight of the drum, but still make the system strong enough, aluminium alloy 1100 is used as drum material. This results in a mass of 131.56 kg.

The drum will be attached to the bed of the pickup truck using bolts. It is assumed that the truck bed will not rupture before the tether fails. Future research is necessary to determine the actual truck bed fatigue, since no information is yet available on the material of the truck bed. The application of 6 rails on the truck bed is necessary to slide the spindle outward near the back of the truck bed and discard the limiting swivel angles

constrained by the truck bed edges. The maximum bending force applied from the kite is equal to the 12.47 kN, each rail thus has to support a maximum bending moment of 531 Nm.

The designed launching equipment will have as its main function to provide enough tension force to pull the kite down and prevent it from coming into an unwanted position and generating lift prematurely. The equipment is designed to be lightweight for storing, and it can be loaded with material from the launching spot, such that the equipment is not being pulled from the ground. A mass of at least 17.8 kg of the launching equipment was calculated to be needed.

Guidance, Navigation and Control System

The guidance, navigation, and control (GNC) system is vital for the successful operation of the entire system, as it is the brain of the operations. Both the kite and the winch are controlled by the system, and it is instrumental for the safety and efficiency of the design. The Navigation part of the system first determines the state of the system and the wind conditions. The state of the kite entails the position, attitude and velocities of the kite and for the winch it is the tether force and reeling speeds. The most vital sensors used here are the Inertial Measurement Unit (IMU) on the kite and the tether force sensor at the winch.

The guidance part then determines a flight path based on the flight conditions and calculates the required heading or course angles to follow this path. The flight path planner makes the kite fly in figures of eight with the use of simple sections of straight lines and turns with a constant turning rate. For a straight line section a heading angle is set, for a turning section a set turning rate is defined. Every cycle, the elevation angle of the figure of eight is reassessed based on the wind conditions. This simple approach has been chosen for reliability reasons, as it limits the number of control commands and has been demonstrated to work on similar kite systems [4]. For the winch guidance in case, the tether force is under the maximum, the reel out speed is calculated to optimise power output based on the Luchsinger model, otherwise the tether force is actively controlled to stay below the maximum tether force.

Finally, the control part actively controls the system to follow the set variables by the guidance system. The kite is controlled by a Kite control unit hanging 10 meters below the kite via depower and control lines. By changing the length of the steering tapes, the local angle of attack of the kite is changed, inducing a steering manoeuvre. Using the depower line creates a pitching movement, and using the control lines creates a change in the heading and course angles. The steering inputs are calculated by a Linear Parameter Varying (LPV) control in addition to using output linearisation. The winch is controlled by changing the rotation speed of the motor. By increasing the rotation speed, the tether force drops and vice versa. When the tether force is limited, a simple Proportional Integral Differential (PID) controller with the tether force as input is used. In addition, the ground control has a moving spindle which assures the tether is not rolled over itself on the drum. Finally, the entire system communicates via a 5 GHz Wi-Fi system, with a backup 2.4 GHz system.

Fault, Detection, Isolation and Recovery System

The Fault, Detection, Isolation and Recovery (FDIR) is a vital part of the risk mitigation strategy of this design. It is a technique often used in industries requiring high reliability, such as in the space industry, and was therefore chosen for this system. The target design for the FDIR is to prevent catastrophic failure scenarios based on the risk analysis performed per subsystem. It is made up of five hierarchical levels, increasing in scope. The first three levels monitor the system on respectively item, equipment and subsystem level with sensors and redundant parts. The last two levels monitor on a system level, with most notably a flight anomaly detection system and the option to cut the safety line between the KCU and the tether. If the FDIR detects a risk, a predefined mitigation measure is taken based on the severity of the issue.

Optimisation and Final Preliminary Design

In line with the design procedure, after having investigated each subsystem in detail, an optimisation of the system is performed. This is done by means of an iterative process in which the power cycle, the airborne system's aerodynamic parameters, and the tether parameters are matched. In order to automate this process, the Luchsinger model, the VSM, and tether diameter calculation codes were merged. Furthermore, the codes that were used for calculation of other subsystem characteristics were integrated as well. The other integrated codes automatically sized, and determined subsystem characteristics based on the obtained values from the power cycle and the aerodynamic analysis. The main parameters that were determined in this way were the drum diameter, the kite mass, tether mass, supercapacitor storage, launching equipment clamp force, motor and generator sizing. The initial values and the results of the optimisation are shown in Table 3. It can be seen that all values either improved, meaning the system got more efficient or lighter, or they stayed the same. The final configuration of the system can be seen in Figure 8.

Table 3: Summary of Optimised Design Data.

Subsystem	Parameter	Unit	Data after initial matching	Data after optimisation
Airborne	Projected area	m ²	16.65	15.19
	Flat area	m ²	21.17	19.32
	Kite mass	kg	5.16	4.81
	Tether Diameter	mm	4.4	4.5
	Lift-over-drag reel-out	-	7.64	7.14
	Tether mass	kg	7.00	7.06
	Tether lifetime	h	2526	2632
	KCU weight	kg	6.65	6.65
Flight Cycle parameters	Optimal γ_{out}	-	0.43	0.41
	Optimal γ_{in}	-	1.78	1.80
	Reel-in duration	s	14	14
	Reel-out duration	s	58	61
	Total cycle duration	s	72	75
	Pumping efficiency	%	89	89
	Duty cycle	%	80.60	81.30
	Cycle efficiency	%	71.73	72.36
Power	Average mechanical cycle power	kW	33.82	33.02
	Average electrical output cycle power	kW	20.00	20.00
	Energy generated during reel-out	Wh	456.72	471.12
	Energy used during reel-in	Wh	50.26	54.67
	Capacitor storage	Wh	60.0	65.6
	Net energy generated per cycle	Wh	406.46	416.45
	Mechanical (Motor) reel-in power required	kW	9.21	9.03
	Electrical reel-in power required	kW	14.12	14.14
	Mechanical reel-out power generated	kW	44.27	42.62
	Electrical reel-out power generated	kW	28.29	27.79
	Gear ratio generator	-	0.12	0.11
	Gear ratio motor	-	0.97	0.98
Ground System	Traction force reel-out	kN	10.33	10.41
	Traction force reel-in	kN	0.52	0.50
	Required friction coefficient	-	0.400	0.404
	Drum diameter	m	0.473	0.475
	Drum width	m	1.10	1.10
	Downforce by launching equipment	N	192	175
	Pulley diameter	m	0.27	0.27
	Swivel rails weight	kg	13.9	13.9

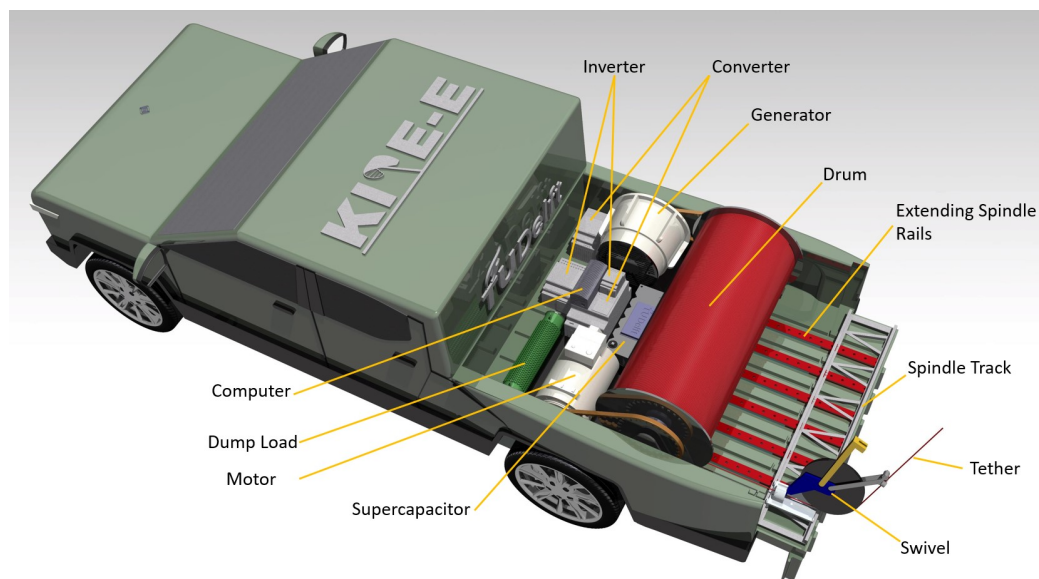


Figure 8: Visualisation of the final configuration.

In addition, for a quantitative analysis of the configuration, a mass breakdown was performed on the final design. The total mass of the system is 409.4 kg. This total mass is broken down in several system aspects, which can be seen in Figure 9.

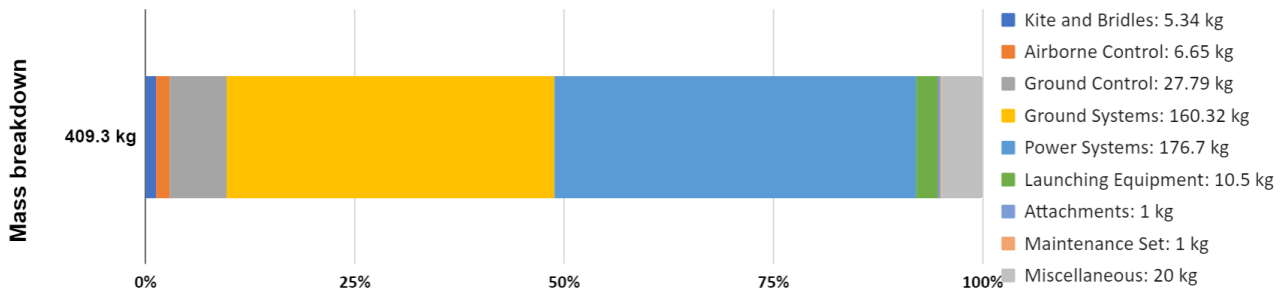


Figure 9: Mass breakdown of optimised design

Design Sensitivity

A sensitivity analysis was done, to clarify how the design interactions that were shown on the N2 chart influence each other, both qualitatively and quantitatively. No anomalies were found, and all parameters were related as expected. This means the design results are expected to be reliable.

Verification and Validation

Verification and validation are a very important step in every design process. It should be performed on both a small and large scale. All the models, or other calculations that were used for the design, were verified by performing unit tests, to ensure their correct implementation in the script.

This calculation verification was found to be successful for every established calculation model. Furthermore, when possible, those models were also validated by comparison with experimental data. Apart from those unit tests, also a product validation was performed by comparing the KITE-E system with an older AWES with a similar configuration. Although the KITE-E system's performance is much better than the older system, good reasons were found when looking at the difference in performance of the two system at subcomponent level. The system was therefore found to be validated.

Reliability, Availability, Maintainability and Safety (RAMS)

To ensure that the system fulfils the reliability, maintainability, availability, and safety, aspects of the design a RAMS analysis was performed. To investigate the reliability of the system, the lifetimes of the different subsystems components were determined, which were mainly deducted from literature. The components from kite system show the lowest reliability, due to the fairly new composite ALUULA Vaepor™ that is used for the kite and the low number of flight hours that the tether can handle due to fatigue bending. The ground system, control system, and power system components showed high reliability, due to the fact that the components in these systems are well established concepts. Following this, the availability of the AWES was discussed. This was assessed in terms of the unavailability of the system, which was determined to be equal to 2.7% after a full week of operation. To improve the reliability and availability, and safety of the system, maintenance is of utmost importance. Therefore, a predictive maintenance strategy is applied, and an in-depth maintenance strategy was established for each subsystem, leading to the identification of the required maintenance intervals. Furthermore, also repair kits and a list of spare parts for specific operating regions is provided. Maintenance is one to improve the safety of the system, however, this is not enough and safety measures should be taken throughout the complete life cycle of the AWES. The different to ensure safety for both the AWES components and people, different safety measures were established and discussed.

Requirement Compliance

After having verified and validated the different analytical and numerical models, also the product itself must be verified and validated. The product verification is done by identifying if each of the requirements are complied with, using a compliance matrix. From this, it was shown that no non-compliance was found. However, to check verification with some requirement, demonstrations or tests still need to be performed.

Finances

The cost of the complete system will be €41532.69, and will be sold for €47999,-. A detailed cost breakdown is shown in Chapter 17. Furthermore, the return on investment is estimated to be 15.57% over the course of 8 years, with the break even point reached around 7.5 years in. When a customer buys this system, it will take around half a year of flight hours to start making a net profit, compared to buying energy directly from the grid.

Sustainable Design

With an equivalence CO₂ emission of 9007 kg, the KITE-E production process and operation over one year emits over 4.5 times less than the operation of a 20 kW diesel generator operation. This result is obtained for an equal energy generation over this timespan and clearly indicates that sustainability was a vital aspect throughout KITE-E's design. Firstly, a sustainable strategy was determined to cover the people, profit and planet aspects. This led to the establishment of four sustainability related requirements. This implied that design decisions should take a sustainability factor into account, which is reflected by the design's trade-off decisions and material choices. Finally, the sustainability approach was reflected on by an equivalence CO₂ emission analysis and comparison to a similar diesel generator system.

KITE-E Future Outline

Since this report contains the outcomes of a 10-week design period, it only covers the system's design to a certain level. Future steps should therefore be taken to ensure a successful product development. The project's timeline was extended to 5 years, eyeing to enter commercial production in 2027. Up to the commercial production phase, the KITE-E's future outline was laid out in depth. Starting with a detailed design phase to further investigate and refine the current design, the used models should be extended to result in more accurate analyses. Once a final design is reached, the testing phase is initiated. This enables design iterations that enable design to converge for compliance with the driving requirements and regulations. After the prototype establishment, the market campaign is initiated and maintained until the commercial production phase start. This future outline is concluded with a production plan for the commercial production phase. After production, full product operation and maintenance is initiated. Finally, the end-of-life phase concludes the KITE-E's operational lifetime.

Recommendations

This report was concluded with the main recommendations for the future development of this project. Although this report already contains detailed analyses on a high level and for the general principles, still a lot of detailed investigation is required to fully verify and validate these outcomes. Additionally, subsystems should be evaluated into every detail to provide a finalised design concept, ready for commercial production. The main recommendations are summarised in the following paragraphs.

The verification and validation for the used numerical models should be extended. This report mainly lacks proper validation of these models due to the unavailability of experimental data. Therefore, these experiments should be carried out in order to better understand the models' limitations and possible model matching extensions.

More structural analysis should be performed. Except for the tether, the current design only briefly investigated components' load carrying characteristics and were sized based on estimations. Therefore, it is recommended to further investigate the load path from the kite's lift production, all the way to the AWES to truck bed connections. Additionally, aeroelastic effects due to kite deformation should be investigated.

Finally, the KCU should be assessed in more detail. Since this component is crucial in the GNC system, more time and research should be invested into this component to ensure reliable operations.

Contents

Acknowledgements	i	9 Design Procedure	44
Executive Overview	ii	9.1 System Design Functionalities, Risks, and Requirements	44
Nomenclature	xiv	9.2 Design Procedure and Interaction . . .	44
1 Introduction	1	10 Main Power Generation System Charac- teristics	47
2 Requirements and Constraints	2	10.1 Power System Requirements, Func- tionalities, and Risks	47
2.1 Project Objectives	2	10.2 Luchsinger's Model	48
2.2 Requirements and Constraints Overview	2	10.3 Design Power Cycle Calculations and Results	50
3 Sustainable Development Strategy	6	10.4 Three-phase Strategy Calculations and Results	52
3.1 Design Oriented Sustainability	6	10.5 Electrical block diagram	53
3.2 Requirement Influence	8	10.6 Power Component Efficiency Analysis	54
4 Market Analysis	9	10.7 Ground Power System Design	54
4.1 Key Stakeholders	9	10.8 In-air Power System Design	57
4.2 Market Exploration	9	11 Aerodynamic Airborne System Charac- teristics	59
4.3 Strengths, Weaknesses, Oppurtini- ties, & Threats Analysis	10	11.1 Aerodynamics System Requirements	59
4.4 Porter's Five Forces	11	11.2 Airfoil Concept Trade-off	59
4.5 System Applications	12	11.3 Kite Design Parameters	61
4.6 Environmental Analysis	13	11.4 Kite Design Layout	63
4.7 Market Size Estimation	16	11.5 Tether and Kite Control Unit Drag Analysis	67
4.8 Social Acceptance	17	11.6 Aerodynamic Characteristics Deter- mination	68
4.9 Market Analysis Conclusion	17	12 Airborne Structures and Materials Char- acteristics	69
5 Trade-Off Study Summary	18	12.1 Structures and Materials Require- ments and Risks	69
5.1 Airborne System	18	12.2 Tether	69
5.2 Control System	18	12.3 Leading Edge	71
5.3 Tether	19	12.4 Struts Configuration	72
5.4 Launching and Landing	19	12.5 Bridle System	72
5.5 Main Power Generation System	19	12.6 Kite Material	75
5.6 Ground System	19	13 Ground System Characteristics	76
5.7 Short Term Energy System	19	13.1 Ground System Requirements, Func- tionalities, and Risks	76
5.8 Trade-off Design Options Summary	20	13.2 Anchoring	76
5.9 Trade-off Sensitivity Analysis	20	13.3 Drum Sizing	79
6 System Configuration and Operations	21	13.4 Extending Spindle Rails	80
6.1 System Configuration	21	13.5 Launching Equipment	80
6.2 Functional Analysis	22	14 Guidance, Navigation, and Control Sys- tem Characteristics	82
6.3 Operating logistics (F.3)	26	14.1 Guidance, Navigation, and Control System Requirements, Functionali- ties, and Risks	82
6.4 Maintenance (F.4)	29	14.2 Navigation	83
6.5 End-of-life Analysis (F.5)	32	14.3 Guidance	84
7 Resource Allocation	33	14.4 Control	86
7.1 Technical Resources	33	14.5 Communication and Telemetry	92
7.2 Organisational Resources	36		
8 Risk Assessment	37		
8.1 Risk Identification	37		
8.2 Launching and Landing	38		
8.3 Airborne System	39		
8.4 Guidance, Control and Navigation	40		
8.5 Ground System	41		
8.6 Power System	42		
8.7 Fault, Detection, Isolation and Recov- ery	43		

15 Optimised Design	94	17.2 Return On Investment	113
15.1 Final Design Optimisation	94	17.3 Operational Profit Analysis	113
15.2 Final Design Configuration	96	18 Reliability, Availability, Maintainability, and Safety Analysis	114
15.3 Budget breakdown	98	18.1 Reliability	114
15.4 Sensitivity Analysis	98	18.2 Availability	115
16 Verification and Validation	102	18.3 Maintainability	115
16.1 Requirement Validation	102	18.4 Safety	115
16.2 Aerodynamic Model Verification and Validation	102	19 Sustainability Compliance	116
16.3 Luchsinger Model Verification and Validation	106	19.1 Use of Sustainable Resources	116
16.4 Structural Calculations Verification and Validation	107	19.2 Requirement Compliance Check	116
16.5 Guidance, Navigation and Control Verification and Validation	108	19.3 CO ₂ Emission Estimates	117
16.6 Code Integration Verification	108	20 Project Future Outline	119
16.7 Product Verification by compliance matrix	108	20.1 Design and Development Logic	119
16.8 Product Validation	111	20.2 Production Plan (F.1 & F.2)	121
17 Financial Analysis	112	21 Conclusions and Recommendations	122
17.1 Cost Breakdown	112	21.1 Conclusions	122
		21.2 Recommendations	124
		References	126

Nomenclature

Abbreviations

AB	Airborne System	MTTF	Mean Time till Failure
AC	Alternating Current	NAA	National Aviation Authority
AMC	Acceptable Means of Compliance	NGO	Non-Governmental Organisation
AR	Aspect Ratio	NMPC	Nonlinear Model Predictive Control
AWE	Airborne Wind Energy	NOTAM	Notice To Air Missions
AWES	Airborne Wind Energy System	OPS	Operations
CFD	Computational Fluid Dynamics	OS	Operation Sites
CS	Control System	P	Probability
CTF	Cycles To Failure	PDRA	Predefined Risk Assessment
DC	Direct Current	PF	Production Facilities
DSE	Design Synthesis Exercise	PID	Proportional Integral Differential
EASA	European Aviation Safety Agency	POS	Project Objective Statement
EEE	External Energy and Emissions	QSM	Quasi-Static Model
EPS	Expanded Polyester	R&D	Research and Development
ESR	Equivalent Series Resistance	RF	Research Facilities
FAA	Federal Aviation Administration	ROI	Return On Investment
FDIR	Fault Detection Isolation and Recovery	RPM	Revolutions Per Minute
FH	Flight Hours	S	Severity
FMEA	Failure Mode and Effect Analysis	SORA	Specific Operations Risk Assessment
FV	Fussell-Vesely	SSL	Safe Service Life
GNC	Guidance, Navigation and Control	STS	Standard Scenario
GNSS	Global Navigation Satellite System	SW	Software
GPS	Global Positioning System	SWL	Safe Working Life
GS	Ground System	SWOT	Strengths, Weaknesses, Opportunities, & Threats
HMPE	High Molecular Polyethylene	TBD	To Be Determined
HPS	Highly Prestretched	TE	Trailing Edge
HW	Hardware	TF	Test Facilities
ID	Indetifier	Triple P	People, Planet, and Profit
IMU	Inertial Measurement Unit	UAS	Unmanned Airborne Systems
KCU	Kite Control Unit	UHMWPE	Ultra-High Molecular Weight Polyethylene
KITE-E	Kite Integrated in Truck Electrical Energy	UN	United Nations
LCA	Life Cycle Assessment	UV	Ultraviolet
LCOE	Levelised Cost Of Electricity	VALID	Verifiable, Achievable, Logical, Integral and Definitive
LE	Leading Edge	VAT	Value-Added Tax
LEI	Leading Edge Inflatable	VLM	Vortex Lattice Method
LFP	Lithium Iron Phosphate	VRF	Vanadium Redox Flow
LPV	Linear Parameter-Varying	VSM	Vortex Step Method
MAC	Mean Aerodynamic Chord	W	Waste
MACHY	Machinery	WHO	World Health Organization
MAWE	Mobile Airborne Wind Energy	WT	Working Tools
MAWES	Mobile Airborne Wind Energy System	WTT	Wind Tunnel Test
MBL	Mean Breaking Load		
MECH	Mechanics		
MF	Maintenance Facilities		
MFG	Manufacturing		
MGMT	Management		
MNS	Mission Need Statement		
MTTF	Mean Time Till Failure		

Greek Symbols

α	Angle of attack	$^{\circ}$
β	Elevation angle	$^{\circ}$
$\beta_{ellipse}$	Ellipse ratio	-
β_{set}	Set average elevation angle	$^{\circ}$
χ	Kite course angle	$^{\circ}$
δ_s	Angle between the swivel and truck bed	$^{\circ}$
δ_{road}	Road angle	$^{\circ}$
$\dot{\phi}_{set}$	Set turn rate	$^{\circ}/s$
ϵ	Oswald efficiency factor	-
η	Efficiency	-
γ	Reeling speed	-
Γ_i	Vortex strength per element	m^2/s
λ	Taper ratio	-
μ	Wind speed ratio v_w/v_n	$^{\circ}$
μ_{ground}	Friction coefficient of the ground	-
ω	Angular velocity	rad/s
Φ	Curvature of the kite	$^{\circ}$
ϕ	Azimuth angle	$^{\circ}$
ψ	Kite heading angle	$^{\circ}$
ρ	Air density	kg/m^3
σ	Stress	N/m^2
σ_b	Bending stress	N/m^2
σ_c	Compressive hoop stress	N/m^2
θ_s	Angle of the tether on the swivel	$^{\circ}$
θ_{et}	Eye-throat angle	$^{\circ}$
ξ	Friction coefficient air with ground	-
E	Elastic modulus	Pa
I_c	Moment of inertia	kgm^2
M	Moment	Nm
y_{NA}	Maximum distance from neutral axis	m

Roman Symbols

μ_k	Kinetic friction coefficient	-
μ_s	Static friction coefficient	-
a	Deceleration	m/s^2
a_s	Projection of the tether length	$^{\circ}$
$A_{contact}$	Contact area	m^2
A_{rotor}	Rotor swept out area	m^2
b	Wingspan	m
C	Capacitance	F
c	Chord	m
c	Cord length	m
C_D	Drag coefficient	-
C_L	Lift coefficient	-
C_P	Power coefficient	-
C_R	Resulting aerodynamic coefficient	-
C_{D_0}	Zero lift drag	-
$C_{D_{ground}}$	Kite drag at the ground	-
C_{D_i}	Lift induced drag	-

D	Diameter	m
D	Drag	N
D	Duty cycle	s
d	Displacement	m
D/d	D_{Pulley}/d_{tether}	-
d_w	Wheelbase distance	m
D_{drum}	Diameter of the drum	m
D_{pulley}	Diameter of the pulley	m
d_{tether}	Diameter of the tether	m
E	Energy	J
E_k	Kinetic energy	J
F_f	Friction force	N
F_L	Loading factor	-
F_t	Tether force	N
$F_{k,\tau}$	Force generated in a turn	N
F_{in}	Force factor during reel in	-
F_{out}	Force factor during reel out	-
F_{res}	Resultant force	N
H_0	Reference altitude	m
H_1	Specific altitude	m
h_{drum}	Height of the drum	m
L	Length	m
L	Lift	N
l_t	Length of the tether	m
l_{et}	Eye-throat length under loading	m
M	Mach number	-
m	Mass	kg
N	Normal force	N
n	Number of struts	-
N_b	Normal force back tires Truck	N
N_f	Normal force front tires Truck	N
N_l	Normal force left tires Truck	N
N_r	Normal force right tires Truck	N
N_{split}	Number of split points	-
P	Power	W
$p_{k,set}^{SE}$	Set position	$^{\circ}$
Q	Tension in the tether	Pa
R	Turning radius	m
r_t	Tether angle	m
Re	Reynolds number	-
t	Thickness of the leading edge strut	mm
t	Time	s
t_s	Drum shell thickness	m
u_s	Steering input	rad
V	Voltage	V
v_a	Apparent wind speed	m/s
v_d	Design wind speed	m/s
v_w	Actual wind speed	m/s
v_0	Wind speed at reference altitude	m.s
v_1	Wind speed at specific altitude	m/s
$v_{k,\tau}$	Tangential velocity vector	$^{\circ}$

v_{tn}	Tether limited wind speed	m/s	in	Reel-In
v_{true}	True airspeed	m/s	k	Kite
$v_{W_{ground}}$	Wind speed at the ground	m/s	KCU	KCU
W	Weight	N	max	Maximum
W_e	Energy density	J/m^3	mech	Mechanical
w_{et}	Eye-throat width under loading	m	min	Minimum
x	X-axis	-	N	Normal force
y	Y-axis	-	out	Reel-Out
z	Z-axis	-	proj	Projected
v	Speed	-	rotor	Rotor

Subscripts

r	Root
t	Tip
c	Cycle
c.g.	Center of gravity
clamp	Clamp
desgin	Design
el	Electrical
flat	Flat
front	Front view
g	Gravity
hor	Horizontal

SE	Small earth
section	Section
stall	Stall
t	Tether
top	Top view
vert	Vertical
w	Weight
w	Wind

Superscripts

E	Electrical
M	Mechanical
opt	Optimal

Introduction

The search for renewable and sustainable substitutes for fossil fuels is becoming more and more urgent as the deadline of the Paris Agreement looms [5]. Solar energy, nuclear energy and wind energy have emerged as possible replacements for fossil fuels to reduce the emission of greenhouse gases. More recently, within the renewable energy sector, airborne wind energy (AWE) has emerged as a new concept to generate energy without the negative side effects of burning fossil fuels. Big advantages of an airborne wind energy system (AWES) are the low environmental impact and the flexibility [6].

Within the transportation sector, the reduction of fossil fuel use is urgent. In 2019, 18% of all CO₂ emissions in Europe originate from road transportation [7]. With hydrogen cars and especially electric cars, solutions for this problem are already widely available. Moreover, the EU is targeting to restrict new car sales to solely comprise fully electric or electric equivalent cars in 2035 [8]. These cars currently have a very limited operational range. Paired with the fact that charging infrastructure is still limited, operation of electrically driven vehicles in remote areas is almost impossible. Furthermore, the electricity and hydrogen that these cars use are also often produced through unsustainable processes [9]. This raises the question whether it is possible to create a system that is energy-autarkic, providing a theoretically unlimited operational range, while minimising the emission of greenhouse gases.

A potential solution to this challenge for autarkic systems would be to create a mobile airborne wind energy system (MAWES), by fitting an AWES to an electric pickup truck. This combination enables the electric pickup truck to push beyond the limitations of other electric cars. Firstly, the AWES provides the pickup truck with green electrical energy for recharging the battery. Secondly, the truck would be ideal to operate in remote areas, where charging infrastructure is missing. In addition, it could operate as a mobile power plant, providing power in disaster-struck areas, where a combination of a pickup truck and an AWES is an ideal solution for operations in destroyed infrastructures.

The aim of this report is to determine the preliminary design of an AWES that can be fitted on the truck bed of the Rivian R1T. In the Midterm Report [10], a design configuration was chosen after performing trade-offs. This provides a starting point for the preliminary design phase to be carried out in this report. The design consists of an assembly of different subsystems that need to adhere to each other. These are designed in adherence with the constraints and requirements, which are imposed by stakeholders and identified by the team. Once the design process is complete, the total system is optimised for power generation. However, for other design aspects, a full optimisation is absent, as this is not possible within the scope and timespan of the ten-week project.

This report starts with a review of all previously identified design constraints and requirements in Chapter 2. Following this, the sustainable development strategy is shown in Chapter 3. Furthermore, Chapter 4 presents the market analysis, including an environmental analysis and regulatory investigation. A summary of the trade-offs is performed in the Midterm Report [10], is given in Chapter 5. Based on this conceptual design convergence, the system configuration, functionalities and operations are introduced in Chapter 6. In Chapter 7, the technical and organisational resources are laid out. The risk assessment for all subsystems is performed and reported in Chapter 8. Before presenting the detailed design analysis, an N2 chart, together with an explanation on the design philosophy, are presented in Chapter 9. This chapter is specifically created to provide an overview of the design steps and subsystems dependencies that lead to an integrated design. All calculations, decisions and explanations for the detailed design of the subsystems are presented in Chapter 10-Chapter 14. These subsystems together form the system, which is optimised and shown in Chapter 15. A sensitivity analysis is also carried out in this chapter, to show how the design interactions both influence each other and the general system's performance. Verification and validation is then performed, as laid out in Chapter 16. These verification and validation processes are vital for ensuring that correct and accurate models are used for simulations and calculations. The cost, return of investment and operational profit are treated by the finance chapter in Chapter 17. In Chapter 18, a reliability, availability, maintainability and safety analysis (RAMS) is performed. A reflection on the sustainable approach is discussed in Chapter 19 and concluded by an equivalence CO₂ emission analysis. Chapter 20 outlines the future of the project. Lastly, the conclusions and recommendations are presented in Chapter 21.

Requirements and Constraints

In this chapter, the system and subsystem requirements and the constraints for the design are discussed. First, the project objectives are laid out in Section 2.1. Afterwards, the current list of requirements is shown, with updated and additional requirements. Since more is known about the layout of the system, additional requirements arise. This is done in Section 2.2.

2.1. Project Objectives

Design Synthesis Exercise (DSE) group 15 was tasked with designing an airborne wind energy system that could be fitted in the trunk of a Rivian R1T. The goal was to create an energy-autarkic system, to allow the electric pickup truck to operate in disaster regions and remote environments. The Mission Need Statement and Project Objective Statement associated with this are the following:

Mission Need Statement:

"Provide an energy-autarkic solution for an electric pickup truck operating in a remote environment." [1]

Project Objective Statement:

"Design an airborne wind energy system with a cost and mass budget of 45,000.- € and 500 kg that can be fitted to the Rivian R1T for self-charging and to be used as a mobile renewable power plant, by 10 students in 10 weeks." [1]

2.2. Requirements and Constraints Overview

This section presents the revised requirements and constraints from the initial established ones in the Baseline Report [10]. Since then, multiple requirements have been altered or added. This results in the removal of certain requirements, as they are subdivided over multiple new requirements. This means their identifier (ID) changes and the old requirement is crossed out. The final set of requirements and constraints is presented in Table 2.1 and Table 2.2 respectively. These tables also include either a justification why the requirement or constraint is added or why it is deleted.

Table 2.1: Technical requirements and justification table.

Requirement ID	Requirement Description	Justification
General Requirements		
AWE-TEC-GEN-01	The airborne wind energy system shall be energy-autarkic.	This requirement is a stakeholder requirement.
AWE-TEC-GEN-02	The airborne wind energy system shall estimate wind speed with an accuracy of TBD %.	This requirement is crossed out here, since it is given a new identifier. This is due to the fact that is not a general requirement, but a requirement on the GNC system.
AWE-TEC-GEN-03	The airborne wind energy system shall estimate wind orientation with an accuracy of TBD %.	This requirement is crossed out here, since it is given a new identifier. This is due to the fact that is not a general requirement, but a requirement on the GNC system.
AWE-TEC-GEN-04	The airborne wind energy system shall determine the attitude of the airborne system with an accuracy of TBD %.	This requirement is crossed out here, since it is given a new identifier. This is due to the fact that is not a general requirement, but a requirement on the GNC system.
AWE-TEC-GEN-05	The airborne wind energy system shall provide acceleration information with an accuracy of TBD %.	This requirement is crossed out here, since it is given a new identifier. This is due to the fact that this is not a general requirement, but a requirement on the GNC system.
AWE-TEC-GEN-06	The airborne wind energy system shall not be intrusive to the internal system of the Rivian R1T.	This requirement is a stakeholder requirement.
AWE-TEC-GEN-07	All personal passenger space shall remain available.	This requirement is a stakeholder requirement.

Continued on next page

Table 2.1 – continued from previous page

Requirement ID	Requirement Description	Justification
Aerodynamics Requirements		
AWE-TEC-AIR-06	The airborne system shall be able to provide a C_L/C_D during reel-out of at least 5.	This requirement results from the desire for an equally or improved aerodynamic performance when compared to similar AWES [11, 3].
AWE-TEC-AIR-11	The airborne system shall have a stall angle larger than 16°.	This requirement ensures a valid operational range [12].
Structures & Materials Requirements		
AWE-TEC-AIR-01	The airborne system shall be softkite based.	This requirement is a stakeholder requirement.
AWE-TEC-AIR-02	The airborne system shall be able to withstand the wing loading generated during nominal operations, including a safety factor of 1.2.	This requirement needs to ensure the structural integrity of the AWES.
AWE-TEC-AIR-03	The tether shall be able to withstand at least two times the tether force experienced under nominal operations.	This requirement needs to ensure the structural integrity of the AWES.
AWE-TEC-AIR-04	The airborne system shall be able to withstand wind gusts of TBD m/s.	This requirement is difficult to verify and is therefore taken into account by including a safety factor during the airborne system analysis.
AWE-TEC-AIR-05	The tether shall be able to withstand wind gusts of TBD m/s.	This requirement is difficult to verify and is therefore taken into account by including a safety factor during the tether analysis.
AWE-TEC-AIR-07	The bridles shall be able to withstand at least two times the bridle force experienced under nominal operations.	This requirement needs to ensure the structural integrity of the AWES.
AWE-TEC-AIR-08	The tether shall have a bending fatigue safe service life SSL of at least 1848 FH.	This requirement needs to ensure the structural integrity of the AWES, and is related to requirement AWE-CON-REL-01, taking into account a margin of half a month.
AWE-TEC-AIR-09	The tether shall have a creep SSL of at least 1848 FH.	This requirement needs to ensure the structural integrity of the AWES, and is related to requirement AWE-CON-REL-01, taking into account a margin of half a month.
AWE-TEC-AIR-10	The airborne system shall be able to operate under an environmental temperature range of -15°C to 35°C.	This requirement comes from the performed environmental analysis, presented in Section 4.6.
Operational Requirements		
AWE-TEC-LL-01	The launching and landing of the airborne system shall be a task for maximally one person.	This requirement is crossed out since it has been given a new identifier to make it more logical.
AWE-TEC-OPS-01	The launching and landing of the airborne system shall be a task for maximally one person.	This requirement is a stakeholder requirement.
AWE-TEC-OPS-02	The airborne wind energy system shall be able to be operated in a reverse pumping mode to bridge wind gaps of maximum 30 minutes.	This requirement is a stakeholder requirement.
AWE-TEC-OPS-03	The AWES shall be able to operate for road angles between -2° and 2°.	The AWES will be operated on a surface as horizontal as possible, however since not all roads are flat the AWES should be able to handle a pre-defined small range of road angles.
AWE-TEC-OPS-04	The extending swivel rail shall not yield under the tether force experienced during nominal operations, including a safety factor of 1.2.	This requirement needs to ensure structural integrity of the AWES.
Power System Requirements		
AWE-TEC-PG-01	The power generation system shall have an efficiency of TBD %.	This requirement is split up in a requirement on the efficiency for the reel-in and reel-out phase.
AWE-TEC-PG-02	The electrical wires shall be able to withstand a maximum current during nominal operation, including a safety factor of 1.2.	This requirement needs to ensure the structural integrity of the AWES, and is related to risk TR-POW-11 in the risk analysis, presented in Chapter 8.
AWE-TEC-PG-03	The power generation system shall have a nominal power output of 20 kW.	This requirement is a stakeholder requirement.
AWE-TEC-PG-04	The power generation system shall be able to operate under an environmental temperature range of -15°C to 35°C.	This requirement comes from the performed environmental analysis, presented in Section 4.6.
AWE-TEC-PG-05	The wing loading produced during nominal operations shall not exceed 750 N/m ² .	This requirement is based on a discussion with an expert.
AWE-TEC-PG-06	The drum shall be able to withstand the maximum reel-in speed achieved during nominal operations, including a safety factor of 1.2.	This requirement comes from operational needs.
AWE-TEC-PG-07	The motor shall be able to support the revolutions per minute (RPM) experienced during reel-in during nominal operations, including a safety factor of 1.2.	This requirement comes from operational needs.
AWE-TEC-PG-08	The motor shall be able to support the RPM experienced during reel-out during nominal operations, including a safety factor of 1.2.	This requirement comes from operational needs.
AWE-TEC-PG-09	The power generation system shall have an efficiency of at least 50% during reel-in.	This requirement comes from the desired operational performance.

Continued on next page

Table 2.1 – continued from previous page

Requirement ID	Requirement Description	Justification
AWE-TEC-PG-10	The power generation system shall have an efficiency of at least 50% during reel-out.	This requirement comes from the desired operational performance.
AWE-TEC-PS-01	The energy storage shall provide an output power of 20 kW.	This requirement is crossed out because of the existing requirement AWE-TEC-PG-03, ambiguity in output power definition.
AWE-TEC-PS-02	The energy storage shall be able to provide the motor with the necessary power to perform the reel-in manoeuvre.	This requirement comes from the operational need that the AWES should be able to perform a reel-in manoeuvre using stored energy.
AWE-TEC-PS-03	The energy storage shall have a capacity of TBD Ah.	This requirement is crossed out because of the unknown value for the storage capacity, which depends on power cycle definition and component energy use.
AWE-TEC-PS-04	The electrical wires shall be able to withstand a maximum current during nominal operation of TBD A.	This requirement is the same as requirement AWE-TEC-PG-02.
AWE-TEC-PS-05	The energy storage shall be able to withstand cyclic loading during the specified lifetime.	This requirement is crossed since due to the modularity of the system no system lifetime has been defined, as subsystems show very different lifetimes. A more detailed discussion on this is presented in Section 6.5.
AWE-TEC-PS-06	The energy storage system shall be compatible with the national power grid standards of the operating environment.	This requirement is based on a combination of operational needs and a stakeholder requirement.
AWE-TEC-PS-07	The kite control unit (KCU) shall be continuously powered to control the kite.	This requirement comes from operational needs.
AWE-TEC-PS-08	The power management system shall be fully automated.	This requirement is based on a combination of operational needs and a stakeholder requirement.
AWE-TEC-PS-09	The energy storage system shall be able to operate under an environmental temperature range of -15°C to 35°C.	This requirement comes from the performed environmental analysis, presented in Section 4.6.
AWE-TEC-PS-10	The energy storage shall be able to provide the ground GNC system with the necessary power to continuously operate.	This requirement comes from operational needs.
AWE-TEC-PS-11	The energy storage system shall be equipped with an electrical load dump element.	This requirement is related to risk TR-POW-10 in the risk analysis, presented in Chapter 8. It is a risk mitigation to protect the electrical components of the Rivian R1T.
AWE-TEC-PS-12	The generator power voltage shall match the required voltage level of the car battery.	This requirement comes from operational needs and is necessary to ensure compatibility between the generator and the car battery.
AWE-TEC-PS-13	The voltage level of the motor shall match the voltage of the power provided by the short term power storage.	This requirement comes from operational needs and is necessary to ensure compatibility between the motor and the short term power storage.

Guidance, Navigation and Control (GNC) System Requirements

AWE-TEC-CS-01	The GNC system shall have a response time below 100 ms.	This requirement is deducted from literature [13].
AWE-TEC-CS-02	The kite shall achieve a minimum turning radius of TBD m.	This requirement is crossed out, since no specific information is available on a required minimum turn radius to ensure proper functioning of the global navigation satellite system (GNSS) sensor. Therefore, a direct requirement for the functioning of the GNSS sensor is included by requirement AWE-TEC-CS-14.
AWE-TEC-CS-03	The control unit shall have a sensitivity of TBD units.	This requirement is crossed out because it is not directly relevant for the current state of this project.
AWE-TEC-CS-04	The GNC system shall provide fully automated pumping cycles.	This requirement is a stakeholder requirement.
AWE-TEC-CS-05	The AWE system shall be able to be operated in a reverse pumping mode to bridge wind gaps of maximum 30 minutes.	This requirement is crossed out here, since it is given a new identifier. This is due to the fact that this more a requirement on the operations.
AWE-TEC-CS-06	The GNC system shall determine wind speed on the ground with an accuracy of 5%.	This requirement is deducted from literature [4].
AWE-TEC-CS-07	The GNC system shall determine the wind orientation at least once every power cycle.	This requirement is deducted from literature [4].
AWE-TEC-CS-08	The GNC system shall determine the attitude of the airborne system with an accuracy of 5°.	This requirement is deducted from literature [4].
AWE-TEC-CS-09	The control system shall provide acceleration information with an accuracy of TBD%.	This requirement is crossed out because the acceleration information is not used by the GNC system as input.

Continued on next page

Table 2.1 – continued from previous page

Requirement ID	Requirement Description	Justification
AWE-TEC-CS-10	The GNC system shall determine the tether force with an accuracy of 1%.	This requirement is deducted from literature [4].
AWE-TEC-CS-11	The airborne wind energy system shall determine the reel-out speed with an accuracy of 2%.	This requirement is deducted from literature [4].
AWE-TEC-CS-12	The KCU shall not be damaged during nominal operations.	This requirement needs to ensure the structural integrity of the KCU.
AWE-TEC-CS-13	The KCU shall not be damaged during emergency landings.	This requirement needs to ensure the structural integrity of the KCU.
AWE-TEC-CS-14	The GNSS sensor shall be able to determine the position of the kite with an absolute error of maximum 4 m.	This requirement is deducted from literature [14], and is necessary to ensure for precise control.

Table 2.2: Constraints and justification table.

Constraint ID	Constraint Description	Justification
Cost		
AWE-CON-CO-01	The total cost per airborne wind energy system shall be below 45,000- €	This constraint is a stakeholder requirement
Scheduling		
AWE-CON-SCH-01	The preliminary design of the airborne wind energy system shall be delivered within ten weeks of the start of the project.	This is a project description requirement of the DSE.
AWE-CON-SCH-02	The preliminary design of the airborne wind energy system shall be delivered by ten students.	This is a project description requirement of the DSE.
Safety		
AWE-CON-SAF-01	The pickup truck shall remain static under the specified operational loads.	This requirement comes from risk TR-GR-03 of the risk analysis, presented in Chapter 8.
AWE-CON-SAF-02	People shall not get injured during the operation of the airborne system.	This requirement comes from the sustainability analysis presented in Section 3.2
AWE-CON-SAF-03	The airborne wind energy system shall not get damaged during operations.	This requirement is crossed out because it is not defined enough.
Legislation		
AWE-CON-LEG-01	The final design shall comply with road regulations.	This comes from the legal constraints imposed by local authorities.
AWE-CON-LEG-02	The final design shall comply with country specific airspace regulations.	This comes from the legal constraints imposed by local authorities.
Sustainability		
AWE-CON-SUS-01	At least 70% of the airborne wind energy system components shall be recyclable.	This comes from the sustainability analysis presented in Section 3.2.
AWE-CON-SUS-02	The airborne wind energy system shall provide a non-helium based solution.	This is based on the combination of a stakeholder requirement and the conducted sustainability analysis presented in Section 3.2.
AWE-CON-SUS-03	The AWES operations shall stay below a noise level of 45 dB.	This comes from the sustainability analysis presented in Section 3.2.
AWE-CON-SUS-04	50 % of the components of the airborne wind energy system shall be reusable.	This requirement is crossed out since it is not verifiable. Furthermore, as discussed in Section 6.5 due to the modularity of the system no system lifetime has been defined, as subsystems show very different lifetimes. Each component will therefore be used until the end of its lifetime.
Reliability		
AWE-CON-REL-01	The airborne wind energy system shall have an operational lifetime of at least 1488 FH before heavy maintenance needs to be conducted.	This requirement comes from the system applications that are analysed during the market analysis, presented in Section 4.5.
AWE-CON-REL-02	The airborne wind energy system shall be able to withstand the environmental temperature range of -15°C to 35°C.	This requirement comes from the performed environmental analysis, presented in Section 4.6.
AWE-CON-REL-03	The airborne wind energy system shall be able to operate for TBD h before re-launch is needed.	This constraint is crossed out because of the inability to predict environmental dependencies with integrated reverse pumping cycles.
Design		
AWE-CON-DES-01	The preliminary design shall fit within the truck bed of the Rivian R1T.	This requirement is a stakeholder requirement.
AWE-CON-DES-02	The preliminary design shall not exceed 500 kg.	This requirement is a stakeholder requirement.
AWE-CON-DES-03	The preliminary design shall be compatible with the rechargeable batteries of the Rivian R1T.	This requirement is a stakeholder requirement.

Sustainable Development Strategy

The sustainability development strategy is explained in Chapter 3 in the Midterm Report [10]. A recap is presented in this chapter. This chapter aims to come up with a general strategy to enable a sustainable project development. It is important to realise that not all sustainability approaches discussed in this chapter are achievable in every aspect of a design process. For this reason, the sustainability approaches should mainly be considered as guidelines. Except for legal constraints and material choices, most of the sustainability approaches can not be considered to be hard requirements. In Section 3.1, sustainability strategies are defined and explained. This is followed by Section 3.2, which describes the effects of the sustainability approach on the requirements and concludes this chapter.

3.1. Design Oriented Sustainability

Sustainability is aimed to be achieved through the triple bottom baseline (triple P) of 'people', 'profit' and 'planet' [15]. Essentially, the business principle behind the sustainable development should not only focus on the economic aspect but needs to take multiple aspects into account to ensure a fully feasible and integrated sustainability approach.

The aim of this section is to provide general instructions to ensure sustainable development throughout a design process that takes into account the triple P approach. The three elements of the triple P approach are further discussed and elaborated on in Section 3.1.1, Section 3.1.2, and Section 3.1.3 for the people, planet and profit elements respectively.

3.1.1. People

This subsection aims at describing the sustainability goals on a social level, especially taking into account all people related to a project. It is therefore important to assess both the direct and indirect social effects that a project or process can have on any stakeholder. The list below summarises the most important topics to achieve a sustainable project on a social level:

- **Politics and Regulations:** Certain requirements can be set up by external parties, for example the government and environmental agencies. These agencies might introduce killer requirements which can have high financial consequences. For Airborne Wind Energy (AWE) systems, one should look into the required aviation specifications to publicly operate such airborne systems. Additionally, the product processing phases should be in congruence with the working forces' legislatures, both labour and safety regulations. Since these regulations were devised to ensure safety, they should be directly taken into account in the design phase.
- **Community Impact:** It is important to assess what the effects of the design will be on the environment it is operated in, for example the visual and noise impact. Therefore, one should assess the public opinion of those affected by the operation of the AWE system and make a critical analysis of how the adverse effects could be mitigated. Next to the human disturbance, the effects on the biosphere should also be evaluated to check whether animal harm is caused.
- **Materials Sourcing and Processing:** During the production phase, the people aspect also plays a vital role in the working environment. For example, the production of metal from iron ore produces a lot of heat which forms an unpleasant working environment, or manufacturing of laminates using toxic filaments, can also harm people if they do not wear the proper equipment. Therefore, it is vital to invest in the required equipment. The material choice is highly influenced by the sourcing/mining methods. The materials to be considered for the design choices should be verified to be harvested from dignified mining operations. This includes a correct workers' salary and non-harmful working environment. An example for this situation is the sourcing of toxic materials that should be performed under safe circumstances, therefore, the material choice is influenced by the means of material gathering.
- **Team Participants:** This project is aimed at providing the team participants their first experience with an integrated and multidisciplinary aerospace system design work experience. In this process, the TU Delft proves to be an important partner as this project is part of the AE3200 Design Synthesis Exercise course during the third year of the Aerospace Engineering Bachelor of Science. The successful completion of this project would mark the final stage in their Bachelor's curriculum and add significant value to their personal resumes.

- **Use of Human Resources:** Since people are complex living organisms, it is important to maintain a healthy and pleasant working environment. Therefore, design processes should be developed to optimise the utilisation of human resources while keeping a healthy working atmosphere. This can be done by taking into account people's expertise and assigning the correct people to each department. Weekly evaluations are important to improve the group dynamic. Also, the waiting time between different process phases has to be minimised to keep everyone working together.

3.1.2. Planet

To ensure a sustainable design, one should consider sustainability approaches to minimise the environmental footprint and impact on the planet of a project. Therefore, this subsection is divided into three parts: material choice considerations, lean manufacturing and end of operations.

Material Choice Considerations

Material resource sustainability refers to the long-term availability of a raw material. This availability can be split up into two groups: renewables, which are materials that Earth can replenish and non-renewables, of which the natural reserves will eventually run out.

Most of the materials that will be used in the production phase are metals, fabrics and composites, which are mainly non-renewable. Concerning the use of metals, it is important to notice the negative sustainable aspects, but also realise it can be recycled almost 100 percent into a new component. One of the concerns is soil and groundwater pollution while digging the ore. Secondly, not all materials can be mined close to the manufacturing site, leading to a deterioration of the ecological footprint of the product due to transportation. Thirdly, plenty of heat is dissipated into the air during the cycle of forming ore into a component and contributing in this way to global warming.

The use of scarce material should be limited. Since there is only a limited natural capacity for certain metals, they should only be used in extreme necessity to adhere to key requirements.

Lean Manufacturing

This project will focus on incorporating the lean manufacturing philosophy for the production and manufacturing processes [16]. As there is no set method to achieve a lean process, lean manufacturing is a way of thinking that aims at maximising value creation by eliminating several types of waste, while delivering customer oriented products. This is especially reflected in trying to minimise the environmental footprint related to the manufacturing process. The main aspects of waste reduction from the lean manufacturing philosophy are listed below.

- **Overproduction:** A process should aim at not producing more than required products or sooner than what is required by a client. In this sense, the losses by a decrease in demand are limited, and material waste is eliminated. On the other hand, the need for additional storage locations is reduced.
- **Processing Waste:** During every processing phase, all wastes should be limited. These environmental wastes range from material to energy consumption and even water usage. One should try to optimise production and development processes by analysing the wastes and optimising the design phases.
- **Transportation:** Transportation of products and general resources should be limited as much as possible in a manufacturing process. It does not only cause increased emissions and energy losses, but also introduces operational challenges with respect to planning and logistics.
- **Rework:** Rework is caused by re-processing a defective product [17]. As there is only a small room for error in the aerospace industry, any production process should be well planned, verified and validated before entering operation. By limiting defective products and hence waste creation with rework as a consequence, the environmental impact can be reduced. This is a direct result from the fact that material and invested resources that were invested in the defective product have to be discarded. Rework can thus be avoided by frequent monitoring and quality control of a process and by appropriate crew training.

End of Operations

During the lifetime of the product, it is beneficial to have as many components as possible that can last for the entire product lifetime. In this way, the need for replacement and hence discarding degraded components is minimal. However, this is a very idealised and non-realistic solution. Apart from this long lifetime, one should also allow for maintainability to increase components' lifetimes. This greatly reduces the inefficient use of dedicated components and hence decrease environmental impact by eliminating direct component wastes.

Next to the reusability assessment made in the material choice discussion, one should also consider the recyclability and reusability of entire (sub)systems. Depending on the wear of individual components, e.g. the power generation systems and the control unit could be reused in other AWE or power generating operations.

Next to reuse, the final end-of-life option is to disassemble systems and recycle components that allow for that operation. In this way, scarce materials could be re-captured from electrical components and processed for use in new products. Similarly, the kite canopy and snapped tether lines could be re-purposed for other operations.

3.1.3. Profit

The profit aspect is highly related to the presence of market competitors and market advantages. Therefore, this aspect is not discussed within the sustainability development, but is further elaborated on in the market analysis in Chapter 4. It is important to keep track of technological development to continuously fill existing market gap and contain a competitive edge.

One important aspect related to the profitability of a project is its ability to obtain possible subsidies. With the current interests and goals in terms of sustainability, it is beneficial to have a clear sustainability strategy in order to obtain subsidies as financial benefits to fulfil the project.

3.2. Requirement Influence

In this section, the sustainability requirements are specified. Which are formed from the sustainability analysis performed above. In the analysis, the triple P concept was used to make sure each area where sustainability plays a role is covered. Requirements are set to make sure all sustainable criteria are covered and to maximise the sustainability of the system.

The first four requirements are determined to take into account the sustainability impact on the planet. The last requirement is determined to ensure safety on a people's aspect. The sustainability related requirements are:

- **AWE-CON-SUS-01:** 70% of the components of the airborne wind energy system shall be recyclable
- **AWE-CON-SUS-02:** The airborne wind energy system shall provide a non-helium based solution.
- **AWE-CON-SUS-03:** The airborne wind energy system shall stay below a noise level of 45 dB.
- **AWE-CON-SAF-02:** People shall not get injured during operation of the airborne system.

These can be achieved through material choice and lean manufacturing to reach these percentages. Helium can simply not be used because it is scarce and therefore not sustainable. The percentages for reusability and recyclability were determined by the group and seemed both reasonable and achievable for this project's application.

Secondly, to improve the sustainability concerning the people's aspect, the maximum noise level was set to 45 dB. In this way, the social life of people and animals is not harmed. This is further explained in the regulations discussion in Section 4.6.2.

Finally, no people should get injured during operation. This requirement relates to the system operator, as well as the surrounding people. Since the system will be operated mostly in remote areas, the latter will most likely not cause significant issues. Nonetheless, the system should be designed for safety and should include additional safety aspects.

Market Analysis

In this chapter, the market analysis is performed. In Section 4.1 the most important stakeholders are listed. Secondly, the market is explored in Section 4.2. This will be done with the use of a SWOT analysis in Section 4.3 and an exploration of Porter's Five Forces in Section 4.4. Using these findings, in Section 4.5 the applications of the system are defined. Furthermore, an environmental analysis is performed to determine the possible operation locations in Section 4.6. With the characteristics of the market and environment defined, the size of the market is explored in Section 4.7. Then, for the operational locations, the social acceptance of the system is explained in Section 4.8. Finally, the conclusions of this chapter are summarized in Section 4.9. Note that Section 4.6 is adapted from Sections 4.2-4.4 in the Midterm Report [10] and that in general, this chapter is adapted from Chapter 3 in the Baseline Report [18].

4.1. Key Stakeholders

It is vital for any project to determine the key stakeholders. These are the parties most strongly involved with or influenced by the system. In the case of this MAWES, the key stakeholders are:

1. Kitepower, a company that builds AWE systems using leading edge inflatable (LEI) kites. Kitepower can be defined as a key stakeholder, as the idea of integrating an AWES in an electric pickup comes from them. Furthermore, they might want to use the MAWES for illustration purposes in the future.
2. Rivian, a company that builds electric pickup trucks. Rivian can be considered a key stakeholder, as the MAWES shall be designed to be integrated into the Rivian R1T.
3. TU Delft, for the reason that the MAWES should be designed as an exercise for the final bachelor project of Aerospace Engineering.
4. Authorities of the countries where the system will operate, as they will set and enforce regulations for the MAWES.
5. The customer, as they will be using the MAWES, and the functionality and usability of the system is directly influenced by their needs.

4.2. Market Exploration

The system will operate in two different markets: the electric pickup truck market and the mobile energy generator market. Both markets will have their own influence on the system.

In the electric pickup truck market, over one and a half million orders have been placed for the five most popular electric pickup trucks, as can be seen in Table 4.1. However, as the pickup truck is often more of a status symbol than a utility vehicle, this should be accounted for in the analysis. Furthermore, the production of electric pickup trucks is starting to ramp up now, but it will take some time for the production to meet the demand. Seen the growth in market share of electric vehicles [20], it can be assumed that the same trend will set through for pickup trucks and orders will keep rising.

The second market is the mobile airborne wind energy market. The Mobile Airborne Wind Energy (MAWE) market has a high threat of substitutes, which is important to take into account when performing a market size analysis. To compare a MAWES with substitutes, one can first look at the costs of the electricity generated. The different technologies can be compared in terms of cost by expressing the cost in the form of the Levelised Cost Of Electricity (LCOE). The LCOE is a measure of the average net present cost of generation of electricity for a generating plant over its lifetime [23]. The LCOE for different energy sources is given in Table 4.2.

Table 4.1: Current orders for the five most popular electric pickup truck [19].

Model	Orders
Tesla Cybertruck	1225 k
Ford F-150 Lightning	160 k
Chevrolet Silverado	110 k
Rivian R1T	71 k
GMC Hummer EV	59 k
Total	1.625 M

Table 4.2: Levelised cost of energy (LCOE) for different energy sources [21, 22].

Energy Source	LCOE (\$/MWh)
AWE	126
Wind Turbines	64
Solar	48
Portable Generator	132

For mobile energy supply, portable generators and solar power could be good substitutes for AWE. Portable generators are more expensive than AWE, and do not provide an energy-autarkic solution. This strengthens the position of MAWES in its target market. However, portable generators also have a higher reliability than solar and wind power, because they are not dependent on natural resources, but only on the available fuel. As portable generators are strong competitors, a look into their market size might provide valuable insights. The portable generator market is currently about 2 Billion USD[24], and is estimated to grow to 2.5 Billion USD by 2026. The main use of portable generators is in emergency situations.

The second competitor is solar power. It is cheaper compared to the AWES, but it does not provide a high and continuous power supply [25]. The amount of solar irradiation in the operational environment will heavily influence the competition with the MAWES. In regions with plenty of solar energy, foldable solar panels can provide a mobile energy-autarkic solution. For example, the continents of Africa and Australia have the highest overall solar irradiance, which is defined as the daily number of peak sunshine hours on a horizontal surface at an intensity of 1 kW/m² [26]. The middle and southern regions of the Americas and the middle and southern regions of Asia follow, and the more northern regions of the Americas, Asia, and Europe have the lowest solar irradiation per day.

4.3. Strengths, Weaknesses, Oppurtunities, & Threats Analysis

In this section, a SWOT analysis is performed for the AWES. This analysis aims to identify the strengths, weaknesses, opportunities, and threats of any system or organisation. This SWOT analysis focuses on KITE-E's market position. The four aspects of this analysis are summarised in Figure 4.1 below and elaborated on in the following subsections. This section is adapted from Section 3.5 from the Baseline Report [18].

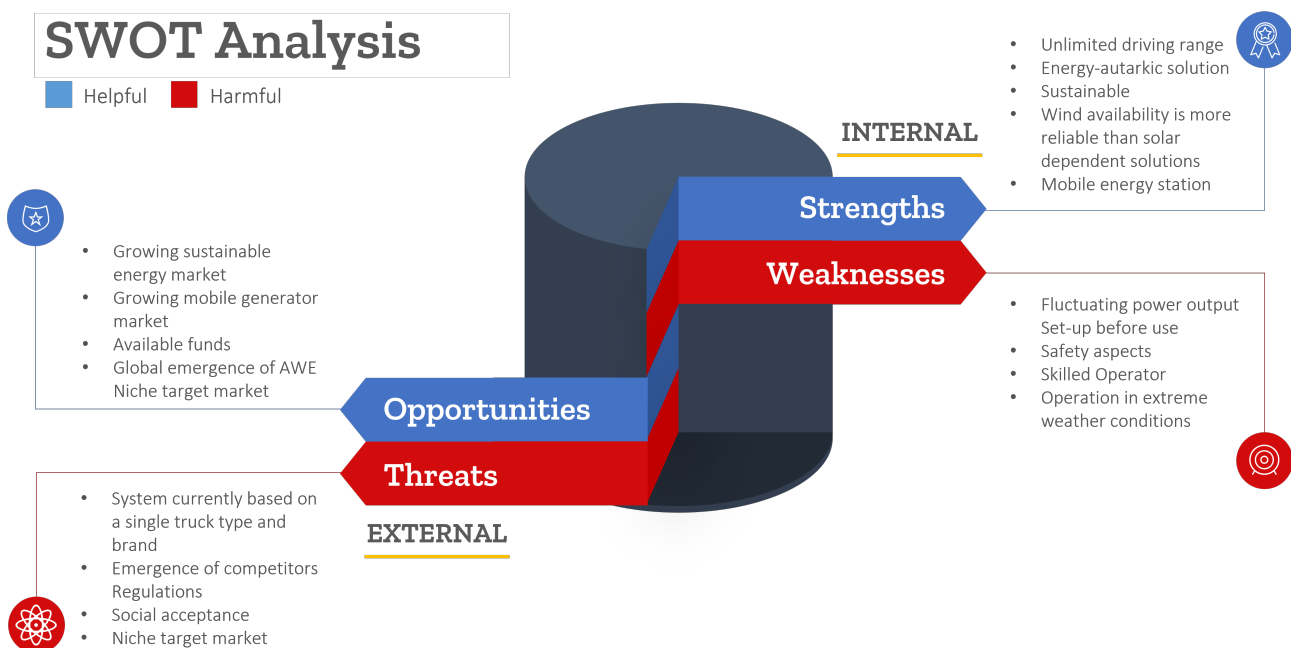


Figure 4.1: SWOT analysis for the market position of a kite power integrated in an electric truck.

Strengths

The main strengths of the AWES that defend its market position are the unlimited driving range it provides with the energy-autarkic solution, the sustainability, the high availability of wind and that it can be used as a mobile energy station.

The main issue with electric vehicles right now is their range, and the time it takes to replenish that range, especially compared to fossil fuel. This design would theoretically unlock unlimited range for the truck, without the need of any extra fuel or supplies, thus providing an energy-autarkic solution. With an eye on the urge to lower humanity's footprint and globally achieve carbon neutrality, the sustainability of the system is an important strength over other energy generation systems. Furthermore, compared to other sustainable energy sources, wind energy has a higher reliability. Solar energy, for example, is not available during the night, while wind energy still is. This is especially interesting for charging the truck, since this is done at random times or during the night. Lastly, this system can also be used as a mobile energy station for external systems, which extends the market even further.

Weaknesses

The main weaknesses of KITE-E that compromises its market position are the facts that it has fluctuating power output, needs to be set-up before use, has several safety considerations, the operator needs to be skilled and operation in extreme weather conditions is restricted.

First, even though wind energy is more reliable than, for instance, solar energy, it is still prone to fluctuations, and it is impossible to guarantee a full power output at all times. Next, the kite power system requires constant automated control and should be deployed, launched, and stored by the user. This requires training and licensing, as explained in Section 4.6.2. Operating the system is thus more demanding than possible substitutes. Furthermore, some safety aspects imposed by the system may also result in a large spatial footprint, due to which it could only be operated in remote areas. In case of a catastrophic failure of the system, all people in the operating radius of the kite could get in a life-threatening situation if no precautions are taken. Lastly, the use of the system is limited by weather conditions, it will have an operating window with a minimal and maximal wind strength, imposed by the defined limit loads, and a minimal and maximal temperature for nominal performance of all electrical components.

Opportunities

The team sees big opportunities for the system in the growing sustainable energy market, the available funds for sustainable development, the global emergence of AWE, and the niche target market.

Humanity is facing huge challenges in limiting climate change [27]. Switching to renewable energy sources is one of the important solutions to tackle this problem. This leads to an opportunity for airborne wind energy being widely implemented. Big funds are made available for exploration of the topic. Next, also the mobile generator market is expected to grow in the coming years [24]. The main application for this market is emergency power during power outages. North America is expected to account for the largest market share due to the rising number of power outages, whereas airborne wind energy companies and research institutes are mainly European based. AWE is getting global recognition as an interesting wind energy source, which provides the opportunity to jump on the bandwagon. Lastly, providing a MAWES that is to be fitted in a pickup truck bed aims to a niche target market. As this is a unique solution for specific regions, the system could dominate this niche market.

Threats

Next to the opportunities of this system, the threats should also be taken into account. The following threats are identified: the dependency on a specific pickup truck type, the emergence of competitors, regulations, the social acceptance, and the niche target market.

This project is based on a specific truck type and brand, and thus relies on a single manufacturer. When this manufacturer stops the production of this type, also the designed MAWES loses its relevance. However, slight modifications can make the system more universal. Another threat is the fact that competitors can come up with similar, potential substitutes for the system. This goes together with the niche market, which is an extra threat, as a system that outperforms the team's design, would cause the sales to go down significantly. Furthermore, the regulations could also pose problems. Most countries have strict regulations on their airspace. Therefore, permits possibly will be needed to operate the system. Finally, the social acceptance also plays an important role in making the system succeed in its target market. The AWE is a very new idea and yet unknown to the broad public. Target costumers could be sceptical about this concept as it has never proven its abilities, as for example photovoltaics, a possible substitute, has already done.

4.4. Porter's Five Forces

To investigate the profitability and viability of the MAWES within the electric pickup truck market and the MAWES market, a Porter's Five Forces analysis is performed. The Porter's Five Forces is a model used in market analysis to identify five competitive forces related to a target market. It consists of existing rivalry, the threat of new entrants, the threat of substitutes, supplier power, and buyer power [28]. These forces are explained below and are explored for the MAWES in Table 4.3.

Existing Rivalry

The intensity of competition plays a significant role in the attractiveness of an industry. Many competitors lead to a rather challenging environment, diminishing the individual power of a company. As an example, price wars might severely undermine the profitability of a company. Conversely, when rivalry is low, a company potentially has more room to increase prices and thus increase profitability, without the risk that customers will immediately go to a rival.

Threat of New Entrants

New entrants result in an increase in competition, which reduces profitability. If the entrance barriers are high, for example in the case of patent intensive industries or economies of scale, new entrants only have a low chance of entering the market.

Threat of Substitutes

Substitutes can replace the product or service being offered. Having a low threat of substitution means companies can set higher prices, without the risk of customers opting for a substitute.

Supplier Power

When suppliers have a large amount of power, they can easily raise prices, resulting in an increase in input costs, and decreasing profitability of a company. When there are few suppliers or if they offer unique solutions, they are arguably more powerful.

Customer Power

The power of customers lies in their ability to influence prices and negotiate terms. A few larger customers and many sellers, means the significance of one customer is quite high. This is favourable for their negotiation position. However, with many small customers, a company has a higher ability to dictate deals and set prices, increasing profitability.

Table 4.3: Analysis of Porter's Five Forces in the electric pickup market and the mobile airborne wind energy market.

Porter's Five Forces	Electric Pickup Truck Market	Mobile Airborne Wind Energy Market
Current Rivalry	The rivalry is quite high, as there are many companies starting with the production of Electric Pickup Trucks, such as Ford, Hummer, and Tesla.	Rivalry can be described as moderate, due to the fact that the market is still developing and growing. As the technology is still new, the main objective of most companies is to get a working product, and competition is not yet the main focus.
Threat of New Entrants	There is moderate threat of new entrants, as the electric car industry is growing heavily, but still a large initial investment is needed to start the production of electrical vehicles, which is to be expected from the main pick-up truck producers.	The threat of new entrants in this market is moderate, as technologies are patent protected.
Power of Suppliers	Suppliers have a large amount of power since demand for electric pickup trucks is higher than the supply, which naturally gives more power to the supplier. Furthermore, most of these suppliers are already well established car manufactures.	Suppliers for the time being have moderate power. This is due to the relatively unestablished market in the mobile airborne wind energy. This power is most likely going to increase when this technology advances, as parts are often custom made, or very specific.
Power of Customers	Individual customers have low buying power as the demand is higher than the supply. Some large customers who buy in bulk have larger bargaining power.	Customers have relatively high power, since the commercialisation of these systems is highly dependent on the specific customer needs. Together with the small demand for the time being, this leads to quite a large influence customers can still have, especially if these are bigger organisations that want to buy in bulk.
Threat of Substitutes	There is a high threat of substitutes. Substitutes are petrol, diesel or hydrogen fueled pickup trucks. When the sustainability of the truck is more important to a customer, this threat does however decrease.	There is a high threat of substitutes. Sustainable alternatives can be autarkic or not. Autarkic substitutes can use wind or solar energy. For example, the Lightyear cars [29] and the EF1-T pickup truck of Edisonfuture [30] use solar panels. Non-autarkic but still possibly sustainable substitutes are a portable hydrogen fuel cell station, or a battery station. Lastly, also non-sustainable portable petrol generators can be a substitute.

4.5. System Applications

The first application for the AWES on an electric pickup truck could be for well-off adventurers. The system would provide them with unlimited freedom as they can drive their pickup truck to wherever they want without depending on external power sources to recharge their truck. The demand for adventures vehicles is also quickly rising, people tend to escape to remote places for holidays but still want some luxury. This is the ideal target customer for this application. For this operation, the AWES would only be used to recharge the pickup truck. It was found earlier that with a nominal output power of 20 kW, the system should be operated for 6.75 hours. In case the user would go on a three-month mission and charge the battery completely every day, that would lead to 621 required FH over his mission. Ideally, the system should be able to reach this amount of FH, without requiring any heavy maintenance. The maintenance schedule is explained in Section 6.4.3.

Secondly, the system could also be used for emergency relief missions. In the 21st century, already more than 4 billion people have been affected by natural disasters [31]. Regions that are affected by natural disasters

often also face loss of power resources. Here the MAWES can be a great solution and can even become an essential addition to the tools of an emergency relief team. One single system is able to provide enough power to provide 40 households. Thanks to its off-road capabilities, it can also easily reach those locations affected by natural disasters. For this application, the system should be able to provide continuous power until the conventional power supplies are restored. In an extreme case, the system should ideally be able to provide quasi continuous power for two months. This would require the system to perform 1488 FH, without needing any heavy maintenance.

Lastly, it could also be of great use for humanitarian peace missions. The MAWES could recharge mission vehicles in between operations, when there is no other power source available, or could power remote field hospitals. An energy-autarkic solution would thus be very interesting during humanitarian crises, as the grid power could be cut-off due to intentional destruction by hostile groups. The president of General Motors Defence said in an interview with the CNBC that the Hummer EV, which is an electrical pickup truck, will also be transformed into a utility vehicle, apart from the civilian models [32]. These electric vehicles aim to partly replace the 'High Mobility Multi-purpose Wheeled Vehicles', also known as the Humvees. The MAWES on this pickup truck is, however, not intended to serve or ease any hostile purposes, but shall solely be used for humanitarian and peaceful intentions. The continuous FH required for this application depends on how the truck shall be used for these missions. It seems unlikely that they would use one of these trucks to permanently power a big base field hospital, as it would be more convenient and efficient to use a fixed MAWES. The trucks could be used for medical evacuation missions, as its off-road capabilities, enable to go to remote or rough surfaced places. In this case, the truck shall be recharged, when not in use. Assuming a full recharge every day, 210 FH per month are required. Another application in these kinds of missions would be to power a small temporary field hospital in difficult to reach places. In this case, continuous operation is required. As for emergency relief, for continuous operation for two months, 1488 FH are required.

4.6. Environmental Analysis

In this section, an analysis of the operating environment is presented. A choice is made on the locations where the kite-powered Rivian R1T will operate, in order to determine the boundaries of the market size analysis. Therefore, research is done on the suitability of different environments, which is presented in Section 4.6.1. Furthermore, the regulations on AWE systems are an important factor, discussed in Section 4.6.2. Lastly, the chapter concludes with an environmental analysis and a trade-off table of the region selection in Section 4.6.3.

4.6.1. Applications Environment Analysis

As identified in Section 4.5, the applications of the MAWES fitted on the Rivian R1T are adventuring, disaster relief and humanitarian peace missions. The environment for adventuring consists mostly of unpopulated areas with a lot of nature. With regard to disaster relief, an overview of regions often struck by disasters is given. For humanitarian peace missions, regions of conflict are investigated.

Scarcely populated nature

For adventuring, areas with a lot of untouched nature, consequently often scarcely populated, are desirable. As can be seen in Figure 1 in [33], the most scarcely populated areas are found in the northern part of the Americas, southern parts of Africa, Australia, the rain forests in South-America, the eastern part of China, and north-east parts of Russia. A large part of these regions are arid, extremely arid or semi-arid regions [34]. These are thus suitable areas to travel large distances energy autarkically. Another customer could be people who live off-grid at these locations and want to combine a renewable energy source with their car.

Disasters

Regions that are prone to disasters or emergencies are identified for the application of disaster relief. A map with different types of natural disasters over the world can be seen in the Figure in [35]. Almost all coastal regions in Asia and the east and west coast of middle America can be subject to disasters caused by floods or tsunamis. Attention also has to be paid to possible storms, as the system can be implemented in areas where a storm destructed the local power supply. Furthermore, earthquakes occur in Central America, large parts of eastern and middle Asia, the south-east of Europe, and the Middle East. Lastly, droughts are included in the map, but these are less relevant for the application of the MAWES. This is the case because, unlike the previously mentioned natural disasters, droughts do not destroy infrastructure, and thus access to electricity. One exception for droughts is that they might lead to people displacements, thus resulting in a need for mobile electricity. The regions in which droughts occur are the arid regions [34].

Regions of Conflict

For an analysis of regions for the humanitarian applications of the MAWES system, the regions are investigated with the help of a conflict zone map, as can be seen in the Figure in [36]. In this map it can be seen that less

peaceful zones can be found in the Middle East, and in Central Africa. Peaceful zones are in Central America, Russia, and the Baltic region. More peaceful zones can be found in North America and Europe.

4.6.2. AWE Regulations

Airborne wind energy systems (AWES) operate in large spatial envelopes at elevated altitude. When compared to classical wind turbines, the increased altitude and dynamic activity lead to the driving regulatory challenges, as they lead to the potential interaction with both air and ground based objects. Additionally, these airborne systems can not simply be stopped mid-air, leading to an increased interest for specific regulations. This section will therefore look into the regulations related to the flight operations and the acoustic aspects of AWE systems.

Flight Operational Regulations

There are currently no effective regulations specifically concerning AWES [37]. This is attributed to the fast emergence of these new airborne systems, for which no continuous long-term operations have been performed yet. The need for proving reliable operation includes establishing safety regulations, and is therefore a vital aspect to be considered and estimated for future development in the AWE field.

American AWES regulations prove to be fairly lenient and do not require specific certificates for operational use [38]. The Federal Aviation Administration (FAA) excludes tethered aircraft from general aviation regulations. This includes that AWES are purely considered to be obstacles and should therefore be considered on a case-by-case basis with respect to the surrounding aviation environment to ensure safety. As defined in Federal Regulation 14 CFR Part 157, every operation should submit a requiring notice for operational approval.

Within EU aviation regulations, tethered AWES are categorised among unmanned airborne systems (UAS). This type of aircraft is separated into three categories: open category, specific category and certified category. The open category comprises low risk, low weight UAS. For these aerial vehicles, the altitude limit is set to 120 m (400 ft) and must cohere to the general aviation's regulation to not fly over restricted airspaces. Detailed specifications for the open category are found in UAS.OPEN.010 of the appendix to EU regulation 2019/947 [39].

As the AWES is expected to both fly higher and weight heavier than what is specified in the open category, the current regulations for the specific category need to be adhered to [40]. Furthermore, since the AWES operations do not occur in rural areas, do not fly over crowds and do not transport people in operation, it does not fall under the certified category. In general, the certified category licensing category would be comparable to that of manned aircraft.

Licensing of specific UAS can be done by providing coverage in one of these two manners: standard scenario (STS) or risk assessment [41]. The two standard scenarios (STS1 and STS2) are covered by the appendix to EU regulation 2019/947. The AWES to be designed does not fall into these categories, as its operation is foreseen to be at higher altitudes. Therefore, the AWES should be covered by either a SORA or a predefined risk assessment (PDRA) as an acceptable means of compliance (AMC). The SORA should be carried out according to AMC1 in Article 11 as specified in EU regulation 2019/947. This SORA includes risk assessment, mitigation and must show compliance with the national aviation authority's (NAA) safety objectives. The results of this SORA must be submitted to the NAA for operational approval.

Next to the SORA, an operation might also be covered by a PDRA [41]. This was created as a form of regulation simplification for UAS operators. These PDRA's can be used as an AMC to the UAS regulations. Currently, existing PDRA's are listed in GM1 in Article 11 as specified in EU regulation 2019/947. These PDRA's can omit the need for a full SORA conduction if the intended system operation is already covered. The European Aviation Safety Agency (EASA) is currently intending to publish the most common operations in Europe over the coming years. In order to obtain the required licence, documentation in support of the application must be submitted to the NAA.

Considering the current state of the PDRA list, none of these operations cohere to the intended use of the to be designed AWES [41]. Therefore, a full SORA should be performed in order to operate the AWES. However, with rising interest in airborne wind energy, there is a chance that the AWES operations could be implemented in the PDRA list. Depending on the outcome of the risk assessment, the competent authority might require a design verification through a verification report. When operating in a controlled airspace, the respective air traffic control should be notified in order to issue a NOTAM (NOTice To Air Missions) about the scheduled flight operations.

Lastly, the AWES needs to be operated by a A1/A3 and A2 licensed pilot in remote control as specified by EU regulation 2019/945-947 [41]. This does not mean that the AWES can not operate fully automatic. Rather, the pilot should be a visual observer on site, in potential remote control. Only under these specified conditions, the AWES can be operated in visual line of sight, either at day or at night (when sufficient lighting is provided).

Acoustic Aspects

It is generally accepted that AWES produce less sound emissions than conventional wind energy technologies [37]. Because of the higher operational environment, sound propagation is highly dissipated once it reaches the ground. The issue with acoustic regulations is that they differ per country, therefore, a general approach/recommendation should be obtained.

In order to quantify the maximum acceptable acoustic levels, the same noise recommendations for wind turbines are considered as recommended by the World Health Organization (WHO) [42]. This choice is made based on the similarity in operational application and to allow for equal comparability. An outdoors limit of 45 dB, to be measured at any on-ground location, is specified to be the highest allowable noise level for wind turbines.

4.6.3. Region Selection

In this subsection, a trade-off on the location selection is made. The result of this trade-off is displayed in Table 4.4. In this table, regulations are not included since they are not limiting the operational procedures, as can be read in Section 4.6.2. Moreover, the soil conditions vary to a high extent within climates. This means that for the anchoring system design, all soil conditions are taken into account. For East Asia (India), the mountains around the Himalayas are excluded in the trade-off, since this area is very difficult to reach.

The trade-off is performed per region (1st column). The 2nd until the 4th column display the different use cases of the system, and the last 6 columns give the parameters of every region. The regions are judged on a scale of 0 to 5, from worst to best. The cells are also coloured based on this scale, from *red* (0), *orange* (2), *yellow* (4), and *green* (5). *Red* means that the mobile AWES is not suitable for an application or that the environment is not suitable for the design. Cells are *orange* if the system can work at the desired location, but needs a lot of adjustments. *Yellow* is used for satisfactory locations, where conditions are sometimes marginally outside the boundaries. Lastly, *green* shows a perfect location with outstanding environmental conditions.

Table 4.4: The trade-off table for the different regions of the world. For East Asia (India), the mountains around the Himalayas are excluded in the trade-off.

Region	Use case: Exploration [33]	Use case: Disaster relief [35]	Use case: Humanitarian Peace Missions [36]	Wind speed m/s @10,100,200m height [43]	Air temperature °C [44]	UV Index [45]	Vegetation and terrain[46]
Canada	Suitable <small>Green</small>	None <small>Red</small>	Potentially suitable <small>Orange</small>	5.87, 8.72, 10.52 <small>Green</small>	neg 7.3 - 9.0 <small>Orange</small>	0.5 - 2.5 <small>Green</small>	Treeless tundra <small>Green</small>
USA	Medium suitable <small>Yellow</small>	Drought, flood <small>Green</small>	Potentially suitable <small>Orange</small>	5.98, 8.97, 10.78 <small>Green</small>	neg 1.8 - 24.3 <small>Yellow</small>	2.5 - 8.5 <small>Yellow</small>	Grassland and forest <small>Orange</small>
Caribbean (Cuba)	Not suitable <small>Red</small>	Drought, flood, earthquake <small>Green</small>	Suitable <small>Green</small>	4.79, 7.12, 8.57 <small>Yellow</small>	19.9 - 27.2 <small>Green</small>	8.5 - 14.5 <small>Orange</small>	Savanna and rainforest <small>Orange</small>
Amazon (Brazil)	Suitable <small>Green</small>	Drought <small>Yellow</small>	Medium suitable <small>Yellow</small>	4.04, 7.02, 8.83 <small>Yellow</small>	16.5 - 28.7 <small>Green</small>	12.5 -> <small>Orange</small>	Rainforest <small>Red</small>
Patagonia (Argentina)	Suitable <small>Green</small>	None <small>Red</small>	Not suitable <small>Red</small>	7.89, 11.36, 13.12 <small>Green</small>	neg 7 - 24.2 <small>Orange</small>	4.5 - 10.5 <small>Yellow</small>	Treeless tundra <small>Green</small>
Europe (Germany)	Not suitable <small>Red</small>	Drought, floods <small>Green</small>	Potentially suitable <small>Orange</small>	5.09, 8.45, 10.38 <small>Green</small>	5.8 - 11.4 <small>Yellow</small>	0.5 - 4.5 <small>Green</small>	Grassland and forest <small>Orange</small>
Russia	Suitable <small>Green</small>	None <small>Red</small>	Medium suitable <small>Yellow</small>	5.54, 8.48, 10.42 <small>Green</small>	neg 9.9 - 12.5 <small>Orange</small>	0.5 - 4.5 <small>Green</small>	Treeless tundra <small>Green</small>
North Africa (Libya)	Suitable <small>Green</small>	None <small>Red</small>	Suitable <small>Green</small>	5.28, 8.51, 10.26 <small>Green</small>	18.2 - 24.9 <small>Green</small>	4.5-12.5 <small>Orange</small>	Desert <small>Green</small>
Central Africa (Congo)	Not suitable <small>Red</small>	Drought <small>Yellow</small>	Suitable <small>Green</small>	2.56, 4.77, 5.99 <small>Red</small>	16.0 - 26.4 <small>Green</small>	12.5 -> <small>Orange</small>	Rainforest <small>Red</small>
South Africa	Medium suitable <small>Yellow</small>	Drought, flood <small>Green</small>	Not suitable <small>Red</small>	4.86, 7.33, 9,23 <small>Yellow</small>	11.5 - 23.2 <small>Yellow</small>	10.5 -> <small>Orange</small>	Savanna <small>Green</small>
Middle East (Saudi Arabia)	Medium suitable <small>Yellow</small>	Drought, flood, earthquake <small>Green</small>	Suitable <small>Green</small>	4.92, 7.91, 9.71 <small>Yellow</small>	19.0 - 30.9 <small>Green</small>	4.5 - 12.5 <small>Yellow</small>	Desert <small>Green</small>
East Asia (India)	Not suitable <small>Red</small>	Drought, flood, earthquake <small>Green</small>	Medium suitable <small>Yellow</small>	4.1, 6.58, 8.02 <small>Yellow</small>	18.0 - 29.1 <small>Green</small>	6.5 - 12.5 <small>Yellow</small>	Savanna and rainforest <small>Orange</small>
Indonesia	Not suitable <small>Red</small>	Flood, earthquakes <small>Green</small>	Medium suitable <small>Yellow</small>	2.8, 4.89, 5.92 <small>Red</small>	11.3 - 27.8 <small>Yellow</small>	10.5 -> <small>Orange</small>	Rainforest <small>Red</small>
Australia	Suitable <small>Green</small>	Drought <small>Yellow</small>	Not suitable <small>Red</small>	4.81, 8.01, 10.02 <small>Green</small>	9.9 - 28.2 <small>Green</small>	12.5 -> <small>Orange</small>	Desert <small>Green</small>

Trade-off Reasoning for Table 4.4:

- **Exploration:** Scarcely populated areas with uncharted nature are desirable for remote exploration and will get a higher value based on [33].
- **Disaster relief:** Of the three main types of disasters, floods, earthquakes, and droughts, only the first two will lead to the destruction of infrastructure. Therefore, only for those disasters, a mobile AWES is needed. If those disasters appear in a certain region, the system will be applicable and gets the highest value based on [35].
- **Humanitarian peace mission:** The third use case is for humanitarian peace missions, as can be read in Section 4.6.1. Less peaceful regions therefore have a high value (green). More peaceful zones will have a

low value (red), except for Canada, the USA, and Europe, which have active armies and potentially will use the system in their own country for training, besides use in conflict regions.

- **Wind speed:** Wind speed is the main parameter for the system. With the Global Wind Atlas, annual wind speed values at 10, 100, 200 m can be obtained, which are globally 8.14, 10.61, 11.88 m/s [43]. The higher the values, the more energy can be produced with the kite. Low values are labelled unsuitable, as a power kite needs a minimum wind speed to operate [47]. For the detailed design, the wind speed variations at the chosen locations are taken into account.
- **Air temperature:** The temperature is limiting for the battery performance. An ideal temperature is between 15 and 35 °C [48, 49]. In general, the average annual temperature on a location stays below 35 °C, and will get a high rating (green) based on the Global Solar Atlas [44]. The regions with extreme negative temperatures will get orange rating. The cold temperatures can be overcome with a heating system for the battery. For the detailed design, the temperature variations at the chosen locations are taken into account.
- **UV index:** The UV index will range from 0 to 15 on charts, but can be as high as 40 [45]. All high values are damaging to the kite and the other parts of the system. Materials can be made UV resistant and therefore the system can operate all over the world. For this reason, no UV index will result in an unfeasible design (red).
- **Vegetation and terrain:** The last parameter of influence is the local vegetation and terrain. Which can be a hindrance to the operations of the system. Open areas (deserts, tundras, savanna) will get the highest value (green) [46].

With the whole trade-off in Table 4.4 taken into account, 4 locations are chosen: North-America (Canada + USA) (high market demand for exploring), Patagonia (high wind region), Caribbean (disaster prone region) and the Middle East (less peaceful region). For these four locations, a more in-depth research on the parameters presented in the trade-off table is performed.

4.7. Market Size Estimation

Looking at the possible applications for the system in Section 4.5, Section 4.6.1, and the electric pickup truck market in Section 4.2, it is clear the system targets a small niche market. For a niche market, a trustworthy estimation of the market size is difficult. However, it is clear that the electric pickup truck market is quickly growing and that the competitive position of AWE compared to possible substitutes is in certain regions very strong. The market size is important for the product series, which has a very big impact on the cost of development. Therefore, during the analysis, conservative numbers are used, in order to remain on the safe side, and not overestimate the demand.

In order to estimate the demand for the first application, the adventurers, the team decided to assume that about 10 percent of the people that order an electric pickup truck, will actually use their pickup for this purpose. This leaves 162 500 potential customers. However, the MAWES is for a very specific use case, and will thus not be for every adventurer. Therefore, a conservative estimation is made that only 0.5 percent of those adventurers will buy this solution. This leads to a demand of 810 units for this purpose.

For emergencies or disaster relief, the market size of the portable generators can be used. This market size is estimated to be around 2.5 Billion USD in 2026 [24]. With a market penetration of 1%, and a MAWES cost of 50k USD, about 500 unit sales of the MAWE system are expected. In addition, one can look at the Non-Governmental Organisations (NGO's) which often provide disaster relief. An indicative number of pickup trucks used by NGO's is the number of trucks used by the United Nations (UN) World Food Programme. The UN World Food Programme uses (among other transportation methods) 5600 trucks, which are larger than pickup trucks, to deliver food to about 115.5 million people in 2020 [50]. If the fleet is extended by 0.5% with MAWES equipped pickups to provide emergency electricity, about 28 pickup trucks will be sold. It should be noted that the UN World Food Programme is only one among many NGOs that provide aid in disaster relief, meaning the total demand of NGO's can be about 25 times larger, resulting in a demand of 700 MAWES equipped pickup trucks [51].

Finally, for the humanitarian peace missions, electric pickup trucks are destined to partly replace the US Army's Humvees. Since 1983, 281 thousand Humvees have been built [52]. Assuming that about 30 percent of this production would be replaced by the production of electric pickup trucks and that 5 percent of those pickup trucks would be equipped with an MAWES, the military demand for the system would be 540 units per five years.

The total estimation of demand is achieved by adding up the demand for the different applications, resulting in a demand of 2550 units for the coming five years. The added recurring demand is depended on the lifetime of the system. It should be noted that this is a conservative estimation for the team to base itself on. As the market and demand are unpredictable, the team could investigate after the initial launch if an expansion of production is saleable.

4.8. Social Acceptance

Literature research has been done into the social acceptance of AWES [37]. Since this is based on existing literature, almost all the research is about stationary AWE systems, and not mobile ones like the one discussed in this report. Nevertheless, it is important to look into what could be interesting for this market analysis, and how these factors can impact the reputation of this technology. The sitting of the stationary system is one of the main aspects discussed in the report, but this will not be separately discussed, since this is intertwined with most of the other aspects already.

A large part of social acceptance is the safety aspect of a product. How this is viewed heavily depends on the impact a potential failure of the system has. Regarding the MAWES, this impact could be very large. A kite with a size of around 20 m² that breaks free from the tether and is able to fly, and more importantly, crash anywhere can do some serious damage to structures, animals or people. Even though the system is most likely going to be operated in more remote places, this needs to be taken into account and the system will need to be designed and developed to prevent this from happening.

Looking further at the social acceptance of a design, it is also important to consider who will be effected by it. For safety, it is important to realise that the system intrudes airspace up to a certain degree. The safety aspect of this has to be discussed with the effected groups. This brings up another important factor of social acceptance. People that are impacted need to be included in the decision-making and get an opportunity to share concerns. This is also very useful for the designers as it provides valuable input and could reveal priorities or missed aspects in a design.

Further concerns that are brought up from literature research are the visibility and noise impact. The visibility mostly concerns the ground station in the research[37], since the kite is quite small compared to how high it flies. In the case of the MAWES, the size of the ground system is most likely not a large concern, seeing as it will fit into the back of a pickup truck. Furthermore, the purpose of the system is to be mobile, so there will not be a long term stationary ground station near people's homes, which is mentioned to be a potential issue in the literature research. The system has a higher probability of staying in the same place for a while, closer to civilisation, when it is used to power a grid. There is no mention of this in the literature research, but it can be assumed that the concerns about this system are not of high priority in these situations, since the MAWES will most likely power a grid in disaster struck regions. The noise concerns are similar to the visibility. They can become an issue if the system is stationed for a longer period of time, in close vicinity of populated areas. But with the same conclusions as before, this concern should be minimal. What should be taken into account is the noise the system makes during operations for the user. For this, a dB limit can be introduced, that is assessed to have minimal impact on the user.

Another concern is the ecological impact the system has. One aspect of the system is to be energy-autarkic, such that it is independent of external sources during the generation of energy. Furthermore, the ecological aspect is also taken into account by requiring that the system is largely recyclable. If this aspect is incorporated for especially the components that need regular replacement, this impact can be reduced. Moreover, the ecological impact is also the impact it has on birds and bats, in the form of collisions. In the literature research[37], this is mentioned as taken to be a prominent aspect of this impact. The conclusion of the size of this impact is said to be hard to judge, but logically the size of the kite, and that of the tether, are not that big. Further research could be done into the mitigation of the risk of bird strikes.

4.9. Market Analysis Conclusion

The main aim of this chapter was to get an insight into the applications of the system, and the market size for these applications. To explore the main applications of the system, a SWOT analysis was performed, followed by identifying the Porter's five forces. The conclusion that can be drawn from these, is that the system has an opening in a niche market, providing unlimited range to electric pickup trucks while being energy-autarkic. Furthermore, it has the option to be involved in the mobile generator market, expanding the applications. The three main applications are explored and explained in Section 4.5. The system can be used by well-off adventurers, for disaster relief, or for humanitarian peace missions. Furthermore, in Section 4.6, based on environmental characteristics, and the possible applications, the operation locations were selected. Bringing those two together, it can be concluded that North-America and Patagonia are the primary markets for exploring. Furthermore, the use of the system as a mobile energy system can be done in the Caribbean for disaster relief and in the Middle East for humanitarian peace missions. Combining all these findings, a market size estimation has been made of 2550 units. Lastly, research has been done into the social acceptance of a mobile AWE system.

Trade-Off Study Summary

In this chapter, a summary of the detailed trade-off performed and presented in the Midterm Report [10] is given. Note that the options which were not taken into account during the detailed trade-off due to being an unfeasible concept, a non-concept, or a further development, are not presented again. Furthermore, the detailed trade-off was based on seven different criteria: complexity, cost, mass, performance, reliability, sustainability and volume. Moreover, the trade-off tables for the presented subsystems can be found in Chapter 6 of the Midterm Report [10].

5.1. Airborne System

For the airborne system, first a decision between having a single or multiple lifting surfaces was made, followed by a trade-off on the type of kite that will be used. For this there were two possible options, a ram-air kite or a leading edge inflatable kite.

Based on a comparison between the advantages and disadvantages of having a single or multiple lifting surfaces, it was found that having a single lifting surface is the best concept. This is mainly because of the increase in control, landing and launching complexity when having multiple lifting surfaces.

The type of kite however was decided based on a detailed trade-off. The criteria that led to the final decision were the performance, reliability and complexity, since the results for the other criteria gave the same outcome. In terms of performance, ram-air kites were found to have better aerodynamic performances due to the fact that they approximate an airfoil like shape. However, their performance during reel-in is less efficient compared to leading edge inflatable kites. Furthermore, ram-air kites are designed to fly at high angles of attack, when flying at low angles of attack the stagnation point is not directly at the air intakes, leading to a loss in internal pressure. Moreover, LEI kites have better steering capabilities compared to ram-air kites. Then, in terms of reliability, both types have similar reliabilities, however the ram-air kite has the extra advantage of being more reliable in low wind conditions. Finally, taking a closer look at the complexity, it was found that ram-air kites are a lot more complex compared to leading edge, which will lead to a potential lack of time during the detailed design phase. Ram-air kites are fully dependent on the airflow for its aerodynamic shape. In order to ensure structural integrity, a complex bridle system is required, compared to the LEI kite, which uses inflatable tubes. Furthermore, the pressure difference between the lower and upper skin leads to a ballooning effect. This can be minimised by extra connecting elements inside the ram-air kite, however this increases the structural complexity. Furthermore, due to the enclosed air volume, more complex manufacturing processes are required. Taking all three criteria into account, the choice was made to go for the leading edge inflatable concept.

5.2. Control System

For the control actuation system, first a trade-off was performed between the different types of actuation systems and afterwards a final trade-off was done between airborne or on the ground. From this, the suspended cable robot came out as the best option. Regarding the airborne systems, it scored better in each criterion. Primarily on the performance, since higher angles of attack are achieved. Eventually, it is also better than the ground control system due to the strong weight requirement and the more complex control system of the ground controller.

Further, the ground station requires feedback from the sensors to control the system. One of the sensors placed on the ground station is the wind speed measurement device. From the trade-off, it was concluded that the ultrasonic measurement performed the best. Regarding the relative positioning measurement system, the combination of GPS and barometer performed better in the criteria of performance and complexity, thus this system was chosen. Next, the choice was made which attitude measurement sensor will be used. Based on the performance criterion, the magnetometer was chosen, mainly because it outputs a vector. This will be used in conjunction with accelerometers and gyroscopes.

As power supply for the airborne control system, the wind turbine was chosen as it can deliver a continuous power supply, which is not the case for solar panels. Changing battery with a drone was also not preferred because of the complexity to switch batteries in the air.

Finally, to deliver the information from the computer on the ground to the control system in the air, a communication trade-off was performed between Wi-Fi and Bluetooth. Regarding the performance, Wi-Fi scored better because of the faster data speed. Therefore, it is also more reliable, as the delay speed of 100 ms can not be exceeded [4]. Hence, it can be concluded that Wi-Fi is the best solution.

5.3. Tether

The tether material and concept were determined by performing multiple trade-offs. Firstly, the deduced concept was the conventional tether. This proved to be superior in almost every category. For the material selection, first an analysis of the performance of different tether materials was carried out. Combining this with the established criteria weights for the tether, the material was decided to be Sierra 78 (bio-based) Dyneema®. Dyneema outperforms all other materials that were selected, especially on fatigue resistance and specific strength. Furthermore, the bio-based option gives a boost to the sustainability of the project.

5.4. Launching and Landing

For launching and landing, different strategy concepts were set up. As for the launching, many of these concepts involved large and heavy structures, like the mast and catapult based launch described in the midterm report [10]. This led to the general flat laying approach, which does not require any extra equipment apart from clamps, being the most interesting. On top of this, this launch strategy is also a proven concept, and has low complexity and costs. During this launch strategy, the kite is laid on its back, clamped to the ground by its leading edge and then inflated. When the tether is under tension and the kite is powered by standing on its trailing edge. The tether can be further reeled in, and the kite will be brought airborne.

For landing, it was chosen to bring the kite to the side of the wind window. This strategy works at all wind strengths and can be handled by a single person. The competitors of this strategy were either dangerous or unreliable.

5.5. Main Power Generation System

After having discarded all the unfeasible and future development concepts, the only option that was left for the power generation system was having a motor-generator. The only trade-off that still had to be performed was on the type of motor-generator. This was chosen based on a comparison between the advantages and disadvantages of DC and AC motor-generators. The main advantages which stood out for the DC motor-generator were its fast response time, easier installation and maintenance, and smaller size compared to the AC motor-generator. Since one of the main requirements is that the airborne wind energy system shall fit in the envelope of the Rivian R1T, the DC motor-generator was seen as the best option.

5.6. Ground System

For the ground system, a trade-off had to be done for the anchoring system. Several anchoring methods were investigated. After a worst-case analysis for high traction forces on different application points, it was concluded that a special anchoring system was not needed, as the use of the handbrake was sufficient to keep the car static.

5.7. Short Term Energy System

The main requirement for the short term energy storage is to provide continuous power to the ground control system and to power the reel-in phase. After having discarded all unfeasible options, only lithium-ion batteries, vanadium redox flow (VRF) batteries and supercapacitors remained as potential options. In this trade-off, the supercapacitors resulted as the desired storage option. Their biggest advantage over the VRF and lithium-ion batteries are their high cycle life, high reliability, ideal discharge time and recyclability. The largest drawbacks are cost, mass and volume. Since the supercapacitor is only a minor component in the total AWES concept, these criteria have minor weights assigned to them. Additionally, these characteristics are believed to improve rapidly as supercapacitor operations are rising and research and development is continuously going on [53].

The main drawback of lithium-ion batteries is the toxic waste related to the end of operations and its very limited recyclability. As for the VRF batteries, mainly the performance, sustainability and mass were limiting factors. Additionally, VRF batteries still need research and development to compete with other proven concepts. Therefore, supercapacitors proved to provide the best performance out of these three options.

5.8. Trade-off Design Options Summary

This section aims at providing an easy and quick overview of the final design choices. Therefore, the following list shows the concept per subsystem that resulted from the trade-off performance. The section is adapted from Section 6.4 in the Midterm Report [10].

- **Airborne system (Section 5.1):** A single Supported Leading Edge Inflatable Kite is the chosen design.
- **Control system (Section 5.2):** For control system actuation, a suspended cable robot will be used. The airborne control system will be powered by a separate wind energy system. The sensors (Ultrasonic Wind Sensor, GPS, Barometer, Magnetometer, Accelerometer, and Gyroscope) will be placed on the airborne control system and ground station. The communication between these systems will be through an external Wi-Fi system.
- **Launching and landing system (Section 5.4):** For launching, the general flat laying approach is used. For landing, the reel-in method to the side of the wind-window was determined to be the best option.
- **Tether system (Section 5.3):** A Sierra 78 (bio-based) Dyneema® non-conductive tether, without an electric wire embedded, will be used as tether.
- **Ground system (Section 5.6):** The airborne system will be stored in the truck bed or the gear tunnel of the truck. The ground system anchoring only requires the handbrake to stay stationary. The drum will be fixed with bolts to the truck bed.
- **Power generation system (Section 5.5):** A DC motor-generator will be used for the reel-in/-out of the tether connected to the kite. This decision was however revisited during the detailed design.
- **Short term energy storage system (Section 5.7):** The energy for the reel-in phase will be stored in a supercapacitor.

5.9. Trade-off Sensitivity Analysis

The sensitivity analysis for the trade-offs is performed in the Midterm Report [10]. When changing the weight of the criteria in the trade-off, the outcome of the trade-off is compared to the original outcome. For three out of the fourteen trade-offs, the outcome changed when a criterion was changed to 0% or 200% of its initial value. This indicates that there is a low influence of changing the weights, which gives a high confidence in the performed trade-offs.

System Configuration and Operations

The design convergence resulting from the trade-off execution led to the need for a general system configuration overview. This overview is discussed in Section 6.1. This section emphasises the system's interconnectedness and provides a baseline for a general understanding. This is followed by a functional analysis in Section 6.2, which comprises a functional breakdown structure and a functional flow diagram and wind speed analysis. Section 6.3 discusses KITE-E's operational procedures based on the established system functionalities. Finally, Section 6.4 concludes this chapter with a maintenance plan description.

6.1. System Configuration

In this section, a high level system configuration is discussed. Figure 6.1 shows a schematic system overview of how the subsystems interact both with each other and with the external environment. As observed in Figure 6.1, the AWES is subdivided into five subsystems: the landing and launching system, the ground system, the energy system, the airborne system, and the GNC system. On their turn, these subsystems are further broken down. The connecting arrows indicate an interaction between two items. These interactions are not further specified in this diagram, but are discussed in the operating logistics (Section 6.3) and in the detailed subsystem design chapters (Chapter 10 to Chapter 14).

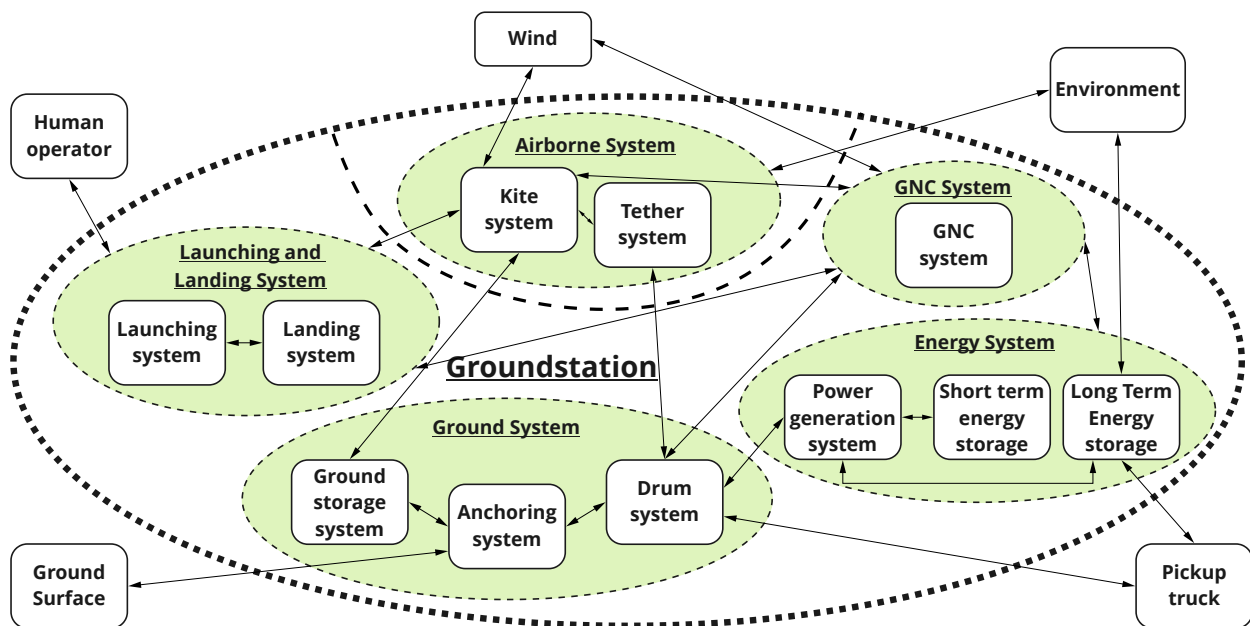


Figure 6.1: KITE-E's general system configuration schematic.

6.2. Functional Analysis

In this section, the functional breakdown structure and functional flow diagram of the airborne wind energy system are presented in Section 6.2.1 and Section 6.2.2 respectively. These are provided in order to provide insight in the functions that will have to be performed and in what order, with a function being defined as a task or activity to be performed by people, equipment, hardware or software [54].

6.2.1. Functional Breakdown Structure

The functional breakdown structure provides an in depth overview of the most important functions that need to be performed during each stage of the life cycle of the airborne wind energy system. However, note that the chronological flow in the functional breakdown structure is not necessarily of primary concern. Furthermore, the five primary stages are the system production phase, the integration and transportation phase, the operations phase, the maintenance phase, and the end-of-life phase, which is shortly discussed.

- **System production phase:** During this phase, all necessary parts need to be manufactured and assembled. During the production process, it is of utmost importance that all components are inspected and tested at several stages throughout the process in order to identify defects on time, such that these parts can be repaired or replaced as early as possible to eliminate waste. After having all the separate parts produced, they will be transported to the assembly facility, where they will be assembled. Furthermore, during the assembly phase, inspection and testing plays also a crucial role. Finally, the product can be packed ready to be transported to the integration facility.
- **Integration and transportation phase:** During this phase, the assembled product will be transported to an integration facility where it can be integrated in the Rivian R1T. Once the integration is finished, the finished product can be delivered to the client.
- **Operations phase:** This is the phase during which the energy is harvested. However, in order to harvest energy, some other steps need to be taken. First, the car as well as the airborne system need to be prepared for operation. Once the complete system is prepared for operations, the kite can be launched and start with its regular operating functions. The operations will proceed until the wind drops or until it is decided by the driver to end the operations and drive to another location. In case the wind drops, there are two possibilities. In case it is estimated that the decrease in wind speed will last less than 30 minutes, the system will start performing reverse pumping cycles in order to bridge the wind gap. When this is not the case, the landing procedure will be performed. Finally, when the operations are finished, the shut-down operations will take place.
- **Maintenance phase:** This phase runs in series with the operations phase, and forms an iterative loop. This is because during the operational lifetime regular maintenance is required, until the end-of-life phase is reached. This includes that all components are cleaned after operation. Furthermore, regular maintenance should be conducted to avoid unrepairable damage. Moreover, inspection should be executed within predetermined time intervals. This is of utmost importance for the detection of defects. Finally, the outcomes of this inspection should always be reported in a logbook.
- **End-of-life analysis:** When the airborne wind energy system is observed not to be able to perform its operations in a safe and efficient way any more or when a part is to be replaced, the end-of-life analysis will be performed. During this analysis, it is decided for each of the system components if they will be reused, recycled or disposed.

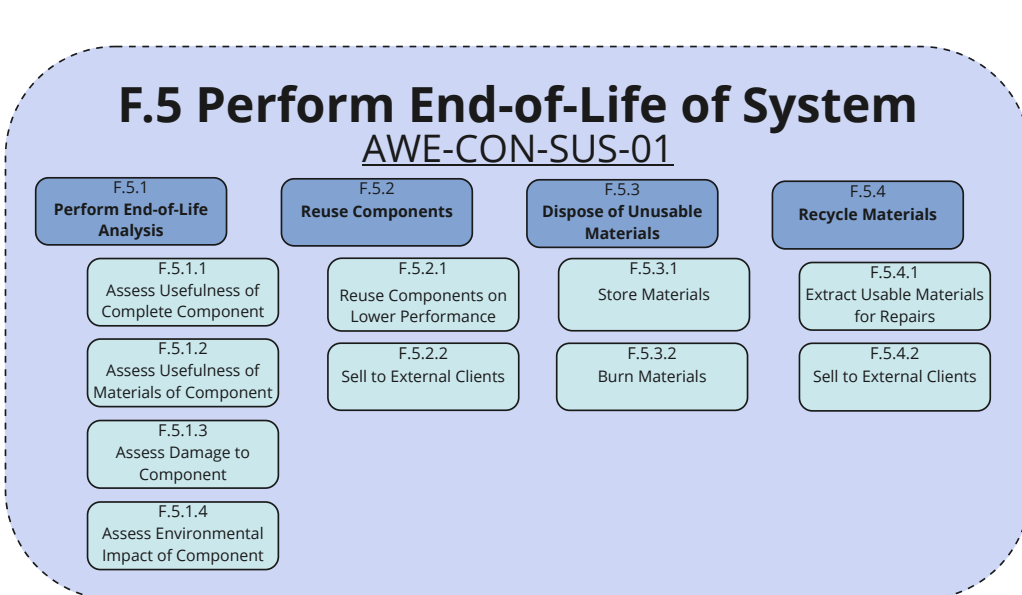
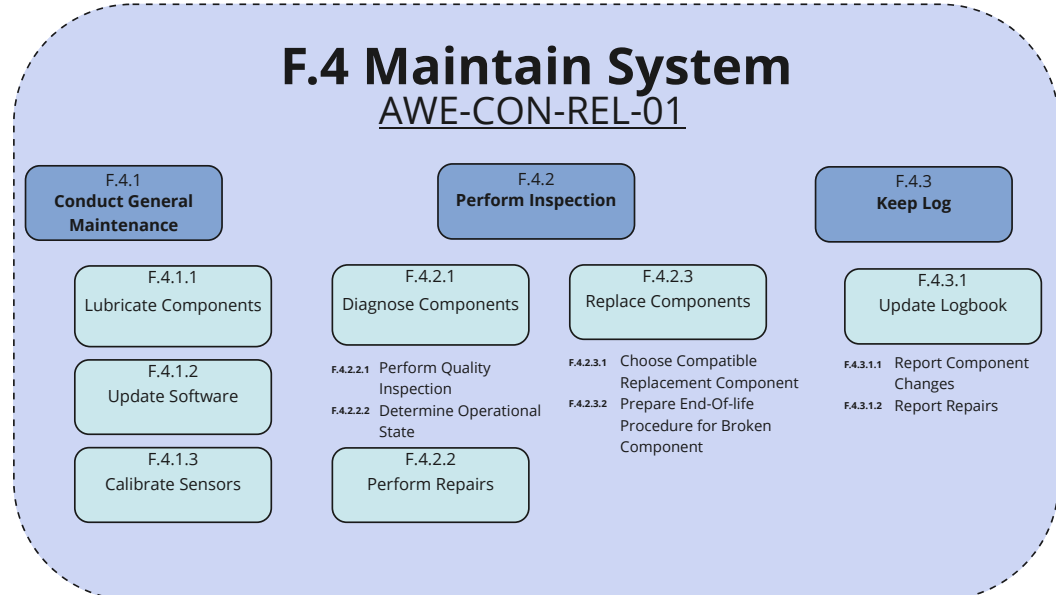
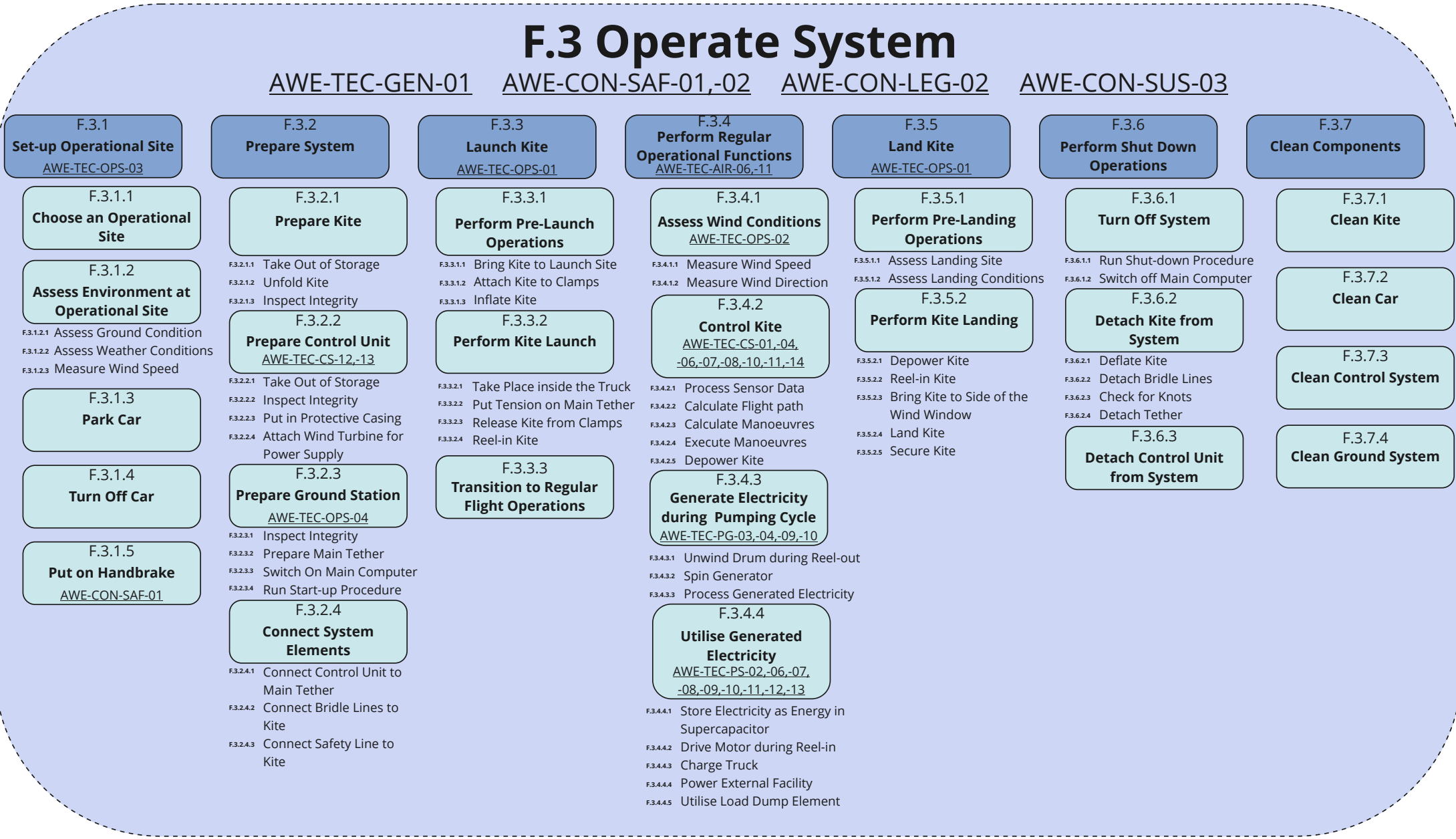
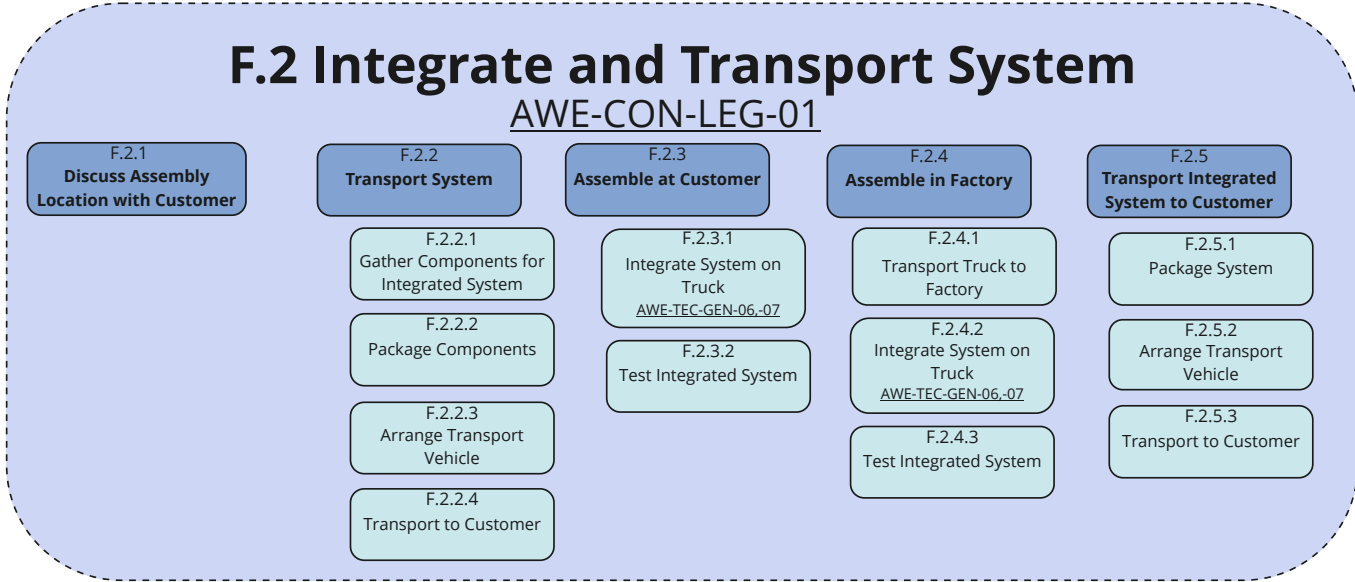
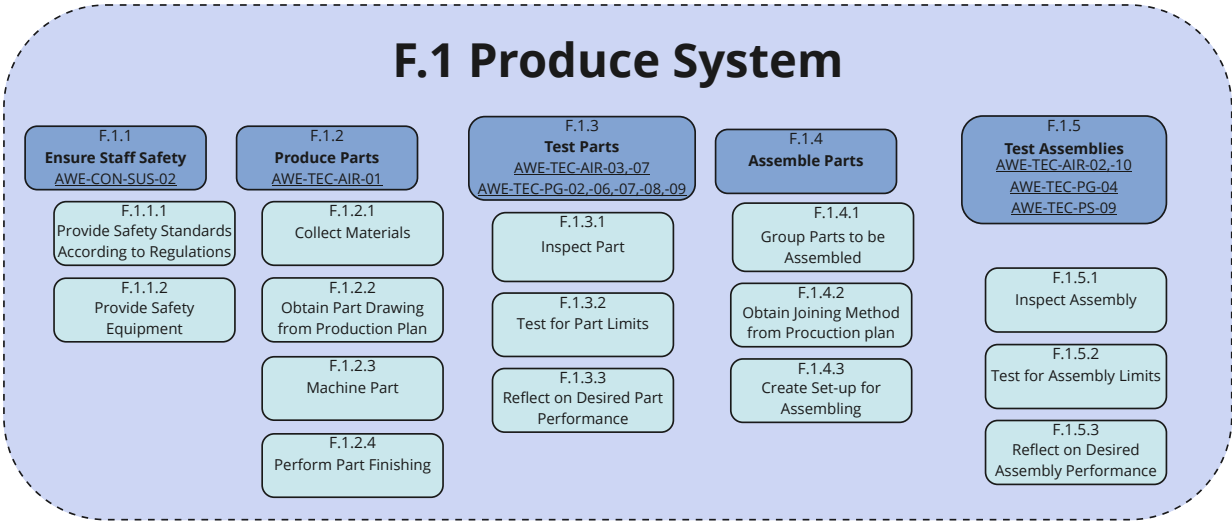
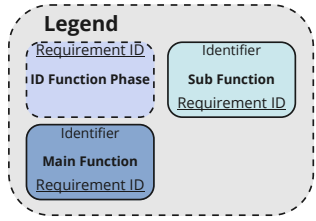
6.2.2. Functional Flow Diagram

Having established a detailed overview of all the functions that will need to be performed during each stage of the life cycle of the airborne wind energy system, a chronological sequence of these functions will be presented in a functional flow diagram. This is necessary in order to understand what the components of the system need to do, and especially when. Furthermore, in Section 6.2.2 the different life cycle stages are shown on top. Then these stages are expanded two levels deeper by dividing each stage and function into the several underlying functions. All functions logically flow from and into each other, and a reference block, as presented in the legend, is used when a branch ends and continues into a new main function.

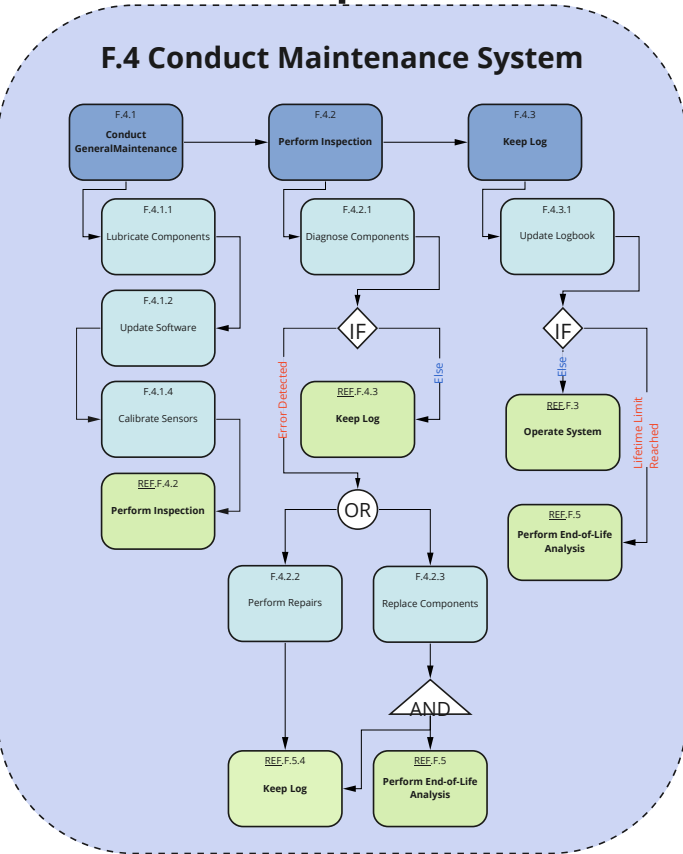
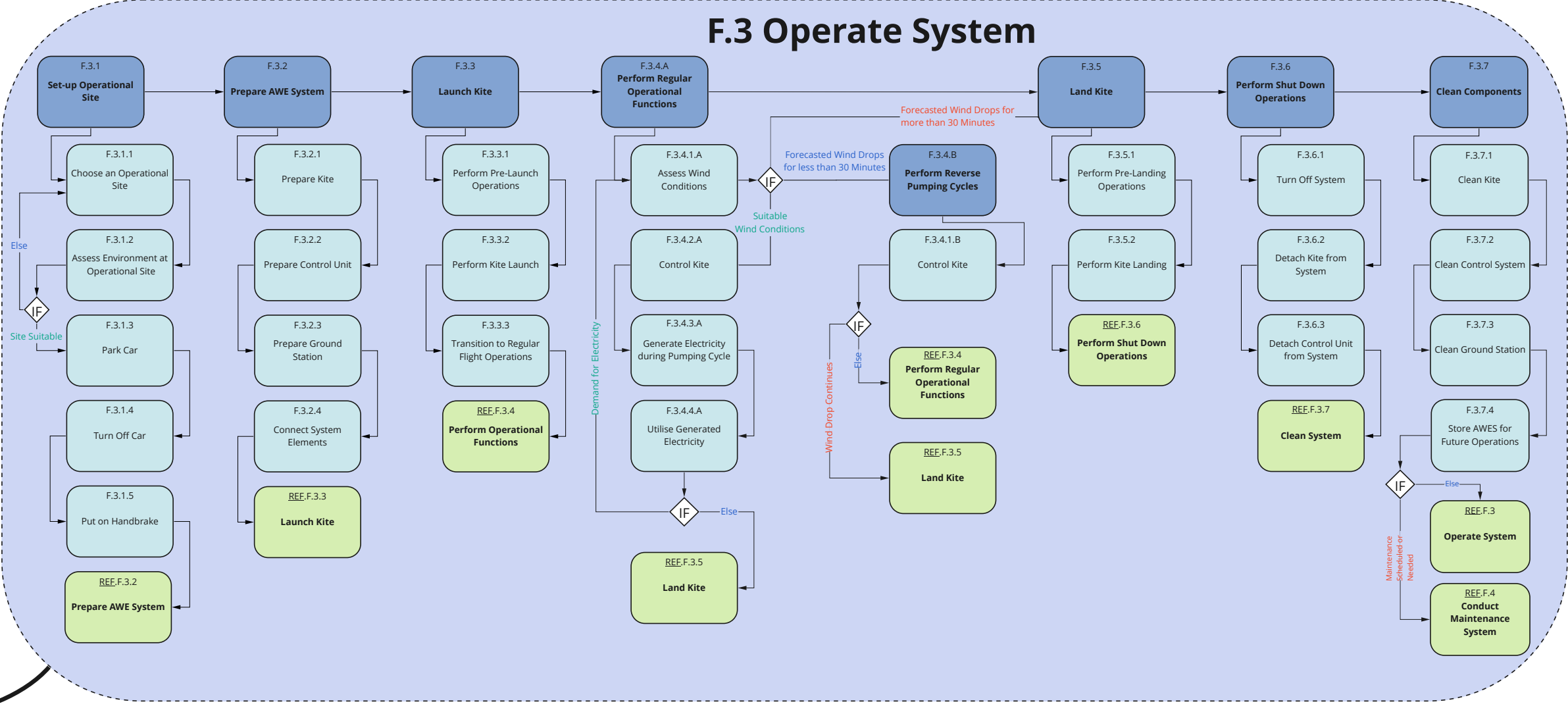
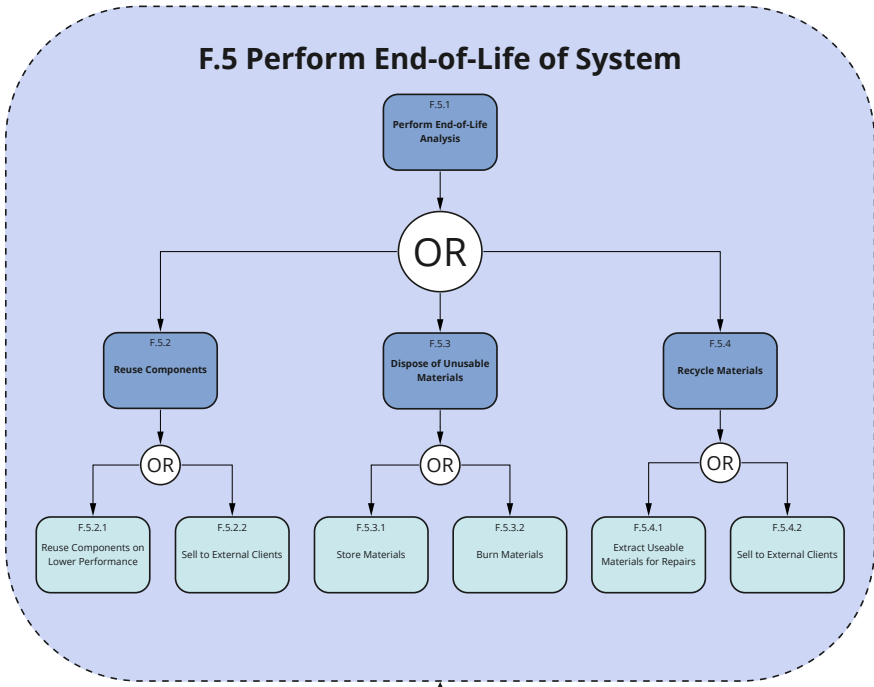
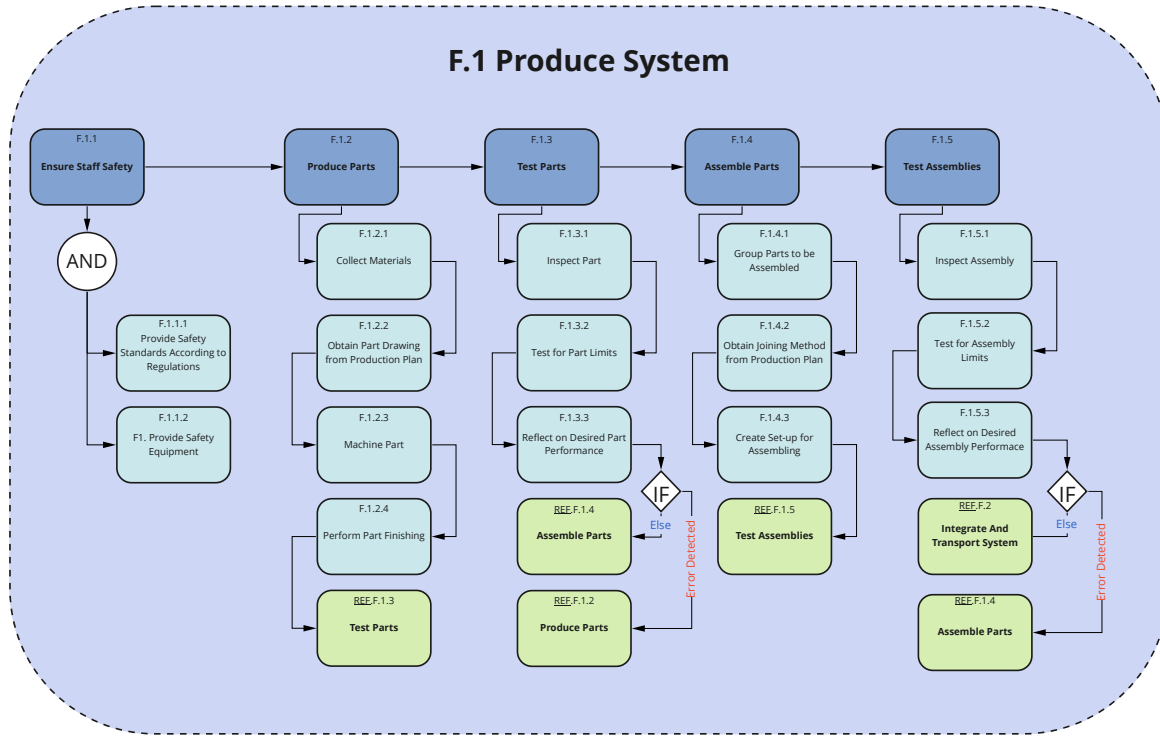
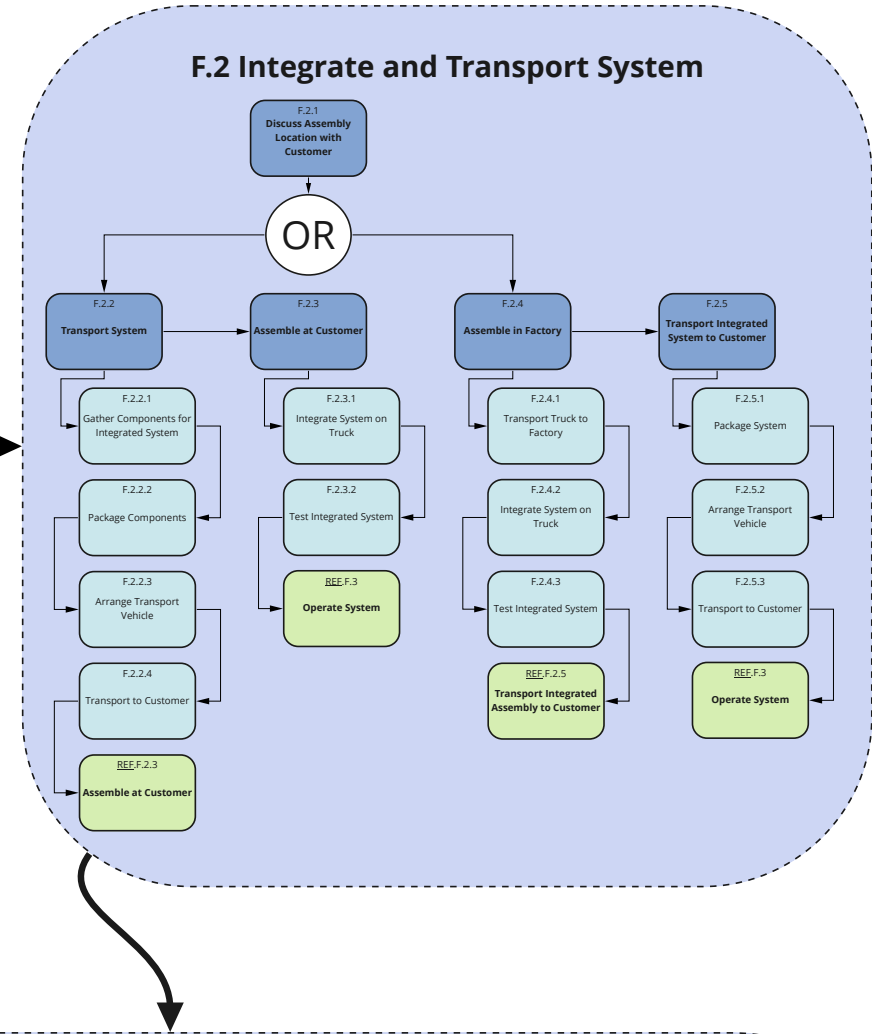
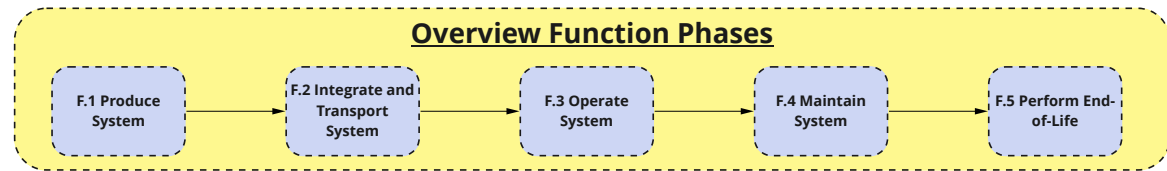
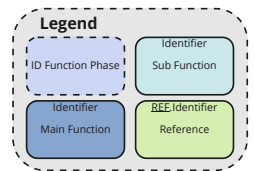
In the functional flow diagram, three statements have been used: "or", "if" and "and" statements. When using an "or" statement, the output of the function before decides the follow-up function. Furthermore, the "if" statement only applies when a certain condition is met, and only then flows towards the function applied afterwards. Lastly, the "and" statement simply means that both functions follow simultaneously.

The identifying functionality codes will be used throughout this chapter's section titles to link functionalities with AWES operational descriptions. Similarly, the functionality codes are linked to their respective subsystem design in Chapter 10 to Chapter 14. The functional breakdown structure and functional flow diagram can be found after Section 6.2.2 on the next two pages.

Functional Breakdown Structure KITE-E



Functional Flow Diagram KITE-E



6.2.3. Wind Speed Parameters

The operating moment and duration of the system is dependent on the wind window of the location. Therefore, a wind analysis is performed on the influence of temperature and humidity daily and seasonal wind speed changes, and last of all the influence of terrain roughness and altitude on the wind speed. A general yearly overview of the average wind speed in the world can be obtained from the Global Wind Atlas [43]. This analysis was retrieved from the Midterm Report [10].

Temperature and humidity effects

Wind is generated due to a difference in pressure between two air masses. A higher temperature will decrease the density of the air mass. A higher temperature gradient, the temperature difference between two locations, will lead to an increased pressure difference and higher wind speeds. The air temperature at a location does not tell something about the wind speed at that place [55]. Air temperature has influence on the relative humidity. If air heats up, it can contain more moisture. For the same moisture level, the relative humidity decreases when the temperature rises [56, 57].

Daily and seasonal effects

Wind speed changes during the day and season, and although a certain pattern is present, there are still some irregular situations. These can be taken into account from a week in advance with a wind forecast. For daily cycles, it can be generalised for most locations that the wind speed is higher during day and drops during night, due to the difference in air mixture. During the day, the sun warms up the air layer near the soil. The warm air will rise and mix with colder air on top, resulting in wind. The heat of the sun will be gone during the night and leaves a cold layer of air near the ground, resulting in little wind. This is visible in Figure 1 in [58] for different locations on Earth. Areas close to large bodies of water will have smaller daily temperature variations [59].

Next to the daily effects, there are also seasonal effects. For example, in the European and American winter, a higher temperature gradient causes larger pressure differences and increases the wind flow. This cycle is represented in Figure 3 in [58].

Altitude and terrain effects

The wind speed usually increases with altitude, because there is less resistance for the air caused by the ground. Furthermore, local topography and weather patterns are influencing factors that change the wind speed and wind availability. On hills and mountains, for example, the wind speed is higher because of the altitude. Additionally, wind speed can increase through a tunnelling effect in narrow valleys or over hills. On the other hand, obstacles also affect the wind flow, such as building, trees. For each surface a different wind speed boundary layer is formed as it strongly depends on the surface roughness. Following the wind speed always increases with increasing altitude while pressure decreases [57]. The surface roughness is given as ξ and different values of ξ can be found in Table 6.1. These values can then be implemented in the following Hellman exponential equation to calculate the wind speed v_1 at specific altitude H_1 [60]. The reference wind speed v_0 at the reference altitude H_0 will be used as baseline. For a more accurate wind speed, local measurements combined with forecasts can be used. If this data is not available, Equation (6.1) can be used.

Table 6.1: Friction coefficients for different surfaces [60].

Landscape type	Friction coefficient, ξ
Lakes, ocean and smooth hard ground	0.10
Grasslands (ground level)	0.15
Tall crops, hedges and shrubs	0.20
Heavily forested land	0.25
Small town with some trees and shrubs	0.30
City areas with high rise buildings	0.40

$$\frac{v_1}{v_0} = \left(\frac{H_1}{H_0} \right)^\xi \quad (6.1)$$

Sea and land breeze effect

The sea and land breeze effect is induced by the difference of thermal properties of land and water. When heated by the sun, the land temperature raises quickly compared to a large body of water. Due to the temperature increase, a low pressure region is formed above land. Air from above the water flows towards the land, the so-called sea breeze [61]. At about 1000-1500 m, the air cools down again, resulting in a relative high pressure region [62]. The high pressure region air flows back to the relative low pressure above sea, closing the cycle. At nighttime, the phenomena reverses, resulting in a land breeze [63]. The figure in [64] shows a visualisation of the sea and land breeze.

6.2.4. In-Depth Wind Analysis

For the in depth wind analysis, the wind speed values for 10, 50, 100, 150, and 200 m are extracted from the Global Wind Atlas [43] for the four chosen locations in Section 4.9. The values are interpolated to find the value of ξ in Equation (6.1). With the value of ξ known and the value of 10 meters used as baseline, the wind speed can be calculated at multiple heights. For the determination of the maximum operational height, the power

increase is determined in steps of 10 m. The power will keep increasing for increasing height, but at a certain moment the increase of the power is so low it is not worth to increase the maximum operational height. This height is set to 290 m, where the power increase is less than 2%. The data of the Global Wind Atlas is for the 10% windiest areas in the region. For a more conservative wind speed estimate, the 20% windiest areas are used. The minimum operational height is determined by the drum sizing and is set to 165 m, as can be read in Section 13.3. For this operational height, averaged for the four locations, the wind speed changes between 9.38 and 10.51 m/s. At the average operational altitude of 227.5 m the wind speed is 10.0 m/s, which is the regular design wind speed. The data is summarised in Table 6.2.

Table 6.2: The friction coefficient and wind parameters at 10 m height and 227.5 m height for the four chosen locations.

Region	Friction coefficient ξ	Wind speed @10m m/s	Wind speed @227.5m m/s
North America (Canada)	0.1964	5.47	10.10
Caribbean (Cuba)	0.217	4.25	8.37
Patagonia (Argentina)	0.1821	6.91	12.21
Middle East (Saudi Arabia)	0.2193	4.72	9.37

6.3. Operating logistics (F.3)

In this section, the system operating steps are covered in the chronological order during the operations of the system. Starting with the pre-flight operations and launching. When the battery is full, the landing and post flight operations are carried out. These operations are discussed in Section 6.3.2-Section 6.3.6. This section is adapted from Section 8.1 from the Midterm Report [10].

6.3.1. Operations logistics Requirements, Functionalities, and Risks

This section's purpose is to highlight the requirements, functionalities and risks associated with the operating logistics. This enables a better integrated operating design and allows for integrating the operation section in the larger project framework. Additionally, the operational procedures should comply with the identified requirements as seen in Table 6.3. The identified risks and the risk reduction measures relevant for certain operating steps are shown in Table 6.4 and the functionalities of the subsystem are linked to the associated subsections.

Table 6.3: Requirements on AWES operations.

Identifier	Requirement
AWE-TEC-OPS-01	The launching and landing of the airborne system shall be a task for maximally one person.
AWE-TEC-OPS-02	The airborne wind energy system shall be able to be operated in a reverse pumping mode to bridge wind gaps of maximum 30 minutes.

Table 6.4: Risks, with risk reduction measures influencing the operation logistics

Identifier	Measure
TR-LALA-04	Include a reserve manual pump in the truck.
TR-LALA-05	Remove sharp objects of the launching and landing area.
TR-LALA-06	Detangle the bridles before launching and check the bridle setup a second time.
TR-LALA-07	Check wind forecast before launching.
TR-LALA-10	Signalling the operator with an alarm.
TR-GR-04	Placing a brush on the tether before reeling in the tether.

6.3.2. Pre-Flight Operations (F.3.1 and F.3.2)

The operation of the system starts with parking the car in a suitable location. A suitable location has favourable vegetation, terrain and wind conditions. For the vegetation, it is important to note that the kite has an operational range of about 500 m around the truck. The height of obstacles is limited to 1 m in a range of 20 m from the car [65]. Secondly, the terrain is important for the anchoring of the truck, as can be read in Section 13.2. Snow and ice should be avoided as operating terrain. Furthermore, the truck can be parked at a maximum road angle of 2°. When deploying the kite, risk TR-LALA-05 should be taking into account to prevent damage during launching. As mitigation, the launching area is inspected for sharp objects and removed in case of occurrence. Lastly, the wind conditions on the ground are important for the operation of the system. The risk TR-LALA-07 of not being able to launch the kite can be mitigated by checking the wind forecast and changing location to a more suitable area. Information can be gathered on websites like Windfinder [66], Windy [67] or Windguru [68]. With the truck parked in a suitable location, the truck can be put in operational mode.

From requirement AWE-TEC-OPS-01 it follows that the operational phases need to be executed by one person and the help of an automated system. The first step on the checklist for the operating person is to put the truck

in the operational mode. It is followed by initiating the hand brake of the truck, lowering the truck to its minimum height and making the air suspension stiffer to avoid vibrations. Following, the operator steps out the truck and lowers the truck bed door to extend the spindle track on the extending spindle rails, visible in Figure 13.5.

The next steps are all about ensuring the integrity of the system after a long drive. Pull the covers from the system, visually check the gears, generator, motor, tether and KCU for damage. If all systems are in good shape, the control unit on the ground station can be turned on. The control unit will run tests on the system, to check whether all actuators and motors work. After the whole ground system is functioning, the tether is laid out downwind by the operator. Launching equipment needs to be placed on the ground, approximately 15 m from the truck and loaded with material from the launching area, to prepare the anchoring point for the kite. The kite is pulled out of its storage bag and while folding it out, the leading edge and trailing edge are connected to the clamps. The front bridles are connected to the power lines, and the back bridles are connected via the pulley to the steering and depower lines. The last connection is made between the KCU and the main tether.

The trailing edge is pointed into the wind. The tether is tensioned before inflating the kite, such that the trailing edge is pushed on the ground. This means the rear bridle lines need to be fully retracted, which is accommodated by the KCU. The inflation of the kite is done with the built-in compressor of the Rivian R1T. A reserve manual pump is included as a redundant part to mitigate this risk, for when the compressor fails, as described in risk TR-LALA-04. The bridles have to be checked a second time by the operator to make sure they are not tangled, which prevents risk TR-LALA-06 for happening. With the kite securely connected to the ground, and the bridle system attached to the KCU and main tether, the KCU will perform steering manoeuvres on the ground to calibrate its sensors, checking the proper functioning of the KCU. After the KCU checks have been performed, the operator will slowly drive the pickup truck to about a minimum distance of 40 meters from the kite, with the tether being reeled out with the same speed as the speed of the pickup truck to prevent dragging of the kite. If sufficient wind is not present for launching, the truck can be placed further from the kite so more tether length can be used to reel in the kite to create a higher apparent wind speed. Increasing the distance to the kite thus provides the possibility to launch at lower wind speeds. These pre-flight operations will take around 30 minutes to execute. However, the first time it can take longer, as the operator is not yet familiar with the system.

6.3.3. Launching Procedure (F.3.3)

During pre-flight operations, the system is made ready for operations. To begin the launching, first the operator walks back to the truck when the kite is standing stable. The operator is now in a safe position and gives a signal to the control system to begin the automated launching procedure. Now a sequence of separate steps are executed, beginning with disconnecting the magnetic clamp from the leading edge. Then, KCU reels out the depower tape and the main tether is reeled in till the kite is standing straight on its trailing edge. Now, if the wind is sufficiently high enough, the kite catches the full wind, and if there is sufficient wind the kite will fly up. If the wind is not high enough, a winch launch is performed. The tether will then be reeled in, increasing the apparent wind speed and thus letting the kite take to the air. The launching method can be seen in Figure 6.2. Now that the kite is safely in the air, the tether can be reeled out. When the tether is not double wended around the drum any more, the power generation of the system can start.

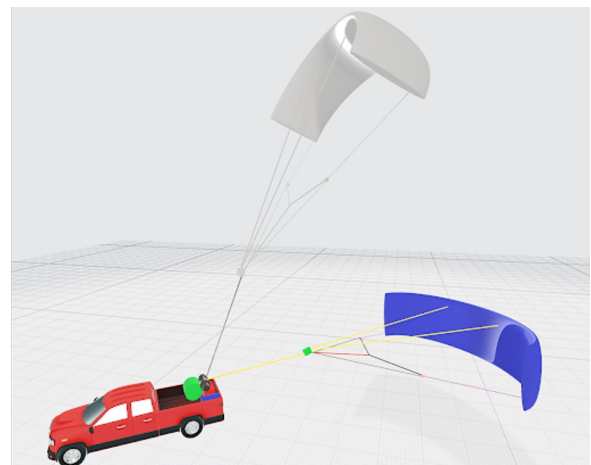


Figure 6.2: Illustrative visualisation of the general flat laying launch. (Tether length is not to scale)

6.3.4. In-Air Operations

The operations of the system are explained in this subsection. For a more specific explanation of the control, Section 14.4 can be read for explanation about the ground control system and KCU. After the kite reaches its minimum operational altitude of 165 m, as visible in Figure 6.3, pumping cycles are used for power generation. The design cyclic power output should be equal to 20 kW. In order to achieve this, the power generation during the reel-out phase should be maximised. This can be obtained by flying figure of eight manoeuvres. During these manoeuvres, the tether unrolls from the drum, which is connected to a generator, resulting in the generation of electrical energy until a maximum regular design operating altitude of 290 m is reached. The kite could fly higher, but this is chosen as the maximal operating altitude, since the wind speed does not change

significantly when going higher. A part of this energy is stored to be used during the reel-in phase. The energy is used to pull the kite back in, from the maximum operational height to the minimum operational height, to start a new pumping cycle. The power consumption should be minimised and this is achieved by depowering the kite, which means lowering the angle of attack. For regular design wind speed, the in-air operation will take around 6.5 h to fully charge the battery of the truck.

When the wind drops, the general pumping cycles are not enough to keep operating. In this case, the system shall operate in a reverse pumping mode for a maximum of 30 minutes (requirement AWE-TEC-OPS-02). During the reverse pumping cycles, the kite will be reeled in, which creates a higher relative wind speed, resulting in enough lift to keep the kite airborne. Once the kite reaches the highest point, the force on the tether is lowered by reeling out the cable. At this moment, the kite will also make a backward turn, creating speed. After the turn, the control unit will move under the kite, because there is no more tension on the tether, and the kite will operate as a glider, gliding down slowly. At a certain altitude, the kite will again make a turn and be reeled in, to restart the reverse pumping cycle. When the wind gap lasts longer than 30 minutes, the kite will be landed. Launching will be performed if the wind speed is again optimal for operation. This method of reverse pumping is a proven way to keep the kite airborne during low wind periods [65].

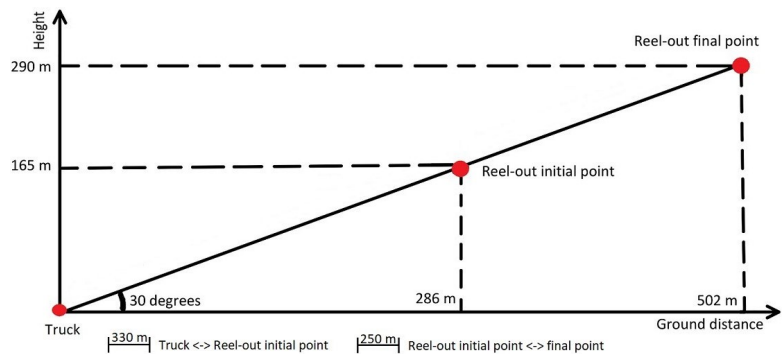


Figure 6.3: Operational envelope during the reel-out phase.

The operational window of the kite spans 180° behind the pickup truck in the horizontal plane. This constraint prevents the tether from hitting the truck's cabin. If the wind turns 50° in one direction, as can be read in Section 13.4 the kite has to be landed to enable the operator to relocate the truck.

The system is grounded when there is a high risk of lighting strikes, during storms, and when there is low visibility. The system is able to operate at high wind speeds, but when the maximum tether is reached, a deviation of the optimal flight path of the kite will be needed to reduce the force on the kite, tether, and the rest of the system. First, the tether is reeled out faster to alleviate the force. Then, the elevation angle is increased to operate the kite outside the power window. If the kite is at its maximum elevation, the kite will be depowered to ensure safe operation of the system. After all these depowering steps are performed, the only remaining operation is to land the kite.

6.3.5. Landing Procedure (F.3.5)

The landing procedure is executed when the battery is full or for another reason, and the system of the kite has to be terminated. The landing procedure is based on the landing explanation in the Midterm Report [10]. The procedure is started by reeling in to a minimum distance, where the kite can still be controlled by the KCU. At that moment, the side of wind window landing approach will start. This landing is performed by bringing the kite to one of the sides of the wind window. The KCU is responsible for this execution and gently steers the kite by shortening one of the steering lines. Before this manoeuvre is performed, an inspection of the landing area is required, to identify any sharp objects and other big objects that can interrupt the landing procedure. In case the system is used to charge the truck, an alarm will signal the operator if the battery is full and the kite has to be landed, in this way risk TR-LALA-10 is prevented. When the kite is positioned at the side of the wind window, the kite is stable and depowered such that the operator can safely walk from the truck to the kite. The operator then grabs the kite at the leading edge and lays it down on the ground with the leading edge pointing to the ground, and the kite positioned into the wind, which blows the canopy downwards. When the kite is in this safe and stable position, the kite can be relaunched when the weather conditions become favourable again, or, if the weather conditions are already favourable, when it is necessary to generate energy. The truck can be relocated to be upwind of the kite and the magnetic clamp is repositioned. If operation of the kite is not necessary any more, the post-flight operations can be performed.

6.3.6. Post-Flight Operations (F.3.6 and F.3.7)

When the kite has safely landed and needs to be stored, the leading edge of the kite is connected to the magnetic clamp. With the kite safely secured to the ground, the kite can be turned over to lay on its topside. To minimise the influence of the wind on the kite, it is first deflated with the middle valve and extra valves at the wing tips. Then the KCU is disconnected from the bridle and tether by the operator and stored on the spindle track in the

back of the truck when the spindles rails are retracted. Before the tether is reeled in, a brush is placed over the tether to prevent dirt from coming in the swivel and drum. In this way, risk TR-GR-04 is prevented. A visual is present in Figure 6.4. Now the tether is rolled completely onto the drum and a cover is put over the entire system. The last post-flight operation step is storing the kite. The kite can be completely deflated by using the compressor of the Rivian R1T as a vacuum pump. The kite will be folded from the wing tips to the middle to keep the structural integrity of the kite intact. The folded kite can be put in a bag and stored in the gear tunnel of the truck. The gear tunnel is located before the truck bed and is visible in Figure 15.1. Storing the kite wet should be avoided to prevent the growth of mould, harming the kite material. The KCU will be stored on the spindle track, when it is retracted to storing mode, as can be seen in Figure 13.5. These post flight operations will take around 20 minutes to execute. However, the first time it can take longer, as the operator is not yet familiar with the system

6.4. Maintenance (F.4)

Proper maintenance of the system is important to ensure continuous operation. Small failures and errors can have big consequences and can lead to system failure. In Section 6.4.1, the maintenance friendly design methods are introduced. The predictive maintenance strategy is explained in Section 6.4.2. After the maintenance strategy is explained, the maintenance is explained per subsystem in Section 6.4.3. Finally, the maintenance of the Rivian R1T, will be explored in Section 6.4.4. This section is adapted from Section 8.2 from the Midterm Report [10].

6.4.1. Maintenance Friendly Design

The required maintenance during the operational lifetime will be taken into account for the design phase. Parts that need frequent maintenance are easily accessible and replaceable. Also, the usage of specialised parts should be avoided, due to their high costs and the availability of replacement parts [69]. Finally, critical parts will be designed with a long operational lifetime. An extra investment in the material and design of the parts saves money in the long run.

6.4.2. Predictive Maintenance

A predictive maintenance strategy is used for critical components of the system [70]. Despite the long operational lifetime, critical components can still fail during operations. When the system is operated in remote locations, spare parts are not widely available. For this reason, critical parts will be actively monitored with sensors and replaced on time if small initial failures are detected. With these on-time replacements, downtime of the system is avoided. To keep track of all the maintenance, repairs, and replacement performed, a logbook should be kept. To conclude, predictive maintenance enables cost and time effective operation.

6.4.3. Maintenance per Subsystem

In this subsection, a more in-depth maintenance strategy per subsystem will be explained. This subsection is adapted from Section 8.2 in the Midterm Report [10]. For the subsystems, there are a few standard maintenance procedures that can be applied. These consist of cleaning, inspection, repairs, or replacement of components and keeping a log. These procedures slightly differ for each component, and different solutions to prevent failures can be used. The differences for every subsystem will be explained in the coming paragraphs. The maintenance can be divided into scheduled and unscheduled maintenance. The system will be mainly damaged due to the rough off-road conditions, high or low humidity, ultraviolet (UV) radiation exposure and the continuous high loading.

Kite

The LEI kite is highly dependent on the pressure in the inflatable structures, so any type of damage that causes a leak is catastrophic for the system. Cleaning the kite is necessary to remove sand and dirt that could tear the fabric [71]. The leading edge and struts are connected via a small rubber hose with a valve to enable a single pump system. The rubber hose is easy to manufacture and thus preferred over connecting the leading edge and the struts internally. The valve on the hose is always open during operation to keep the struts pressurised, and can be closed to localise leaks in separate struts.

The pump placed on the kite measures the pressure inside the inflatable structures. If the pressure is too low, the pump will raise the pressure back to its operational pressure. When the operating time of the pump suddenly goes up, it means there is a leak. If the damage is minor, it can be repaired on site. With the system, a kite repair set will be delivered, containing scissors, special glue for tears, adhesive tape for the canopy and structure, bladders for pinholes and stick-on valves [72]. Next to the pressure readings from the pump, every time the kite lands, a visual inspection is performed on the non-inflatable structures of the kite, such as the canopy. During the launching and landing procedure, the wear and tear on the kite will be minimised by

avoiding sharp terrain.

Kite Control Unit

For the KCU, checking the software is of primary importance. The control computer is a complex system, where bugs can occur. One bug can easily crash the whole system. Therefore, the software should be validated and updated occasionally. Furthermore, the hardware, like sensors, actuators, and the cable management, should be checked, to see whether they are still intact. Lastly, before every flight, the control system should do a test run. The movement of all the actuators is checked just like an aircraft pilot checks the ailerons and rudder. This ensures that the kite can fly the optimal path when in the air. For durability, the KCU is placed in a compartment with an IP65 rating [73].

Tether and Bridle Line System

A critical component is the line system that transfers the aerodynamic forces from the kite to the ground. This system consists of the main tether line and smaller bridle lines. These lines are very thin and damage leads to an inoperative system as catastrophic failure looms. Due to the constant rolling back and forth over the spindle and drum, fatigue due to dynamic bending is expected to be the primary failure mode. Weak parts of the tether will be cut away as tether and bridles can be spliced together, which can be read in Section 12.2 and a splicing set will be provided with the system [74]. Despite that the tether can be spliced together, maintenance on the tether should be avoided, due to the poor reachability of the tether. When the system is not in action, the tether is tightly rolled on the drum. If maintenance is needed, the tether must be unrolled from the drum.

It should be avoided that this dirt will accumulate, or is brought into the drum, potentially causing damage. For example, the coating can sand off, leading to a higher risk of wear. For cleaning of the tether, a small brush cleaning instrument is designed. This cleaning instrument is shown in Figure 6.4. This instrument can be attached to the swivel head when it is to be used. It will only be used after the kite is landed, when the tether is reeled in.

To ensure the tether does not break, a torque sensor in the drum is essential. If the tension in the tether rises above the safely assumed value, the tether is reeled out faster. This way it prevents breaking of the tether. Another component helps with keeping the tether clear of dust and stones. During in-air operations, the kite, tether, and control system will collect dust and other types of dirt. In addition to in-air operations, with launching and for landing, the airborne system will lie on the ground. For the tether, this means it will be dragged over the ground for a short period. This could result in the collection of larger chunks of dirt, or small stones. The last method to increase the operational lifetime of the tether, is by turning the tether around at the end of its operational lifetime. The lowest part of tether is constantly reeled in and out around the drum and will reach its maximum operational life due to fatigue bending. The upper part of the tether is only wound around the drum with low force during the starting and ending phase of the operation, resulting in almost no bending fatigue. When the tether is turned around, the roles are changed and the operational life of the tether will be doubled.

Ground System

The ground system is relatively easy to maintain. The components can be inspected without having to disassemble much. With visual inspection, oil leakages and loose bolts can be found. The lubrication of the drum is important for smooth operation of the system. To check if the lubrication is not contaminated or wrongly applied, an oil analysis sensor can be placed. Next to these sensors, a vibration sensor will be placed on the drum, generator, shaft, and gearbox, to detect vibrations of loose/damaged components or off-axis rotations. Vibrations can harm the bearings, frame or connection bolts of the ground system. Washers will be used to minimise the effect of the vibrations. If the bolts from the system are damaged, they are easy and cheap to replace.

Electrical Circuit

In the electrical circuit, there are three main components: the motor, the generator, and the supercapacitor. The motor is one of the more difficult subsystems to maintain, as it consists of commutators and brushes. These

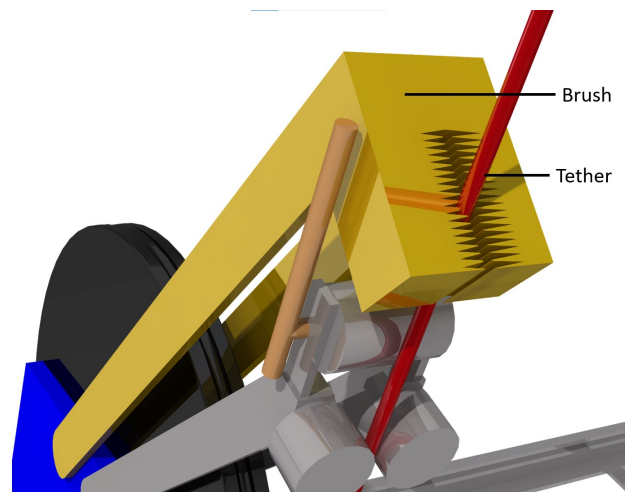


Figure 6.4: Visual of the brush placed on the tether.

can fail through threading, grooving, copper drag and flashover [75]. If the motor or generator malfunctions, the kite won't be able to reel out and reel in any more, resulting in system failure. The components should thus be cleaned properly. The temperature of the generator and car battery will be constantly monitored to prevent them from over- or underheating. If the temperature is out of bounds, the system will be stopped and checked for faults. The motor and generator are placed outside the drum for easy access during maintenance.

The other main component is the supercapacitor, which is used for short-term energy storage. It shows stable performance over long periods of time and needs little to no maintenance [76]. The voltage and current will be constantly monitored to detect deterioration of the system. If the measured values deviate from the nominal values, a check of the supercapacitor and cabling is needed. Only during a full system maintenance will the supercapacitor be checked.

Maintenance Interval

After every flight, the whole system is visually inspected for missing parts, tears in the canopy, cuts in the bridle lines or tether, and leaking lubrication in the drum and generator. Dust and stones will be removed from the canopy and tether to prevent extra wear. Furthermore, the actuation of the KCU will be controlled before every flight.

The number of FH will be measured by the system itself and automatic warnings will be given to the operator. After 336 FH, two weeks of full time operation, a more thorough check-up should be performed. The KCU and generator will be opened to check for internal damage, and the kite will be tested for airtightness with water and soap. Lastly, all the connections will be checked on their integrity and tightened if necessary. For example, bolts can become loose due to vibrations in the system.

Medium maintenance will be performed after 1263 FH, or 1 year if the number of FH is not achieved in those months. Firstly, the truck should be connected to Wi-Fi to check for an available software update for the KCU and ground station. An added benefit is, that with this Wi-Fi connection the health of the system can be monitored by the company and a specific maintenance schedule will be made. In every schedule, there will be standard maintenance tasks. Lubrication liquids will be replaced and bearings will be checked on where. Lastly, after 1263 FH, the tether will be flipped. The tether should be rolled off and on the drum in a clean environment while following the instructions with great care.

After 2526 FH, the operational lifetime of the tether is reached, as can be read in Section 12.2.3 and Section 6.5. The heavy maintenance will occur after 2526 FH, or 2 years if the FH are not met. Heavy maintenance will take the whole system apart and rebuild it up with original and replacement parts if needed. When the system is taken off the truck bed, the structural rigidity of the truck bed will be checked as well. During this heavy maintenance, the tether will be replaced. The kite will be replaced after 4500 FH, as can be read in Section 18.1. The kite will be replaced once for every two times heavy maintenance is performed.

Spare Parts

For the maintenance of the system, tools and spare parts are vital. A basic tool set, splicing set, and kite repair set will be supplied along with the system. The needed spare parts heavily depend on the operational environment and duration. Based on the planned usage, the team can give personal advice about the spare parts list that should be taken along. This advice is based on experience during the testing phase and on feedback from sold systems and customers.

6.4.4. Rivian R1T Maintenance

All the subsystems of the AWES need regular maintenance. The Rivian R1T is not part of the AWES, but if the R1T is not working, it won't be possible to even start the operation [18]. For this reason, the Rivian R1T should be maintained. Rivian has created a phone application, that gives so-called "over-the-air updates" [77]. These updates contain information on important upgrades and improvements to the car. Sensors within the system of the car keep track of defects occurring and give a signal to the computer of the car. As soon as the car is connected to Wi-Fi, it updates the app and the owner receives a message about the errors. If necessary, mobile service technicians and roadside assistance can pass by and repair the car. This subsection is adapted from Section 8.2 in the Midterm Report [10].

6.5. End-of-life Analysis (F.5)

To determine the end of life of the system, one could both look to the amount of FH at which key components start to fail, or the system's lifetime. Firstly, the system is very modular, allowing to easily replace components that reached their end of life. Therefore, it is very hard to determine a point at which the system should be retired. From a sustainability point of view, it is always preferable to repair the system rather than replacing it. As the system does not rely on any critical structures which house the whole system that can age over time, making the system unreliable, replacing items can make the system last very long. However, as the AWE technology is expected to develop at a fast pace, the system will become outdated. A much more efficient system will be brought to the market at some point, making the first generation KITE-E system not interesting to operate any more.

The developments will apply to individual components, and it could be more interesting to refurbish the system, rather than retiring it. As components that reached their end of life, will be replaced by the newest generation of that component, e.g. a kite with better aerodynamic performance, or a thinner tether with a longer lifetime, this refurbishment will happen throughout maintenance systems when components get replaced. Table 6.5 shows the lifetime of every essential component in either FH or years. The kite and bridles lifetime, was determined to be 4500 FH. This was determined from private communication with the kite supplier [78]. When the system would be operated constantly during 30% of the year, this would give the kite a lifetime of 1.7 years. Furthermore, the tether lifetime is determined to be 2526 FH in Section 12.2.3, which would last 1.0 year for the same operation duration. The motor and generator lifetime were obtained from literature leading to 7.6 years and 20 years, before they should be replaced when the system would be operated constantly during 30% of the year. Lastly, for the drum and KCU the team came up with an estimate. The drum is made from aluminium and has a relatively simple design, which makes it a component that ages very slowly compared to other components. Therefore, it was chosen to last for 20 years, without looking at operating FH. The KCU lifetime was put at 5 years. This is because it is a modular system with a very good reparability. However, as kite and KCU technology evolve, the KCU might need to be replaced to fit the demands of the newly developed kite, due to which a lifetime of 5 years was chosen.

Bringing this together, it can be concluded that the user will have a completely 'updated' system after 20 years of operation. However, the driving performance components like the kite and tether will get an update more often, which will be highly beneficial for the system performance. When there is a more efficient kite, or a thinner tether, the area could go down, making either the operations easier, or increasing the power output. The generator can handle an operational output power of 30 kW before it reaches its limit, which leaves room for this increase in performance.

When a component of KITE-E system reaches the end of its lifetime, an end-of-life analysis will be performed. First, all the components are inspected to estimate the state of their condition. When the component is still in a relatively good condition, the component can be reused with little loss of performance. Some components can be reused after performing some repairs. Other components, however, will not be able to be reused. For these components, the materials will be examined and an estimation of the usefulness of the materials will be made. Some materials can be used in other applications, while other materials will not be reused.

Table 6.5: Lifetime of essential system components.

Component	Lifetime
Kite and bridles	4500 FH
Tether	2526 FH
Motor [79]	20 000 FH
Generator [80]	20 years
Drum	20 years
KCU	5 years

Resource Allocation

This section aims to provide an overview of the updated identification and allocation of resources for the AWES project. This process is divided into two categories to structure the allocation. First, Section 7.1 provides a subsystem budget allocation for the technical resource, based on a revision after the preliminary sizing from the Midterm Report [10]. This is followed by an organisational resource allocation in Section 7.2.

7.1. Technical Resources

This section aims to come up with mass, size, power and cost budget allocations for three main AWES systems: airborne, control and ground system. First, a general power budget allocation is discussed. Next, the airborne system (AB) allocations are discussed based on the preliminary design. This is followed by budget estimations for the ground and control systems, based on reviewed historical data. The main assumption for the cost allocation is that development, manufacturing and transportation costs are integrated in the determined budgets.

In order to provide a safety buffer to allow for contingencies, a 15% margin w.r.t. to the maximum allowed budgets is considered (compliant to the established contingency management values [18]). This leads to a current design limit of €38 000 for the total cost, 425 kg for the mass and 1.80 m³ for the total volume, deducted from the budget constraints in AWE-CON-DES-01 to AWE-CON-DES-03.

Power Consumption

The airborne control (consisting of KCU, airborne sensors and pump) is estimated to consume 50 W nominal power, this should be provided by an airborne wind turbine. Secondly, the ground control system (including sensing, communication, actuating) is estimated to consume a nominal power of 150 W. This should be provided by the supercapacitor and produced by the motor-generator during the reel-out phase. Therefore, the AWES nominal cycle output power should be 20150 W to have a nominal net electrical output power of 20 kW.

Airborne System

Using the preliminary estimated 21.54 m² projected area and 26.76 m² total area for the lifting surface, volume, mass and cost estimations were done based on historical data. Assuming a 0.424 kg/m² scaling, the LEI kite and bridle mass is obtained to be 11.34 kg. Considering that a 9 m² fits in a 15 l backpack, the kite's volume is obtained by scaling, using $15 \times 10^{-3} \times \frac{21.54}{9} = 35.9 \times 10^{-3} \text{ m}^3$ [18]. Lastly, the kite's cost is estimated based on a cost of €7/ft² [78]. Scaling this with the total area leads to an estimated and rounded cost of €2000, similarly, the mass and volume are divided by a factor 2.

Using the preliminary estimated 8 mm Sierra Dyneema® tether with a length of 675 m, the volume is estimated to be 34 l. Using a 3.6 kg/100m specific mass, the tether is estimated to weigh 24.3 kg. As discussed in the Midterm Report, these estimations are based on conservative safety factors [10]. Therefore, these values are expected to decrease in value throughout the detailed design. Finally, using a cost of €8.4/m, the original 8 mm tether is estimated to cost €5670. Since the preliminary estimate was highly overdetermined, this eventual cost is believed to be halved. Therefore, a cost budget of €3000 is decided to be allocated for the tether.

The in-air wind turbine should be able to deliver 50 W of power to the KCU, airborne sensors and kite pressure pump. Therefore, a general scaling method based on the wind power equation is used. This equation is presented by Equation (7.1) [81].

$$P = 0.5 \times C_P \times v_{true}^3 \times \rho \times A_{rotor} \quad (7.1)$$

Where v_{true} is the true airspeed (20 m/s), A_{rotor} is the rotor swept out area, C_P the power coefficient (0.25 [81]) and ρ the air density (1.19 kg/m³ [18]). From Equation (7.1), A_{rotor} is obtained. From this swept out area, the rotor diameter is found to be 23 cm and rounded to 25 cm, using $D_{rotor} = \sqrt{4 \times A_{rotor} / \pi}$. The mass estimation is based on a 6.8 kg three rotor blades with a 1.3 m diameter, leading to a 5.23 kg/m ratio. Scaling this with the obtained 25 cm rotors and assuming a safety factor of 2 to account for the needed casing and protection, a mass of 2.5 kg is obtained. Finally, This rotor, including a safety casing, is assumed to have 0.4 m x 0.4 m x 0.1 m dimensions and takes up 16 l of volume. Due to this added casing and design uncertainty, the weight is multiplied by a safety factor of 3 to account for this. Finally, this turbine is estimated to have a specific cost of €9/W [81], leading to a total cost of €450, which is rounded to €500 for this cost allocation.

Control System

The control system (CS) consists of a mix of components with determined parameters from the preliminary design and newly established components that require parameter estimations. Especially for the cost budget, estimations are carried out based on historical data and adjusted according to this project's AWES. Therefore, the cost allocation is performed at the end of this subsection.

The KCU is estimated to weigh 8 kg, based on the existing V3 KCU [82]. Including the casing to prevent damage from falling impacts, the total KCU weight is estimated to be 15 kg, based on the 23 kg KCU system from the 100 kW Falcon system [83]. This 15 kg is used as the Falcon's KCU already includes a wind turbine, battery pack and airborne sensors. The KCU dimensions are estimated based on scaling of an existing KCU for a 6 m² projected area kite [84]. The KCU's dimensions (no casing) are estimated to be 0.4 m x 0.2 m x 0.15 m, and is assumed to consume 50 W of average power.

Next to the KCU, the control system also contains sensors, computers and communication items. Since these elements have not yet been discussed in detail, only raw estimates for mass, size, cost and power consumption can be made. Therefore, the sensors are estimated to take up a combined space of 20 l, whereas the computers and communication items would only take up 10 l each. For power consumption, the computers are the main power demanding elements with an estimated average power demand of 100 W, with the communication elements and sensors each estimated to consume 25 W. Before diving into the cost allocation, the masses for the computers, sensors and communication items are roughly estimated to be 5 kg, or 2.5 kg each.

In total, the control system is allowed to take up €17500 of the current €38000 cost budget. This value corresponds to 46% of the total, margin accounted budget and is found to be in congruence with literature [85]. Within the control system, the costliest elements are determined to be the sensors, mainly due to the costly IMU's (€2500/piece [86]) and hence got a cost budget of €7500. This is followed by the KCU's budget of €5000 and control computers' budget of €3500. Finally, the communication items are allowed to cost €1500 with the current total design budget.

Ground system

The technical resource allocation for the ground system is based on a similar approach when compared to the control system. As some components are already investigated in the preliminary design and other newly identified components are combined, a hybrid between the obtained results from the preliminary design and raw estimates is used for the budget allocations.

Firstly, the drum is estimated to have a 0.65 m diameter and 1.03 m length from the preliminary design [10]. This would lead to a volume of 1.36 m³. During reel-out, a continuous electrical power of 25.9 kW needs to be generated by the motor-generator. For this operation, a 40 kW nominal power DC motor-generator is used [10, 87]. Estimated mass and dimensions based on existing motor-generators are found to be 210 kg and 0.36 m x 0.52 m x 0.36 m respectively, leading to a volume of 67 l.

The supercapacitor needs to provide power to both the ground control system and to power the reel-in phase. In total, the capacitor needs to provide 69.6 Wh/cycle (including a 1.2 safety factor) [10]. Using a 9 Wh/kg specification, the mass is found to be 7.73 kg, with a corresponding volume of 2.32 l (using 30 Wh/l) [10].

The ground system also contains pulleys, a spindle motor, electrical wiring, inverters, charge and motor controllers and the kite's clamps. Since only little information is known about these components, they are grouped as miscellaneous items. This implies that individual component estimates are not possible at this stage, and it is therefore assumed that they fill up the remaining ground station (GS) budgets. For mass and size, this leads to an allowable 55 kg and 0.25 m³ respectively.

In total, €15000 was allocation to the ground station, corresponding to 39% of the total AWES cost budget. This value is in congruence with literature obtained cost splits [85]. The motor-generator was estimated to have a €6500 cost allocation since it is the main component for power generation, followed by an estimated cost of €4000 for the drum. The supercapacitor has a €1500 cost allocation, corresponding to a €21.5/Wh specific cost [88]. Finally, the miscellaneous items have an allocated cost of €3000 to fulfil the foreseen ground station mass budget.

Summarising Overview and Budget Evolution

A summarising overview of the high level technical resource allocation is provided by Table 7.1. As mentioned before, this allocation allows has a 15% margin to the absolute design limits as a contingency measure. Following these estimations, Figure 7.1 to Figure 7.3 show the budget's evolution when compared to the pre-design established budget allocation.

Table 7.1: Budget allocation per subsystem.

		Cost €	Power W	Mass kg	Size m ³
1. Airborne System		5500	50	30.99	0.069
	1.1 Kite and Bridles	2000	0	11.34	0.036
	1.2 Tether	3000	0	12.15	0.017
	1.3 Wind Turbine	500	50	7.50	0.016
2. Control System		17500	-200	27.5	0.042
	2.1 KCU	5000	-50	15	0.012
	2.2 Sensors	7500	-25	2.5	0.02
	2.3 Computers	3500	-100	5	0.01
	2.4 Communication items	1500	-25	2.5	0.01
3. Ground Station		15000	20 150	367,73	1.68
	3.1 Motor-Generator	6500	20 250	210	0.067
	3.2 Supercapacitor	1500	0	7.73	0.00232
	3.3 Drum	4000	0	100	1.36
	3.4 Miscellaneous	3000	-100	55	0.25
Total		38000	20000	426	1.80

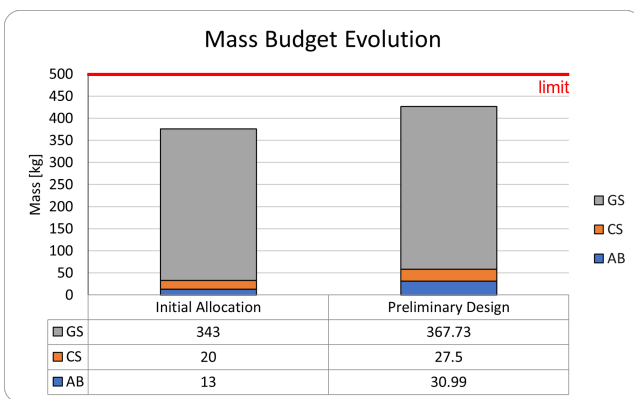


Figure 7.1: Mass budget evolution and split.

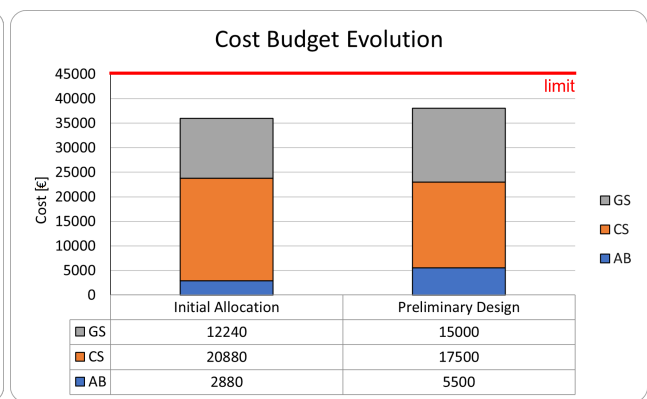


Figure 7.2: Cost budget evolution and split.

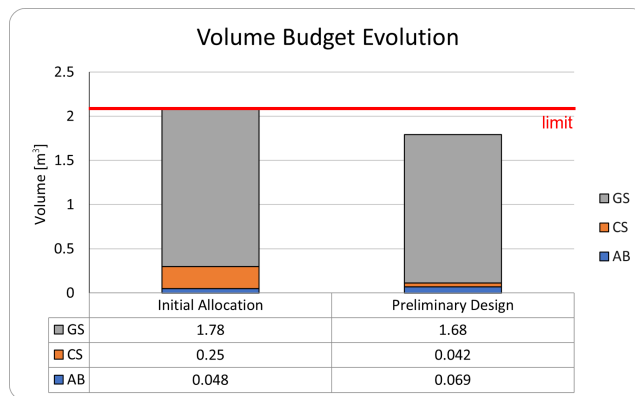


Figure 7.3: Volume budget evolution and split.

As observed in Figure 7.1 and Figure 7.2, the mass and cost budgets have generally risen. This is because of the higher level of available detail. It allows having smaller margins to the specified design limits, while still accounting for contingencies. For the control system cost, the allocated budget has shrunk from the initial cost allocation to the current allocation. This decision was taken based on a revision of the literature’s percentage-wise split. This resulted from the additional gained information throughout the earlier design stages.

Finally, Figure 7.3 shows the updated volume budget. The main observation from this graph is the declining volume. Since there was no margin in the initial allocation, the volume allocation after the preliminary design was decided to include a margin to account for design contingencies and unusable space.

7.2. Organisational Resources

The project is split into seven stages: design (1), prototype testing (2), production (3), integration (4), operation (5), maintenance (6), and end-of-life (7). Each of these phases require their own specific organisational resource allocation to ensure a proper process flow. The main organisational resource aspects are:

- **Working Staff:** Working staff relates to human resources. This includes all personnel required to develop, manage, build, operate and maintain the AWES. The identified working staff is listed below:
 - Management (MGMT) – Mechanics (MECH) – Research and Development (R&D)
 - Operation (OPS) – Manufacturing (MFG)
- **Time:** Time is a major dimension in any project. It is used as a planning resource and induces delay risks.
- **Tools:**
 - Hardware (HW) – Machinery (MACHY)
 - Software (SW) – Working tools (WT)
- **Facilities/Locations:**
 - Research facilities (RF) – Testing facilities (TF) – Maintenance facilities (MF)
 - Production facilities (PF) – Operation site (OS)
- **Sustainability:** Sustainability resources are considered to ensure coherence to the sustainability development strategy. The two items to track sustainability are listed below:
 - Waste (W) – External energy and emissions (EEE)

The waste is defined as excessive and inutile material or effort. This parameter is rated on a scale from 1-10 because of the variety of possible waste sources throughout the project. The energy and emissions resource is evaluated during each step in the project's process. Rating for this parameter is based on a percentage of the total project emission and energy consumption.

Now that all organisational resources are defined, they can be allocated to the different project stages, which were defined above. The allocation of the working staff, tools, facilities and locations is pretty straightforward. The time allocation, however, is difficult to estimate, since it is heavily dependent on the design choices that are made. For now, the design phase was estimated to be around two years based on the development time of already developed kite power systems [89]. Furthermore, the testing of the prototype was estimated to take around a month. Then, since the production phase is the phase that is most affected by the design choice, a rough estimate was made leading to an estimated time span of roughly six months [89]. Furthermore, the time for the integration of the AWES in the R1T, should be limited and was therefore estimated to take two weeks. Finally, the operations time and time for maintenance needed to be estimated. The total operations time of the AWES needs to be around eight years. This was estimated based on the Rivian's warranty on the battery [90]. The time needed for maintenance was estimated to be around a week per three months. This was estimated based on the fact that maintenance includes cleaning of the components, regular maintenance of the system, repairs and replacements.

The largest energy consuming stage is determined to be the production phase. Since material processing requires a lot of mechanical and thermal processes, the energy consumption will be high. Additionally, it is also the main contributor to waste production since a lot of material is discarded. Prototype testing is found to be a large waste contributor. This is because of the destruction related to failed tests and the discarding of inefficient potential components. The AWES operations phase generates energy from the wind and is energy-autarkic. Therefore, it is assumed not to produce emissions, nor use external artificial energy. It does however produce waste since components show degradation and need replacement. Lastly, the end-of-life phase allows reusability and recyclability. In these processes and because not all material can be reused/recycled, there is a significant waste generation. End-of-life processing requires energy consumption, but is limited in operation time. Table 7.2 shows the summary of the organisational resource allocation.

Table 7.2: Organisational resource allocation. Abbreviations in this table are taken from Section 7.2

	Working Staff	Time days	Tools	Facilities	Sustainability W, EE
Design	MGMT, R&D	700	HW, SW	RF	1, 5
Prototype Testing	MGMT, R&D, OPS	30	HW, SW	OS	6, 13
Production	MGMT, MFG	150	MACHY	PF, TF	7, 60
Integration	MGMT	14	WT	PF	2, 13
Operation	OPS	2920	HW, SW	OS	3, -
Maintenance	MGMT, MECH	224	WT	MF	1, 4
End-of-life	MGMT	14	WT	PF	3, 5

Risk Assessment

Unfortunately, with new innovations, come new risks. Therefore, it is essential to perform a risk analysis of the system. The results of the analysis can highlight the most critical risks. These need to be prevented and mitigated to keep the system operational for as long as possible. In Section 8.1 the risk identification method is explained using a scoring system for both the probability (P) and severity (S) of the risk. Afterwards, an analysis is performed per subsystem in Section 8.2, Section 8.3, Section 8.4, Section 8.5 and Section 8.6. In the last section, Section 8.7, the Fault Detection, Isolation and Recovery method is explained.

8.1. Risk Identification

In the previous report [10] a technical risk analysis was performed. Per subsystem, at least one failure event was analysed using the Failure Mode and Effect Analysis (FMEA) method [13]. The risk of the kite detaching from the ground system was established to be the most critical.

This risk analysis is more extensive. The system is divided into five subsystems: the launching and landing, the airborne system, the guidance, control and navigation system, the ground system and the power system. For each subsystem, between eight and eleven failure events have been established that form a risk for the functionality of the system. Each of these risks have a unique ID to use as reference in the continuation of the report. All the failure events have been assigned a score for its probability and severity. These scores are defined in Table 8.1 and Table 8.2.

Throughout the analysis of the subsystems, some mitigation methods are repeatedly used. First there is the "safe kite state". This is a pre-programmed software system in the KCU. If an issue occurs, but the kite is still controllable, the safe state is activated to keep the kite up in the air, but not in full operation until the issue is solved, or a landing is initiated. This state brings the severity score of the corresponding risk to 2. If an issue occurs that makes the kite uncontrollable, the weak link between the tether and the KCU is cut. The tether remains connected through the kite via the safety line, and the KCU stays connected to the kite through the bridle lines. This way an emergency landing can be initiated, and the kite will glide to the ground while slowly being reeled in. This mitigation method brings the severity to a score of 3.

Table 8.1: Probability definition for the failure event [13].

Code	P Value	P Definition
A	1	Extremely unlikely (virtually impossible or no known occurrences on similar products or processes, with many running hours)
B	2	Remote (relatively few failures)
C	3	Occasional (occasional failures)
D	4	Reasonably possible (repeated failures)
E	5	Frequent (failure is almost inevitable)

Table 8.2: Severity definitions and harm of the failure modes [13].

Code	S Value	S Definition	Harm
I	1	No relevant effect on reliability or safety	No harm
II	2	Very minor, no damage, no injuries	Maintenance
III	3	Minor, low damage, no injuries	Harm to environment
IV	4	Moderate, moderate damage, injuries possible	Minor injury (e.g. bruise or small cut, operator harm and third person)
V	5	Critical	Major injury (e.g. by electric shock, by kite crash, from fire, smoke explosion)
VI	6	Catastrophic	Injury by kite collision or crash (many people)

8.2. Launching and Landing

The launching and landing phase is the first system to be analysed on risk. The criteria as described in Section 8.1 are used to score each failure event listed in Table 8.3. As can be seen, risk TR-LALA-10 “The operator being unavailable for landing” is the most critical risk. In Table 8.4 the risk map before risk reduction is visualised, whereas Table 8.5 shows the risk map after mitigation and prevention measures have been taken.

Table 8.3: Possible failure events regarding the launching and landing.

ID	Failure Event	Before Risk Reduction		After Risk Reduction	
		P	S	P	S
TR-LALA-01	The rope connecting the magnetic clamp and the launching equipment breaks.	1	4	1	2
TR-LALA-02	The launching equipment is pulled from the ground.	2	4	1	4
TR-LALA-03	The operator becomes unavailable during launching.	2	2	2	2
TR-LALA-04	The Rivian R1T compressor is malfunctioning and can not pump the kite.	2	2	1	1
TR-LALA-05	The kite is punctured due to sharp objects on the ground.	2	2	1	1
TR-LALA-06	The bridle system is tangled during launching.	2	2	1	2
TR-LALA-07	The wind speed is too low to launch the kite.	3	1	2	1
TR-LALA-08	Wind gusts are too strong, which makes the kite uncontrollable.	2	3	1	2
TR-LALA-09	The clamp release does not work.	2	2	1	2
TR-LALA-10	The operator becomes unavailable during landing.	3	3	1	3

8.2.1. Risk Prevention and Mitigation Methods

Most of the risks already have a relatively low score compared to other subsystem’s risks, but some can still be further improved. Below, for each risk, the possible prevention and mitigation options are listed.

- **TR-LALA-01:** The risk can be prevented by designing a rope that is extra strong, and reliably attached to the launching system. In case the rope disconnects, the risk can be mitigated by performing immediate landing or in when normal landing is not possible, an emergency landing is performed.
- **TR-LALA-02:** The risk can be prevented by ensuring that the launching equipment holds enough weight, so that the kite can not launch unintentionally and pull the equipment in the air. No mitigation strategy is present for this risk.
- **TR-LALA-03:** The risk that the operator becomes unavailable can not be prevented nor mitigated.
- **TR-LALA-04:** The risk can be prevented by installing the Rivian application that gives an update about bugs in the car. This will make it possible to repair the compressor before the operation starts. After failure of the compressor, the risk can be mitigated by bringing an extra air pump to the location.
- **TR-LALA-05:** The risk can be prevented by investigating the ground where the kite will lie, and removing sharp objects. The risk can be mitigated by using a repair kit, and repairing the kite.
- **TR-LALA-06:** The risk can be prevented by detangling the bridle system properly before launch. No mitigation strategy is present for this risk.
- **TR-LALA-07:** The risk can be prevented by checking the weather forecast before launch. This risk does not need to be mitigated any further.
- **TR-LALA-08:** The risk can be prevented by checking the weather forecast before launch. After failure, the risk can be mitigated by deflating the kite.
- **TR-LALA-09:** The risk can be prevented by installing an on/off button, such that the kite can be released once the power is switched off. If this also malfunctions, the power cable can be pulled out of its socket. No mitigation strategy is present for this risk.
- **TR-LALA-10:** The risk can be prevented by setting an alarm to prevent the operator from falling asleep. No mitigation strategy is present for this risk.

8.2.2. Results of Technical Risk Analysis

In the tables below, the risk maps before and after the prevention and mitigation measures have been taken are shown.

Table 8.4: Risk map for the launching and landing before prevention and mitigation.

Probability	Frequent					
	Reasonably possible					
	Occasional	TR-LALA-07		TR-LALA-10		
	Remote		TR-LALA-03, -04, -05, -06, -09	TR-LALA-08	TR-LALA-02	
Extremely unlikely				TR-LALA-01		
	No relevant effect	Very minor	Minor	Moderate	Critical	Catastrophic
	Severity					

Table 8.5: Risk map for the launching and landing after prevention and mitigation.

Probability	Frequent					
	Reasonably possible					
	Occasional					
	Remote	TR-LALA-07	TR-LALA-03			
Extremely unlikely	TR-LALA-04, -05	TR-LALA-01, -06, -08, -09	TR-LALA-10	TR-LALA-02		
	No relevant effect	Very minor	Minor	Moderate	Critical	Catastrophic
	Severity					

As can be seen in the both risk maps above, all the risks have been placed in the green area. Most of the risks were already in the green area, but the most critical risk, TR-LALA-10 "The operator needed for landing is unavailable." and risk TR-LALA-02 "The launching equipment is pulled from the ground." have been reduced to the green zone by applying prevention measures. The measures of risk TR-LALA-01 and TR-LALA-02 are directly related to its design, so during the final design phase, these measures should be taken into account.

8.3. Airborne System

The airborne system risk analysis in this section is performed conform to the described conventions in Section 8.1. The airborne system is considered to be the softkite, bridle system and tethering line, excluding the KCU, KCU power generator and airborne control sensors. An overview of the identified risks for the airborne system is displayed in Table 8.6.

Table 8.6: Possible failure events regarding the airborne system.

ID	Failure Event	Before Risk Reduction		After Risk Reduction	
		P	S	P	S
TR-AIR-01	The tether breaks.	3	6	1	6
TR-AIR-02	Kite control line breaks.	3	5	2	2
TR-AIR-03	Bridle line snaps due to high loads.	4	5	2	3
TR-AIR-04	Loss of pressure in inflatable tube system.	2	3	2	2
TR-AIR-05	Canopy ruptures at bridle attachment points.	2	5	2	3
TR-AIR-06	The kite canopy tears due to fluttering.	3	3	2	2
TR-AIR-07	Kite damage due to wet storage.	3	3	1	3

8.3.1. Risk Prevention and Mitigation Methods

The identified risks in Table 8.6 cause potential threats for the AWES. Therefore, prevention and mitigation strategies corresponding to individual risks are explained below.

- **TR-AIR-01:** The risk can be prevented by applying a safety factor and a tether coating during the design phase. In addition, the tether force is actively limited, and wind gusts should be anticipated based on the wind sensor positioned upstream of the kite. A weak link is introduced above the safety line to ensure that this part breaks first instead of the line. No mitigation strategy is present for this risk.
- **TR-AIR-02:** This risk can be prevented by providing a safety factor on the control line load. After failure, this risk is mitigated by the addition of a safety line, which breaks and depowers the system in case of an unsteerable kite.
- **TR-AIR-03:** This risk can be prevented by adding safety factors to the encountered bridle line loads. In case of a failure event, the safety line is cut and a controlled emergency landing is performed.
- **TR-AIR-04:** This risk can be mitigated by separating the strut elements from the leading edge tube by small one-way pressure valves, to separate leading edge (LE) and strut pressurised regions. A pump can be added to pump the inflatable tubes up in case of small pressure losses.
- **TR-AIR-05:** This risk can be prevented by placing the bridle attachment points to the struts in such a manner that the force is evenly divided over all the bridle points. The risk can also be mitigated by locally increasing canopy thickness at critical attachment points.
- **TR-AIR-06:** Since fluttering occurs at more freely moving elements, the trailing edge (TE) shape can be adjusted to limit the canopy fluttering.
- **TR-AIR-07:** This can be prevented by drying the kite after operation and applying a waterproof coating to the canopy.

8.3.2. Results of Technical Risk Analysis

The identified risks in Table 8.6 are displayed in Table 8.7 to visualise the probability and severity. A mitigated risk map is shown by Table 8.8, in which the prevention and mitigation adjusted risks are displayed.

As observed in Table 8.7, the most critical risks are TR-AIR-01,-02 and -03. These and other risks have been brought to acceptable risk levels by prevention and mitigation, as observed in Table 8.8. The majority of airborne system risks can be reduced by making appropriate design choices and should therefore be considered during the airborne system design development.

Table 8.7: Risk map for the airborne system before prevention and mitigation.

Probability	Frequent								
	Reasonably possible							TR-AIR-03	
	Occasional			TR-AIR-06, -07				TR-AIR-02	TR-AIR-01
	Remote			TR-AIR-04				TR-AIR-05	
	Extremely unlikely								
		No relevant effect	Very minor	Minor	Moderate	Critical	Catastrophic		
		Severity							

Table 8.8: Risk map for the airborne system after prevention and mitigation.

Probability	Frequent								
	Reasonably possible								
	Occasional								
	Remote			TR-AIR-02, -04, -06				TR-AIR-03, -05	
	Extremely unlikely							TR-AIR-07	TR-AIR-01
		No relevant effect	Very minor	Minor	Moderate	Critical	Catastrophic		
		Severity							

8.4. Guidance, Control and Navigation

The GNC system risk analysis performed in this chapter uses the criteria and scores as described in Section 8.1. The identified risks are defined in Table 8.9 together with their probability and severity, before and after applied risk reduction measures. Before the measures, the failure of the IMU or force sensor together with the malfunction of the GNC software of the kite are identified as the greatest risks. These risks before measures can also be seen graphically represented in Table 8.10.

Table 8.9: Possible failure events regarding the GNC system.

ID	Failure Event	Before Risk Reduction		After Risk Reduction	
		P	S	P	S
TR-GNC-01	IMU or force sensor malfunctions.	3	6	1	2
TR-GNC-02	General sensor failure.	3	4	2	2
TR-GNC-03	Actuator motor in KCU malfunctions.	3	5	2	3
TR-GNC-04	Steering lines fail.	3	5	2	3
TR-GNC-05	Main processor malfunctions.	2	6	2	2
TR-GNC-06	Communication system malfunctions.	3	5	1	2
TR-GNC-07	GNC software for the kite malfunctions.	3	5	3	3
TR-GNC-08	GNC software for the winch malfunctions.	3	6	3	2

8.4.1. Risk Prevention and Mitigation Methods

Many risks defined before are too large to be kept, and therefore risk reduction measures will be taken. Both measures to prevent the risk and measures to mitigate the effects are discussed.

- **TR-GNC-01:** The risk can be prevented by using a redundant tether force sensor and IMU, in addition the sensors can be frequently calibrated. The risk can be mitigated by generating a safe kite state and performing an immediate landing if the sensors malfunctions.
- **TR-GNC-02:** The risk can be prevented by calibrating the sensors frequently. The risk can be mitigated by generating a safe kite state until the issue is resolved.
- **TR-GNC-03, -04:** By introducing a large safety factor for the actuators and steering lines, the risk of failure is reduced. Otherwise, the risk is mitigated by cutting the safety line and performing an emergency landing.
- **TR-GNC-05:** The status, for example the temperature, of the main processor will be monitored and controlled to keep it in optimal conditions, to reduce the chance of failure. To mitigate the failure when it does happen, a safe kite state will be generated and landing will be initiated immediately.
- **TR-GNC-06:** Redundancy will be used as a prevention method to reduce the chances of failure. If it does occur, the kite will be put in a safe state and will be landed immediately.
- **TR-GNC-07:** This failure will not be prevented, but since the kite cannot be controlled anymore, the risk will be mitigated by cutting the safety line and performing an emergency landing.
- **TR-GNC-08:** There will not be a prevention method for this failure event, the severity will be lowered by placing the system in a safe kite state, and it will be further evaluated if landing is required or if the problem can be resolved in air.

8.4.2. Results of Technical Risk Analysis

In the tables below, the risk maps before and after the prevention and mitigation measures are shown.

Table 8.10: Risk map for the GNC system before prevention and mitigation.

Probability	Frequent	Green		Yellow		Orange		Red	
	Reasonably possible	Green		Yellow		Orange		Red	
	Occasional	Green		Yellow		Orange		Red	
	Remote	Green		Yellow		Orange		Red	
	Extremely unlikely	Green		Yellow		Orange		Red	
		No relevant effect	Very minor	Minor	Moderate	Critical	Catastrophic		
Severity									

Table 8.11: Risk map for the GNC system after prevention and mitigation.

Probability	Frequent	Green		Yellow		Orange		Red	
	Reasonably possible	Green		Yellow		Orange		Red	
	Occasional	Green		Yellow		Orange		Red	
	Remote	Green		Yellow		Orange		Red	
	Extremely unlikely	Green		Yellow		Orange		Red	
		No relevant effect	Very minor	Minor	Moderate	Critical	Catastrophic		
Severity									

When comparing the risk map before and after the prevention and mitigation, it can clearly be seen that the risk after is almost all in the green boxes. This means the prevention and mitigation methods proposed lowered the risk sufficiently. Especially, the risks resulting in catastrophic failure are well mitigated. Important to note is that some parts require a second one for redundancy, which needs to be taken into account for the budget.

8.5. Ground System

The ground system forms the basis on the ground for subsystems as the spindle and the drum. The criteria as described in Section 8.1 are used to score each failure event. From Table 8.12 it can be concluded that risk TR-GR-04 “The tether wears due to dirt/stones that get on the swivel and drum.” is the most critical risk. In Table 8.13 and Table 8.14 the risk maps before and after mitigation and prevention measures have been taken into account are shown.

Table 8.12: Possible failure events regarding the ground system.

ID	Failure Event	Before Risk Reduction		After Risk Reduction	
		P	S	P	S
TR-GR-01	The tether hits the sides of truck bed.	3	4	1	3
TR-GR-02	The motor malfunctions.	2	6	1	2
TR-GR-03	The car starts to slide.	3	4	2	2
TR-GR-04	The tether wears due to dirt/stones that get on the swivel and drum.	4	5	2	2
TR-GR-05	The operating person gets stuck in the drive train.	2	5	1	4
TR-GR-06	The spindle breaks.	2	3	2	2
TR-GR-07	The connection band between the gears of the drum and the motor breaks.	2	6	1	3

8.5.1. Risk Prevention and Mitigation Methods

Below, prevention and mitigation methods have been described per failure event corresponding to the ground system.

- **TR-GR-01:** The risk can be prevented by placing rails on the truck bed underneath the spindle. This way, the spindle and swivel can be shifted in front of the truck bed sides. Besides, the risk can be mitigated by placing small bumpers to soften the impact of the hit on both the tether and the truck bed sides.
- **TR-GR-02:** The risk can be prevented by properly maintaining the motor and checking it before usage on damage. Another way to prevent failure is to add sensors on the components, which measure their current status and condition, such as the power, voltage, current, and temperature. After failure, the risk can be mitigated by generating a safe kite state until the issue is solved.
- **TR-GR-03:** The risk can be prevented by placing the truck on its hand brake. Also, snow chains can be placed around the wheel to further prevent the failure occurring. For mitigation, a sensor in the car can be used to register its movement, after a set distance the tether forces can be lowered by depowering the kite.
- **TR-GR-04:** The risk can be prevented by guiding the tether through a brush that is placed on top of the spindle. To mitigate the failure, a safe kite state will be generated and landing will be initiated immediately.
- **TR-GR-05:** The risk can be prevented by placing warning stickers on the machinery and letting the operator follow a course regarding the usage of the machinery. The risk can be mitigated by placing emergency buttons within reach to shut down the whole system.
- **TR-GR-06:** The risk can be mitigated by disconnecting the spindle and letting the tether move freely over the drum. This way the tether can be reeled in with minimal damage.

- **TR-GR-07:** This risk can be prevented by placing a redundant band. The risk can be mitigated by placing brakes on the drum to still have the minimal controllability over the reeling in and out of the tether.

8.5.2. Results of Technical Risk Analysis

Table 8.13 and Table 8.14 are the risk maps where each risk discussed above is placed based on its probability and severity score. On the left, the risk map before prevention and mitigation is shown, and on the right after the measures are taken.

Table 8.13: Risk map for the ground system before prevention and mitigation.

Probability	Frequent					
	Reasonably possible				TR-GR-04	
	Occasional			TR-GR-01, -03		
	Remote		TR-GR-06		TR-GR-05	TR-GR-02, -07
	Extremely unlikely					
	No relevant effect	Very minor	Minor	Moderate	Critical	Catastrophic
Severity						

Table 8.14: Risk map for the ground system after prevention and mitigation.

Probability	Frequent					
	Reasonably possible					
	Occasional					
	Remote			TR-GR-03, -04, -06		
	Extremely unlikely		TR-GR-02	TR-GR-01, -07	TR-GR-05	
	No relevant effect	Very minor	Minor	Moderate	Critical	Catastrophic
Severity						

The situation before prevention and mitigation was not optimal, since only one risk was in the green area. However, after the measures have been taken into account, all the risk have been scored such that all of them are no longer a threat for the system. Risk TR-GR-01, -04, -06, -07 all have a prevention method directly related to the design of the system. It can therefore be concluded that these risks need to be taken into during the design phase of the system.

8.6. Power System

For the power subsystem, several risks can be identified. The risks are listed in Table 8.15. When the risks are known, methods for prevention and mitigation will be explored. The risks before the reduction strategies are applied are plotted in the risk map in Table 8.16, and after implementation of the reduction strategies in Table 8.17.

Table 8.15: Possible failure events regarding the power system.

ID	Failure Event	Before Risk Reduction		After Risk Reduction	
		P	S	P	S
TR-POW-01	Inverter, converter, or essential grid connection malfunctions.	2	6	2	2
TR-POW-02	The turbine on the KCU malfunctions.	2	5	2	1
TR-POW-03	The battery in the KCU is full, but still receives power from the turbine.	3	2	1	2
TR-POW-04	The generator receives too much mechanical power, harming the generator.	4	4	1	4
TR-POW-05	The generator malfunctions.	3	3	2	2
TR-POW-06	The supercapacitor is full and is still charged by the generator.	4	2	2	2
TR-POW-07	The battery of the car is full and is still charged by the generator.	3	2	1	2

8.6.1. Risk Prevention and Mitigation Methods

Many risks defined before are too large to be kept, and therefore risk reduction measures will be taken. Both measures to prevent the risk and measures to mitigate the effects are discussed below.

- **TR-POW-01:** The risk is prevented by adding sensors on the components, which measure their current status and condition, such as the power, voltage, current, and temperature. The risk can be mitigated by generating a safe state until the issue is solved or landing is initiated.
- **TR-POW-02:** The risk is prevented by increasing the size of the buffer battery in the KCU. The battery will be sized it can power the KCU for half an hour, the required time the system can perform reversed pumping. Furthermore, the battery enables the kite to use its normal landing procedure if the turbine fails.
- **TR-POW-03:** The risk can be prevented by adding a brake to the turbine, such that it stops producing power when the battery reaches 80% of its capacity.
- **TR-POW-04:** The risk can be prevented by adding brake on the drum, placing power sensors in the generator, and adding a safety factor to the maximum power of the generator.

- **TR-POW-05:** The risk is prevented by adding sensors on the components, which measure their current status and condition, such as the power, voltage, current, and temperature. The risk can be mitigated by using the motor to reel in the kite until it can land safely.
- **TR-POW-06:** The risk can be prevented by adding a charge control to the system, which has sensors on most components for measuring the power, voltage, current, and temperature, thereby performing monitoring at both component and subsystem level. The charge controller divides the current over the right component to prevent an overload.
- **TR-POW-07:** The risk can be prevented by adding a dump load in the system, which can convert the excessive power into heat to protect the system for an overload. Again, a charge control can be added to the system.

8.6.2. Results of Technical Risk Analysis

Table 8.16 and Table 8.17 are the risk maps where each risk discussed above is placed based on its probability and severity score. On the left, the risk map before prevention and mitigation is shown, and on the right after the measures are taken.

Table 8.16: Risk map for the power system before prevention and mitigation.

Probability	Frequent Reasonably possible	TR-POW-06		TR-POW-04			
	Occasional	TR-POW-03, -07		TR-POW-05		TR-POW-02, TR-POW-01	
Remote							
Extremely unlikely							
	No relevant effect	Very minor	Minor	Moderate	Critical	Catastrophic	
	Severity						

Table 8.17: Risk map for the power system after prevention and mitigation.

Probability	Frequent Reasonably possible						
	Occasional						
Remote	TR-POW-02		TR-POW-01, -05, -06				
Extremely unlikely			TR-POW-03, -07		TR-POW-04		
	No relevant effect	Very minor	Minor	Moderate	Critical	Catastrophic	
	Severity						

As can be seen in the risk maps in Table 8.16 and Table 8.17, with the current mitigation and prevention of the risks, the risks can be scaled down to a manageable level. TR-POW-07 was a critical risk, and is mitigated properly. Only TR-POW-01,-02,-04 can pose a risk to the system. The main risk prevention method is the charge controller, which measures the outputs, such as the power, voltage, current, and temperature, of the power subsystem.

8.7. Fault, Detection, Isolation and Recovery

FDIR is a vital part of the risk mitigation strategy of this design. Due to the high reliability necessary in both space industry and this AWE system, it is based on the FDIR framework used in the space industry with five hierarchical levels [91]. The target design for the FDIR is to prevent catastrophic failure scenarios based on the FMEA analysis performed per subsystem above. It combines a large part of the risk prevention and mitigation measures proposed above into the different levels of the FDIR architecture. The five levels work as follows:

- Level 0 is built-in monitoring on item level. Often software and hardware watchdogs are integrated into components and are examples for this level.
- Level 1 performs equipment level monitoring of the system for parts that cannot detect and recover issues by themselves. The use of redundant parts is an example for this level.
- Level 2 operates at the subsystem level and monitors their performances. An example is looking at the output voltage of the power system.
- Level 3 performs monitoring of the system level performance. If faults remain undetected through the lower levels of the FDIR they are caught by a flight anomaly detection system.
- Level 4 is a system level hardware-only monitoring aimed at preventing events with high severity. An example is the cutting of the tether for an emergency landing in the case of a major flight anomaly.

The mitigation measures, described in the subsystem risk chapters above, will be integrated into the level 0, level 1 and level 2 of the FDIR. Level 3 and level 4 will run independent of the flight software, preventing malfunctioning of the flight software to influence the performance of these vital levels of the FDIR.

The flight anomaly detection system, which is found in level 3 will use acceleration measurements, position data and steering motor commands. Three criteria are used to assess whether the flight is safe. These are that the kite is under control, the kinetic energy of the kite remains in a predefined region, and the position of the kite stays in the allowed operation zone. If this is no longer the case, and the issue has not been found on a lower level of the FDIR, the flight is terminated. A timer is used of a second before the FDIR system terminates the flight to prevent false activation of the system.

Design Procedure

Design is an integral part of product and system development. A well-organised and streamlined design process is therefore a necessity to ensure a detailed and consistent design. In this chapter, the design procedure for the KITE-E system is explained. First, in Section 9.1 the main functionalities, risks, and requirements that drive the design process are discussed. These are taken into account throughout the entire design process. Second, in Chapter 9 the design procedure described. The design procedure is a concurrent process, with many iterative and interdependent design elements of the system. The determination and calculation methods of the system element characteristics are fully integrated with each other, and are verified and validated as well. Finally, at the end of this chapter, an N2 design interaction is presented. This chart was used in the design process itself, and aids in giving an overview of all interdependencies and iterative design elements.

9.1. System Design Functionalities, Risks, and Requirements

The aim of the design process is to ensure that the system has the desired functionalities, and meets the requirements. As identified in Section 6.2, the main functionalities of the system during operations lie within the launching (F.3.3.2), landing (F.3.5.2), control (F.3.4.2), electricity generation (F.3.4.3) and utilisation (F.3.4.4). These are thus the main functions for which the system is designed. The main requirements driving the design, coming from Chapter 2, are the following:

- AWE-CON-CO-01: The total cost per airborne wind energy system shall be below €45,000-
- AWE-CON-DES-01: The preliminary design shall fit within the truck bed of the Rivian R1T.
- AWE-CON-DES-02: The preliminary design shall not exceed 500 kg.
- AWE-CON-SAF-01: The pickup truck shall remain static under the specified operational loads.
- AWE-TEC-PG-03: The power generation system shall have a nominal power output of 20 kW.
- AWE-TEC-CS-04: The control system shall provide fully automated pumping cycles.
- AWE-TEC-OPS-01: The launching and landing of the airborne system shall be a task for maximally one person.

Furthermore, there is a selection of risks, for which the prevention and mitigation strategies have a large impact on the design of all subsystems. The main technical risks which drive the design are the following:

- TR-AIR-01: The tether breaks.
- TR-GR-03: The car starts to slide.

9.2. Design Procedure and Interaction

The design of the total system was done in line with the idea of concurrent and integrated systems engineering. Throughout the design procedure the requirements were leading, in particular AWE-CON-DES-01 and AWE-CON-DES-02, as these requirements had a large role in the determination of the whole system integration and configuration. In addition, risk mitigation and prevention is practised in the whole design process, especially with regard to the risks TR-AIR-01 and TR-GR-03. Before initiating the design procedure, all subsystems, their characteristics and the ways in which they should be analysed were determined. Ways in which these analyses could be verified and validated were determined as well. Verification and validation has been performed throughout the design, this is presented in Chapter 16.

For the actual design, subsystems were parallelly analysed and designed at first, and then iterated and integrated with each other. This was done as the design of many subsystems and elements are dependent on design parameters of other subsystems. To have a complete overview of the way in which elements of the total system influence each other with respect to design, an N2 chart was made. This chart shows the design interaction between all system elements, and what specific parameters of these elements have an influence on other elements. The N2 chart can be seen at the end of this chapter.

In the N2 chart, it can be seen that there are a couple of subsystems which contain a reciprocal design dependency. Foremost, design interdependency is present between the power cycle, the tether geometric properties, and the kite aerodynamic and geometric properties. The power cycle, which is discussed in depth in Chapter 10,

determines operational characteristics such as the reel-out and reel-in speed, the traction force of the tether, and the kite area that is needed to optimise the power output of the system to meet requirement AWE-TEC-PG-03. Based on the characteristics of the power cycle, the power subsystems and element are sized in Chapter 10 as well. However, to determine these operational characteristics of the power cycle, initial aerodynamic parameters are needed, such as the lift over drag coefficient of the airborne system. These aerodynamic properties are determined in Chapter 11 via a vortex step model. The parameters that are determined by the power cycle optimisation, have in turn an effect on the aerodynamic properties.

Furthermore, the power cycle determines the traction force, dictating the tether diameter, which has a significant effect on the drag of the airborne system, and thus the lift over drag ratio. The tether dimensions are determined in Chapter 12, just like the bridles, kite material and configuration. The traction force also has a large effect on the anchoring design, as the truck might potentially be dragged or tilted due to a force that is too large. This would violate requirement AWE-CON-SAF-01, and is therefore investigated in Chapter 13. While a large part of the analysis to comply with requirement AWE-TEC-OPS-01 has been done in Section 6.3, the launching equipment has to be designed, which is done in Section 13.5 as well. In Chapter 14 a thorough analysis of the control system is done, and a KCU is designed to ensure compliance with requirement AWE-TEC-CS-04.

The power cycle, aerodynamic, structural, control, and ground system properties all have their own model and calculation programs. For a full design optimisation, all programs are integrated, meaning all inputs and outputs match, ensuring a consistent preliminary design. The result of this integration and optimisation is discussed in Chapter 15.

Main Power Generation System Characteristics

In order to produce the required output power, a power cycle has to be defined, that determines how fast the kite should fly during reel-in and reel-out. This, together with the wind speed and kite performance, defines how much power is generated on average during a power cycle. From this, a detailed analysis of all power cycle parameters can be performed, which allows for the sizing of many components of the system. Among these parameters are the kite area, the traction force carried by the tether, the power required or generated during the different phases of the power cycle and many more.

This chapter starts by defining the power system specific requirements, functionalities and risks that influence the design in Section 10.1, which sets the base of what should actually be achieved by the power cycle. Next, in Section 10.2, the Luchsinger model, which is used to define the power cycle is explained, followed by the calculation model and results of this model in Section 10.3 and Section 10.4. Afterwards, Section 10.5 shows a visual overview of how all the components of the power system are organised, followed by Section 10.6 which defines the efficiencies of those components. Next, the ground power system design, and all its components, is discussed and sized in Section 10.7 and lastly, the same is done for the in-air power system, presented in Section 10.8.

10.1. Power System Requirements, Functionalities, and Risks

This section's purpose is to highlight the isolated power related requirements and functionalities. This enables a better integrated subsystem design and allows to more easily integrate the subsystem in the larger project framework. The aerodynamics subsystem requirements are shown by Table 10.1. The main functionalities are electricity generation (F.3.4.3), and utilisation (F.3.4.4), as can be read in Section 9.1. Next to these requirements, the power subsystem is in charge of functionalities F3.4.3.A and F.3.4.4.A to generate and distribute the wind energy.

Table 10.1: Requirements on AWES Power Properties.

Identifier	Requirement
AWE-TEC-PG-02	The electrical wires shall be able to withstand a maximum current during nominal operation, including a safety factor of 1.2.
AWE-TEC-PG-03	The power generation system shall have a designed power output of 20 kW.
AWE-TEC-PG-04	The power generation system shall be able to operate under an environmental temperature range of -15 °C to 35 °C.
AWE-TEC-PG-05	The wing loading produced during nominal operations shall not exceed 750 N/m ² .
AWE-TEC-PG-07	The motor shall be able to support the revolutions per minute (RPM) experienced during reel-in during nominal operations, including a safety factor of 1.2.
AWE-TEC-PG-08	The motor shall be able to support the RPM experienced during reel-out during nominal operations, including a safety factor of 1.2.
AWE-TEC-PG-09	The power generation system shall have an efficiency of at least 50% during reel-in.
AWE-TEC-PG-10	The power generation system shall have an efficiency of at least 50% during reel-out.
AWE-TEC-PS-02	The energy storage shall be able to provide the motor with the necessary power to perform the reel-in manoeuvre.
AWE-TEC-PS-06	The energy storage system shall be compatible with the national power grid standards of the operating environment.
AWE-TEC-PS-07	The KCU shall be continuously powered to control the kite.
AWE-TEC-PS-08	The power management system shall be fully automated.
AWE-TEC-PS-09	The energy storage system shall be able to operate under an environmental temperature range of -15 °C to 35 °C.
AWE-TEC-PS-10	The energy storage shall be able to provide the ground control system with the necessary power to continuously operate.
AWE-TEC-PS-11	The energy storage system shall be equipped with an electrical load dump element.
AWE-TEC-PS-12	The generator power voltage shall match the required voltage level of the car battery.
AWE-TEC-PS-13	The voltage level of the motor shall match the voltage of the power provided by the short term power storage.

From the risk analysis performed for the power subsystem, a few extra components have been added. These are a charge controller, a dump load for the generator and a brake on the wind turbine on the KCU. Furthermore, the buffer battery on the KCU is increased in size to be able to provide power to the KCU for 30 minutes. The risks are shown in Table 10.2.

Table 10.2: Risks, with risk reduction measures influencing the power design.

Identifier	Measure
TR-POW-02	The size of the buffer battery is increased.
TR-POW-03	A brake is added to the turbine on the KCU.
TR-POW-06	A charge controller will be added to the system.
TR-POW-07	A dumpload will be added to the system.

10.2. Luchsinger's Model

In order to size most of the ground systems, a detailed analysis of the power and traction forces during different phases and conditions should be performed. This can be done by making an estimation of the power cycle of the kind using the Luchsinger model [2]. This model provides a set of equations, relying on and defining many parameters, with which the complete power cycle can be optimised.

10.2.1. Design Power Cycle

This model starts with the assumption that the traction force in the tether is equal to the lift produced by the kite. From this Equation (10.1) and Equation (10.2), which evaluate the traction force during reel-out and reel-in, are derived, based on the assumption that the traction force equals the lift generated by the kite. Here, the dimensionless force factors F_{out} and F_{in} , that depend on the aerodynamic coefficients, and dimensionless factors $\gamma_{out} = v_{out}/v_w$ and $\gamma_{in} = v_{in}/v_w$ are introduced. Furthermore, θ is the elevation angle of the tether.

$$T_{out} = \frac{1}{2} \rho v_w^2 A (\cos \theta - \gamma_{out})^2 F_{out} \quad \text{with} \quad F_{out} = \frac{C_{L_{out}}^3}{C_{D_{out}}^2} \quad (10.1)$$

$$T_{in} = \frac{1}{2} \rho v_w^2 A (1 + 2\gamma_{in} \cos \theta + \gamma_{in}^2) F_{in} \quad \text{with} \quad F_{in} = C_{D_{in}} \quad (10.2)$$

Next, knowing the traction force during both phases and the reeling speeds, the reel-out power, reel-in power, and the average mechanical cycle power can be calculated with Equation (10.3), Equation (10.4), and Equation (10.6) respectively, where P_w is the power density of the wind, defined by Equation (10.5). This is the actual power exerted on the generator by the tether, without accounting for any losses due to inefficiencies.

$$P_{out} = T_{out} v_w \gamma_{out} \quad (10.3) \quad P_{in} = T_{in} v_w \gamma_{in} \quad (10.4) \quad P_w = \frac{1}{2} \rho v_w^3 \quad (10.5)$$

$$P_c^M = P_w A (F_{out} (\cos \theta - \gamma_{out})^2 - F_{in} (\gamma_{in}^2 + 2 \cos \theta \gamma_{in} + 1)) \left(\frac{\gamma_{out} \gamma_{in}}{\gamma_{out} + \gamma_{in}} \right) \quad (10.6)$$

In Section 10.6 a power generation analysis is performed and the efficiency factors for the reel-in and reel-out phase, $\eta_{in} = 0.65$ and $\eta_{out} = 0.64$ respectively, are defined. Implementing those in Equation (10.6), the average electrical output power can be calculated with Equation (10.7). The electrical power generated during reel-out and required during reel-in can be found by multiplying Equation (10.3) by η_{out} and by dividing Equation (10.4) by η_{in} .

$$P_c^E = P_w A \left(F_{out} \eta_{out} (\cos \theta - \gamma_{out})^2 - \frac{F_{in}}{\eta_{in}} (\gamma_{in}^2 + 2 \cos \theta \gamma_{in} + 1) \right) \left(\frac{\gamma_{out} \gamma_{in}}{\gamma_{out} + \gamma_{in}} \right) \quad (10.7)$$

Now that the reeling speeds of the tether are known, and the complete power cycle is determined with the previous set of equations, the apparent speed of the kite can be determined during both reel-in and -out, with Equation (10.8) and Equation (10.9). Furthermore, the kite's cross wind speed during the figure of eight manoeuvres, $v_{k,c}$, explained in Section 14.3.1, can be calculated. This kite's cross wind speed can be found by assuming that the traction force during reel-out equals the aerodynamic force of the kite, with which the required apparent wind speed can be calculated. Then, by reforming Equation (10.8), with Equation (10.10), the kite's cross wind speed can be calculated.

$$\mathbf{v}_a = \mathbf{v}_w - \mathbf{v}_{out} - \mathbf{v}_{k,c} = \begin{pmatrix} v_w - v_{out} \cos \theta \\ -v_{k,c} \\ -v_{out} \sin \theta \end{pmatrix}, \quad v_a = \sqrt{v_w^2 - 2v_w v_{out} \cos \theta + v_{out}^2 + v_{k,c}^2} \quad (10.8)$$

$$\mathbf{v}_a = \mathbf{v}_w - \mathbf{v}_{in} = \begin{pmatrix} v_w + v_{in} \cos \theta \\ 0 \\ v_{in} \sin \theta \end{pmatrix}, \quad v_a = \sqrt{v_w^2 + 2v_w v_{in} \cos \theta + v_{in}^2} \quad (10.9)$$

$$v_{k,c} = \sqrt{v_a^2 - v_w^2 - v_{out}^2 + 2v_w v_{out} \cos \theta} \quad (10.10)$$

Furthermore, also based on the defined reeling factors, γ_{out} and γ_{in} , and the tether length used during operations, l_c , which was found to be 250 meters in Section 13.3, the total cycle duration can be calculated with

$$t_c = \frac{l_c}{v_{out}} + \frac{l_c}{v_{in}} = \frac{l_c}{v_w} \left(\frac{\gamma_{out} \gamma_{in}}{\gamma_{out} + \gamma_{in}} \right). \quad (10.11)$$

The individual durations of reel-out and reel-in can then be defined with Equation (10.12) and Equation (10.13) respectively [11]. Furthermore, the duty cycle, D, can be obtained, by taking the ratio of the reel-out duration

over the total cycle time, as can be seen in Equation (10.14). Next, those reeling durations can also be used to calculate the energy generated, E_{out} , or used, E_{in} , during both phases, by multiplying them with the power generated or required during that phase. Using those energies, the pumping efficiency, η_p , can be defined with Equation (10.15). Finally, the cycle efficiency can be calculated with Equation (10.16).

$$t_{out} = t_c \frac{\gamma_{in}}{\gamma_{out} + \gamma_{in}} \quad (10.12) \quad t_{in} = t_c \frac{\gamma_{out}}{\gamma_{out} + \gamma_{in}} \quad (10.13) \quad D = \frac{t_{out}}{t_c} \quad (10.14)$$

$$\eta_p = \frac{E_{out} + E_{in}}{E_{out}} \quad (10.15) \quad \eta_c = D\eta_p \quad (10.16)$$

10.2.2. Limitations

Even though the system is designed for a set design wind speed, during operations the wind speed is never constant. These fluctuations can become a serious issue when the limits of the system are reached. The limits that have been looked at and are of main concern are the limit imposed by the tether, at some point the force becomes too high, and the power limit, where the generator reaches its maximum power that it can generate. These limits will first be discussed separately, and then a so-called three-phase strategy will be discussed.

Tether limit

In the case that the tether will be limiting, the strategy to keep the tether force constant is to increase the reel-out speed, and consequently reduce the reel-in speed. These speeds are determined by again maximising power output, normalised in this case, for different reel-in and reel-out gammas. But in this case, the equation to maximise is slightly different, namely a new factor μ is introduced, which is the ratio between the current wind speed and the design wind speed. Furthermore, the reel-out gamma scales with μ and the optimal reel-out gamma, γ_{out}^{opt} , determined before, and this leads to a new expression for the reel-out speed:

$$\gamma_{out} = 1 - \frac{1 - \gamma_{out}^{opt}}{\mu} \quad \text{with} \quad \mu = \frac{v_w}{v_n} \quad (10.17)$$

$$v_{out} = v_w - v_n + \gamma_{out}^{opt} v_n \quad (10.18)$$

Combining this into the equation for power, this leads to the following equation to be maximised for varying γ_{in} :

$$\frac{P_c}{AF_{out}} = P_w \left(\frac{1}{\mu^2} \eta_{out} (\cos \theta - \gamma_{out}^{opt})^2 - \frac{F_{in}}{F_{out}} (\gamma_{in}^2 + 2 \cos \theta \gamma_{in} + 1) \right) \left(\frac{(\gamma_{out}^{opt} + \mu - 1) \gamma_{in}}{\gamma_{out}^{opt} + \mu \gamma_{in} + \mu - 1} \right) \quad (10.19)$$

Power limit

When the power limit, the wind speed at which the generator produces maximum power, is reached, the power, and with that the tether force, needs to be kept constant. Since the power and tether force are directly related, with the reel-out speed being the factor between the two, this means that this is also kept constant. This means γ_{out} needs to scale down, shown in Equation (10.21). To keep the power and tether force constant with increasing wind speed during the reel-out phase, the kite is depowered, which means that the F_{out} changes, shown in the following equation.

$$F_{out,\mu} = \frac{F_{out} (1 - \gamma_{out}^{opt})^2}{\mu^2 (1 - \frac{\gamma_{out}^{opt}}{\mu})^2} \quad (10.20) \quad \gamma_{out} = \frac{\gamma_{out}^{opt}}{\mu} \quad (10.21)$$

Combining these equations to find the optimal reel-in gamma leads to

$$\frac{P_c^E}{AF_{out}} = P_w \left(\frac{1}{\mu^2} \eta_{out} (\cos \theta - \gamma_{out}^{opt})^2 - \frac{F_{in}}{F_{out}} (\gamma_{in}^2 + 2 \cos \theta \gamma_{in} + 1) \right) \left(\frac{\gamma_{out}^{opt} \gamma_{in}}{\gamma_{out}^{opt} + \mu \gamma_{in}} \right). \quad (10.22)$$

10.2.3. Three Phase Strategy

To get a clear overview of what happens when the wind speed increases, the reeling speeds are divided into three phases. The first is the design case, where the wind speed is below any limit and the reeling speeds are optimised as discussed before, using

$$\frac{P_c^E}{AF_{out}} = P_w \left(\eta_{out} (\cos \theta - \gamma_{out})^2 - \frac{F_{in}}{F_{out}} (\gamma_{in}^2 + 2 \cos \theta \gamma_{in} + 1) \right) \left(\frac{\gamma_{out} \gamma_{in}}{\gamma_{out} + \gamma_{in}} \right). \quad (10.23)$$

At some point, the wind speed reaches a value at which the tether force would increase beyond its designed limited value. Here, the case of the tether limit is used to find the optimal reeling speeds. Lastly, the system reaches its design power at the design wind speed, the power limit. At this wind speed, the equations from the

power limit are used. What should be noted is that for both cases, the scaling factor μ should be based on the wind speeds at which the new phase is initiated.

10.3. Design Power Cycle Calculations and Results

The equations from Section 10.2 for a design power cycle with fixed wind speed, were all brought together in a python script to allow for an efficient and iterative design process. This is very important, as the power generation results are highly influenced by the aerodynamic characteristics, and the aerodynamic characteristics, on the other hand, are highly influenced by the required projected area of the kite, determined by the power cycle.

10.3.1. Calculation Model

The script used to perform all the calculations is visualised in a simple code block diagram in Figure 10.1. As an input it takes the design wind speed of 10 m/s which is defined in Section 6.2.4, the initial estimated projected area of the kite, which is also iterated during the calculation process, and the aerodynamic coefficients, defined in Section 11.4.1 and Section 11.6. This input data is stored in a python dictionary, which is then passed along from function to function, to add the calculated data, as can be seen in the code block diagram.

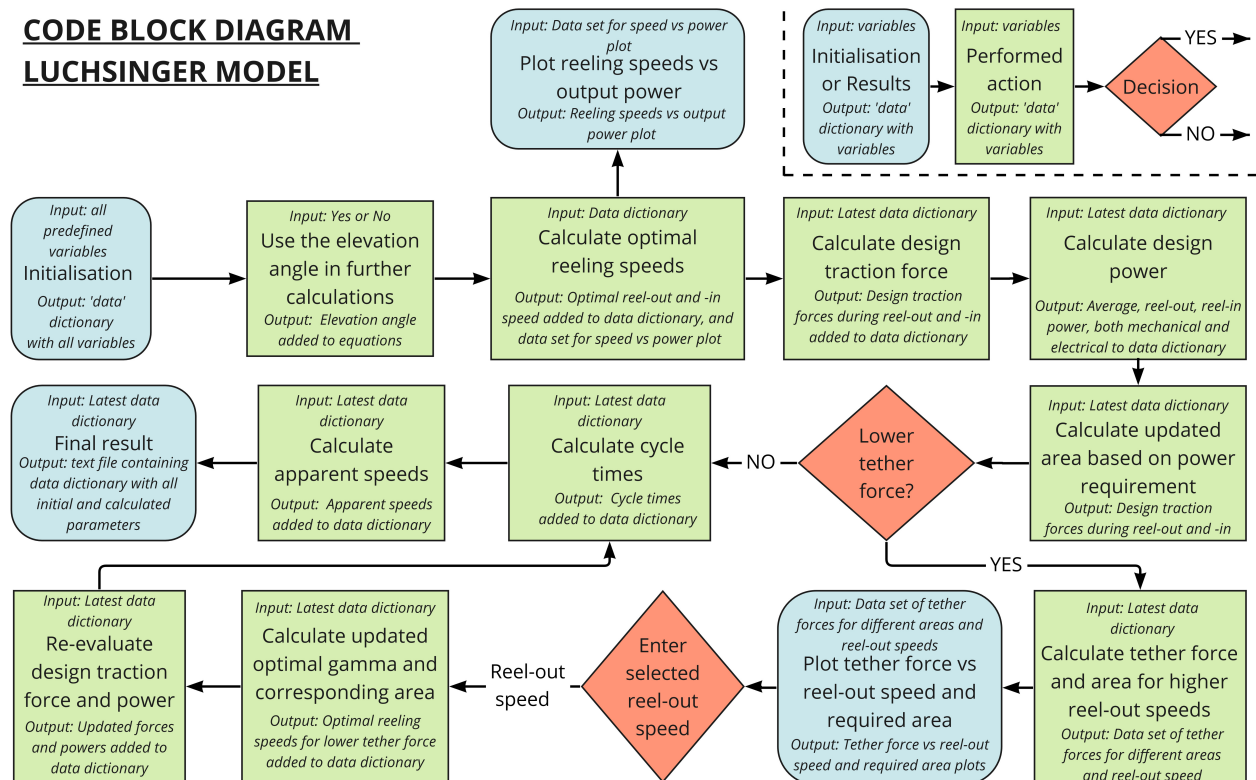


Figure 10.1: Code block diagram for the design power cycle calculations

Based on this initial input, the reeling speeds are defined. This is calculated based on Equation (10.7), which is evaluated for a set of different combinations of γ_{in} and γ_{out} . The combination that gives the highest average power over a cycle is then used to define the reel-in and reel-out speed. This is also plotted in Figure 10.2, using a heat map. It can be seen that high reel-in speeds, in combination with reel-out speeds around 30 percent of the wind speed, lead to the highest output power.

Once those parameters are known, the script goes on to define the traction forces during reel-in and -out with Equation (10.1). Those are then again used to define the output power generated during reel-out and the power required during reel-in with Equation (10.3) and Equation (10.4). Hereafter, the projected area of the kite is re-evaluated based on the power requirement AWE-TEC-PG-03, using Equation (10.7). If this newly calculated area does not match with the initial one, the user gets a message that this should be adjusted for optimal power generation and the projected area in the dictionary is updated. The functions calculating the traction force and power are then also rerun, so that the values are up-to-date with the latest projected area. Thereafter, based on everything that is known, the apparent wind speed and cross wind speed of the kite are calculated, and the duration of the cycle and different phases is determined in two separate functions.

When running this analysis, it was found that the traction force was too high during reel-out and would lead to

dangerous situations moving the car. As anchoring systems were already found to be very heavy, a solution had to be found to lower this force without lowering the output power. As the power depends on the force, multiplied by the speed, it was chosen to opt for a higher reel-out speed. Changing the reel-out speed, also changes the required area and has a different optimal reel-in speed, which is directly found using the optimal reeling speed function explained earlier. To understand how the traction force goes down, and how this influences the area, the traction force was plotted versus the reel-out speed and corresponding projected area in Figure 10.3. From this figure, a certain traction force can be chosen, after which the corresponding area and reel-out speed required to still meet the power requirement can be read off.

Once the new reeling speeds are set, the traction forces and powers during reel-in and -out are recalculated one more time, as well as the apparent wind speed, the kite cross wind speed, and the total cycle duration together with the duration of reel-out and reel-in.

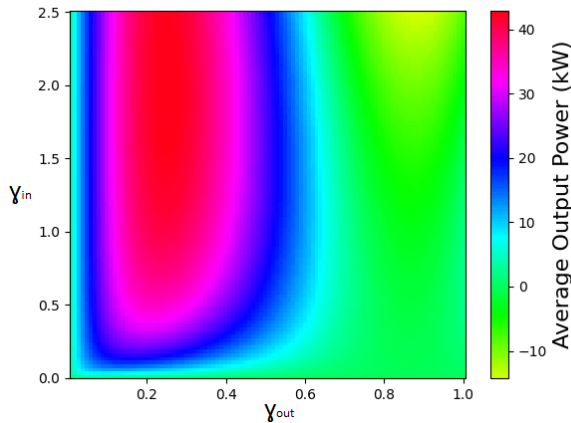


Figure 10.2: Heatmap showing the optimal reeling speed combination.

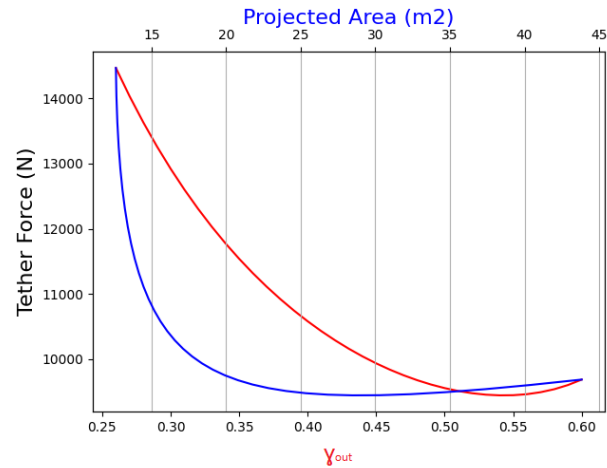


Figure 10.3: Traction force versus reel-out speed and the corresponding required projected area.

At the moment every power parameter was known, extra functions were added to the script, that help sizing the power components. In those functions, the reeling speeds are linked to a certain rotational velocity and this, together with the generated or required power, then allows to size the generator and motor. Furthermore, the energy produced during reel-out and needed during reel-in are computed to size the supercapacitor.

10.3.2. Results

The results for both the analysis without lowering the tether force and using the optimal reeling speeds, and the analysis where the tether force is lowered are shown in Table 10.3. All the initial inputs are defined in Table 10.4.

Note that the projected area increased significantly, as a compensation for the lowered traction force, which was lowered from 15 kN for the optimal case, to 10 kN. For this, the reel-out speed was increased, leading to a less optimal pumping cycle. The output table shows, the cycle efficiency decreased from 82% to 72%. As the reel-out phase goes faster, the duty cycle, which is the amount of time spent for reel-out relative to the total cycle duration, decreases significantly, causing a negative impact on the cycle efficiency. Furthermore, the total cycle duration consequently also goes down. As the cycle is shorter, there is also less energy produced over one cycle. Finally, because of this less efficient cycle, the power generated during reel-out is higher in order to still meet the required average electrical output power.

Table 10.3: Design power cycle output parameters.

Parameter	Unit	Before lowering traction force	After lowering traction force
Projected area	m ²	12.30	16.65
Optimal γ_{out}	-	0.25	0.43
Optimal γ_{in}	-	1.97	1.78
Traction force reel-out	kN	15.18	10.33
Traction force reel-in	kN	0.45	0.52
Average mechanical cycle power	kW	32.69	33.82
Average electrical output cycle power	kW	20.00	20.00
Mechanical reel-in power required	kW	8.84	9.21
Electrical reel-in power required	kW	13.55	14.12
Mechanical reel-out power generated	kW	37.96	44.27
Electrical reel-out power generated	kW	24.25	28.29
Total cycle duration	s	113	72
Reel-in duration	s	13	14
Reel-out duration	s	100	58
Energy generated during reel-out	Wh	673.73	456.72
Energy used during reel-in	Wh	47.74	50.26
Net energy generated per cycle	Wh	625.99	406.46
Pumping efficiency	%	93	89
Duty cycle	%	88.50	80.60
Cycle efficiency	%	82.36	71.73

10.3.3. Power and Aerodynamic Model Matching

As mentioned in Chapter 9, the power and aerodynamic characteristics heavily influence each other. It is therefore important that both calculation models are matched. In this case, the aerodynamic coefficients determined by the aerodynamic calculation model have a large influence on the power generation. The power generation calculation model then gives a projected area that is needed to generate the required power output. This change in projected area then changes the aerodynamic coefficients again, as different sizes lead to a change in kite drag, and a relative change in tether drag to the kite drag. Therefore, a script was written that uses both models, and iterates to a final set of aerodynamic coefficients, and a final projected area. This process was found to be convergent. The results of this process are already included in Table 10.3 above.

Table 10.4: Input parameters for calculating the design power cycle

Parameter	Unit	Value
Initial Projected Area	m ²	21.54
Design wind speed	m/s	10
Required average electrical output power	kW	20
Reel-out lift coefficient	-	1.06
Reel-out drag coefficient	-	0.15
Reel-in drag coefficient	-	0.10
Elevation angle reel-out	°	30
Elevation angle reel-in	°	70
Atmospheric density	kg/m ³	1.18
Tether reel-out length	m	250
Reel-in efficiency	%	63.5
Reel-out efficiency	%	65.2

10.4. Three-phase Strategy Calculations and Results

To create the diagrams for the limited cases, the wind speeds at which each of these occur, need to be determined. Since a limit is set on the tether force, when it reaches its maximum design load case, the power curve transitions into the tether limited case at the wind speed, v_{t_n} , at which this force is reached. This value is found by using Equation (10.1) and the design reel out gamma found, and setting this to the maximum tether force. The power limit is reached when the generator is at its limit, and cannot generate more power with increasing wind speed, which in most cases will be at the required power output. However, from the environmental analysis, it became clear that at places of interest, like Patagonia, the average wind speed is 13 m/s rather than 10 m/s, which is the average over all chosen locations. This brought up two options: sizing a different kite for every location, but this is thought to be too time intensive for the DSE project. This however leads to the system not reaching its full potential at all locations, which means a trade-off between the extra mass, volume and cost of a generator that is able to reach higher powers was made. This was found to be a minimal increase and fit in the design envelope. The decision was thus made to choose for a generator that was over designed for some locations, but allowed to get the full potential from the wind at all locations. This leads to a power output curve that has a higher possible wind speed than the design case, which can be seen in Section 10.4. Here the reeling speeds, both in and out, are shown in the left graph. In the right graph, the power output is shown, increasing up until the power limited wind speed. The red dotted line indicates the design wind speed, which will be used to further design and size the rest of the system.

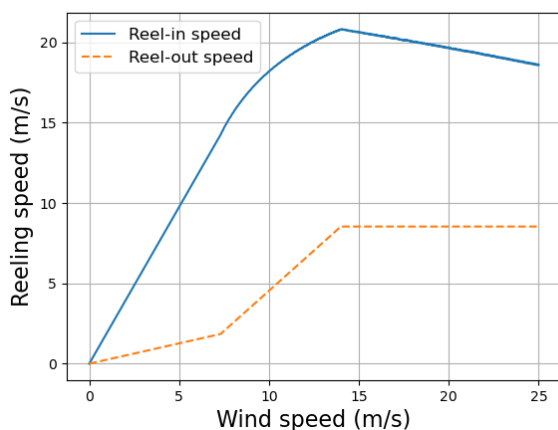


Figure 10.4: Reeling speeds versus to wind speeds

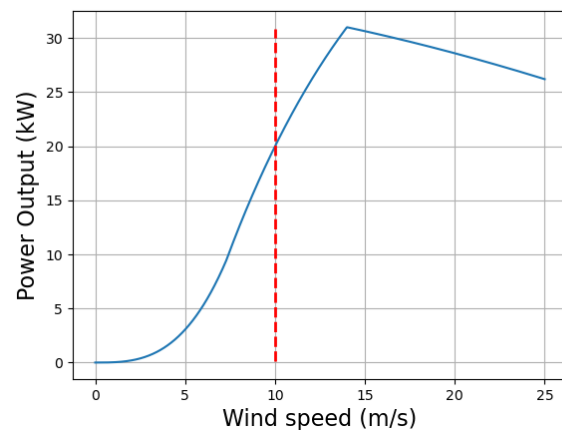


Figure 10.5: Power outputs versus wind speeds, with the red dotted line indicating the design wind speed

It is also of interest to look at what to do when these limits are reached. First, when the tether limit is reached at a certain wind speed, the tether should be reeled out faster, so that the tension force does not increase any further. How the traction force evolves over different wind speeds, can be seen in Figure 10.6. Secondly, once the power limit is reached, the tether cannot be reeled out any faster. In order to ensure that no more power or force in the tether is generated, there are two options. One could choose to either lower the angle of attack of the kite, so that it pulls less on the tether and generates less power, or to increase the elevation angle of the

tether. The second option is visualised in Figure 10.7 This causes the system to be less aligned with the wind, lowering the traction force and power.

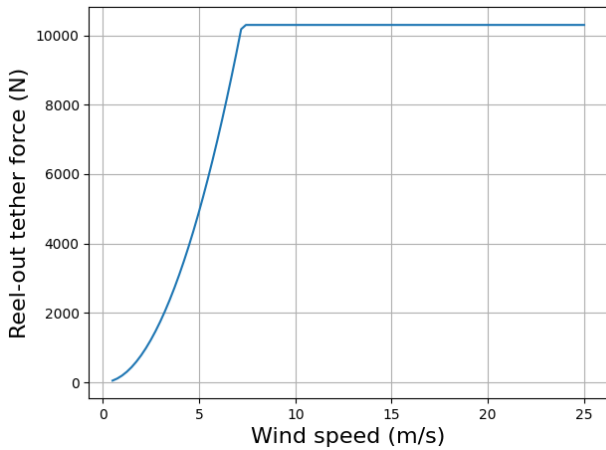


Figure 10.6: Reel-out tether force versus wind speed.

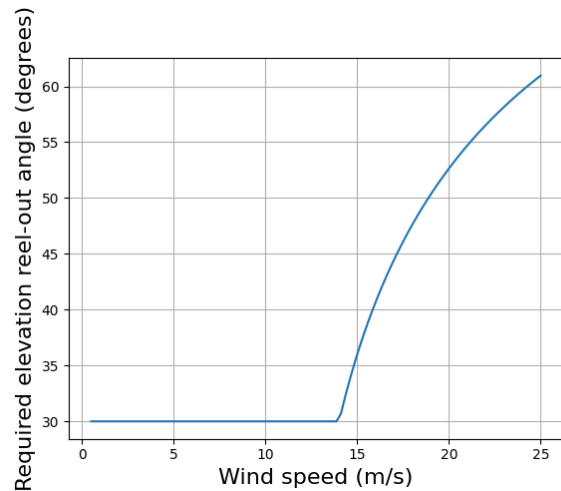


Figure 10.7: Reel-out elevation angle versus wind speed.

10.5. Electrical block diagram

The power system configuration will be explained with the help of Figure 10.8. The power flow for each operational phase can be seen with the four differently coloured arrows. The power flows along mechanical and power components, such as the drum and generator. If the model name and number of a component is known, it is portrayed in italics at the bottom of the component. The same is done for the power usage or storage capacity for a power component. The components that are specifically designed for the system’s purpose, will have the label "Own design". With the following example, the electrical block diagram is explained in more detail. When the kite is reeled out (Green full line arrow), the kite force is transmitted to the drum via the tether. With the gear and clutch, the mechanical energy is transferred to the generator, which transforms it to AC electricity. The AC electricity is divided by the charge controller over the supercapacitor, car battery, grid connection, and if needed, the dump load. Between these four components and the charge controller, an inverter or converter can be used to change the electrical current to DC or change the voltage. In the diagram, a connection between the car battery and the motor can be seen. This connection supplies the motor with electricity when the supercapacitor is empty, as can happen during the 30 minutes of reverse pumping.

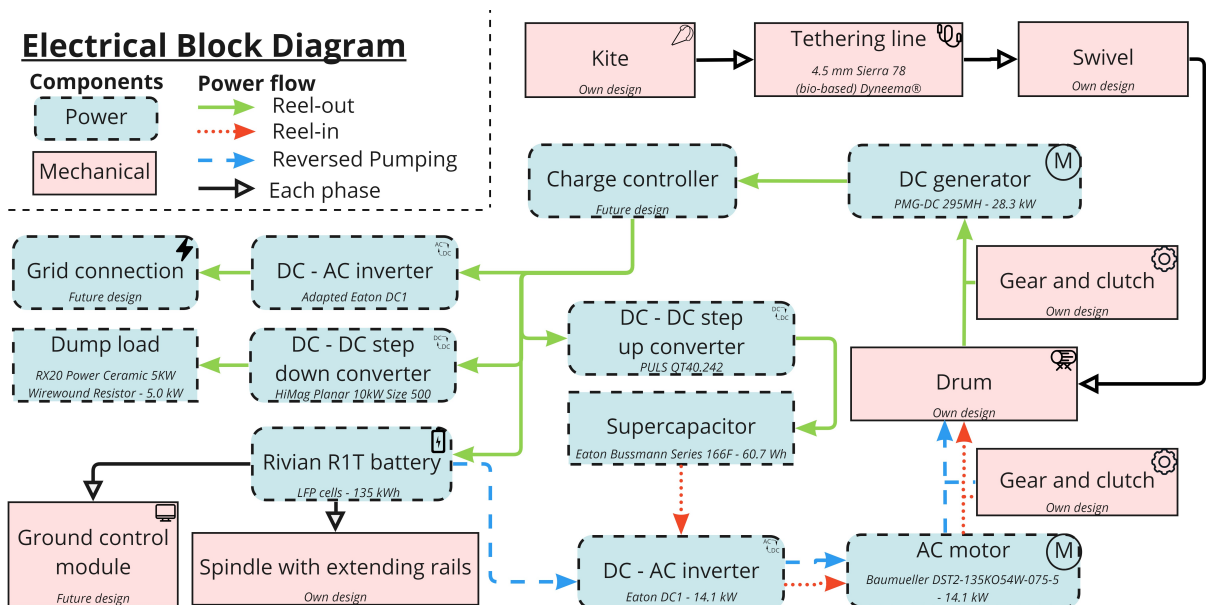


Figure 10.8: Electrical block diagram.

10.6. Power Component Efficiency Analysis

Losses are unavoidable during the conversion of mechanical energy to electrical energy. Equation (10.24) shows the equation for design electric energy, in relation to the phase duration and reel-in and reel-out mechanical power and efficiencies. This section is adapted from Section 9.2.4 in the Midterm Report [10].

$$E_{el\,design} = t_{cycle} \times P_{el\,design} = t_{out} \times P_{out\,mech} \times \eta_{mech \rightarrow el} - t_{in} \times P_{in\,mech} / \eta_{el \rightarrow mech} \quad (10.24)$$

where $P_{out\,mech}$ is the mechanical power that the kite can provide during the reel-out phase, $P_{in\,mech}$ is the mechanical energy invested during the reel-in phase. In order to transfer the mechanical power to electrical power and vice-versa, efficiency losses need to be taken into account.

Mechanical to electrical power efficiency and vice-versa are calculated as the product between the electrical path components' efficiencies as well as losses in the power cycle. A simplified approach for the power harvesting cycle efficiency would be to multiply the transition efficiency, which accounts for the fact that transition from reel-out to reel-in does not happen instantaneously, motor and generator efficiency, controller efficiency and frictional losses. At wind speeds in between 8-10 m/s, the transition efficiency is estimated to be 0.85 [11]. For a 20 kW system, the efficiency is 0.77, based on measurements and simulations from 2013. This paper achieved a simulated efficiency of 0.90 for the nearby future [11]. Table 10.5 shows an overview of the main contributors to both electrical and non-electrical efficiency losses. The motor and generator have an efficiency of 0.85 [92, 93]. Motors and generators have an efficiency curve depending on the load and rpm [94]. The gear will be chosen such that, under design conditions, the motor and generator operate near their maximum efficiency. The electrical power controller has an efficiency of 0.95 [93]. The electricity used by the main computer is neglected. The rotating drum and pulleys will have friction with the stationary frame. The friction can be minimised with bearings and lubrication to value of 1-2% [95]. The friction will increase if the rotational speed or torque on the bearing is raised [96]. For the reel-in efficiency, the reel-out efficiency is multiplied by the storage efficiency. Supercapacitors are a suitable storage system with an efficiency of 0.98 [94]. Multiplying all those losses, efficiencies of 0.652 and 0.639 during reel-out and reel-in respectively were found. All the efficiencies will be applied on the maximum theoretical power percentage that can be extracted from the wind, 4/27th of the total energy of the wind [97].

Table 10.5: Power efficiency overview (generator efficiency assumed to be equal to motor efficiency) [11].

Parameter	Transition	Motor/Generator	Controller	Frictional losses	Storage
Efficiency	0.85 [11]	0.85 [92, 93, 98]	0.95 [93]	0.95 [95]	0.98 [94]

10.7. Ground Power System Design

Now that the characteristics for the ground power system are calculated, it is time to start sizing components. These components are discussed in this section. First, the generator and motor are sized in Section 10.7.1. Secondly, in Section 10.7.2 the supercapacitor is designed. After that, the power overflow dump is discussed in Section 10.7.3. Lastly, the inverters and converters that are needed for the connection between components are presented in Section 10.7.4.

10.7.1. Generator and Motor

During the reel-out phase, the mechanical power generated by the kite should be converted to electrical power. For that conversion, a generator is used. On the other hand, during the reel-in phase, a motor will be used to drive the drum for reeling in the cable. Both systems will be coupled to one side of the drum via a gear with a clutch that can be decoupled. The team chose to size those to systems separately instead of using a motor-generator set, as the power during reel-in differs in magnitude from the power during reel-in and a motor-generator set would therefore not provide an optimal solution. Therefore, first, the generator will be sized and afterwards the motor.

Generator

For selecting a generator, the driving requirement is the electrical output power during reel-out, such that the average electrical output power from requirement AWE-TEC-PG-03 is met. This electrical output power during reel-out was found to be 28.38 kW in Section 10.3. Furthermore, it was decided to use a generator with a direct current (DC) output. This is discussed in the Midterm Report [10]. Taking the DC requirement and the required power output into

Table 10.6: Characteristics of the generator [99].

Parameter	Unit	Value
Max output power	kW	50
Max rotational speed	rpm	3000
Output power at 1500 rpm	kW	28
Output power at 2000 rpm	kW	36
Output power at 2400 rpm	kW	40
Mass	kg	63.5
Size (diameter x depth)	mm	450 x 281

$$RPM = 69.12P - 436.25 \quad (10.25)$$

account, a market analysis was done to find a suitable DC generator. A permanent magnet generator (PMG), made by 'NSM', a powertrain manufacturer, was found to be the best option [99]. More specifically, the 'PMG-DC 295MH' is selected, which is shown in Figure 10.10, of which the parameters are summarised in Table 10.6. The different powers for certain rpm from Table 10.6 were interpolated linearly, as speed and power are directly related and the values given in the table already follow a linear relation. This interpolation is given by Equation (10.25), where P is the output power.

First, this relation was used to evaluate the rotational velocity required for design conditions. This design condition requires an output power of 28.38 kW, from which a design speed of 1525 rpm follows. This differs from the speed of the drum during design operations, which was found to be 176 rpm during reel-out, based on the reel-out velocity and drum diameter. Therefore, a gear ratio between the drum shaft and the generator shaft of $176/1525 = 0.115$ was established. Furthermore, this relation is also important to rate the power at different turning speeds, as the speed of the drum will vary w.r.t different wind speeds. In order to keep the traction force, determined in Section 10.3, constant, the reel-out velocity of the tether changes with the wind velocity. After calculating this reel-out speed for different wind speeds, it was converted into rotational velocity of the drum, which with the chosen gear ratio results in a rotational speed and corresponding power based on Equation (10.25). This calculation was done for a range of wind speeds and plotted in Figure 10.9, for this plot the reeling speed changes such that the traction force is kept constant, after the tether limit has been reached. This happens at 7.3 m/s wind speed, which explains the slope change at that point. It can also be seen that the maximal rotational speed of 3000 rpm is met at a wind speed of 14 m/s. At higher wind speeds, the kite can not be accelerated any more, and thus needs to be either slightly depowered, or the elevation angle of the tether should be increased in order not to overload the tether. This means the power curve flattens out at the same wind speed.

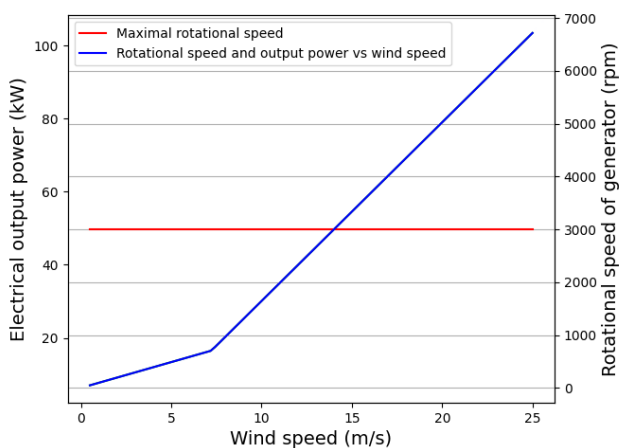


Figure 10.9: Rotational speed of the generator and corresponding power vs wind speed.

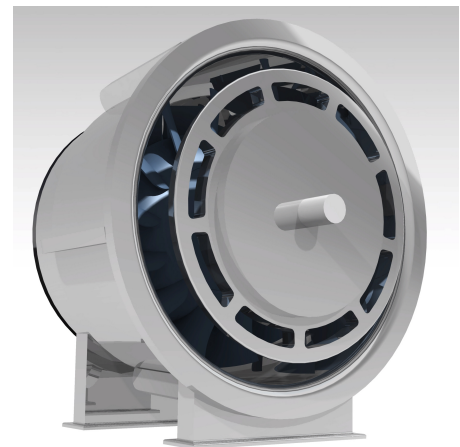


Figure 10.10: Visualisation of the generator.

Motor

The motor, on the other hand, should provide enough power to reel-in the kite. From Section 10.3, it is known that the mechanical power needed during this phase, and thus the power that this motor should output, is 9.34 kW. Furthermore, the torque, which is the radius of the drum times the reel-in tether force, also defined in Section 10.3, was found to be 122 Nm. Again, taking those needs into account, a market analysis was done, from which an AC motor with a maximal output power of 11 kW and torque of 140 Nm was chosen, providing some margin. More specifically, the 'Baumueller DST2-135KO54W-075-5' was selected [100]. A render of the motor is shown in Figure 10.11. Although the choice for a DC motor was taken in the Midterm Report [10], more detailed analysis showed that AC motors better fit the purpose of the system, as finding a DC motor with similar torque and power performance was very difficult. Therefore, as can also be seen on Figure 10.8, an inverter from DC to AC should be placed in between the supercapacitor and the motor. This inverter will be sized in Section 10.7.4.

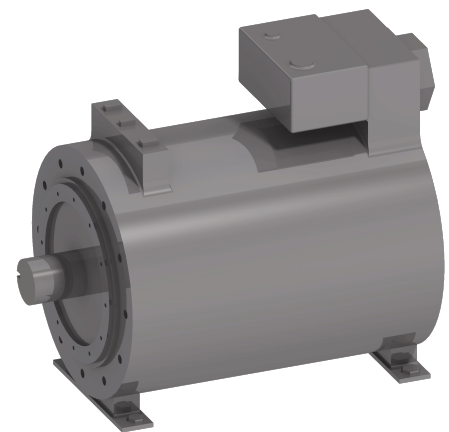


Figure 10.11: Visualisation of the motor.

10.7.2. Supercapacitor module

During the reel-in phase, energy being is consumed. This is a small part of the energy being produced during reel-out. However, this energy is not stored in the pickup truck's battery, but in a supercapacitor module, which is ideal for many repetitive recharge cycles. Those modules consist of supercapacitors which are connected in a combination of parallel and series connections.

From Section 10.3, it is known that the electrical power needed during reel-in is 14.32 kW for a duration of 13 seconds, resulting in a required storage of 50.26 Wh, using $E = P \times t$, where E is the energy, P is the power and t the duration. Adding a safety factor of 1.2, the amount of energy that should be stored is 60.31 Wh. This was formulated into requirement AWE-TEC-PS-02.

The team choose to select a supercapacitor that is available on the market and meets the requirement. After a broad analysis of this market, the Eaton Bussmann Series 166F Supercapacitor was found to give the best fit. Its characteristics have been summarised in Table 10.7 [101].

The energy stored in this supercapacitor can be evaluated with Equation (10.26).

$$E = \frac{1}{2} CV^2 \quad (10.26)$$

Using the parameters from Table 10.7, this equation gives an energy capacity of 60.68 Wh, which meets the required storage including the safety factor. The supercapacitor is visualised in Table 10.8

Table 10.7: Characteristics of the Eaton Bussmann Series 166F supercapacitor [101].

Parameter	Unit	Value
Capacitance	F	166
Max Operating voltage	V	51.3
Capacitance tolerance	%	-0 to +20
Operating temperature range	°C	-40 to +65
Equivalent series resistance (ESR)	mΩ	5
Mass	kg	14.7
Volume (W x L x H)	mm	177 x 421 x 196

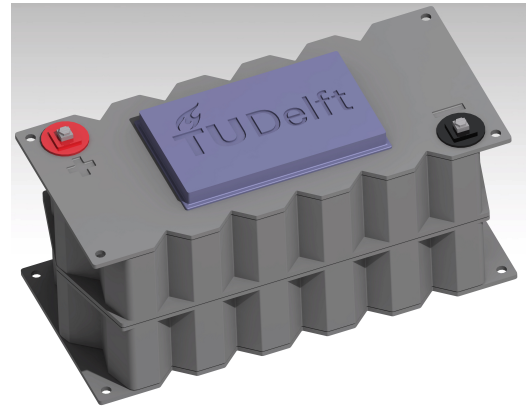


Table 10.8: Visualisation of the supercapacitor.

10.7.3. Power Overflow Dump

As the battery is being charged, the generated power is used for energy storage. When the battery is fully charged, the power generated at that instant can not be stored any more and should be used for other purposes. In this case, where the energy can not be internally absorbed any more, the excess electricity should be redirected to prevent an overload. For this system, an overload can be prevented in two ways, either the excess power is redirected to a power grid, or it is dissipated by an electric load dump.

When the system is connected to a power grid, a battery overcharge can easily be prevented by redirecting the generated power to the grid. This is controlled by the charge controller, which is responsible for sensing the battery charge levels and directing the generated electricity. In this operation, overcharging and its related overheating and potential burnout are omitted.

In the case where the kite system is solely used for battery recharging, the surplus electrical energy needs to be dissipated to prevent component damage. The most widely used application for this operation is resistive heating [102]. In resistive heating, electrical power is fed to a resistor, which dissipates the energy as heat. Because of this energy dissipation, the kite is assumed to be depowered right after full battery charging. As such, it is not producing design power. As an estimate, the system is assumed to produce 5 kW of power while transitioning from a fully powered state to the reel-in configuration.

Therefore, the AWES is equipped with an RX20 Power Ceramic 5KW Wirewound Resistor, produced by TongYueXin Commercial and Trading Co. Ltd. [103]. A visualisation of the dump load can be seen in Figure 10.12 An electrical load dump equipment with the aforementioned requirement is found to have a size of 0.1 m x 0.1 m x 0.55 m, an estimated mass of 20 kg and has a cost of \$30.04. Lastly, it requires an electric current ranging from 500 V to 10000 V.

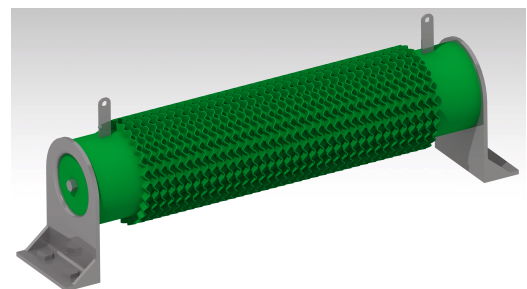


Figure 10.12: Visualisation of the dump load.

10.7.4. Inverters and Converters for Power Utilisation

When the system is working properly and the generator is producing power, the next step is to utilise this energy. The main purpose of the system, especially for the adventures, is to charge the batteries of the car. Secondly, the system will have an option to connect to a grid, for emergency relief or humanitarian peace missions. These uses require different kinds of electrical current. Some components need DC and others AC, at varying voltages. Therefore, inverters and converters are needed to change the type of current. Research has been done into this topic, which concluded that the detail level of this system is limited, both by a time constraint and a knowledge gap. This means that in this section the needs for this system are explored and documented, and a concept of a solution is presented, but to get the exact right solution for this problem, further designing needs to be done, by a person with more experience and knowledge in this field.

Charging Truck Battery

To get an idea of what is needed to be able to charge the truck, the properties of the truck's battery and charging options were researched. The truck can be charged by plugging into an outlet at home, so between 120 V and 240 V, to charge the batteries with 11.5 kW, which is the standard overnight charging power. Alternatively, there is a fast charging option, capable of charging with over 200 kW, with a voltage of around 400 V. Rivian also announced that they are working on increasing this voltage to 800 V. The output of the generator is around 350 V for the design case [99]. Since these voltages are quite close, it needs to be evaluated if a converter is needed to change this to the desired voltage or if it can directly charge the batteries. Again, a person with more knowledge in this field needs to look at this solution, especially the decision whether the system will hook into the fast-charging or the lower voltage option, since the power output is not close to this 200 kW at all, but also it is still more than the 11.5 kW.

Internal Power Usage

When reeling in, the motor needs to be supplied with power from the system. This is done by storing energy in a supercapacitor, which has been discussed before. But the connections between the system components have not been explained yet. These are the connections from the generator to the supercapacitor and then to the motor. The former requires a converter, since both are DC, but it needs a lower voltage, shown in Table 10.7, for this a DC-DC step-down converter will most likely be used. For the connection towards the motor, an inverter is needed, since the motor is AC. This inverter was sized based on the power input the motor needs, which from Section 10.7.1 is known to be 11 kW. AN inverter was found on the market that fulfils this need. More specifically, the 'Eaton DC1' outputting a three-phase 400 volts alternating current [104]. Lastly, the power dump will need a converter to operate properly, since its voltage range is much higher than the voltage output of the generator, discussed in Section 10.7.3. The inverter for the dump load is designed for its specific purpose.

Power Output to Environment

The power that is generated is not only used to charge the batteries of the Rivian R1T. It can also be used to supply a small village with power or to provide power in disaster regions, when the local power grid is out of use. Over the world, different power grids exist, which use different voltages and frequencies. The main four regions for operations are North-America (United States of America and Canada), Patagonia, the Caribbean, and the Middle East. For these regions, the power grids require a voltage of 120 V, 220 V, 110 V, and 220/230 V respectively [105]. Also, the output of the generator is DC and that of the grid is AC. For this reason, an inverter needs to be installed, that also changes the output voltage of the generator to the desired voltage of the grid. Notably, Rivian is planning on implementing bidirectional charging, meaning the battery pack can be charged and discharged at the same time, delivering power back to the grid, basically acting like a buffer storage. This system could be used to skip the implementation of this separate connection to the grid, and with that the inverter. What should be noted is that this degrades the battery capacity quite heavily, so it will depend on the development of this technology how viable this option will be.

10.8. In-air Power System Design

The last power components that need to be sized are those of the in-air power system. First, the pump for pressure control of the kite is discussed in Section 10.8.1. After that, KCU power will be evaluated and a solution to generate this is given in Section 10.8.2.

10.8.1. Pump on Kite

During operation of the kite over extended periods of time, air will leak out of the inflated leading edge and struts. A poorly inflated kite can result in dangerous situations due to the strongly decreased performance and steerability. To overcome this problem, an air pump will be placed at the leading edge of the kite. Based on Section 12.3, the internal volume of the leading edge and struts is 0.392.6 m³ and the maximum internal pressure is 83 kPa (12 psi). Little data is available on the pressure loss in inflatable kites, therefore an example

calculation is performed, for a pressure drop of 5% per hour. This pressure results in a volume loss of 16.08 L. The Baencyr Air Pump is a 2.4 W pump, able to reach the required pressure 83 kPa (12 psi) and able to pump 3.2 L/min [106]. The pump needs approximately 5 minutes of operation per hour, resulting in a power consumption of 0.21 Wh per hour. The pump mainly there as a safety measure, for example if the kite is punctured and starts leaking, it will still be able to fly. The weight of the pump is 62 grams.

10.8.2. Kite Control Unit Power

The kite control unit power usage mainly consists of the communication power and the control lines actuation power. The communication system for the 2.4 or 5GHz Wi-Fi uses about 6 W continuous power [107, 108]. The control lines actuation power has peak loads in the turns of the figure-eight pattern and uses little energy on the straights of the reel-out phase. The actuation motors have a 100 W design power and 300 W peak power [109]. During reel-out, the kite is cornering about 25% of the time, for which actuation is needed [65]. It is assumed that the actuation consists of 75% design power and 25% peak power. In the rest of the reel-out phase and the whole reel-in phase, almost no control is needed, and it is assumed no power is used. This results in an average control power of 30.5 W. Combined with the communication power and a 10% (3.65 W) safety factor for the pump, the light on the kite, all the sensors, and sensor data handling, the power consumption of the KCU ends up at 40.2 W average power consumption. The requirement to provide this power continuously is stated in AWE-TEC-PS-07.

The power for the KCU is produced by an onboard wind turbine, a scaled down Rutland 504 turbine [110]. The Rutland 504 is chosen because of the ring touching the blade tips for extra strength. The apparent wind speed for the KCU is 32.75 m/s for reel-out and 23.35 m/s for reel-in, which are determined in Section 10.2. The Rutland 504 turbine has a diameter of 55 cm and generates 142.8 W on average for those wind speeds. The power production is extrapolated from the existing performance graph. To be able to generate the required 40.2 W, the turbine is scaled to 28 cm in diameter [111]. Due to the fluctuations in power usage by the control line actuation and power production by the wind turbine, a battery is used as a buffer [112]. The battery has a storage capacity of 30.5 Wh, which weighs about 300 grams. The battery is able to power the whole KCU for 30 minutes, for example during the reverse pumping cycle where little power will be produced by the turbine. Furthermore, the battery capacity will be cycled from 20% to 80% to elongate the battery life. When the battery is charged to 80%, the turbine will be stopped with a brake to overcome overloading the battery.

Aerodynamic Airborne System Characteristics

In this section, the aerodynamic characteristics of the AWES are presented. First, an overview of the main requirements, risks, and functions corresponding to the aerodynamics of the AWES is given in Section 11.1. Secondly, a trade-off, on the type of airfoil that will be used, is presented in Section 11.2. Then, the influence of specific kite design parameters is assessed in Section 11.3. This is followed by a discussion on the used aerodynamic model and the resulting kite design layout in Section 11.4. Furthermore, the framework to incorporate the tether and KCU drag is discussed in Section 11.5. Lastly, the results of the aerodynamic analysis are shown in Section 11.6.

11.1. Aerodynamics System Requirements

This section's purpose is to highlight the isolated aerodynamics related requirements, risks, and functionalities. This enables a better integrated subsystem design and allows to more easily integrate the subsystem in the larger project framework. The aerodynamics subsystem requirements are shown by Table 11.1. Unlike other subsystems, there are no direct system functionalities linked to the system's aerodynamics to take into account during the kite system's planform and shape design. Furthermore, there are also no specific risks or functionalities that have an effect on the aerodynamics design of the kite, as can be read in Chapter 8 and Section 9.1.

Table 11.1: Requirements on AWES Aerodynamic Properties.

Identifier	Requirement
AWE-TEC-AIR-06	The airborne system shall be able to provide a C_L/C_D during reel-out of at least 5.
AWE-TEC-AIR-11	The airborne system shall have a stall angle larger than 16° .

11.2. Airfoil Concept Trade-off

As discussed in Section 5.1, the trade-off showed that the LEI kite is the optimal option for the final concept of the AWES. In this section, a trade-off is performed between five LEI kite airfoil designs. First, each of the designs is briefly explained, which is followed by a comparison and a final decision on the LEI kite airfoil.

Firstly, the aerodynamic characteristics of the conventional LEI tube kite airfoil concept are described. As shown in Figure 11.1, the conventional airfoil simply consists of an inflatable tube connected to a canopy. Furthermore, a 2D cross-section is shown in Figure 11.2. From this, it is clear that due to the lack of a streamlined aerodynamic shape on the pressure side of the kite, a recirculation zone is formed. In this recirculation zone, vortices are created, which leads to extra drag generation. As a consequence, the aerodynamic efficiency of this type of kite is limited.

The formation of a recirculation zone can however be delayed or prevented by reshaping the leading edge inflatable tube or by adding a fabric membrane on the pressure side, as shown in Figure 11.1. This is due to the fact that in this way, the profile of the LEI kite can more closely resemble an airfoil shape, leading to a better aerodynamic performance. Lastly, LEI kites can also be made more lightweight by discarding the tubular inflatable structure and replacing this by rigid reinforcements at the places where the bridle system is attached to the leading edge. This concept is called, a single skin airfoil and is presented by the bottom airfoil in Figure 11.1.

A major aspect to be discussed for the airfoil selection are the aerodynamic characteristics, since these have a significant influence on the performance of the airborne wind energy system. This can be derived from Equation (11.1), as it shows that the power that can be generated is related to C_L^3/C_D^2 [115]. Therefore, a better aerodynamic performance will lead to an overall better performance of the AWES in terms of power generation.

$$P = \frac{2}{27} \rho A v_w^3 \frac{C_L^3}{C_D^2} \quad (11.1)$$

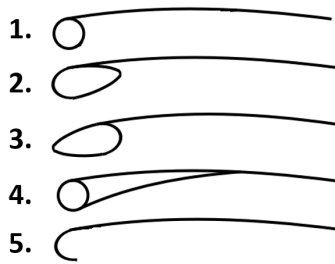


Figure 11.1: Different Airfoil Concepts [113].

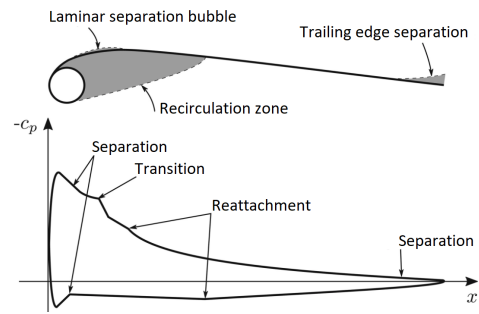


Figure 11.2: Aerodynamic Characteristics of Leading Edge Inflatable Kites [114].

Now comparing the aerodynamic efficiency of the different concepts, it is clear from literature that compared to the conventional LEI kite airfoil, the airfoils of concept 2 and 3 will lead to a slight increase in aerodynamic efficiency [113]. Looking at concept 2, this increase in efficiency is due to the fact that the airflow is guided towards the canopy, which will lead to a reduction in the recirculation zone. Furthermore, in the case of concept 3, this is due to the fact that the nose of the airfoil has a more streamlined shape. However, concept 3 will still have a recirculation zone, due to the fact that the flow is not guided towards the canopy. Therefore, this airfoil has only a small advantage compared to the conventional LEI kite in terms of aerodynamic efficiency. Then, in the case of concept 4, the recirculation zone is bridged due to having a lower skin. This leads to an increase in aerodynamic performance due to a decrease in drag due to vortex creation [113, 116]. Finally, concept 5 has a similar aerodynamic performance compared to conventional LEI kite airfoils [117].

Besides the aerodynamic performance, also the mass of the kite design is of importance, in order to ensure that the mass budget is achieved. Compared to the conventional LEI kite, concept 4 has a much lower mass. This is due to the fact that the inflatable tubes take up the most of the mass, which are discarded when a single skin airfoil is used. When looking at concept 2 to 4, on the other hand, extra fabric or tubes are added in order to approximate the airfoil shape. For example, concept 2 and 3 can be realised by connecting two inflated tubes, one with a small diameter and one with a larger diameter. This will lead to an increase in mass. Furthermore, concept 4 will also weigh more compared to the conventional LEI kite design, due to the fact that the structure behind the leading edge inflatable tube will add to the mass. Furthermore, to ensure no deformation occurs during flight of this larger inflatable structure, an internal system for rigidity is necessary, further increasing the mass.

Another important factor that plays a role in choosing an airfoil concept is the complexity that it brings to the system. During operations, the leading edge will have to endure high loads, which need to be completely absorbed and distributed by the leading edge. The best shape for the leading edge tube to absorb these high loads is a cylinder, as is used in the conventional LEI kite concept. When other shapes are used, such as in concept 2 and 3, a structural analysis to identify possible load bearing problems and deformations of the leading edge should be performed. Furthermore, since in concept 3 the leading edge slims down towards the front, also an analysis on the formation of indents should be performed, since there is less area to distribute the high loads. Then, the fourth concept will also lead to a more complex structure, due to the extra interface between the leading edge inflated tube and the inflated structure behind it, which approximates an airfoil shape. Furthermore, the manufacturing complexity will increase. Lastly, compared to the LEI kite, the single skin airfoil requires an elaborate bridle system, comparable to that of ram-air kites, increasing the complexity.

Taking a look at the launching and landing operations, the launching and landing performances of concept 1 to 4 are fairly similar. These concepts can make use of the established launching and landing concepts provided in Section 5.4, since the kite would already contain structural rigidity without wind. Except for differences in kite mass and size, the same operational procedures can be performed. On the other hand, concept five relies much more on the airflow for its structure and would therefore require a launching concept similar to those used for ram-air kites. This is undesired and potentially adds weight as a mast or larger structural component would be needed to induce the initial required airflow for rigidity. On the other hand, an advantage of these lightweight kite structures is that they can be operated at lower wind speeds compared to their more rigid competitors.

Lastly, the achievability and operational knowledge of the concepts should be considered. For this assessment, concepts 2 and 3 are found to be the most limiting concepts, since these concepts have only been analysed once by performing a wind tunnel experiment using a single integrated, rigid structure [113]. Therefore, these concepts were deemed to be unfeasible to be analysed reliably within the short project duration. Concept 4 is an interesting concept to better guide the airflow around the airfoil, but lacks detailed documentation and research. Additionally, an in-depth aerodynamic performance requires an extensive Computational Fluid Dynamics (CFD)

analysis, which is not achievable within the project's time constraints. Lastly, concepts 1 and 5 share the same aerodynamic flow mechanism and can therefore be analysed using a vortex step method, which has already been developed at the TU Delft. Furthermore, both of these concepts have already been proven to be feasible for real world applications [65]. Additionally, these concepts have been analysed in detail in numerous research documents [116, 117, 118].

To summarise the discussion on the different concepts, a trade-off is presented in Table 11.2. This is just a high-level trade-off, to provide a visual insight into the discussion presented above. For each airfoil concept, a score from one to three is assigned. One, meaning it scores lower than desired. Two, meaning that for a certain criterion, the concept has average properties. Lastly, a score of three indicates that it has beneficial properties. Based on this, a total score was computed. This led to the choice of a conventional LEI airfoil.

Table 11.2: Trade-off Airfoil Concepts.

	Aerodynamic Performance	Weight	Complexity	Operations	Application Knowledge and Achievability	Total Score
Concept 1	1	2	3	2	3	11
Concept 2	2	1	2	2	1	8
Concept 3	2	1	2	2	1	8
Concept 4	3	1	1	2	1	8
Concept 5	1	3	1	1	2	8

11.3. Kite Design Parameters

This section aims at investigating the kite's general layout. This contains the investigation into the effects of several design aspects on a kite's aerodynamic performance. The influences of camber and thickness, taper ratio, aspect ratio, planform shape and anhedral are discussed below. The results of this assessment and the full layout of the LEI kite are then presented in Section 11.4.

11.3.1. Camber and Thickness Influence

First, the effect of having a certain thickness on the aerodynamic performance will be discussed. In general, thicker airfoils experience stall at higher angles of attack and have a higher maximum lift coefficient. This leads to a larger operational range in terms of angles of attack [119]. Furthermore, an increase in the maximum obtainable lift coefficient also leads to a better overall performance of the AWES, due to the dependence of the power generation on the aerodynamic properties of the kite. However, thicker airfoils also lead to an increase in drag, which will reduce the aerodynamic performance. Therefore, the airfoil thickness influence is investigated in more detail using a vortex step method (VSM) program in Section 11.4.5 in order to evaluate which thickness results in the best aerodynamic performance.

Then, investigating the influence of camber on the aerodynamic performance of airfoils, it was concluded that a larger camber leads to an increase of the lift coefficient. Furthermore, especially at higher angles of attack, a larger camber also leads to an increase in drag. This is presented in Figure 11.3 [120]. Therefore, applying some camber to the kite's airfoil can significantly improve its aerodynamic performance, since higher lift coefficients are desirable, however at the same time, the drag should be kept minimal. The camber influence will therefore be evaluated in more detail in Section 11.4.4 using the VSM.

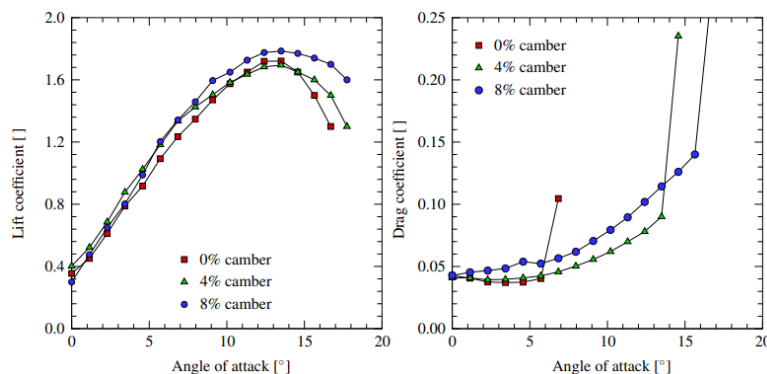


Figure 11.3: C_L and C_D versus α for different cambers [120].

11.3.2. Taper Ratio Determination

The taper ratio is a parameter that greatly defines the kite's planform geometry. It is defined as the ratio between tip and root chord lengths, shown by Equation (11.2). The taper ratio mainly influences the spanwise lift distribution and correlated wing efficiency. Since an elliptic lift distribution is the optimal spanwise distribution, its Oswald efficiency factor is set to 1 [121]. Therefore, the Oswald factor gives an indication of a wing's similarity to an elliptical lift distribution.

$$\lambda = \frac{c_t}{c_r} \tag{11.2}$$

Furthermore, the drag coefficient consists of two components, the zero-lift coefficient (C_{D_0}) and the induced drag coefficient (C_{D_i}). Equation (11.3) shows that, it is desired to have the highest possible Oswald efficiency factor, ϵ , as this leads to a reduction of C_{D_i} .

$$C_D = C_{D_0} + C_{D_i} \quad C_{D_i} = \frac{C_L^2}{\pi e AR} \tag{11.3}$$

As shown by Figure 11.4, a taper ratio of 0.4 is found to be the optimal taper ratio for the lowest induced drag and the highest Oswald efficiency factor, hence it best approximates the elliptical lift distribution. This spanwise lift distribution is shown by Figure 11.5, where it is compared to an actual elliptical lift distribution. Lowering the taper ratio would increase the local lift coefficients at the tip, leading to a wing-tip stall. Conversely, increasing the taper ratio beyond 0.4 increases the wing-tip vortices and adds induced drag. Based on these results, a taper ratio of 0.4 is used for the design of LEI kite [121].

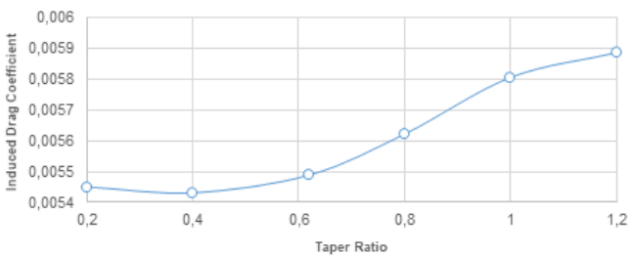


Figure 11.4: C_{D_i} variation versus taper ratio [121].

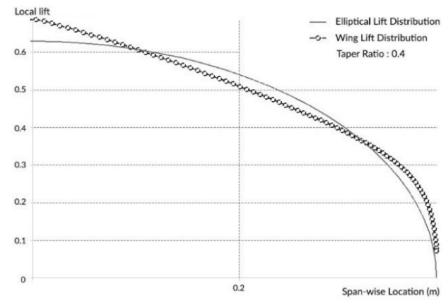


Figure 11.5: Lift distribution for $\lambda = 0.4$ compared to an elliptical lift distribution [121].

11.3.3. Aspect Ratio Influence

The aspect ratio also has an influence on the aerodynamic performance of the LEI kite. Figure 11.6 shows that higher aspect ratios lead to a higher maximum obtainable glide ratio and traction force. The increase in traction force subsequently leads to a better power generation capabilities of the AWES, as can be concluded from Equation (11.1). However, with a low aspect ratio, a wider range of possible angles of attack can be obtained [122]. From performed research on similar concepts, an aspect ratio of five was found for comparable AWES [82]. Therefore, it was aimed to obtain a flat aspect ratio for the LEI kite around five. The final value of the aspect ratio is, however, highly dependent on the planform design and will therefore be presented in Section 11.3.4.

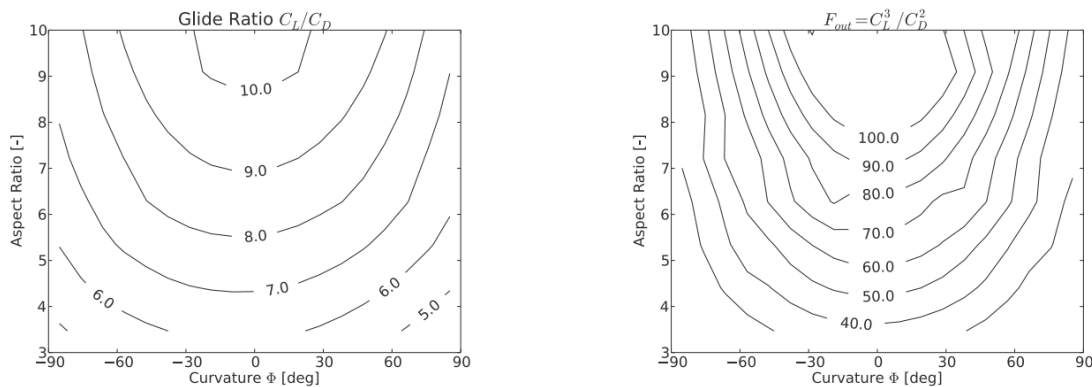


Figure 11.6: The influence of curvature of the kite Φ and aspect ratio on the maximum glide ratio and maximum traction force factor [123].

11.3.4. Planform Shape

As discussed in Section 11.3.2, having an elliptical lift distribution is beneficial for the aerodynamic performance of the LEI kite. The lift distribution depends on the taper ratio, but also on the overall planform geometry of the kite. The optimal shape for the planform is an ellipse. However, for this project's landing and launching procedures, a curved trailing is undesirable. Therefore, only the leading edge will be curved in order to approximate the elliptical planform shape, which is desirable in terms of aerodynamic performance [124]. Furthermore, the lower the values for ellipse ratio, $\beta_{ellipse}$, the lower the aspect ratio. From an analytic analysis, a semi-elliptic leading edge with ellipse ratio $\beta_{ellipse} = \frac{1}{3}$ was found to be ideal, leading to an aspect ratio equal to a flat aspect ratio of five.

11.3.5. Anhedral Influence

A planar wing is most optimal in terms of aerodynamic performance. However, this is not feasible to obtain when using a LEI kite concept. Therefore, LEI kites have an elliptical shape. From comparison between different ellipse ratios, it was found that at L/D_{max} , an elliptical wing with an ellipse ratio of $\beta_{ellipse}=0.5$ has 14% more lift and only a 6% lower L/D ratio compared to the planar wing with the same projected area [116]. From this, it was concluded that it is optimal to have an ellipse ratio of $\beta_{ellipse}=0.5$.

11.4. Kite Design Layout

Having determined and explained the different kite parameters, a detailed layout of the LEI kite is presented in Section 11.4.1. Then, the VSM, that is used to generate insights in the aerodynamic performance of the designed LEI kite, is provided in Section 11.4.2. Additionally, the limitations of the VSM are presented in Section 11.4.3. This is followed by an analysis of the camber and thickness influence on the aerodynamic performance as discussed in Section 11.4.4 and Section 11.4.5 respectively, since no specific value for these parameters has been determined yet. Lastly, the results from the numerical analysis using the VSM are presented in Section 11.4.6.

11.4.1. Design Layout

Most of the LEI kite parameters were defined in Section 11.3, except for the camber and thickness, which will be determined in Section 11.4.4 and Section 11.4.5 respectively. A summary of the other design parameters and the kite layout parameters, based on the projected area of 21.54 m^2 provided in the midterm report [10], is provided in Table 11.3. Furthermore, Figure 11.7 and Figure 11.8 show the planform and the 3D view of the LEI kite based on the presented design parameters. Note that the twist angle is not included in this analysis. This design choice was taken to not increase the complexity level beyond the achievable limits.

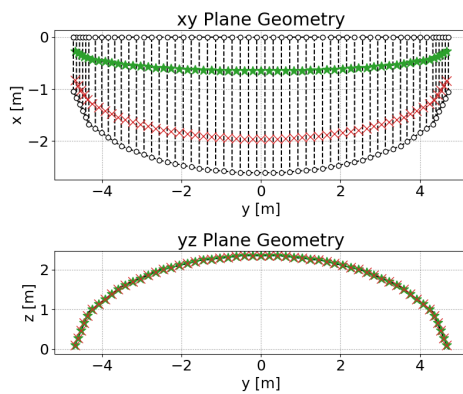


Figure 11.7: 21.54 m^2 LEI kite xy- and yz-plane geometries. (Segments = 12, $N_{split} = 5$, # Points = 10^6)

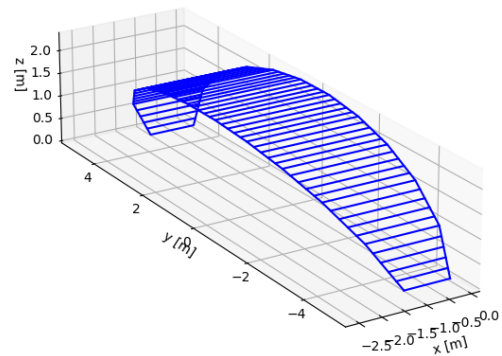


Figure 11.8: 3D view of the 21.54 m^2 LEI kite. (Segments = 12, $N_{split} = 5$, # Points = 10^6)

Table 11.3: Kite design layout parameters summary. In this table, the subscript (proj) relates to the projected planform, whereas the subscript (flat) relates to the flat planform.

Parameter	A_{proj}	b_{proj}	A_{flat}	b_{flat}	AR_{proj}	AR_{flat}	MAC	λ	c_t	c_r	Front $\beta_{ellipse}$	Top $\beta_{ellipse}$
Value	21.54 m^2	9.43 m	26.09 m^2	11.43	5.00	4.13	2.28 m	0.4	1.05 m	2.62 m	0.50	0.33

11.4.2. VSM Explanation and Code Overview

The vortex step method belongs to the vortex lattice method and approaches the Prandtl's lifting line theory [125]. However, compared to the Prandtl's lifting line, which sheds a continuous trailing vorticity from the wing's quarter

chord, the VSM approximates the vortex sheet with a finite number of horseshoe vortices [126]. In general, the VSM can be split into five main steps. First, the kite's planform is divided into a lattice of quadrilateral panels. On each of these panels a horseshoe vortex with strength Γ_i is placed. Then, the bound vortex of the horseshoe vortex is placed on a quarter chord of each individual panel. This is followed by placing the control point on the three-quarters chord. Lastly, the strength of each Γ_i that is required to satisfy the boundary conditions can be determined using a system of linear equations.

An overview of the general aerodynamics code flow is shown by Figure 11.9. It shows the main inputs and outputs of the program, as well as the main code actions and functions. As seen in Figure 11.9, two functions have been further detailed to increase the ease of comprehension and highlight the most important code purposes.

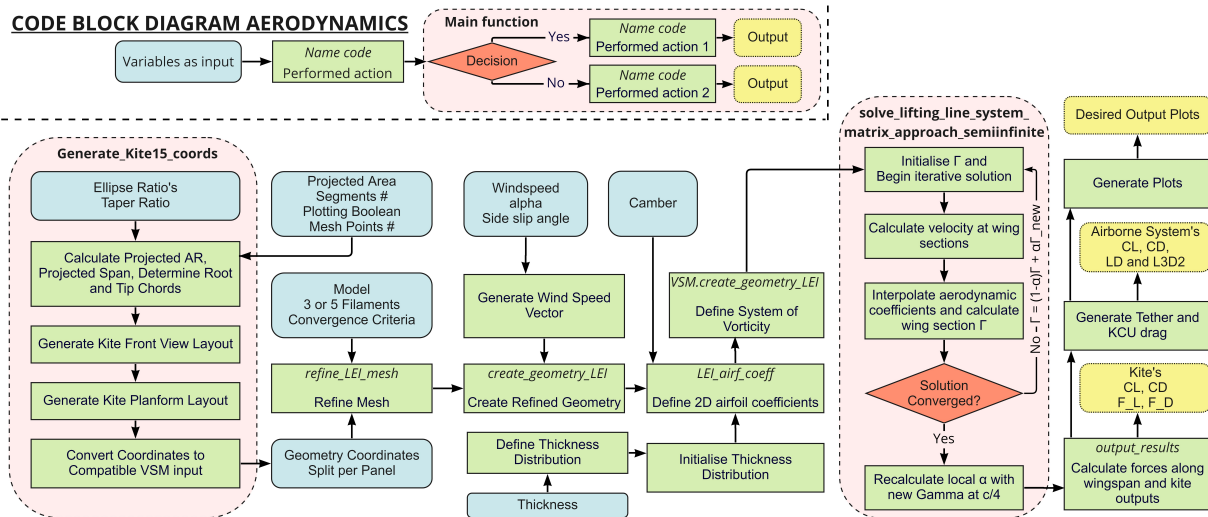


Figure 11.9: Aerodynamics code block diagram for VSM implemented program [127].

As shown by Figure 11.9, the aerodynamics simulation code functions based on specified kite geometry inputs. These geometry parameters enable the generation of the 3D coordinates to be used in the main program. In order to have the desired mesh refinement, the number of points is specified as input for the coordinate generation, while the splits per panel and number of segments further subdivide the modelling geometry. During the geometry creation, 2D polars are implemented based on nonlinear airfoil polar data, using the defined spanwise thickness and camber implemented in the chosen airfoil. After this implementation, the vortex system is created and looped until convergence is reached. When convergence is not obtained, the loop is run again with an updated vortex system. After reaching convergence, the spanwise forces are generated based on the recalculated vortex system, followed by the tether and KCU component drag implementation for the full AWES system aerodynamic properties.

11.4.3. Program Limitations

The program used to simulate the VSM has five main limitations. The aim of this subsection is to address and clarify the identified limitations. Next to this, mitigation possibilities are discussed to omit the encountered program limits.

1. Airflow outside the defined geometry is inviscid, irrotational and incompressible [127]. These assumptions are necessary to obtain a potential flow solution, but introduces errors in the drag approximations, leading to an underestimation of a geometry's drag generation.
2. The aerodynamic simulation tool only models the kite's aerodynamics. Therefore, it lacks the tethering/bridle lines' and KCU's aerodynamic influences. This limitation is solved by implementing drag estimations for these elements in a separately integrated code.
3. The VSM does not model the aerodynamic effect of struts. Since these struts are chordwise structural elements, their effect on the overall kite drag should be evaluated. According to Viré et al.: "The results show that the struts have little influence on the overall aerodynamic performance of the wing, independent of the degree of side-slip. Therefore, for analysing performance in the flow regime investigated here, these geometrical characteristics of the wing can be omitted without a noticeable loss of accuracy." [118] Therefore, the limitation of not including the aerodynamic effect of struts leads to the program's assumption of negligible strut drag.

4. The kite's layout needs to be segmented into linear elements. As it is conventional with code to be used for simulation, complex shaped objects need to be segmented into small parts to be implemented. This reduces the continuous shape to an interrupted, segmented shape. This segmentation influence can be reduced by creating numerous segments to accurately model the desired, more complex contour. The downside of this approach is the increase of mesh size and computational time with increasing level of segmentation.
5. Flexing, wing deformation, foil fluttering and ballooning are not taken into account by the VSM program. These structural phenomena are considered to be too complex to accurately model. Nonetheless, these effects will be present in real-world applications and should therefore be looked at more carefully for future applications. Experimental tests are therefore advised to obtain more accurate results.
6. The VSM is unable to correctly model stalled flight conditions. In this highly turbulent airflow range, the program is unable to reliably determine aerodynamic properties. The stall region is, however, clearly visible on the polar curves. Therefore, the program user should stay within the linear, unstalled region when analysing the aerodynamic performance of a desired configuration. This stall limitation is visualised by Figure 11.10. Stalling occurs at an angle of attack α of 17.5° , after which a sawtooth behaviour is observed for C_L , C_L/C_D and C_L^3/C_D^2 . An increasing C_D is observed after stalling.

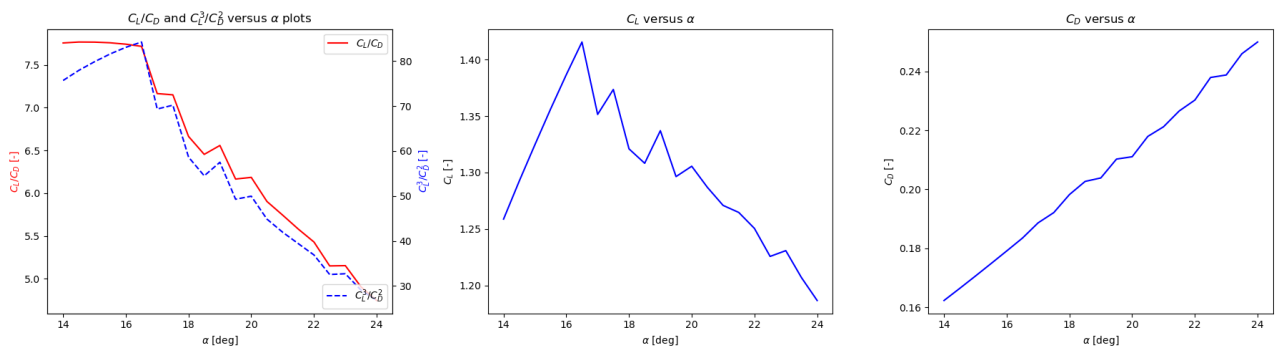


Figure 11.10: Detailed stall plots for the 16.65 m^2 projected area AWES. (Segments = 12, $N_{\text{split}} = 5$, # Points = 10^6)

7. The VSM assumes a flat wake [127]. The consequence of this limitation is an overestimation of vortex strengths, leading to an overestimation of lift and induced drag.
8. The model uses quasi-steady flow, meaning that every flow condition can solely be solved in the spatial domain [127].

11.4.4. Camber Determination

The camber of a LEI tube airfoil with a single skin is defined as the ratio between the maximum height (measured from the line connecting the centre of the LEI tube and the trailing edge) and the chord length. A visualisation of this camber determination is shown in Figure 11.11. For this design, only a non-varying camber along the span is considered. The main reasoning for this choice is the higher level of complexity and the limited available project duration. Therefore, Figure 11.12 to Figure 11.15 show the aerodynamic performance of different cambered kite configurations.

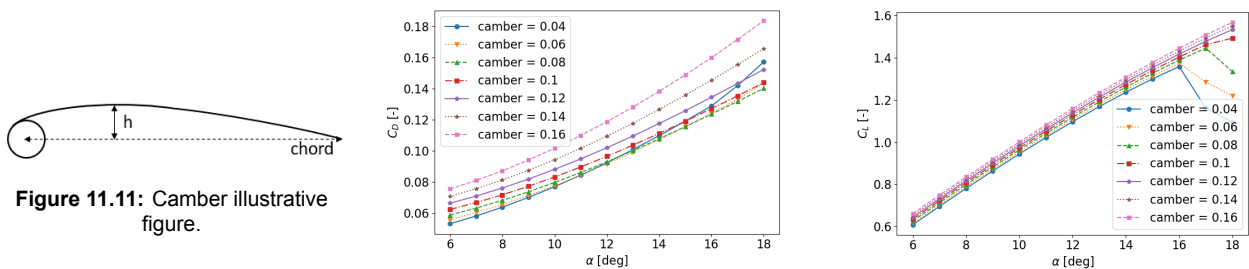


Figure 11.12: C_D versus α for different cambers. Figure 11.13: C_L versus α for different cambers.

Based on Figure 11.12 and Figure 11.13, it is observed that higher cambered wings produce more lift and show stall at higher angles of attack. Additionally, higher cambered wings generate more drag at the same angle of attack when compared to their less cambered counterparts. However, from the lift and drag polars alone, no decision on camber could be taken.

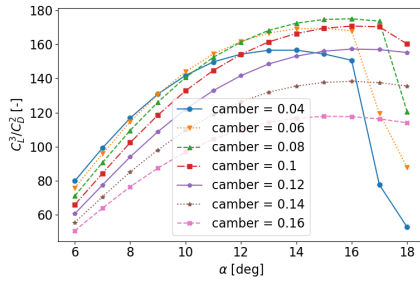


Figure 11.14: C_L^3/C_D^2 versus α for different cambers.

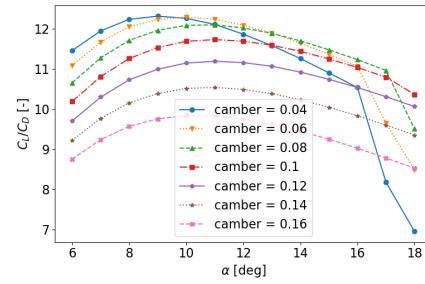


Figure 11.15: C_L/C_D versus α for different cambers.

Contrary to the lift and drag polar plots, the C_L^3/C_D^2 and C_L/C_D versus α curves in Figure 11.14 and Figure 11.15 show bigger differences for varying camber configurations. In Figure 11.14, the 8% cambered wing shows the best performance for C_L^3/C_D^2 . Also in Figure 11.15, the 8% cambered configuration shows high L/D values. Although the 4% and 6% cambered configurations show higher absolute L/D values, the 8% cambered wing maintains its high L/D values for a more desirable angle of attack range (8°-15°). These ideal performance parameters, combined with an acceptable stall angle of attack, led to the decision to use an 8% cambered airfoil in the kite's design.

11.4.5. Thickness Determination

In the design of this project's LEI kite, the thickness is defined as the diameter of the LEI tube. The kite's thickness will be determined based on either a constant t/c ratio or a constant t/MAC ratio. Since there is a varying chord length, the first option would indicate a changing thickness along the span. The latter option indicates a constant spanwise thickness. In order to decide on the optimal design choice and t/c or t/MAC value, Figure 11.16 to Figure 11.19 show the simulated aerodynamic performance parameters based on several thickness settings.

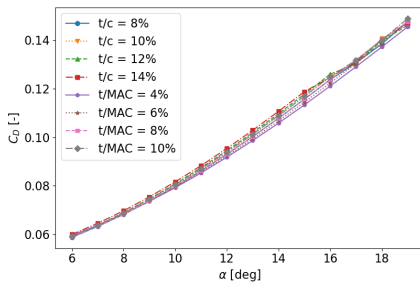


Figure 11.16: C_D versus α for different thicknesses of the kite's leading edge.

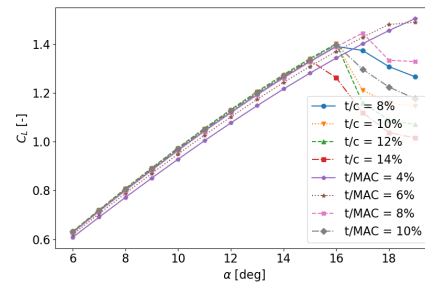


Figure 11.17: C_L versus α for different thicknesses of the kite's leading edge.

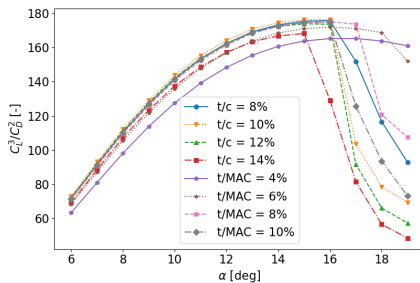


Figure 11.18: C_L^3/C_D^2 versus α for different thicknesses of the kite's leading edge.

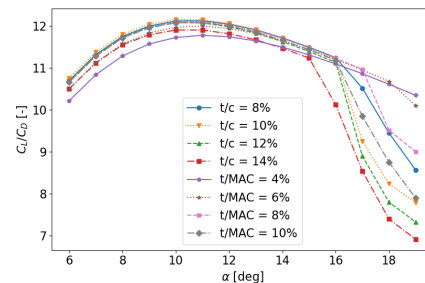


Figure 11.19: C_L/C_D versus α for different thicknesses of the kite's leading edge.

Compared to the camber influence analysis, the LEI tube thickness is found to be less influential on the aerodynamic performance. Nonetheless, there are still performance differences to be considered. The first observation from the aerodynamic polar plots is that a kite with a constant t/c ratio stalls at lower angles of attack when compared to a constant thickness kite. Inspecting Figure 11.17, the stall angle for 0.10-0.14 t/c configurations are found to be just 16° or below, which is not complying with requirement AWE-TEC-AIR-11. Therefore, these

configurations are discarded. Additionally, Figure 11.17 displays the expected higher lift coefficients for thicker airfoils. Similarly, Figure 11.16 shows a higher drag generation for thicker airfoils.

A t/MAC of 0.08 is found to provide the optimal aerodynamic performance for this project's kite configuration. Looking at Figure 11.19 and Figure 11.18, the 0.08 t/MAC design option shows great aerodynamic and power efficiencies. Combined with the delayed stall properties of constant thickness kites, the higher lift coefficients and easier production process when compared to variable spanwise thickness kites, a 0.08 t/MAC kite is desired.

This thickness will be used as the initial kite thickness and needs to be checked on its load carrying performance by a structural analysis. Since this level of detailed load analysis is not performed in this report, future iterations should assess the feasibility of an 8% t/MAC constant thickness LEI kite. In case a higher thickness should be required, the aerodynamic performance will be negatively affected.

11.4.6. Kite Polars

This section displays the main aerodynamic polar plots for this project's kite. Based on the earlier presented kite geometry parameters, the lift coefficient, drag coefficient, C_L/C_D , and C^3_L/C^2_D versus α plots are generated and shown in Figure 11.20. From these VSM simulations, a maximum C_L of 1.42 is found, with an α_{stall} of 17° . For this kite's configuration, an L/D_{opt} of 12.15 and a C^3_L/C^2_{Dopt} of 184 is obtained.

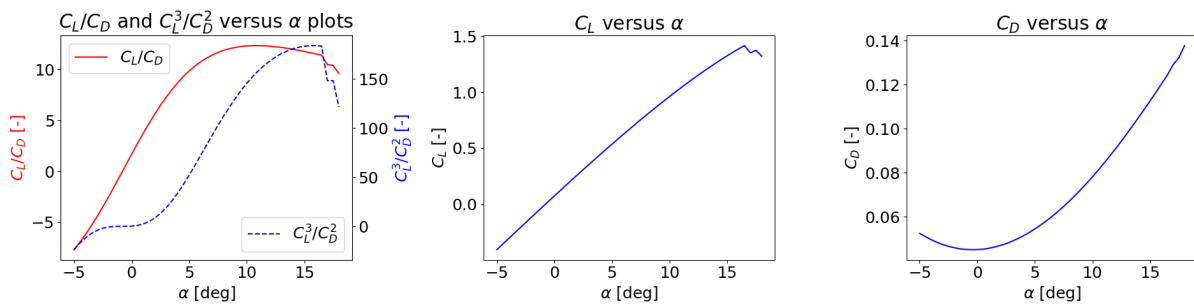


Figure 11.20: Aerodynamic polars for the 21.54 m² projected area kite. ($N_{split} = 5$, Segments = 12, #Points = 10⁶)

11.5. Tether and Kite Control Unit Drag Analysis

The total drag is calculated as the sum of the kite's, KCU's and tether's component drag contributions. The drag contribution of the kite itself is estimated using the VSM program, which is also used to approximate the other aerodynamic performance parameters, such as the lift coefficient. Furthermore, the method used to estimate the tether drag will be discussed in Section 11.5.1, while the drag contribution of the KCU is presented in Section 11.5.2.

11.5.1. Tether Drag Determination

In this section, the tether drag (D_t) is described in more detail. Tether sag is not taken into account [128, 129]. It was validated that the aerodynamic drag of the tether can be taken into account by adding one fourth of the tether drag area to the kite drag area ratio, as shown in Equation (11.4). Furthermore, Equation (11.4) shows the tether drag formula and its resulting contribution to the general system's drag coefficient [3].

$$D = D_k + D_t + D_{KCU} \quad D_t = \frac{1}{8} \rho d_t l_t v_a^2 C_{D,t} \quad C_D = C_{D,k} + \frac{1}{4} \frac{d_{tether} l_t}{S} C_{D,c} \quad (11.4)$$

With d_t being the tether diameter, l_t the airborne tether length, $C_{D,t}$ the tether drag coefficient, S the projected kite area and v_a the apparent wind velocity. For this application, the apparent wind velocity of the tether is, as an overestimation, assumed to be equal to that of the kite. The value for $C_{D,t}$ is approximated by the drag coefficient of a cylinder in cross flow and is found to be 1.1 [3]. This is valid for the bridle line drag estimation, since these cables can be seen as long cylinders with a circular cross-section hanging in the air. Using an airborne tether length of 580 m (determined in Section 13.3), a tether diameter of 4.4 mm, as determined in Section 12.2.1, and a kite projected area of 21.54 m² from the Midterm Report [10], the tether drag coefficient is found to be equal to 0.033.

11.5.2. KCU Drag Determination

The KCU will be approximated as a blunt body with a circular cross-section. Based on in situ flow measurements, the drag of the KCU was found to be approximately equal to 10% of the combined wing and tether drag [130]. Therefore, the KCU drag is a function of the angle of attack, α . This will be used to approximate the KCU drag

contribution to the total drag. Note that the drag contribution of the propeller attached to the KCU is included in the KCU drag contribution.

11.6. Aerodynamic Characteristics Determination

In order to determine the AWES aerodynamic performance parameters, an estimation on reel-in and reel-out angles of attack is carried out. Based on Figure 11.21, the range of reel-out angles of attack is determined to be 8° to 15° . These values are considered by looking at the fully powered system (corresponding to the red colour in Figure 11.21). Similarly, a range of -5° to 0° is determined for reel-in angles of attack. In order to get an estimation of the aerodynamic characteristics for these operational phases, the $C_{L_{out}}$, $C_{D_{out}}$ and $C_{D_{in}}$ are determined as the averages over their respective α ranges.

Up to this point, the aerodynamic performance of the LEI kite is solely assessed based on the kite area determined during the midterm report [10] and its characteristics. However, the kite area needs to comply with the required power output of 20 kW based on the power cycle. In order to meet this requirement, an initial matching with the power cycle model presented in Section 10.3 is performed. This leads to an updated kite area of 16.65 m^2 . Furthermore, the drag coefficient of the complete airborne wind energy system is determined and added to the kite's polars. The complete kite-tether-KCU system's aerodynamic performance and geometry parameters are presented in Table 11.4. A 3D render of this 16.65 m^2 projected area kite is displayed by Figure 11.23.

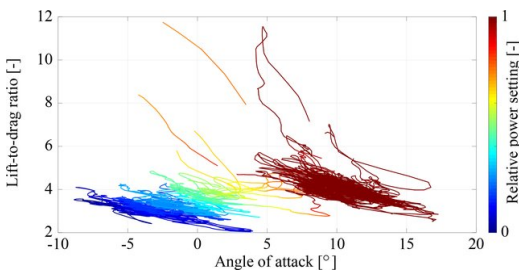


Figure 11.21: Measured L/D of the kite plotted versus angle of attack. The colours are relative to power settings. The colouring ranges from blue, for lower values during retraction, up to dark red, for a fully powered kite during the traction phase [12].

Table 11.4: Aerodynamic and geometry summarising table for the 16.65 m^2 projected area kite system. (Segments = 12, $N_{split} = 5$, # Points = 10^6)

Geometry			Aerodynamics		
Parameter	Unit	Value	Parameter	Unit	Value
A_{proj}	m^2	16.65	$C_{D_{fether}}$	-	0.043
b_{proj}	m	8.29	$C_{D_{KCU}}$	-	$f(\alpha)$
AR_{proj}	-	4.13	Reel-Out System	-	-
AR_{flat}	-	5.00	$C_{L_{out}}$	-	1.07
C_t	m	0.92	$C_{D_{out}}$	-	0.14
C_r	m	2.30	$C_L/C_{D_{out}}$	-	7.41
MAC	m	2.01	$C_L^3/C_{D_{out}}^2$	-	60
A_{flat}	m^2	21.17	Reel-In System	-	-
b_{flat}	m	10.04	$C_{L_{in}}$	-	-0.16
$\beta_{ellipsetop}$	-	0.33	$C_{D_{in}}$	-	0.099
$\beta_{ellipsefront}$	-	0.50	α_{stall}	$^\circ$	16.5

Based on the results in Table 11.4, AWE-TEC-AIR-06 is met, since the $C_L/C_{D_{out}}$ of 7.41 exceeds the minimal required value of 5. The second aerodynamics related requirement, AWE-TEC-AIR-11, is also met, since the obtained stall angle from simulations is 16.5° , which exceeds the minimum required value of 16° .

The kite's flat area is calculated based on the multiplication of the projected area and the $\frac{b_{flat}}{b_{proj}}$ ratio. This relation is based on the assumption that the kite is curved in a single direction, implying a straight plane connection between LE and TE. This assumption leads to a minor underestimation of the actual kite's flat area, since the camber effect is not accounted for. Therefore, a 5% addition to this obtained flat area is taken to initially account for this effect, compliant with the allowable 5% contingency margin as defined in the Baseline Report [18].

Lastly, the reel-in angle of attack range should be re-assessed. Using the range specified above, resulted in an average value of -0.16 for the $C_{L_{in}}$. During reel-in, however, the kite should gain altitude, which is not possible for negative C_L values in normal operations. Therefore, a new reel-in α range will be determined in Chapter 15.

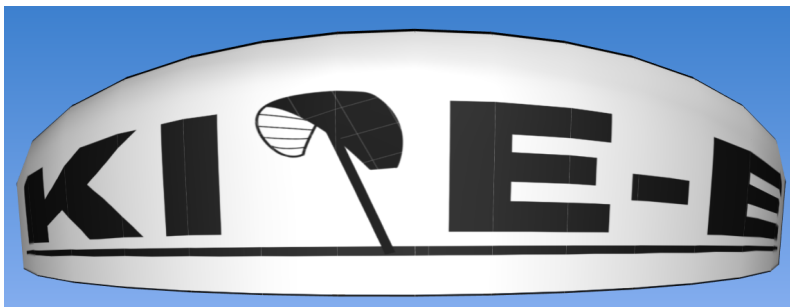


Figure 11.22: Kite design top view made in SurfPlan.



Figure 11.23: Visualisation kite design obtained made in SurfPlan.

Airborne Structures and Materials Characteristics

In this chapter, the structural components of the AWES will be thoroughly discussed and the results of this detailed design will be presented. Firstly, the main requirements are shown in Section 12.1. In Section 12.2, the tether characteristics are presented. The leading edge characteristics are given in Section 12.3. The strut configuration is shown in Section 12.4. The configuration of the bridle system is justified and presented in Section 12.5. Lastly, Section 12.6 explains the kite material choice.

12.1. Structures and Materials Requirements and Risks

This section's purpose is to highlight the requirements, functionalities and risk associated with structures and materials. This enables a complete design taking into account both the expected specifications and the vital safety and reliability. The requirements for the structures and material properties are shown in Table 12.1. Furthermore, there are no functionalities that have an effect on the structural design, as can be read in Section 9.1.

Table 12.1: Requirements on AWES Structures and Material Properties.

Identifier	Requirement
AWE-TEC-AIR-01	The airborne system shall be softkite based.
AWE-TEC-AIR-02	The airborne system shall be able to withstand the wing loading generated during nominal operations, including a safety factor of 1.2.
AWE-TEC-AIR-03	The tether shall be able to withstand at least two times the tether force experienced under nominal operations.
AWE-TEC-AIR-07	The bridles shall be able to withstand at least two times the bridle force experienced under nominal operations.
AWE-TEC-AIR-08	The tether shall have a bending fatigue safe service life (SSL) of at least 1848 FH.
AWE-TEC-AIR-09	The tether shall have a creep SSL of at least 1848 FH.
AWE-TEC-AIR-10	The airborne system shall be able to operate under an environmental temperature range of -15 °C to 35 °C.

The risks driving the design process for certain parts of the structural design are shown in Table 12.2.

Table 12.2: Risks, with risk reduction measures influencing the structural design.

Identifier	Measure
TR-AIR-01	A safety factor and a coating is added on the tether.
TR-AIR-03	A safety factor and is added on the bridle lines.

12.2. Tether

The tether is one of the most important components in the AWES. The tether connects the kite to the drum on the Rivian R1T. Without the tether, no energy generation would be possible for the system. Designing the tether is therefore a very intrinsic part of the design process. First, the diameter and material of the tether are discussed. Afterwards, the possible ways to connect tethering lines is discussed. Lastly, the fatigue characteristics of the tether are analysed.

12.2.1. Diameter and material

As presented in the Midterm Report [10], the choice for the tether material fell on Sierra 78 (bio-based) Dyneema®. Because of inconsistencies in the data sheet of Yale Cordage, the producer of the material [131], the mean breaking load (MBL) of the 6 mm variant of the material was reduced by 1100 kg. This means the assumed strength is not 4765 kg, but 3665 kg. This value was established after contact with the company.

Two new developments in the design process alleviated the tether and drum dimensioning issues. Firstly, due to new computations of the aerodynamic loads, the nominal tether force decreased to 10329.3 N. This can be seen in Section 10.3. In addition, the safety factor has been decreased to 2, assuming peak loads can be covered by reeling out quicker. The decrease follows from extensive research of the possible failure modes and the needed safety factors. This safety factor is added to comply with AWE-TEC-AIR-03. These two changes in the design parameters mean that the diameter, along with other parameters of the

Table 12.3: Tether characteristics

Parameter	Unit	Value
Diameter	mm	4.4
Mass	kg/100m	1.0509

tether, can be interpolated between 4 and 5 mm. Using a value of 20658.6 N, the tether characteristics shown in Table 12.3 were determined.

12.2.2. Splicing

In order to connect the tether and bridle lines to the KCU, the ropes have to be either knotted or spliced. From this a loop can be created and hooked on to the KCU. Several methods of knotting and splicing will be discussed. First, a choice is made between knotting and splicing. An important factor that plays a role is the loss of strength in the rope after being adjusted. The tether is a sensitive subsystem and if it breaks, the whole system becomes inoperative. Therefore, the tether should be reliable. Research has shown that a knotted rope can lose up to 50% of its strength [132], whereas splicing preserves the strength of the rope for at least 90% [133]. The figure-of-eight loop knot keeps around 85% of its strength and is the strongest knot, but the eye splice can keep 100% of the rope's strength [134]. Therefore, the knot options are discarded.

The chosen Dyneema rope is a single-braided rope, so only single braided splicing methods will be discussed. The rope consists of twelve strands, thus making the splicing slightly more complicated [135, 136]. There are two different splicing techniques suitable: the Twelve-Strand Class II Smooth Eye Splice, and the Twelve-Strand Class II Tuck-Bury Eye Splice. The smooth eye splice is a technique where the rope as a whole is spliced into the braided rope. Once a load is applied to the rope, it will contract and tighten itself around the inserted rope. The rope is finished by lock stitching (locking the adjusted rope by stitching a thin line through it) and whipping (winding a thin line around the rope's end). This is necessary to prevent the rope from opening up and fraying when no load is applied. One of its disadvantages is that it needs some extra tools (whipping twine and sewing set) and it will become slightly bigger in diameter. However, the surface remains roughly the same, thus the influence on aerodynamics performance is minimal. The tuck-bury splice does not need any extra tools to create the splice. Multiple strands are separately spliced back into the ropes, giving it extra security under alternating loads. One of the disadvantages is that it is slightly more complicated to perform this splice, due to the many strands that need to be pulled apart. Also, its aerodynamics performance will decrease due to out-sticking pieces of strand and a thickening of the rope. These are necessary to prevent the strands from sliding back into the splice and losing their strength.

Due to the difference in aerodynamics performance, it has been decided to use a Twelve-Strand Class II Smooth Eye Splice with whipping. Splicing by yourself after some practice gives the same result as a professional, thus it is not necessary to invest more money in a professional manufacturer [134]. However, some tools as a fid, pusher and whipping twine need to be bought [137].

The size of the eye is important to determine the extra amount of length is necessary to splice the rope. The splice, without measuring the eye, should be as long as 60 times the diameter of the rope, so $4.4 \times 60 = 264$ mm [138]. In addition, it has been determined that rope consisting of Dyneema, require an angle of the eye with the throat (where the rope is becoming one piece) when it is loaded of less than 15° . This comes from the fact that the eye has to fit around the attachment point of the KCU. With

$$L_{et} = \frac{w_{et}}{\theta_{et}}, \quad (12.1)$$

the length of the eye can be determined. Here, l_{et} the length in m of the eye when it is loaded, w_{et} is the width of the attachment in m and θ_{et} the angle with the throat in radians. Since r represents only half of the length, the complete extra length for the eye can be established by multiplying it with two [132].

If the tether or bridle lines break, a different splicing technique can be applied to connect the two separate rope pieces together. This technique is the end-to-end splicing method [139]. Instead of creating an eye, the rope ends are directly splice-connected to each other. By braiding the rope ends through each other, the local thickness of the rope increases by approximately 1 mm and shortens the total rope length by half a meter. Splicing the rope can be done until the minimum tether or bridle line length is achieved. This makes the material reusable and thus sustainable.

12.2.3. Fatigue Characteristics

There are multiple ways which can cause a tether to fail. The most important fatigue characteristics for a tether in an AWES are explained below.

Abrasion

Abrasion is one of the fatigue failure modes of the tether that might arise. It occurs when a rope is moving/sanding along the drum, but can also happen internally when the yarns move past each other [140].

Due to the limited amount of space for the drum, it is necessary to investigate the possibilities of double winding the tether around the drum. However, this causes the tether to move past itself, possibly creating abrasion and

eventually cutting itself [141]. After speaking with an expert from the company Kitepower, which uses the same tether material, it could be determined that during the set-up phase the tether can be doubly winded around the drum. This is possible, because a very low force is applied on the tether by pulling the tether away from the car and laying it on the ground by hand. Precautions should still be applied to ensure the tether safety, especially since it will constantly rub over the pulleys. Lubrication can be used to make the tether move more smoothly from the drum. The drum should be dirt and sand free before the kite is reeled-in, such that the small pieces can not sand/scrub and damage the tether.

Yarn-on-yarn abrasion is the movement of the strands past each other. This can happen when the rope is put under pressure. Also, if the tether is not cleaned properly, dirt can get in between the yarn and abrade the rope. Microplastic-fibres can cut loose and be released into the environment [140]. This can be prevented by applying a coating. Dyneema has the option for a coating and claims to create an abrasion resistance four times better than other High Molecular Polyethylene (HMPE) [142]. This coating also increases the external abrasion resistance. As long as the tether is coated and regularly cleaned, abrasion is not a constraining factor for the design.

Creep

Creep is the rate of irreversible stretching of the tether over time [143]. There are three factors that improve the creep lifetime. Firstly, the day/night temperature changes affect the creep lifetime. A 10 °C reduction in temperature, reduces creep by a factor of 3. Seasonal temperature variations have a similar influence. The factor used for both these to estimate the service life is 1.5. Lastly, a loading factor is introduced, since the tether is not constantly bearing a high load. The factor can be determined using Equation (12.2), using the fact that the system reels out for 58 seconds, and a cycle is 72 seconds, which is determined in Section 10.3.2.

$$F_L = \frac{\text{Cycle time}}{\text{Reel-out time}} = \frac{72}{58} = 1.241 \quad (12.2)$$

This means the Safe Working Life (SWL), which can be read from Figure 33.16 in [143], will be multiplied by $1.5 \times 1.5 \times 1.241 = 2.792$. This SWL is assessed at 20 °C, which is not necessarily the temperature the MAWES will be operating at. The tensile stress in the tether can be calculated using Equation (12.3).

$$\text{Tension} = \frac{\text{Regular design traction force}}{\text{Cross section}} \quad (12.3)$$

This results in a tension of 0.668 GPa for the material chosen in Section 12.2.1. Looking at Figure 33.16 in [143] and taking making a conservative approximation, the creep SWL is 0.5 years. Multiplying this by the previously mentioned factor, the SSL is 12237 FH. This means that creep, assuming a continuous operational time of 2.5 months, will not be a problem for the system. Operating at a temperature of 30 °C will have a negative influence, but the creep life will still be 4079 FH, in which the system is continuously operated. This is in compliance with AWE-TEC-AIR-09.

Fatigue bending

Fatigue bending is the process of dynamic loading that occurs over the drum and swivel of the system [143]. At these points, the tether constantly bends under a high force during operations. This causes tether fatigue. The $D_{\text{pulley}}/d_{\text{tether}}$ is taken as the critical D/d, 60. This is the diameter of the pulley in the spindle motor over the diameter of the tether. Ideally, this ratio would be infinite, since then there would be no bending. Using Figure 33.17 in [143] and a tension of 0.668 GPa, the cycles to failure (CTF) can be determined to be approximately 28000. Taking a safety factor of 1.33, a cycle time of 72 s and two bending points, Equation (12.4) can be filled in.

$$\text{Safe Service Life} = \frac{\frac{\text{CTF}}{1.33} \times \text{cycle time}}{\text{number of sheaves}} \quad (12.4)$$

Filling in the previously mentioned values, the Safe Service Life (SSL) is 211 FH. XBO coating is applied to the tether, increasing the SSL of the tether by a factor of 3 [143, 144, 145]. Additionally, the tether can be flipped, as explained in Section 6.4.3, increasing its lifetime by a factor of 2. The rope can be braided in a way that increases the resistance against bending fatigue by a factor of 2. This means the SSL is 2526 FH, meaning that the system complies with AWE-TEC-08.

12.3. Leading Edge

The size of the leading edge largely influences the performance of the kite. An increase in its diameter gives the kite more power and stability, but makes it more difficult to steer the kite. The diameter of the leading edge of the kite is 0.1606 m, as follows from the t/MAC mentioned in Section 11.3. The diameter of the struts is assumed to be 75% of the leading edge thickness, based on visual inspection of similar kites [116]. The

internal pressures of the leading edge and struts are assumed to be equal, and the lowest maximum pressure is limiting. Based on the Rise A-series from Ocean Rodeo, the pressure in the leading edge is 62 kPa (9 psi) [146]. If more stiffness is required in windy conditions, the kite can be pumped to 83 kPa (12 psi). A thicker leading edge will result in a lower internal pressure.

12.4. Struts Configuration

Struts are a key element in the design of a kite. It provides stability, stiffens the kite and creates the shape. Since the system has to generate power, it needs to resist a relatively high load compared to a low/moderate wind speed. To resist this high load, more struts need to be placed on the kite, however this will also increase the mass.

Not only the leading edge will be an inflatable tube, but the struts as well. This way, the kite can be folded and packed to a small size, which will make it easier to store the kite. A cylindrical shape is chosen for the struts, since it is known to give the best aerodynamic performance [147].

Research has shown that kites with approximately the same surface area of 20 m², five struts are enough for stability and rigidity [109]. In case a sensor and a compressor have to be placed between the struts, an additional sixth strut can be placed. The centre will not have a strut placed directly on top, but two struts on either side of the centre. Attachments can then be placed in the centre of the canopy. Since the system needs to have at least a compressor, the six struts configuration is chosen for the kite.

The struts are positioned evenly over the kite. Two struts are attached to both centre sides of the canopy, the other four are placed evenly divided over the span of the kite [148, 149]. The centre struts mostly influence the stability of the kite, whereas the others prevent the canopy from fluttering, thus making it more steerable. The flat span of the kite is determined to be 10.045 m, and the average section span is calculated with

$$b_{section} = \frac{b_{flat}}{n + 1}, \quad (12.5)$$

where b is the wing span of the kite and n the amount of struts. This results in an average section span of 1.435 m.

The chord length varies over the kite, so the struts have different lengths and are summarised in Table 12.4. Each strut has a number allocated to it, where number one is the most left strut when facing the leading edge of the kite and six the most right strut. The diameter of the struts is estimated to be 75% of the diameter of the leading edge, based on previous designed kites [109]. This results in a diameter of 12 cm.

Table 12.4: Strut sizes for the 16.65 m² (projected area) kite.

Strut Number	Strut Length in m
1	1.704
2	2.109
3	2.283
4	2.283
5	2.109
6	1.704

The struts can be fastened in either a fixed or floating manner [150]. If it is fixed, the struts are directly sewed to the canopy, giving the kite proper tension and a more predictable airflow. With the floating configuration, the space between the canopy and the strut are filled with ripstop. This makes the kite more controllable and increases the resistance against front stall. However, the chance that the canopy will flutter is large. Front stall can be prevented by the KCU, so a fixed strut configuration will be applied. The struts are directly sewed to the canopy.

12.5. Bridle System

The bridle configuration is essential for the introduction of the forces on the kite into the tether. Furthermore, another function of the bridle system is steering the kite and changing its angle of attack, in order to be able to depower the kite during the reel-in phase. The bridle system consists of power lines and steering lines. The power lines bear most of the load, typically 70%, while the steering lines are used to manoeuvre the kite and therefore only carry 30% of the load [151]. In order to introduce all the loads in a gradual way, most bridle systems show a branch-like structure, as can be seen in Figure 12.1. Furthermore, the attachment of the bridle lines to the leading edge is, in most cases, at the locations where also the struts are located. Moreover, for the steering line system, a lot of different configurations are possible based on how the control of the kite is executed. The bridle configuration for this project is shown in Figure 12.2.

Based on research on existing bridle systems, it was chosen to go with a branch-like structure, with an attachment to the leading edge at each strut location [13, 65]. Figure 12.2 shows the bridle configuration that follows from available literature and will be used. The green lines are the power lines, the red lines the steering lines. The power lines are split close to the leading edge, in order to also attach them to the struts at 25% of the chord, as shown in Figure 12.2, to provide more rigidity. Furthermore, the bridles are spliced together at each bifurcation, ensuring no loss of strength. Moreover, in order to not limit the manoeuvrability of the kite, the amount

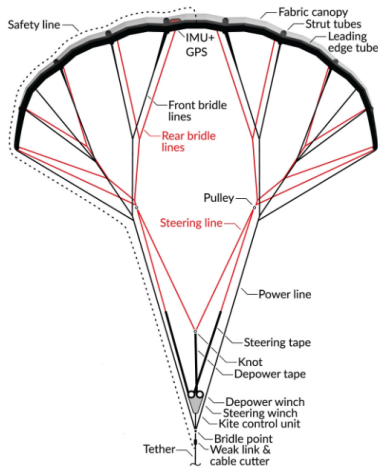


Figure 12.1: Bridle system of the Kitepower V3 kite [13].

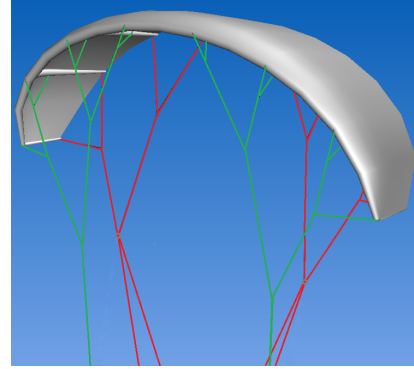


Figure 12.2: Designed bridle configuration.

of bridles is minimised. A system of pulleys is used to steer the kite, which can be seen in Figure 12.1 and Figure 12.2. The steering system that will be used is described in more detail in Chapter 14. This is very similar to the steering system of the V3 kite, since the KCU is based on the same principles as the KCU of the V3 kite. A compact bridle system is used, to allow better feedback to the KCU. The only downside of this compactness is that the forces in the bridles are higher, because the angles at the bifurcations are higher. These angles are therefore minimised, while still keeping a compact bridle system.

12.5.1. Load Analysis

The bridle system has to be arranged in such a way that it effectively guides the load from the kite to the tether. The angles between bifurcations of the bridle lines contribute to the effective introduction of the loads in the tether. Therefore, a static load analysis is performed to give insight into the bridle configuration design.

Using a static load analysis, the forces in the bridles are determined. The equations used to perform the static load analysis, are given by Equation (12.6) and Equation (12.7), and are based on the principle that the summation of all forces in the x- and y-direction equals to zero (force equilibrium). Furthermore, Figure 12.3 shows how the bifurcation angles and forces that used in the equations are defined.

The bifurcation angles used to determine the load in each bridle are initially determined from the bridle system configuration that was designed in SurfPlan. However, in order to obtain a desired loading, the angles were adjusted by changing the location of the bifurcation points. Note that since all angles are linked to each other, changing one bifurcation location influences numerous other angles. Therefore, a full optimisation of the bridle system configuration is not possible in the timespan of this project. A 2D view of the bridle configuration showing all the angles is presented in Figure 12.4. Note that only half of the angles are shown, since the kite is symmetric.

The load that is introduced in the power line bridle configuration is equal to 70% of the tether load, as presented at the beginning of this subsection. Furthermore, the load in the tether that is used for the static load analysis is obtained from the power cycle analysis, and is equal to 10329 N, as presented in Section 10.3. The results of the static load analysis are presented in Table 12.5. The labels for each load in this table are shown in Figure 12.4.

Based on this load analysis, the bridle diameter is determined. The bridle system can be divided into three levels. Level one contains the two bridle lines that originate from the first bifurcation. The second level contains the bridle lines that originate from the following bifurcation. The third level contains the bridle lines that are attached to the kite. Since the aerodynamic loading of the kite is not predictable, a safety factor of 2 is chosen for the sizing of the bridles, in compliance with AWE-TEC-AIR-07. Furthermore, to make the process of splicing

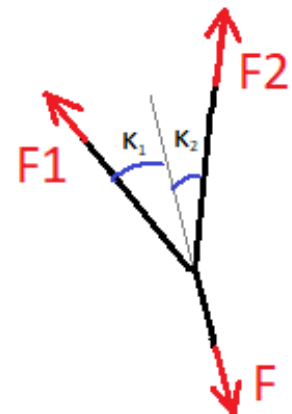


Figure 12.3: Schematic view of the forces acting on a bifurcation.

$$F1\cos(\kappa_1) + F2\cos(\kappa_2) = F \quad (12.6)$$

$$-F1\sin(\kappa_1) + F2\sin(\kappa_2) = 0 \quad (12.7)$$

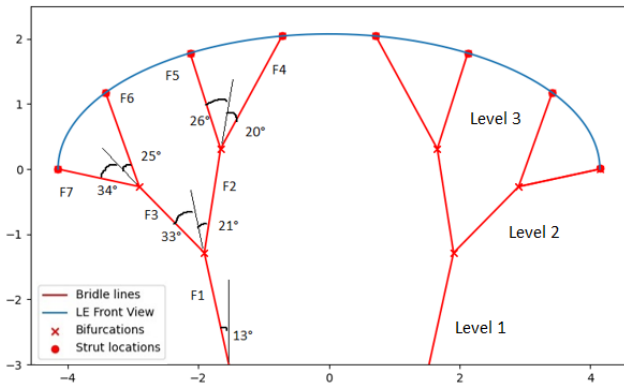


Figure 12.4: Bridle angles at bifurcations.

Table 12.5: Loads in bridles.

Bridle Line	Load in N	Bridle Line	Load in N
Level 1		Level 3	
F1	3710.24	F4	1522.16
Level 2		F5	1187.60
F2	2497.78	F6	1072.19
F3	1643.51	F7	810.32

easier in case of a bridle failure, a diameter of 1 mm is not used after consulting an expert in the field [152]. Because there is little data on low diameter Dyneema®, the diameter will not be interpolated, in case a bridle only carries a low force. Furthermore, it is chosen that the lines on the same level, as shown in Figure 12.4, have the same diameter. This is done, since dynamic loading is not being analysed, and during turns the loading might shift towards the tips of the kite. Based on the same method of determining the diameter of the tether, it is found that the bridles on level 1 and level 2 have a tether diameter of 3 mm and the bridles on level 3 have a diameter of 2 mm. Furthermore, the mass density for 2 mm and 3 mm Sierra 78 (bio-based) Dyneema® are equal to 0.2 kg/100 m and 0.5 kg/100 m respectively. Having determined the lengths of each of the bridle lines, the total mass of the bridle system is found to be equal to 0.145 kg.

12.5.2. Wing Loading

Now that the bridle system load distribution is known, a closer look is taken into how this load is generated. The tether and bridle loads are a result of the kite's pulling forces. In order to visualise this, the kite's lift distribution is shown in Figure 12.5. In this case, the lift is defined as the vertical force with respect to the axis system in Figure 11.8. As seen from Figure 12.5, the central part of the kite generates the majority of the lift, which will influence the bridle system's layout. From this general lift distribution, a percentage estimation on the to be carried lift at every attachment point is generated. This leads to the identification of the lift loads to be carried at the struts, considered from tip to root, to carry 1.66%, 9.88%, 17.72% and 20.74% of the total lift respectively. These percentages are based on the summation of the lift contributions from the middle of one control panel to the middle of the adjacent control panel, where the strut location is the control point between those panels, as used in the aerodynamic VSM program (see Figure 11.9). The force distribution can be seen in Figure 12.6.

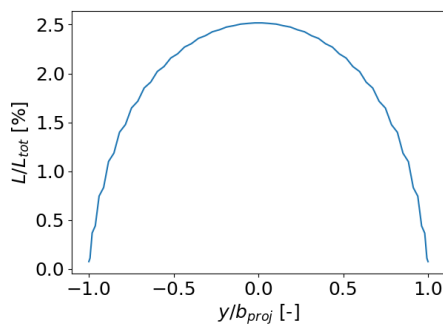


Figure 12.5: Wing Lift Distribution.

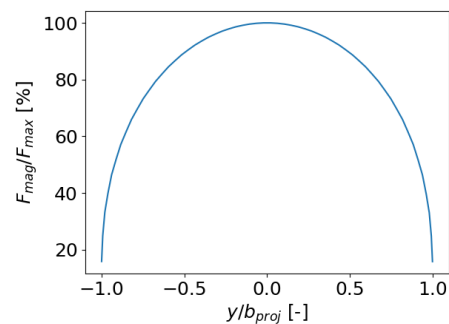


Figure 12.6: General Force Distribution.

The total lift force is the resultant traction force to be carried by the tethering line. However, this is not the total generated force by the kite. For this, the distribution of the general force should be considered. Similarly to the lift distribution, the general force generation at the tips is considerably less than at the kite's root, as observed from Figure 12.6. This is an expected result since the largest contribution of force generation is perpendicular to the kite's surface. These results add to the conclusion that the central bridle lines should be designed to carry higher loads than the tip bridle lines. With a nominal load of 10.3 kN, the average wing loading for this project's kite is calculated to be 618.62 N/m², based on the projected area.

This force analysis is unable to match the wing loading with the bridle loading. This is because of the unknown

load carrying capacity of the LEI tube, struts and canopy. In addition to this, the xy-plane force calculations are not considered. Hence, this load analysis is missing an integrated load path analysis from the lifting surface through the bridles and tether, down to the winch. This should be considered for future work, as well as a dynamic load analysis and aero-elastic deformation model to be integrated with the aerodynamics simulation.

12.6. Kite Material

To finalise the kite design, the material of the kite has to be determined. For over two decades, Dacron was the leader in the kite material industry, however due to development and innovative manufacturing techniques, a new material is on the rise, the ultra-high molecular weight polyethylene (UHMWPE) composite ALUULA [153]. Kite producing companies such as Ocean Rodeo use both Dacron and the ALUULA Vaepor™ fabric for their kites and have tested and compared both materials.

First, the mass of the ALUULA fabric is very low. Where Dacron has a mass of 160 g/m^2 , ALUULA only weighs 82 g/m^2 . This almost 50% mass reduction makes it much easier to steer the kite and improves the light wind performance of the kite. The strength of ALUULA has also increased a lot compared to Dacron. Its tensile strength is approximately 1200 N, which is double the strength of Dacron (580 N) [153, 154]. This means that a kite made from ALUULA has an increased lifetime compared to a kite made from Dacron. Its stiffness is measured by the E-modulus. ALUULA has a modulus of 927 N/mm^2 and Dacron 351 N/mm^2 . From this, ALUULA again outperforms Dacron, since it has a better resistance against deformation, leading to a more durable and reliable kite [155]. Furthermore, from talking to experts, it was clear that the kites using Dacron can handle a wing loading of up to 750 N/m^2 . Since ALUULA performs better than Dacron, the wing loading of 618.62 N/m^2 , which is equal to 742.34 N/m^2 including a safety factor of 1.2, is achievable. This is in compliance with AWE-TEC-AIR-02. A coating is applied before the yarns are woven together [153, 156]. This coating does not have to be reapplied and protects the kite against abrasion and UV-radiation. Dacron kites get a special coating after it is woven, but this coating is not recyclable and has to be reapplied. Over time, this coating degrades, polluting the nature and ecosystems it is operating. The ALUULA fabric is 100% recyclable, thus making the system extra sustainable.

The only disadvantage of the new technology is the price. It is 30% more expensive than Dacron [157]. However, since the durability is better, it will take longer before it needs to be replaced. Thus, in the course of time, it will become a relatively cheaper fabric than Dacron.

The kite mass is determined using a datasheet of a Rise A-Series kite [146]. This kite was used since it has an aspect ratio of 5 and 7 struts, for which it is easier to approximate an 8-strut system with the same aspect ratio compared to using a 3-strut system. An approximation is necessary, because the mass of the valves and reinforcements cannot be accurately determined. The flat kite area is used as input, to extrapolate the percentage of mass that the struts take. This can be seen in Figure 12.7. The extrapolation is based on a Teijin D2 54 gsm canopy and a full ALUULA airframe. To make the system fully ALUULA, the mass of the canopy is subtracted and the mass of an ALUULA canopy is added. Using an averaged value of the surface of all struts (0.687 m^2), a single strut can be added to the system to approximate the mass. This mass is multiplied by a factor of 2.5, because the material used in a strut is assumed to be 2.5 times as thick as the canopy. Using this assumption, the mass of the valves and reinforcements of the canopy, like a small thickness increase at the connection between the leading edge and the canopy, is determined. This mass is equal to 1.15 kg. A 5% margin on the mass is taken, to keep possible inaccuracies of the used data into account. The total mass and the individual contributions of the canopy and the airframe can be seen in Table 12.6.

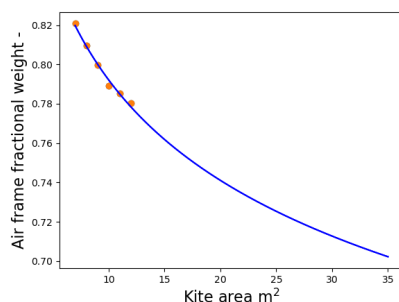


Table 12.6: Kite mass.

Parameter	Unit	Percentage	Value
Canopy mass	kg	34	1.65
Airframe mass	kg	66	3.26
Total mass	kg	100	4.91
Total mass + 5%	kg	105	5.16

Figure 12.7: Extrapolated kite airframe mass factor. (Teijin 54 gsm canopy)

Ground System Characteristics

This chapter will explain the characteristics of the ground system. In Section 13.1, the requirements, functionalities, and risks that are applicable for the ground system will be portrayed. With those inputs known, the anchoring for the truck can be sized in Section 13.2. After the anchoring type is determined, the drum dimensions are explained in Section 13.3. In Section 13.4, the extending rails mechanism for the spindle system will be explained. Finally, the launching equipment is explained and sized in Section 13.5.

13.1. Ground System Requirements, Functionalities, and Risks

This section's purpose is to highlight the requirements, functionalities and risks associated with the ground system. This enables a better integrated subsystem design and allows to more easily integrate the subsystem in the larger project framework. Additionally, it ensures the design follows the set expectations and remains reliable and safe. The ground system requirements are shown by Table 13.1. The identified risks and the risk reduction measures relevant for the design of this subsystem are shown in Table 13.2. The main functionalities of the subsystem the launching (F.3.3.2), landing (F.3.5.2), as can be read in Section 9.1.

Table 13.1: Requirements on AWES Ground System Properties.

Identifier	Requirement
AWE-TEC-OPS-01	The launching and landing of the airborne system shall be a task for maximally one person.
AWE-TEC-OPS-03	The AWES shall be able to operate for road angles between -2° and 2° .
AWE-TEC-OPS-04	The extending swivel rail shall not yield under the tether force experienced during nominal operations, including a safety factor of 1.2.
AWE-TEC-PG-06	The drum shall be able to withstand the maximum reel-in speed achieved during nominal operations, including a safety factor of 1.2.
AWE-CON-SAF-01	The pickup truck shall remain static under the specified operational loads.
AWE-CON-SAF-02	People shall not get injured during operation of the airborne system.

Table 13.2: Risks, with risk reduction measures influencing the ground system design.

Identifier	Measure
TR-LALA-02	It is possible to place extra weights on the launching equipment.
TR-LALA-09	An on/off button is installed to manually release the kite when the power is switched off
TR-GR-01	Rails are placed on the truck bed underneath the spindle. Small bumpers are placed on the sides of the truck bed.
TR-GR-02	Sensors are placed on the motor to monitor the status of the part.
TR-GR-03	The car is placed on the hand brake. A sensor is placed in the car to measure car movement.
TR-GR-05	Emergency buttons are placed within reach to shut down the whole system.
TR-GR-06	Include a connection the spindle that can be disconnected from the tether.
TR-GR-07	Including a redundant band and a brake on the drum.

13.2. Anchoring

The anchoring of the ground station must prevent the truck from sliding and tilting over when the kite system is active. This is vital for the safety of the product users. In previous estimations, a maximum force of 8 kN applied by the tether was assumed, based on older work for 25 m² kites [13]. However, in further design, it was found that the nominal load applied by the tether on the pickup truck will be approximately 10.33 kN, as calculated in Table 10.3. This means that it must be reassessed whether the pickup truck remains stationary during operations, and therefore whether an additional anchoring system is needed.

13.2.1. Sliding of the pickup truck

To estimate the sliding of the truck, a schematic view of the forces acting on a wheel at an angle can be seen in Figure 13.1. Here F_t is the force exerted by the tether on the car, F_f the friction force, N the normal force, W the weight, δ_{road} the road angle and β the elevation angle of the kite. For the car to be stationary, all forces in tangential direction should not exceed the maximum stationary friction force. Equating all forces in tangential direction to the friction force results in Equation (13.1). Here the forces in the normal direction are represented in Equation (13.2) and the relation between the normal force and the friction forces in Equation (13.3). Here, μ_s represents the static friction coefficient. The friction coefficients, necessary to remain stationary under a certain pull force at a specific angle, are calculated with Equation (13.4).

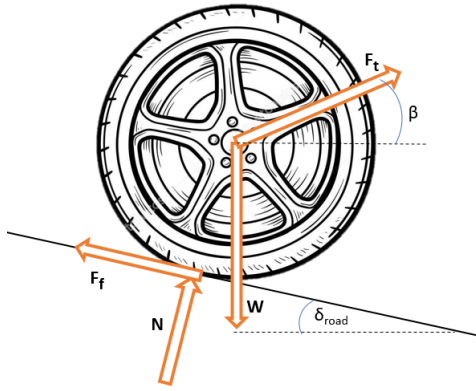


Figure 13.1: Schematic view of the forces acting on a wheel.

$$F_f = W \sin(\delta_{road}) + F_t (\cos(\delta_{road} + \beta)) \quad (13.1)$$

$$N = W \cos(\delta_{road}) - F_t (\sin(\delta_{road} + \beta)) \quad (13.2)$$

$$F_f = N \mu_s \quad (13.3)$$

$$\mu_s = \frac{W \sin(\delta_{road}) + F_t (\cos(\delta_{road} + \beta))}{W \cos(\delta_{road}) - F_t (\sin(\delta_{road} + \beta))} \quad (13.4)$$

With these equations, the worst case estimation can be assumed. Here, the mass of the pickup truck is taken at 3692 kg, which is the mass of an empty Rivian R1T[158] including the ground station with a conservatively estimated weight of 450 kg. The tether force is estimated at a nominal value of 10.33 kN. The tension is controlled by the winch at this value. To take into account the peaks caused by a delay in reaction time of the control system, a safety factor of 1.2 on top of this tension force has been taken. This is based on force peaks of 12.6% measured in similar wind conditions but with a smaller kite [4]. To take into account the uncertainty introduced by the increased kite size, the larger safety factor of 1.2 has been chosen. A maximum road angle for operation of 2° was chosen based on requirement AWE-TEC-OPS-03. This resulted in a necessary friction coefficient of the wheels for different elevation angles of the kite, β , that can be seen in Table 13.3. In Table 13.4, the static friction coefficients can be seen for rubber tires on different surface types.

Table 13.3: Friction coefficients necessary for a static pickup truck under varying elevation angles with a road angle of 2°.

Elevation angle, β	Friction coefficient, μ_{ground}	Elevation angle, β	Friction coefficient, μ_{ground}
0	-	0	-
25	0.40	31	0.40
26	0.40	32	0.39
27	0.40	33	0.39
28	0.40	34	0.39
29	0.40	35	0.39
30	0.40		

Table 13.4: Static friction coefficient values for rubber tires on different surface types [159].

Surface	Peak Value
Asphalt and concrete (dry)	0.8-0.9
Asphalt (wet)	0.5-0.7
Concrete (wet)	0.8
Gravel	0.6
Earth road (dry)	0.68
Earth road (wet)	0.55
Snow (hard-packed)	0.2
Ice	0.1

Based on the values obtained from the calculations, it becomes clear that the car would only start to move on hard-packed snow. This was also expected based on the initial estimations in the midterm report. A snow chain could increase the friction coefficient to a range of 0.2 to 0.3 on snow.

For safety reasons, in case the car is moved by a peak force on snow, the possible displacement should be determined. It is important to note that displacement will only take place for a very short period. When a peak load is registered by the winch control unit, the control system has two options to decrease the loading. The first option is increasing the reel-out speed, the second option is depowering the kite. However, there is a delay before the control system performs either one of these load decreasing mechanisms. This displacement is dependent on the reaction time of the control system. To calculate the maximum expected displacement, a reaction time of the control system of 100ms is used. This reaction time is the maximum, because slower reaction times would mean the control system cannot function properly, as will be discussed in Chapter 14. The displacement caused by this delay can be calculated with

$$d = \frac{1}{2} \frac{F_{res}}{m} \times t^2 \quad (13.5)$$

where d is the displacement of the truck, m is the mass of the truck and ground station, together 3692 kg, t is the duration of 0.1 s, F_{res} is the resultant force of 4407 N, calculated in Equation (13.6):

$$F_{res} = F_f - N \times \mu_{ground} \quad (13.6)$$

where N is the normal force of 28736 N determined for a road angle of 2°, and an elevation angle of 25°. The kinetic friction coefficient, μ_{ground} of 0.2 was obtained for tightly packed snow [159]. This gave a displacement

of 6 mm. As explained, this displacement is the maximum displacement to be expected for a peak load. This isn't estimated to occur frequently, as the control system is to be expected to react much quicker. As a very rough estimate, with an operation duration of a full day and maximum peak loads occurring every 30 minutes, the pickup truck will move a total distance of about 0.286 m per day, when placed on snow. Although this is not preferred, the distance is deemed sufficiently small to be accepted at this point in the design.

13.2.2. Tilting of the pickup truck

The anchoring of the car must also prevent the tilting of the pickup truck, as this would create a hazardous situation. Tilting can occur over the transverse axis of which a schematic view can be seen in Figure 13.2, where the kite force is angled to the side, because of which only the vertical component, F_{t-vert} is visible. In addition, N_b is the normal force on the tires at the back and N_f the normal force on the front tires. Tilting can also occur over the longitudinal axis, of which the schematic view can be seen in Figure 13.3. Here, N_l is the normal force on the left tires and N_r is the normal force on the right tires. The rest of the symbols used in both figures correspond to the symbols used in Figure 13.1.

During tilting, the pickup truck will tilt over one set of tires. For the tilting over the transverse axis that is the front tires and for the tilting over the longitudinal axis that is the right set of tires. The larger the load on the car, the larger the created moment around these tires and the smaller the force on the other set of tires. At some point, the force on the other set of tires would become zero and the car would start to tilt. For both tilting mechanisms, the normal force on the set of wheels that would start moving during tilting was calculated. As the normal force can only be positive, the pickup truck is static as long as all the required normal forces are positive. The equation for the normal force on the rear tires, N_r , is given in Equation (13.7):

$$N_r = \frac{W \cos(\delta_{road})(l_w - l_{c.g.}) - F_t \sin(\beta - \delta_{road})l_w - W \sin(\delta_{road})h_{c.g.}}{l_w} \quad (13.7)$$

where the symbols match those given in Figure 13.2, l_w is the distance between the wheels in longitudinal direction and $l_{c.g.}$ the distance from the back to the c.g. in longitudinal direction. For the tilting over the transverse axis, a worst case situation is taken, where the kite is pointed to the side of the truck and at an elevation angle of 35°. Pointed to the side is the extreme case as the tangential component of the tether force has no stabilising effect for tilting, because it is given that the kite will only operate at full power within 180° behind the truck as defined in Section 6.3.4. 35° is the maximum elevation angle within the operational window and is the extreme case for these maximum loads. As before, the mass of the pickup truck is estimated at 3692 kg. The kite force is estimated at 10330 N on top of which a safety factor of 1.2 was taken. Furthermore, l_w is 3.43 m [158], $l_{c.g.}$ is 1.54 m, based on the wheel loading and the location of the ground system, and $h_{c.g.}$ is 0.4 m, based on measurements in pictures of the Rivian and the fact that heavy batteries are situated at the bottom of the car. For this worst case, the normal forces on the tires remain positive, therefore the pickup truck is not expected to tilt over the transverse axis.

The equation for the normal force on the left tires, N_l , is given in Equation (13.8),

$$N_l = \frac{W(\frac{1}{2}\cos(\delta_{road})d_w - \sin(\delta_{road})h_{c.g.}) - F_t(\frac{1}{2}\sin(\beta + \delta_{road})d_w + \cos(\beta + \delta_{road})h_{drum})}{d_w} \quad (13.8)$$

In this equation, the symbols match those given in Figure 13.3, d_w the distance between the wheels in transverse direction, and h_{drum} the height of the drum. For the tilting over the longitudinal axis, the worst case situation was taken as well, where the kite is pointed at 35° to the side. d_w is taken at 1.9 m [158], h_{drum} is 1.1 m based on estimates from the preliminary layout of the drum. Again, it was found that the normal forces on the tires remain positive. Therefore, the pickup truck is not expected to tilt over the longitudinal axis

13.2.3. Dynamic loading

Dynamic loading is the remaining important loading for the anchoring system. If the applied dynamic loads have a similar frequency as the car response, unwanted resonance can occur. This can lead to unpleasant bouncing of the car or even damage. If necessary, extra damping could be implemented to prevent the unwanted

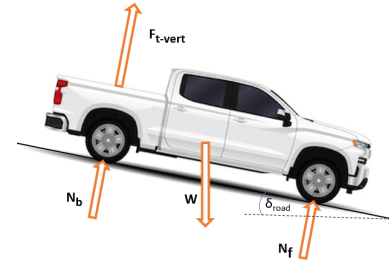


Figure 13.2: Schematic view of the forces acting on a pickup truck for tilting over the transverse axis.

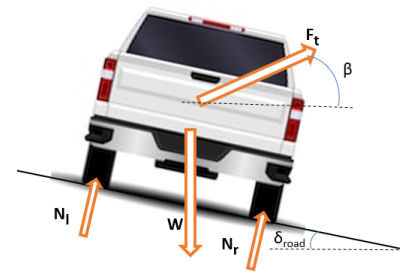


Figure 13.3: Schematic view of the forces acting on a pickup truck for tilting over the longitudinal axis.

resonance. Although the exact specifications of the dampers in the Rivian R1T are not publicly available, an estimation will be made based on similar damping systems.

During reeling, both in and out, oscillations were found with a frequency of 1.2 Hz. These are associated with the reeling controller on the ground system. The kite manoeuvres are estimated to create some oscillations as well, but at a much lower frequency of 0.1 Hz [12]. The damping system of the Rivian R1T is a hydraulic roll control system, that is also used in the McLaren MP4-12C and 720S [160]. This means that it has a damping system that is also used in sport and racing cars. Therefore, the natural frequency of the damping of the R1T is estimated at a range of 1.5 - 2.5 Hz [161]. As this natural frequency is significantly higher than the oscillations caused by reel in and reel out, it is expected that no resonance will occur and that no additional modifications to the pickup truck will be necessary.

13.3. Drum Sizing

The drum dimensions follow from the tether diameter. Firstly, since the $D_{\text{drum}}/d_{\text{tether}}$ is 105, the diameter of the drum is 0.47 m. Secondly, the length of the drum is determined by the tether length. The maximum operational altitude is 290 m, as can be read in Section 6.2.4. With an elevation angle of 30° , the required length is 580 m. A 30% safety factor is added to the operational range, resulting in 75 m extra tether. Due to volume constraints, the tether will be partially double wound on the drum. Due to the high forces during the operational phase, the tether can not be double wound, because it will cut in itself. This problem is solved by unwinding the outer layer completely during the starting phase before the operational altitude is reached. The drum is optimally used when the required drum length for the starting phase is equal to the operational phase. The tether is wound on the drum with a 0.5 mm spacing to avoid damage due to the tether rubbing against itself during winding. This 0.5 mm is an additional safety factor. With these constraints, the operational range starts at 165 m and ends at 290 m. This leads to a drum length of 1.1 m.

From research, it was shown that Gray Iron Grade G1800 is an optimal material to be used for the drum [162]. However, due to its high density of 7300 kg/m^3 , this material was not used, due to the tight mass budget of 500 kg. Based on the material density and performance properties, aluminium alloy 1100 is found to be desirable as drum material [162]. Using this material, the mass of the drum can be determined. First, the drum shell thickness can be estimated using Equation (13.9) as presented by Budynas and Nisbett [163].

$$t_s = \frac{Q}{\sigma_c d_t} \quad (13.9)$$

where d_t is the tether diameter, Q is the tension in the tether, which is assumed to be constant over its length, and σ_c is the allowable compressive hoop stress in the drum shell material [162]. The tether diameter, d_t , is equal to 4.4 mm, the tension in the tether is equal to 10329 N, and the allowable compressive hoop stress is equal to 0.85% of the yield stress, using a safety factor of 1.2. The yield stress for Aluminium Alloy 1100 is equal to 117 MPa, leading to an allowable compressive hoop stress of 97.5 MPa [162]. Using these values, the drum thickness was found to be equal to 2.4 cm. Moreover, for this thickness, the critical load in the tether is determined using Equation (13.10).

$$Q_{\text{critical}} = \frac{E d_t t_s^3}{D_d^2} \quad (13.10)$$

where E is the elastic modulus, and D_d the drum diameter. The elastic modulus of Aluminium Alloy 1100 is equal to 69 GPa, resulting in a critical load in the tether of 19203.44 N.

The mass of the drum can now be calculated using the drum dimensions, and knowing that the density of Aluminium Alloy 1100 is equal to 2710 kg/m^3 [162]. The mass of the clutches is determined separately from CATIA. The volume of the drum, without the clutches, is found to be equal to 0.0485 m^3 , which leads to a mass of 131.36 kg. Adding the mass of the clutches, which is equal to 0.2 kg, gives a total mass of 131.56 kg for the drum.

The drum will be attached to the bed of the pickup truck using bolts. It is assumed that the truck bed will not rupture before the tether fails. Future research is necessary to determine the actual truck bed fatigue, since no information is yet available on the material of the truck bed. Although contact was made with an engineer from Rivian, no further information was found since he was not able to disclose any information that is not public. The drum is visualised in Figure 13.4

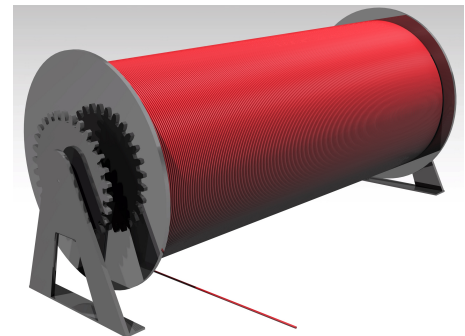


Figure 13.4: Visualisation of the drum.

13.4. Extending Spindle Rails

The application of rails on the truck bed is necessary to slide the spindle outward near the back of the truck bed and discard the limiting swivel angles constrained by the truck bed edges. In this way, the large swivel wheel diameter can be maintained while making it possible to operate the swivel 180° in azimuth direction and for elevation angle range from 0° till 90°.

One of the driving requirements of designing the rails was to minimise the height, and accordingly to minimise the height of attachment of the tether for operational stability of the truck. Secondly, from requirement AWE-TEC-OPS-04, the rails should be sturdy enough to transfer the tether loads to the truck bed without yielding in bending motion. These requirements lead to a design with 6 rails to keep the rail height as low as possible. The critical load for which the rails are designed is the maximum tether load with a safety factor of 1.2 applied in vertical direction at the end of the rail. The maximum bending applied from the kite is then equal to the 12.47 kN divided by 6 rails and multiplied by the maximum extracted distance of 0.27 m. This results in a design in which each rail has to support a maximum bending moment of 531 Nm. To design the rail profile and choose a suitable material, the bending stress equation, Equation (13.11) is applied [164].

$$\sigma_b = -\frac{My_{NA}}{I_c} \quad (13.11)$$

where σ_b is the maximum stress. This is constrained by the yield stress of the material. y is the maximum distance to the centroid and is 10 mm for this profile, and I_c is the moment of inertia of the beam which is $132 \times 10^{-9} \text{ m}^4$. For the rails, aluminium alloy 2024 is chosen, which is much stronger than normal aluminium alloy 1100 to minimise the rail height. Aluminium alloy 2024 with T4 temper has a yield stress equal to 40 MPa and is therefore a good material. Rearranging Equation (13.11) gives a maximum capable bending moment of 557 Nm, which is larger than the maximum tether load. Additionally, the load will be distributed over the extending rail, hence decreasing the real life bending moment. In the Figure 13.5, the placement and profile of the extending spindle rails are shown.

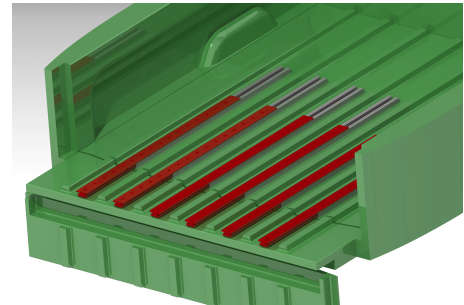


Figure 13.5: Rendering of the extending spindle rails.

13.5. Launching Equipment

Before the kite is launched, it is inflated and put in a pre-launch position, as discussed in Section 6.3. To prevent that wind comes under the trailing edge, blowing the kite away, the tether is kept under tension while the kite is blown up. It is then put into pre-launch position. To prevent the kite from being blown in an undesirable position in the pre-launch phase, launching equipment is designed. This launching equipment will have as its main function to provide enough tension force to pull the kite down and prevent it from coming into an unwanted position and generating lift prematurely. The equipment, as can be seen in Figure 13.6, is designed to be lightweight for storing. The handle bar is 0.83 m, and the width is 1 m. The equipment can be loaded with material from the launching spot, such as rocks or sand, in order to obtain the desired mass to mitigate risk TR-LALA-02, such that the equipment is not being pulled from the ground.

The main clamp is a rope that is magnetically attached to the leading edge of the kite, with the kite being in a tilted-back position. The end of the rope contains an electromagnet that can be turned off, to release the kite. The leading edge contains a thin plate of aluminium in the middle of the span of the kite. This aluminium strip will be concealed and integrated in the kite canopy, such that aerodynamic performance of the kite will not be jeopardised. When the clamp is disconnected, the rope itself will automatically wind up by a spring mechanism in the launching equipment. Similarly, the trailing edge contains a metal strip, which is connected to an electromagnetic clamp as well. This clamp is much smaller than the main clamp, as it needs to provide much less force, since it's only meant to prevent the wind from lifting the trailing edge up. It could be that for some reason the magnetic clamps do not come loose, which is described as risk TR-LALA-09. This is mitigated by the implementation of a separate button, to separate the electromagnets and the strips.

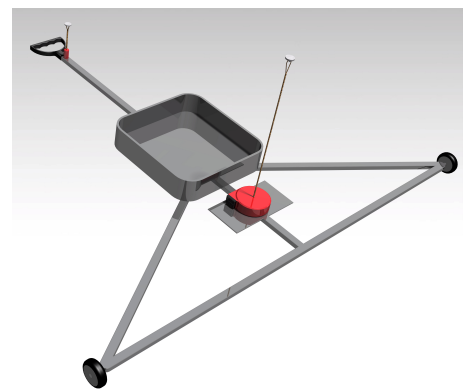


Figure 13.6: Visualisation of the launching equipment, containing a box to put in extra weight.

To determine the weight of the launching equipment, and the strength of the magnets that will be needed, a force and moment analysis was done. A visualisation of the relevant forces in the pre-launch position is given by Figure 13.7. Because the clamp force needed at the trailing edge is much smaller than the clamp and wind force, and it is located at nearly the same position as the normal force (F_N), it is neglected in the force and moments equations. The tether is assumed to stay in straight tension, as the weight of the KCU is assumed to be negligible compared to the tension force that is present on the tether.

The wind force (F_{wind}) was calculated with Equation (13.12),

$$F_{wind} = 0.5 \times \rho \times \sin(35) \times A_{flat} \times C_{d,ground} \times vw_{ground}^2 \quad (13.12)$$

where ρ is the air density, A_{flat} is the flat surface of the kite, and $C_{d,ground}$ is the drag coefficient. Lastly, vw_{ground} is the ground wind speed. The largest angle will mean the highest wind force. Normally, an angle of about 30° will be used for pre-launch positioning of the kite. However, for scaling the launching equipment, a more extreme case is assumed, with an angle of 35° before the launching procedure is initiated. A $C_{d,ground}$ value of 0.8 from Figure 5 from [165] is used to approach the drag coefficient of the kite on the ground at an angle of 35° , with an aspect ratio of 5, as was calculated in Section 11.6. A ground wind speed of 12 m/s was used, this is 50% as large as the nominal ground wind speed of the highest wind operational region, as described in Table 6.2, and therefore a realistic approach of high wind conditions of the system.

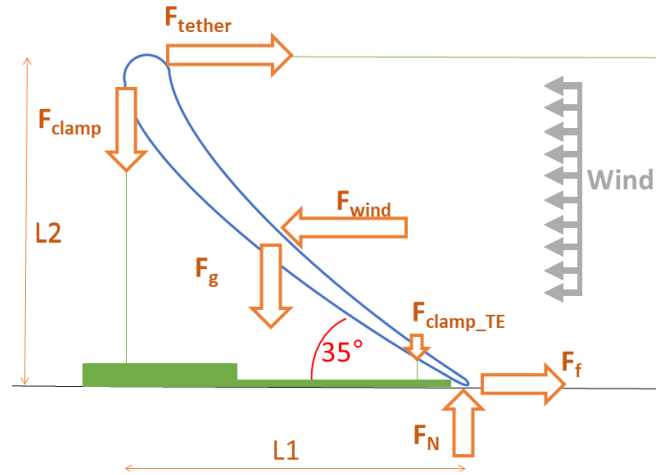


Figure 13.7: Visualisation of forces and kite position in pre-launch position.

The normal force (F_N) can be calculated using Equation (13.13),

$$F_N = F_g + F_{clamp}, \quad (13.13)$$

where F_g equals the mass of the kite (5.16 kg) times the gravitational constant (g). Lastly, the friction force is calculated using Equation (13.3), where μ_{ground} is the minimal static friction coefficient required, as calculated in Section 13.2. Furthermore, F_N equals the sum of F_{clamp} and F_g . By rewriting the force and moment equations for static equilibrium, the force that needs to be provided by the clamp can be calculated using Equation (13.14).

$$F_{clamp} = \frac{F_{wind}/2 - \left(\frac{L1}{2 \times L2} + \mu_{ground}\right) \times F_g}{\frac{L1}{L2} + \mu_{ground}} \quad (13.14)$$

This results in a clamp force that needs to be provided by the launching equipment of 191.8 N. The electromagnet should be able to hold at least of 191.8 N. Multiplying this with a factor of 5.5 [166], gives a magnetic clamping force of 1050 N. This results in an electromagnet weight of 0.55 kg [167]. Although the force needs to be smaller, an electromagnet at the trailing edge with the same strength is chosen, for simplicity and redundancy. To determine the actual force that is needed for the trailing edge, experimental data is needed. It is therefore recommended to do perform an experiment determining the clamp force that is needed. Furthermore, a mass of at least 19.6 kg of the launching equipment is needed, since it can not be assumed that the equipment can always be inserted into the ground. However, as mentioned before, the launching equipment doesn't always need to be of this weight. Think for example of transporting the system. The equipment can be lighter, and weights (for example a sack of stones or sand) can be used to lay on the launching equipment, thus making the equipment reach the appropriate weight.

Guidance, Navigation, and Control System Characteristics

The guidance, navigation, and control (GNC) system is vital for the successful operation of the entire system, as it is the brain of the operations. Both the kite and the winch are controlled by the system, and it is instrumental for the safety and efficiency of the design. First, the requirements, risks and functionalities of the system are discussed in Section 14.1. Then, the system is divided into three separate parts, which are discussed separately. The navigation, where the state of the system is determined, is discussed in Section 14.2. The guidance, where the path of the kite and the reel out speeds are calculated, is discussed in Section 14.3. The control, where the states of the kite are actively changed to follow the calculated paths from navigation, is discussed in Section 14.4. Finally, the communication and telemetry within the system are discussed in Section 14.5.

14.1. Guidance, Navigation, and Control System Requirements, Functionalities, and Risks

This section's purpose is to highlight the GNC related requirements and functionalities. This enables a better integrated subsystem design and allows to more easily integrate the subsystem in the larger project framework. The GNC subsystem requirements are shown by Table 14.1. The main functionality is control (F.3.4.2), as can be read in Section 9.1.

Table 14.1: Requirements on AWES Control Properties.

Identifier	Requirement
AWE-TEC-CS-01	The GNC system shall have a response time below 100 ms.
AWE-TEC-CS-04	The GNC system shall provide fully automated pumping cycles.
AWE-TEC-CS-06	The GNC system shall determine wind speed on the ground with an accuracy of 5%.
AWE-TEC-CS-07	The GNC system shall determine the wind orientation at least once every power cycle.
AWE-TEC-CS-08	The GNC system shall determine the attitude of the airborne system with an accuracy of 5°.
AWE-TEC-CS-10	The GNC system shall determine the tether force with an accuracy of 1%.
AWE-TEC-CS-11	The airborne wind energy system shall determine the reel-out speed with an accuracy of 2%.
AWE-TEC-CS-12	The KCU shall not be damaged during nominal operations.
AWE-TEC-CS-13	The KCU shall not be damaged during emergency landings.
AWE-TEC-CS-14	The GNSS sensor shall be able to determine the position of the kite with an absolute error of maximum 4 m.

Next to these requirements, the GNC subsystem is in charge of functionalities F3.4.1.A, F.3.4.2.A, F.3.4.B and F3.4.1.B. Firstly, the GNC system should autonomously perform a wind conditions assessment to determine the efficiency of operation start-up/continuation. This is performed by sensor data processing. For favourable wind conditions, the GNC system will take control of the pumping cycle (F.3.4.1.A). After a full cycle, wind conditions should be re-assessed for operation continuation. In case the forecasted wind drops for less than 30 minutes, reverse pumping cycling should be initiated (F.3.4.B) automatically. In this operating mode, the GNC system will also be in charge of the cycle control (F.3.4.1.B). Based on wind conditions and energy evaluations, the GNC system should decide to either land the kite or return to the nominal operation mode.

The risks that have an impact on the design of the GNC system are listed in Table 14.2. The biggest interest for the whole system is the redundancy of the components, since this will be quite expensive, and it needs to be budgeted for. Furthermore, the safety factor in the actuators and control lines needs to be taken into account when sizing.

Table 14.2: Risks, with risk reduction measures influencing the GNC design.

Identifier	Measure
TR-GNC-01	A redundant IMU and tether tension sensor are added
TR-GNC-03,-04	A large safety factor is used for both the actuators and the control lines
TR-GNC-06	A redundancy will be introduced into the communication and telemetry components

14.2. Navigation

In this section, the first part of the GNC system is discussed, the navigation. The navigation part determines the state of the system based on sensor inputs. In Section 14.2.1 the different reference frames are discussed. Then the system kinematics are presented in Section 14.4.2. Lastly, the different sensors, both in the air and on the ground, are listed and selected in Section 14.2.2.

14.2.1. Reference Frames

To understand the GNC system, it is necessary to explain the earth reference frame, which can be seen in Figure 14.1. The kite position with reference to the ground system are measured in the "Earth Centred Earth Fixed" reference frame. This can be seen as a half sphere with the ground system as origin. By the use of GPS location, the position of the kite in the earth reference frame can be determined. Now, the earth reference frame is converted to the "Wind Reference Frame" (x_w, y_w, z_w) with the y_w axis pointing in the wind direction [168, 169]. In this way, the kite can be controlled near the power zone of the wind window as the y_w is used as reference and this vector always points in the wind direction. From the "wind reference frame" the azimuth angle ϕ with respect to the wind direction and elevation angle β with respect to the ground can be obtained. These form the spherical coordinate (r_t, ϕ, β) with r_t the tether angle. If it can be assumed the tether is straight, the z_k vector and z_{se} are pointing in the same direction. The heading also called yaw angle can then easily be defined as the rotation around the z_k axis and is the angle between the x_{se} and x_k vector. The other rotations around the kite body x_k and y_k axis are denoted as roll and pitch.

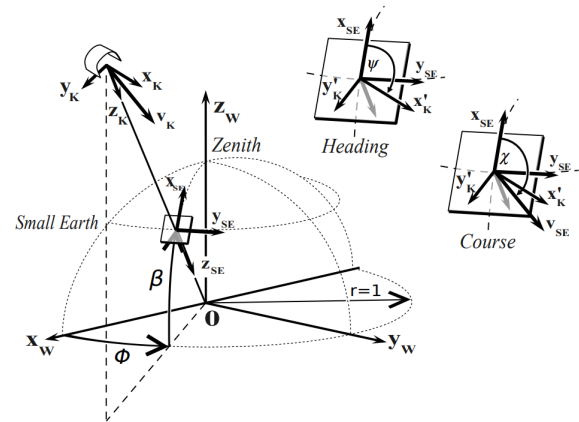


Figure 14.1: Earth reference frame, wind window reference frame [168].

14.2.2. Sensing

In this subsection, the sensors of the system are discussed. The sensors are listed and their outputs and accuracies are discussed. There will also be mention of why these measurements are done and how they impact the system. Furthermore, the sensors are split up into a ground sensing and in-air sensing.

A vital part of the GNC is determining the state of the system, such as the position, attitude and velocity, and the conditions that the system operates in, such as wind speed and wind direction. This is done by multiple sensors, both on the ground and in the air. The accuracy and the measuring rate of the sensors is an important factor when choosing. Because specific requirements are difficult to find for these accuracies and measuring rates, a lot of the specifications are based on existing systems.

In-air sensing

The biggest source of data for the aerial system is going to be the inertial measurement unit (IMU) [86]. The IMU chosen is the vectornav VN-200, and will be placed on the kite itself. It will be fitted behind the leading edge, and since this sensor is very small, it should not interfere with the kite's performance at all. This IMU consists of a gyroscope, accelerometer and magnetometer, with this specific one additionally equipped with an integrated high sensitivity GNSS receiver. The data this IMU will measure is the position, attitude and velocity of the kite. The accuracies of these are 1.0 m horizontal and 1.5 m vertical position accuracy, 0.2° dynamic heading and 0.03° dynamic pitch/roll accuracy and a velocity accuracy of <0.05 m/s. The range and measuring rate of this module is very high, and it can definitely be assumed that this will not cause an issue. To mitigate risk TR-GNC-01 a second IMU will be placed on the KCU.

To increase the accuracy of the altitude, and to get a good relative altitude between the car and the kite, a barometer is also integrated in the KCU. This is done by comparing the air pressures at the kite and car and relating this to altitude. For this, a chip, the SEN-11084 by SparkFun Electronics [170], is used that will result into obtaining the altitude with an accuracy of 0.1 m. This chip has added function to measure the temperature as well, with an accuracy of 1-3 °C, depending on the operating range. This is good enough since the temperature is not directly used by the GNC system, but if the need would arise to have a more accurate temperature measurement an additional chip could be implemented, that increases the accuracy to 0.25 °C, which is the Adafruit Industries LLC 1782 [171].

Furthermore, a pitot tube will be installed on the KCU, to measure the apparent velocity of the kite [172]. For this, a standard pitot tube is used. To have an estimate of the range and accuracy of a manometer, a handheld one is looked at, which has a range of 5-80 m/s with an accuracy of 0.01 m/s. This pitot tube will need to be placed

into the wind, a solution to this could be to make the tube rotatable and put vanes on this rotating structure, so it is automatically pushed into the wind, and for redundancy it can be equipped with angle sensors to get another reading of the heading. This is a solution that has been seen in current kite systems, but a system that is specific for the design of the KCU will need to be produced in the future. For now, it will be placed statically on the KCU, which will be shown in Section 14.4.4.

Lastly, there will be sensors to monitor the status of the components in the KCU, like the motors, battery and wind turbine. This is to see if these components are functioning properly. The energy production and storage of the wind turbine and the battery also needs to be monitored to make sure the wind turbine is stopped when the battery in the KCU is fully charged.

Ground sensing

An ultrasonic anemometer is used to measure the wind speed and direction on the ground [173]. These measurements are then interpolated, and used in tandem with a pitot tube on the KCU, to find reliable measurements for the wind speed at the operational altitude. A sensor comparable to the Rk120-03 is used. This sensor has a wind speed range of 0-45 m/s, with an accuracy of 0.2 m/s for wind speeds under 10 m/s and 2% of the value above 10 m/s. The direction is measured in all directions with an accuracy of 3°.

The main control of the winch speed is done by a force sensor in the drum. This needs to be done because the tether force varies with wind speed, and cannot exceed a certain level, so the winch speed is varied to compensate. This sensor will measure the force exerted on the drum by the tether.

The purpose of control of the tether at the ground station is to make sure that it is wound up neatly on the drum and that the angle under which it is fed into the air is controlled. This is done with a spindle motor that is placed just before the drum and is able to move along the length of the drum. Then to be able to not just let the tether be free to move after spooling off from the drum, a pulley is used. The principle of this is discussed in more detail in Section 14.4, but there will also be sensors in this system, to measure the angle of the pulley itself, and the angle the tether makes through the pulley. This data, together with the reeled-out length of the tether, and the tether force, can be used to estimate the position of the kite. These sensors need to have a high accuracy to get an accurate estimate, since a small angle change can make a large difference over a long distance. The accuracy of the angle times the length of the tether is proportionate to the accuracy of the position. This can be improved since the full range of 360° is not needed for this application. This system is a redundant system to the primary position measurement, which is performed in the air. Some truck data is needed, as well as the environment around the truck. To calculate the relative attitude between the kite and the truck, the magnetometer on the kite, together with a second one on the truck, is used. For this a separate chip is used since the full IMU is very expensive. This chip is called Mikroe-3522 and is made by MikroElektronika [174]. Furthermore, to get an accurate measurement of the relative position of the kite to the car, for which the data necessary is measured by a barometer and the IMU on the kite, these measurements also need to be performed at the car. For this the same barometer chip [170] is used as in the kite, but the GPS sensor, RF Solutions GPS-622F [175], is a different chip, for which the accuracy is a bit lower, 2.5 m, but since the car will be stationary, this could potentially be increased on, but the need for this should be reassessed in the future.

Similar to the in-air components, the components on the ground should be monitored to make sure they are in proper working conditions. It is especially important to monitor the status of the power related components, like the generator and batteries, since these are hard to inspect by person, but vitally important to the system. Furthermore, a system of sensors will need to be set up for the purpose of predictive maintenance, this could for instance be a camera on the tether to look for faults that are too hard to spot for a human. The specifics of this system are also considered for future research.

14.3. Guidance

Following the navigation of the kite, the next step is to have a look at the way the system is flown. The planning of the flight path is discussed in Section 14.3.1.

14.3.1. Flight Path Planner

The kite system uses a flight path planning system to define its flight path. This allows the kite to fly an optimal flight path for power production, but also to stay within the constraints of the kite system. The flight path planning system adapts to changing wind conditions, therefore ensuring more efficient operations in the entire operational range. It uses a combination of straight lines and circle segments when projected on a sphere to create a figure-of-eight shaped flight path. This is achieved by using two attractor points and two constant turn rates for every figure-of-eight. It is based on the flight path planner presented in [4].

This method and pattern has been chosen due to various advantages over alternative methods. For the accuracy and stability of the GNC, the influence of control loop delays are important to minimise. By choosing a relatively simple system based on two attractor points and two turns with constant turning rate, relatively few control commands have to be issued at the same time, reducing the issue of control loop delays. This issue is for example much larger for a GNC system which uses many attractor points [4]. The figure-of-eight pattern also has advantages over the alternative circular pattern for the tether and the adaptability to high wind conditions. Due to the figure-of-eight pattern, the tether does not twist, which would occur in a circular pattern. Lastly, down loops (flying directly downwards) cannot be avoided in a circular pattern, whereas with a figure-of-eight pattern it can be prevented in the case of high wind.

The flight path of an entire power cycle, including the reel-in phase, reel-out phase and transition states, can be seen in Figure 14.2. The angles depicted in this figure are not the angles that are used in this kite system, but serve as an example. A similar figure with the correct angles as proposed for this design can be seen in Figure 14.3. It must be noted that this is a projection of a half sphere on a flat plane which causes distortions of the lines and circles, however for the ease of understanding of the reader these effects have been neglected in the figure. The starting point for the power production is the kite parked at a high elevation angle with a short tether. This is the point P_p . Then the kite goes into the power state, where the angle of attack is increased to a set value for the reel-out phase. The kite then flies downwards to P_1 , makes a turn via C_1 and flies to P_2 until it reaches the target elevation and azimuth angle, after which it starts the figures-of-eight. During the figures-of-eight, the kite is navigated to points P_3 and P_4 and is turned around points C_2 and C_3 , all the while the tether is being reeled out. When either the maximum tether length or the maximum altitude is reached, the kite turns itself towards zenith and flies upwards, slowing down all the while still producing power. The kite flies upwards until the wind speed dependent reel-in elevation angle, β_{ri} , is reached, after which the kite is depowered. Following a short transition period, the tether starts reeling in. During the reel-in phase, the elevation angle will increase due to the lift, finally resulting in the kite ending up at the starting position, after which the cycle begins again.

Looking at the flightpath defined above, the inputs and outputs of the flight path planner can be identified. The first input of the planner is the set average elevation angle, β_{set} . This is the elevation angle around which the figure-of-eights are flown. In the case of this design, the initial estimation for this parameter is 30° . A representative visualisation of a projected figure-eight flight path can be seen in Figure 14.3. The other inputs are the kite course angle, χ , heading angle, ψ , and the Azimuth angle of the kite, ϕ . From these parameters the planner can identify where the kite is in the figure-of-eight pattern, how it is oriented and where it is going. The first important output of the planner is whether the kite is flying in a straight line towards an attractor point or in a turn with a constant turning rate. If it is flying in a straight line, the planner outputs a set position, $p_{k,set}^{SE}$, made up of the heading angle and course angle based on the location of the kite and the location of the attractor point. In the case of a turn, the planner outputs a set value for the turn rate, $\dot{\phi}_{set}$. When the kite has performed a kite state, the flight path planner outputs an exit state command to the top level controller. It then receives the new state command from the top level controller.

Figure 14.4 shows the decision process that is done at the start of every new cycle. First, it is checked whether a landing command had been given by the operator. If this is the case, the landing procedure is initiated. This procedure is also initiated when the battery would be fully charged. Furthermore, also the ground wind speed over the last 60 seconds is averaged, and transformed to the estimated wind speed at operational altitude. If this wind speed is lower than the minimal wind speed, the reverse pumping cycles are initiated. Afterwards,

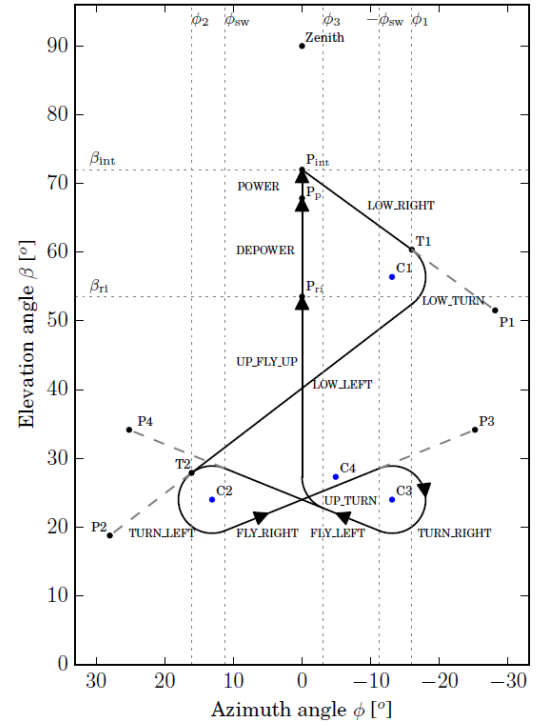


Figure 14.2: Schematic representation of the flight path during a single power cycle, with the reel-out phase at an average elevation of 24° . Four turns (around C_1 to C_4) and five attractor points (P_1 to P_4 and Zenith) are needed [4].

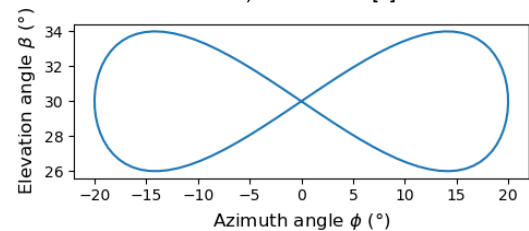


Figure 14.3: Schematic representation of the flight path during a single figure-of-eight manoeuvre at an average elevation of 30° , as proposed for the current design [176]

this wind speed is multiplied with a gust factor, in order to have an estimation of the maximal wind speed that is expected to occur during the coming cycle. If, under the standard average elevation angle of 30° and at this gust wind speed, the power limit is reached, a new elevation has to be set for the next cycle. This elevation angle is chosen such that the power limit shall only be reached at the gust wind speed. In Section 14.4.6, it is explained what should be done when a wind gust occurs that is higher than the foreseen gust wind speed.

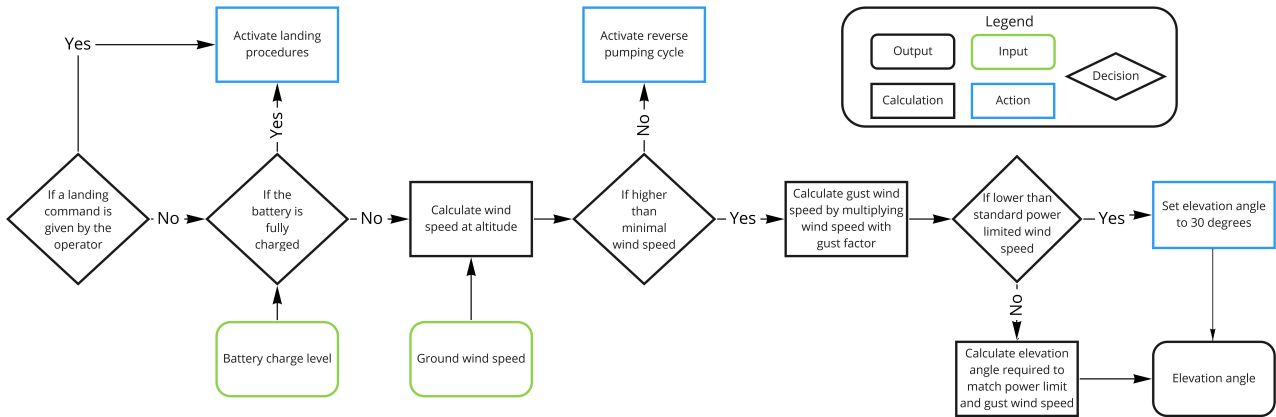


Figure 14.4: Decision process at the start of every cycle.

14.4. Control

The last major part of the GNC system is control. First, the top level control is explored in Section 14.4.1. After this, the kite control is designed and sized, first the software and then the hardware, presented in Section 14.4.3 and Section 14.4.4 respectively. Lastly, the same is done for the ground system discussed in Section 14.4.5 and Section 14.4.6.

14.4.1. Top Level Control

At the top of the entire GNC system stands the top level control. This system determines the mode of the and passes it on to the flightpath planner and winch controller. It makes the rest of the switch between the operational modes such as the launching, landing, pumping cycles, reverse pumping cycles and, if necessary, safety states, which is further defined in Chapter 8. For every operational mode, different states are defined. The exact states for the pumping cycle have been discussed in Section 14.3.1. The states of the other operational modes are outside the scope of this report.

The top level control starts in the launch mode at the start of an operational cycle, after the human input to launch. After the kite has been launched, the flight path planner outputs a signal to indicate the launch is complete. The top level now starts the pumping cycle mode. Until the top controller receives a human input to land or a signal that the battery is full from the charge controller, this is performed continuous, after which the landing mode is started. In case of an input from the wind sensor of too low wind, the reverse pumping cycle mode is started. Finally, if the FDIR, as defined in Chapter 8, identifies a fault for which an emergency mode is needed, the top controller initialises the required mode.

14.4.2. Kite Control Mechanics

Steering of a kite has been made very easy for humans these days. By changing the length of the steering lines, the kite responds quickly with a left or right turn, and it can be brought in a straight flight path by holding the steering lines at the same length. This manoeuvre seems very intuitive for humans, but to understand the aerodynamic forces that act on the kite when the length of the steering lines is changed is very complex. Therefore, to design a flight path planner, simplification are made and relations are formed to link the flight path to the steering inputs. In Section 14.2.1, the three degrees of freedom are already explained and are the spherical coordinates (r_t, ϕ, β) of the kite. Pitch and roll are two rotations that are kinematically coupled as they are tangential motion of the kite. However, the third heading ψ is non-tangential with the kite. This leads to a fourth degree of freedom, mainly the rotation around the tether.

The system responsible for these kinematic motions consists of the kite, KCU and bridles lines which all work together. The KCU actuates the bridles and the bridles morph the kite to change the aerodynamic characteristics which lead to a rotation in the reference frame of the kite. The KCU consists of 2 motors which actuate a depower motor and a steering motor. The depower motor is easy to control. The change in length of the tape corresponds to a change of angle of attack of the kite. The steering motion is more complex as this serves to change the heading. It consists of one tape that is connected to the left steering line and one to the right

steering line, When the motor rotates the length of the left and right tape can be changed. For example, if the left tape is made longer than the right tape, then this will roll the kite clockwise with the corresponding lift vector of the kite. Also, the right wing tip will be reeled into the wind, which increases the local lift vector of the right wing tip.

These two behaviours lead to a change in heading, also called yaw motion. To design this motion in the flight path planner, the empirical turn rate law,

$$\dot{\psi} = c_1 v_a (u_s - c_0) + \frac{c_2}{v_a} \sin \psi \cos \beta \quad (14.1)$$

is used, where c_0 , c_1 and c_2 are experimentally obtained coefficients and u_s , the steering input [177]. So, instead of using a dynamic model of the kite, the turn rate $\dot{\psi}$ is coupled to the steering input of the tape length. The coefficients are reassessed every few days to compensate for kite wear and bending. Another flight angle to design the flight path planner is the course angle, χ which describes the direction of the tangential velocity vector $v_{k,\tau}$. In straight trajectories, it can be assumed that the heading and course angle are the same because kites are designed like aeroplanes which align with the wind direction. This holds if it is not required to compensate for inertial and gravitational forces. For example, in a turn for a real kite with a certain mass, gravitational force are present and have to be balanced by an aerodynamic side force. This force is generated by inclining the heading and the corresponding shift of the lift vector. The force that is generated in a turn is calculated in the equation below [177].

$$F_{l,\tau} = m \frac{v_{k,\tau}^2}{R}, \quad (14.2)$$

with R the radius of the turn, $v_{k,\tau}$ the tangential kite velocity and m the mass of the kite system. The rate of change of the course angle can then be described by the following relation

$$\dot{\chi} = \frac{v_{k,\tau}}{R} = \frac{l_t}{R} \omega. \quad (14.3)$$

In this equation, ω is the angular velocity and r the tether length. The objective is then to implement the change of the course angle and turn rate in the flight path planner to fly to certain attractor points in the small earth reference frame shown in Figure 14.1 [177].

14.4.3. Kite Control Software

The kite system relies on a reliable flight control system to be able to operate safely and produce power efficiently. The kite controller ensures that the kite follows the optimal flight path as determined by the guidance system. The kite system is highly complex, and the inputs relate non-linearly with the outputs. Multiple methodologies for the control of these kinds of systems are possible. As the control of airborne wind energy systems is still a growing field, a lot is still uncertain or unexplored. However, a few different control methodologies will be discussed and compared.

One of the first ideas for the control of kite systems was the use of Nonlinear Model Predictive Control (NMPC) [178]. NMPC uses a model to predict the system behaviour and determines the steering input based on a cost function optimisation. For the kite system, this function could incorporate the maximisation of the power production and stability criteria, but allows for more options if deemed necessary. However, the modelling of kite systems remains complex. Pulling the bridle lines to control the kite changes the geometry of the bridle and deforms the kite itself. In addition, a strong coupling is present between the structure of the kite and the external aerodynamic loading. In essence, a balance is found during flight between the aerodynamic loading deforming the kite and the changing kite shape influencing the aerodynamic loading. All this physical complexity causes the computational cost for a kite model to be very high. Although this option could be interesting when more research is performed on efficient modelling of a kite system, it is unfeasible for the current design.

Another option is based on evolutionary robotics or neural network controlling [179, 180]. The appeal of such a system is its ability to adapt to change. However, the use of these kinds of systems in the control of airborne systems is limited and has had varying success. Due to these reliability issues, it has been deemed unfeasible for airborne systems at this point in its development.

A third option can already be seen in use by large traction kites on large cargo ships [178]. These systems use a nonlinear bang-bang-controller, also called an on-off controller. It uses empirical correlations between steering inputs and yaw rates of the kite. A large advantage is that the system is relatively simple. However, an important disadvantage is that the control is limited. It allows for the kite to fly a figure-eight manoeuvre, but the shape of the trajectory can only be changed by advanced tuning of the commands of the operator.

The final approach is the use of linear controller methods in the form of a Proportional Integral Differential (PID) controller. To compensate for the nonlinearity of the system, output linearisation is often applied. Here,

the output is linearised based on empirical data and some additional inputs. These additional inputs vary, but entail at least the apparent wind speed and often some attitude parameters of the kite [178]. An advantage of PID controllers is that they are well known and widely used, however for very dynamic systems such as a kite system improved techniques exist. One of these improvements to increase the accuracy of the controller is a Linear Parameter-Varying (LPV) controller. Here, different parameters are controlled in different flight conditions according to the linearity of their behaviour in set flight conditions. This allows a non-linear system to be controlled with linear PID methods. In the case of this kite system, mainly the course angle is controlled at high angular velocities, only the heading angle is controlled at low angular velocities and in between these speed regimes both are controlled [4]. As this kind of system has been used before in prototypes of a kite system, this design will also use a LPV controller in combination with output linearisation. It is expected that this allows the kite to be accurately controlled, without the need of an extensive, computationally heavy model of the kite system.

The kite control receives inputs on required actions from the flight path planner. Based on the output of the flight path planner, the controller switches to the control for a straight section or a turn. In the case of a straight section, the LPV controller controls for the set heading and course angle as outputted by the flight path controller. This is done by the LPV and output linearisation as described before, and results finally in a steering input defined by the distance the steering lines must be displaced, which vary for the apparent speed of the kite. When turning, the steering input is calculated based on the inputted set turn rate and the turn rate law described in Section 14.4.2 with its necessary inputs. This directly gives a steering input.

14.4.4. Kite Control Hardware

The kite is controlled by an airborne control unit also called KCU. This device is located 10 m under the kite and is responsible to change the pitching and heading of the kite. The main performance specification of the KCU are the mass and drag, as the more drag directly relates to a lower flight speed and hence lower tether force [13]. Mass also has to be minimised to operate the kite in light wind conditions. In this way, the operating wind window can be increased. From the structural design of the KCU in CATIA and the implemented hardware, the total mass of the KCU is determined to be 6.71 kg. The drag on the other hand can be approximated to be 10% of the total kite drag with $C_D = 1.0$. The frame of the KCU is for these reasons made of lightweight aluminium alloy 1100 which can easily be shaped in an aerodynamic profile. An analysis on the KCU structure will not be performed in this report, but is recommended to optimise the mass and drag. For the dimensions, a size of 0.390 x 0.360 x 0.310 m is obtained to include the hardware and protect the KCU with a 6 cm foam layer. The main components of the KCU are present in Figure 14.5 and Figure 14.6 which are the following: the actuation drive trains, board computers, antenna, safety release pin, pitot tube, a wind turbine and a battery for consistent energy. For the actuation drive trains both consists of gearboxes, tape drums and servo motors. Additionally, the depower motor is also provided of a depower break mechanism to keep the kite at a certain angle of attack. Both servo motors have a reeling speed of about 0.4 m/s [84]. If the depower motor would be stuck in full power mode, a safety release pin is installed at the bottom of the KCU to prevent extensive stress on the tether or braking the weak link. So, if the controller detects a malfunctioning depower motor and the operating force on the tether is too high, then the safety release pin detaches the KCU from the main tether and swings below the kite. If this doesn't work or an unanticipated gust increases the load on the tether too fast, then the weak link will rupture and prevents the main tether to brake. The weak link is located just below where the tether splits up in two power lines and the line to the KCU. When This happens, the kite is still connected to the main tether via a safety line, attached in the middle of the leading edge of the kite. If it ruptures it has to be replaced by a new one, but the main tether is protected.

From the damage prevention requirements AWE-TEC-CS-13 & AWE-TEC-CS-14, it is chosen to apply a foam layer to protect the KCU during nominal operations and emergency landings. The thickness and foam material is designed in the following way. First the design crash speed is set to 40 km/h which seems reasonably higher than an emergency glide landing or operational landing. The KCU foam will absorb the energy by compressing the material. Following, the thickness of the foam should be minimised, by also taking into account that the crash deceleration is not too large to protect the structure and the electronic devices. The thickness of the foam is calculated with

$$t = \frac{E_k}{W_e \cdot A_{contact}}, \quad (14.4)$$

where E_k is the kinetic energy obtained from the design crash speed, W_e the energy density of the foam and $A_{contact}$ is the smallest contact area for which a corner of the KCU is the critical design case. The deceleration can be calculated using

$$a = \frac{F}{m} = \frac{\sigma \cdot A}{m}. \quad (14.5)$$

In this equation, σ is the exerted stress from the compressed foam and A is the contact area. In this case, the largest area, which is the critical design case for deceleration, and m is the weight of the KCU.

The thickness and deceleration follow from the foam material for which the energy density is linearly related to the optimal stress on a double log scale [181]. In Figure 19 from [181], a material with a larger energy density is favourable to lower the thickness, however a material with a smaller stress and energy density allows for a smaller deceleration. Hence, a smaller deceleration has to be compensated with a larger foam layer thickness. An optimum is found for expanded polyester (EPS) with a foam thickness of 6 cm and a deceleration of 330 g which is only 30 g higher than the design of a bike helmet to protect a human brain. The foam layer thickness relative to the KCU is visible in Figure 14.5.

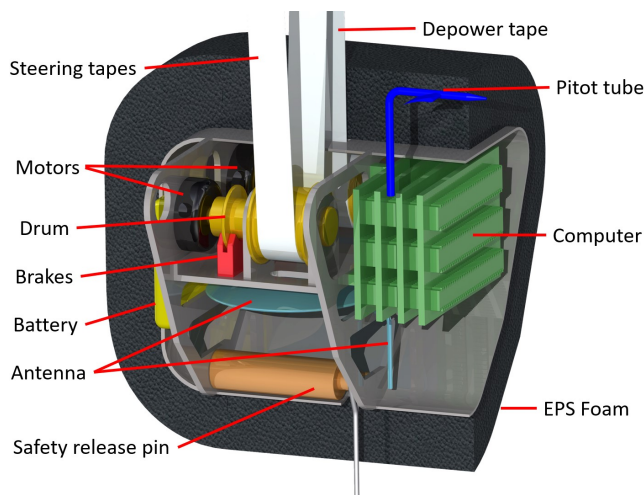


Figure 14.5: KCU hardware overview

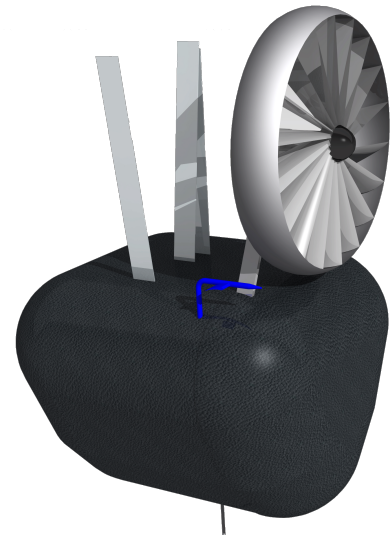


Figure 14.6: KCU foam protection with integrated wind turbine

14.4.5. Ground Control Software

During operations, the winch must be controlled to ensure optimal performance in the different states of the operational phase [4]. For the different operational phases, different controllers are designed and switched between. The winch control must ensure that the tether forces do not exceed the set minimum and maximum tether forces per operational state, therefore preventing that the tether breaks and ensuring controllability of the kite. When the winch is actively reeling, which is during the reel-out and the reel-in phase, the winch control also ensures optimal performances. During reel out, optimal performance means that power production is optimised and during reel in, this means that the reel-in time is minimised. During reel out, the power production is optimised according to the Luchsinger model as described in Section 10.2. Special commands may be necessary for launching, landing and safety modes, but these will be discussed separately in their respective chapters, namely Chapter 13 and Chapter 8.

The winch controller has several inputs: first, the minimum and maximum tether force [4]. When outside this force range, the force is actively controlled. Secondly, the set speed. The set speed is the set reeling speed of the winch for optimal performance in varying scenarios. When in between the allowable force range, the set speed is based on the Luchsinger model for reel out and ensures minimum reel-in time during reel in. When outside the force range, it is based on active force control to keep the forces at the maximum or minimum force. The controller also has the actual measured tether force and the actual reel-out speed as inputs. The only output of the controller is the set speed of the motor controller, which controls the reeling speed of the winch.

Figure 14.7, shows the decision process that is constantly repeated during operation. First, it checks whether there are any safety issues reported by the FDIR system. If there are any, the system is commanded to follow the safety procedure for that issue. Furthermore, it constantly measures the wind speed at the ground station, and converts this to the estimated wind speed at the operational height. When a wind gust is measured that, for the chosen average elevation angle for the current cycle, would be higher than the wind speed at which the power limit is reached, the system calculates when this gust is expected to arrive at the kite. When the gust arrives, the tether cannot be reeled out any faster, as the power limit is reached, which is explained in Section 10.4. Therefore, the system also checks if there is a wind gust expected to arrive within the coming 10 seconds. If this is the case, the kite should be depowered, as changing the elevation angle during a cycle takes time, and is therefore not a short-term effective measure. Next, the decision cycle also checks if the reel-out is completed, in order to initiate the reel-in process at the right time. The optimal reel-in speed is then calculated

with the Luchsinger model, based on the current wind speed and the average reel-out speed. Lastly, the most probable thing to happen, is that the reel-out speed is adjusted based on the measured tether force, which should be kept under the traction force limit.

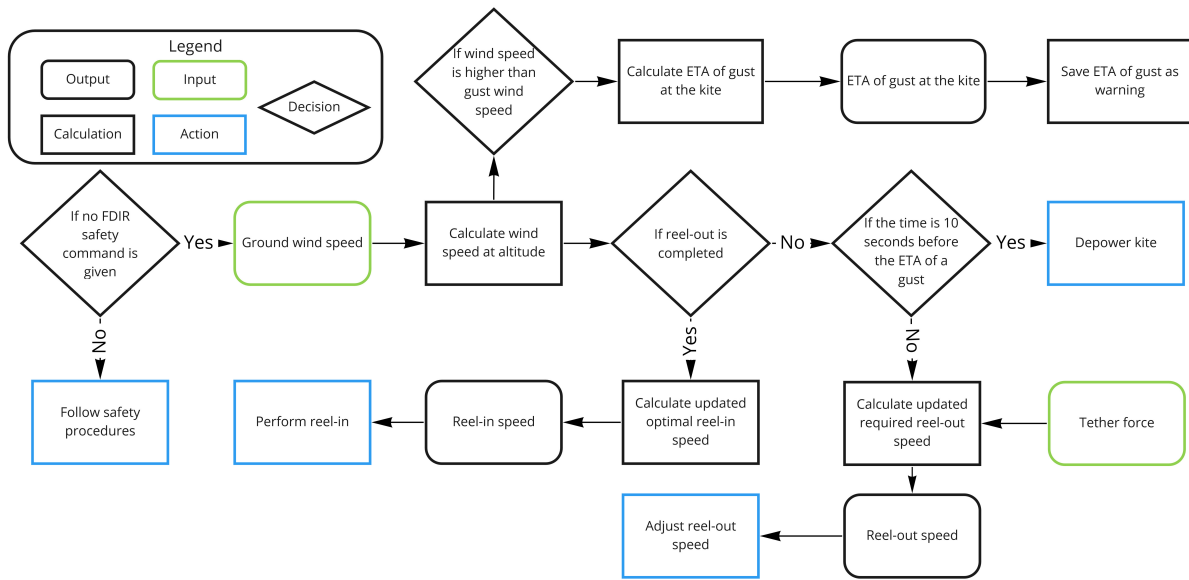


Figure 14.7: Repeated control loop during reel-out.

The winch control controls a simpler system than for example the kite controller. The relation between the set speed of the motor controller and the speed of the winch is influenced by less external parameters, and the speed of the winch is either directly found from the Luchsinger model or from a required tether force. This relation between the tether force and the winch speed is then again also influenced by little external factors. This allows the controller to be simpler than those described in Section 14.4.3. That is why PID controllers are chosen for the different phases, with different gains per phase.

The ground system control also controls the motor of the spindle. The spindle guides the tether onto the drum and moves over the length of the drum, ensuring the tether doesn't wind on top of itself. The speed of this motion is dependent on the reeling speed, therefore the motor moving the spindle is controlled with the reeling speed as input. A more in depth description of the spindle will be given in Section 14.4.6.

14.4.6. Ground Control Hardware

The main purpose of the ground control is to regulate the tether, the guidance of it into the air and back on the drum, and the reeling speeds at which this is done. For this first task, a combination of a motor and swivel is used, and the second is performed by a separate motor and brake system.

The motor and swivel combination, from here on called the spindle motor, is used to guide the tether from and onto the drum, to ensure the tether does not wind on top of itself, and still fits completely onto the drum. Furthermore, it guides the tether to have a straight line towards the kite, which is generally done by a set of pulleys. The control department has come up with a design to use a single pulley integrated into the spindle motor, which can be seen in Figure 14.9. The diameter of the spindle is set at 0.27 m, to comply with requirement AWE-TEC-AIR-08. The angle of rotation of this pulley is around the axis of the tether coming from the drum, and then the tether is free to make the bend towards the kite on the pulley. These angles, of the pulley and the angle the tether makes on this, are measured, and together with the reeled-out length of the tether, the position of the kite can be determined. In Figure 14.9 and Figure 14.10 the angle the swivel makes with the truck bed, δ_s and θ_s , and the angles the tether makes with the ground, β and ϕ , are shown. These last two are to be derived from the first two. For this, the length of the tether, l_t , is needed also. A schematic overview of the reference frame is shown in Figure 14.8.

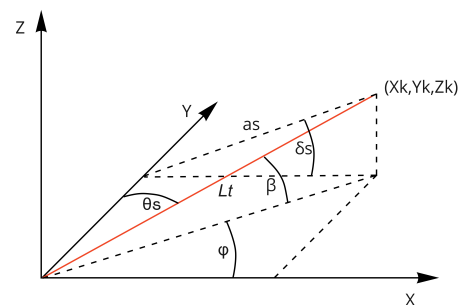


Figure 14.8: Reference frame used to obtain the relative position of the kite compared to the truck (origin). It shows the angles δ_s and θ_s that the spindle motor makes, the elevation angle β and the azimuth angle ϕ .

With angle θ_s , the projected length, a_s , onto the x-z planes and the Y-coordinate of the kite is calculated, as is shown in Equation (14.6) and Equation (14.7).

$$a_s = \sin(\theta_s) \cdot l_t \quad (14.6) \quad Y_k = \cos(\theta_s) \cdot l_t \quad (14.7)$$

With the length of a now known, the X- and Z-coordinate of the kite can be calculated, using Equation (14.8) and Equation (14.9) respectively.

$$X_k = \cos(\delta_s) \cdot a_s = \cos(\delta_s) \cdot \sin(\theta_s) \cdot l_t \quad (14.8)$$

$$Z_k = \sin(\delta_s) \cdot a_s = \sin(\delta_s) \cdot \sin(\theta_s) \cdot l_t \quad (14.9)$$

The last thing to do to get the elevation angle β and the azimuth angle ϕ is to use simple trigonometry, shown in Equation (14.10) and Equation (14.11).

$$\beta = \sin^{-1} \left(\frac{Z_k}{L} \right) = \sin^{-1} \left(\frac{\sin(\delta_s) \cdot \sin(\theta_s) \cdot l_t}{l_t} \right) = \sin^{-1} (\sin(\delta_s) \cdot \sin(\theta_s)) \quad (14.10)$$

$$\phi = \tan^{-1} \left(\frac{Y_k}{X_k} \right) = \tan^{-1} \left(\frac{\cos(\theta_s) \cdot l_t}{\cos(\delta_s) \cdot \sin(\theta_s) \cdot l_t} \right) = \tan^{-1} \left(\frac{\cos(\theta_s)}{\cos(\delta_s) \cdot \sin(\theta_s)} \right) \quad (14.11)$$

Note that this calculation does not take into account the sag of the tether, which will change its length and the outgoing angle θ_s . This should be accounted for when designing the GNC system in more detail. To be able to maximise the power output of the system, the reel-in and reel-out speed need to be controlled. For the reel-in speed, a separate motor is used. When the kite transitions to the reel-in phase, the generator is decoupled from the winch, through a clutch, and the motor is coupled in the same manner. Simple motor control will then determine the reel-in speed. While reeling out, the generator is producing energy, and with that providing a braking force. But to set the optimal reel-out speed, especially when the winch is going too fast and the tether force increases too much, a brake is applied that is connected to the drum.

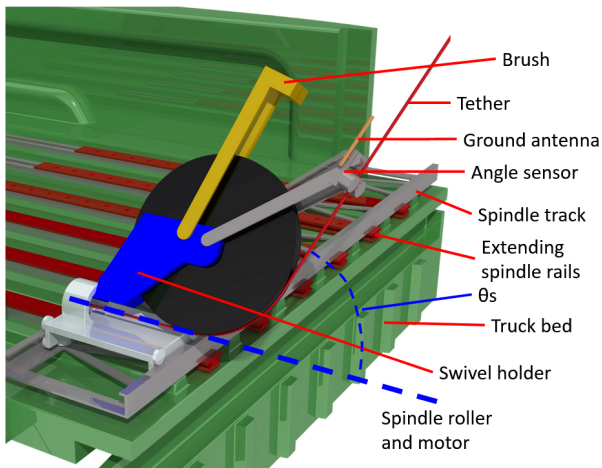


Figure 14.9: Overview of the spindle and swivel components on extending spindle rails on the back of the truck bed.

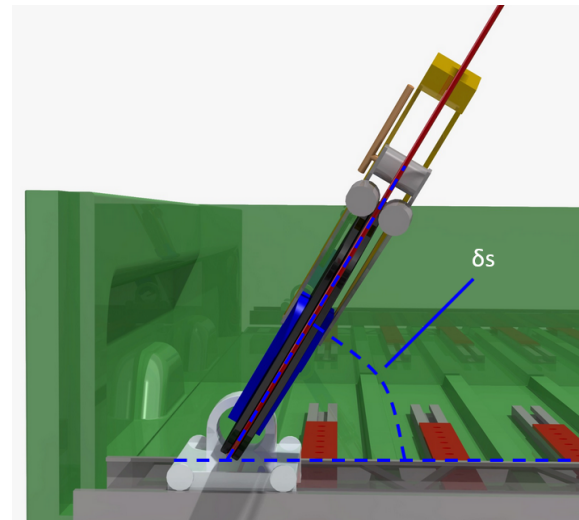


Figure 14.10: Front view of the spindle and swivel, indicating the angle of the swivel.

14.5. Communication and Telemetry

A vital part of the entire system is the communication and telemetry. It allows the system to communicate internally and to transfer vital data from system to system. As a large part of the communication within the system is associated with the GNC system, it is discussed in this chapter. In Figure 14.11 the top level control, communications, and data handling within the system can be seen. The data streams between parts of the system and the function of the blocks in the diagram are shown, in addition to the location of the blocks within the system. The interfaces between hardware and software, as described in previous sections, are thereby visualised.

The interface between the in-air system and the ground system is formed by both the receiver and antenna of the Wi-Fi system in the KCU and the ground system [13]. This interface and these parts were assessed to carry high risk, and therefore a redundant system is also included. The layout is based on similar systems and contains a main 5GHz directional antenna and a backup 2.4 GHz system. To ensure correct pointing of the antennas, the antennas on the ground station are mounted on a swivel. This causes the antennas to roughly be pointed along the tether, therefore pointed towards the KCU. In the KCU, the antennas are aimed downwards along the tether, ensuring continuous pointing towards the ground station.

The last important parameter for control regarding the communication and telemetry that will be discussed, is the control response time. Following from requirement AWE-TEC-CS-01, the response time must be below the 100 ms. Research performed on similar GNC systems shows that the total delay time for the control in the current set up will meet this requirement. The delay time values per subpart of the system can be seen in Table 14.3. These add up to 100 ms.

Table 14.3: Time delay values per subpart of the communication and telemetry system [4].

Component	Unit	Max delay
IMU	ms	20
Wired link, kite to KCU	ms	5
Wireless link, round trip	ms	30
Kite state estimator	ms	5
Flight path controller	ms	20
Motor controller	ms	20
Total	ms	100

Control, Communications, and Data Handling Diagram

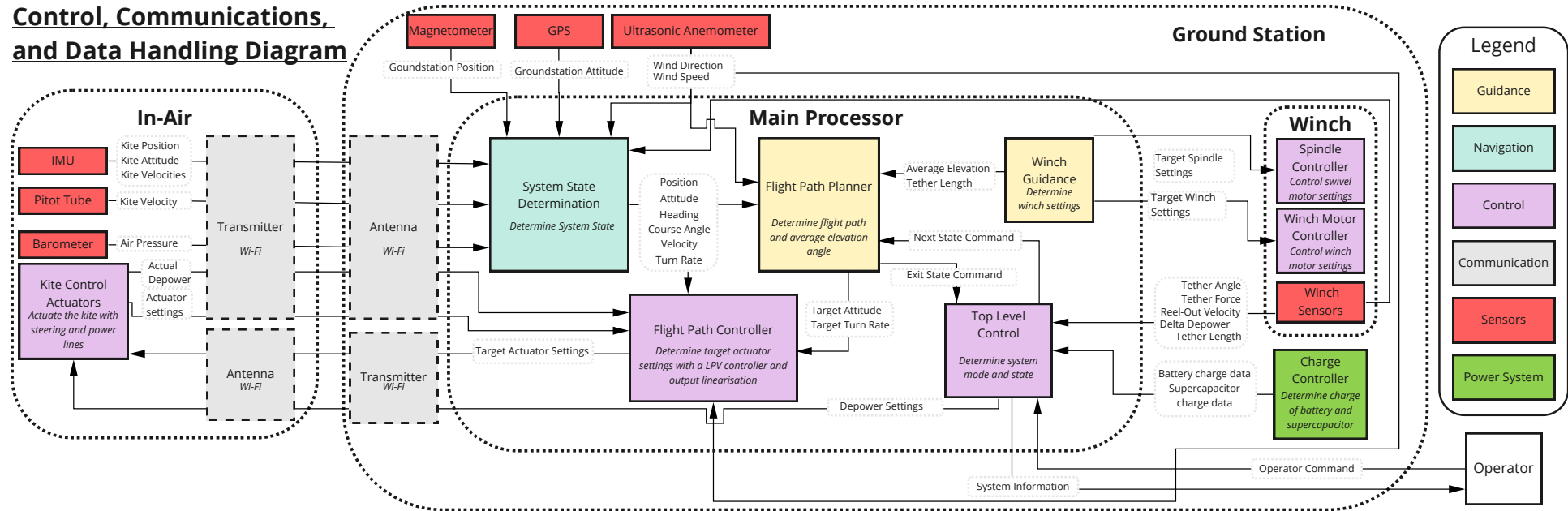


Figure 14.11: A top level Control, Communications, and Data Handling Diagram.

Optimised Design

As discussed in Chapter 9 the system design contains many elements which are interdependent, and thus need to be integrated and iterated with each other for an optimised design. The optimisation method and results will be discussed in Section 15.1. Following these results is Section 15.2, where the final design configuration is presented with a hardware diagram and a CATIA render. In addition, for a quantitative analysis of the configuration, a mass breakdown is performed on the final design as well. Finally, a sensitivity analysis is carried out, to clarify how the design interactions that were shown on the N2 chart in Chapter 6, influence each other, both qualitatively and quantitatively.

15.1. Final Design Optimisation

In line with the design procedure determined in Chapter 9, after having investigated each subsystem in detail, an optimisation of the airborne system is performed. This is done by means of an iterative process in which the power cycle, the airborne system's aerodynamic parameters, and the tether parameters are matched. In order to automatise this process, the Luchsinger model, the VSM, and tether diameter calculation codes were merged. Furthermore, the codes that were used for calculation of other subsystem characteristics such as the drum diameter and the launching equipment clamp force were integrated with the Luchsinger model, VSM, and tether diameter codes. The optimisation and iteration process is explained in Section 15.1.1. The optimisation results are presented in Section 15.1.2.

15.1.1. Optimisation Method

As discussed in Chapter 9 and Section 10.3.3, to obtain a consistent design, the aerodynamic model and the Luchsinger model, which defines the power cycle, are matched. The required projected area influences the aerodynamic coefficients, which again results in a new required projected area, defined by the Luchsinger model. During this analysis, the traction force is kept constant. The reason for this choice is that during regular design operations, the maximum traction force is already reached, this maximum traction force is set by the ground station that should remain static under all loads. The power cycle is thus optimised while keeping the maximal traction force constant. This means that the tether diameter, which heavily influences the drag coefficient of the flying system, can also remain constant and should not be iterated during the optimisation. Therefore, the optimisation process starts by finding a converged projected area, so that the Luchsinger model and the aerodynamic model are perfectly matched.

In order to converge on a projected area, the optimisation loop starts by simulating the projected area that was found before optimisation from Table 10.3. For this area, the aerodynamic model is run, returning the aerodynamic coefficients for a kite with that projected area. This is then taken as an input for the Luchsinger model, which calculates the new power cycle for these coefficients and returns a required projected area. This area is then returned to the aerodynamic model, which recalculates the aerodynamic coefficients. Typically, when the area would be smaller than the previous one, the drag coefficient will go up. This is a direct result from the tether drag assumption in Chapter 11. Returning this to the Luchsinger model, results in a higher projected area to generate required power with this lower aerodynamic performance. Now that the kite has become bigger, in the aerodynamic model the opposite happens as before, returning lower drag coefficients. This cycle is repeated until the previous and newly calculated area differ by less than 0.001 m^2 (user specified value). If the calculated areas would be plotted over time and connected, this would look like a damped oscillation. Therefore, instead of performing the new aerodynamic analysis with the newly calculated area, it was done with the average of the newly calculated area and the previous area. This speeds up the optimisation a lot. In the end, starting from a projected area of 16.65 m^2 , 9 cycles were needed to converge to a projected area of 15.19 m^2 .

After this iteration, the other integrated codes automatically sized and determined subsystem characteristics based on the obtained values from the power cycle and the aerodynamic analysis. The main parameters that were determined in this way were the drum diameter, the kite mass, tether mass, supercapacitor storage, launching equipment clamp force, motor and generator sizing.

15.1.2. Optimisation Results

The initial values and the results of the optimisation are shown in Table 15.1. It can be seen that all values either improved, meaning the system got more efficient or lighter, or the values stayed the same.

Table 15.1: Summary of Optimised design Data

Subsystem	Parameter	Unit	Data after initial matching	Data after optimisation
Airborne	Projected area	m ²	16.65	15.19
	Flat area	m ²	20.16	19.32
	Kite mass	kg	5.16	4.81
	MAC	m	2.01	1.92
	Root chord	m	2.30	2.20
	Tip chord	m	0.92	0.88
	Tether Diameter	mm	4.4	4.5
	Lift coefficient reel-out	-	1.07	1.07
	Drag coefficient reel-out	-	0.14	0.149
	Lift-over-drag reel-out	-	7.64	7.14
	Lift coefficient reel-in	-	-0.16	0.17
	Drag coefficient reel-in	-	0.099	0.103
Flight Cycle parameters	Tether mass	kg	7.00	7.06
	Tether lifetime	h	2526	2632
	KCU weight	kg	6.71	6.71
	Optimal γ_{out}	-	0.43	0.41
	Optimal γ_{in}	-	1.78	1.80
	Reel-in duration	s	14	14
	Reel-out duration	s	58	61
	Total cycle duration	s	72	75
	Pumping efficiency	%	89	89
	Duty cycle	%	80.60	81.30
	Cycle efficiency	%	71.73	72.36
Power	Average mechanical cycle power	kW	33.82	33.02
	Average electrical output cycle power	kW	20.00	20.00
	Energy generated during reel-out	Wh	456.72	471.12
	Energy used during reel-in	Wh	50.26	54.67
	Capacitor storage	Wh	60.0	65.6
	Net energy generated per cycle	Wh	406.46	416.45
	Mechanical(Motor) reel-in power required	kW	9.21	9.03
	Electrical reel-in power required	kW	14.12	14.14
	Mechanical reel-out power generated	kW	44.27	42.62
	Electrical reel-out power generated	kW	28.29	27.79
	Gear ratio generator	-	0.12	0.11
	Gear ratio motor	-	0.97	0.98
Ground System parameters	Traction force reel-out	kN	10.33	10.41
	Traction force reel-in	kN	0.52	0.50
	Required friction coefficient	-	0.400	0.404
	Drum diameter	m	0.473	0.475
	Drum width	m	1.10	1.10
	Downforce by launching equipment	N	192	175
	Pulley diameter	m	0.27	0.27
	Swivel rails weight	kg	13.9	13.9

15.2. Final Design Configuration

In Figure 15.1 the whole ground system configuration can be seen and in Figure 15.2 the total system is presented. Furthermore, a hardware diagram for the system is presented in Figure 15.3. This diagram shows how all the ground station systems and in-air systems are connected and interact with each other, as well as how those two hardware groups are related.

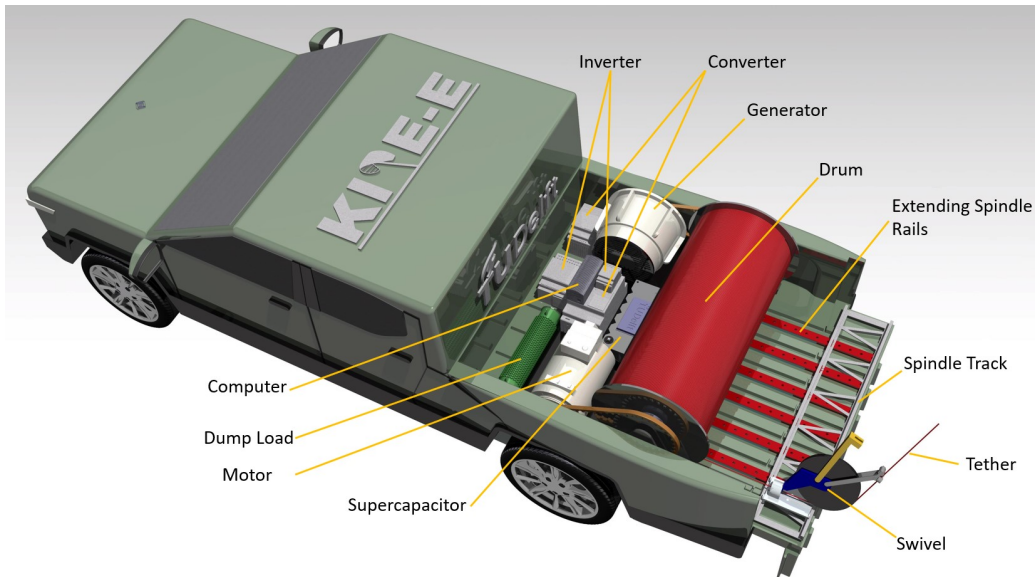


Figure 15.1: CATIA rendering of the final ground systems.



Figure 15.2: CATIA rendering of the final ground and airborne systems.

HARDWARE DIAGRAM

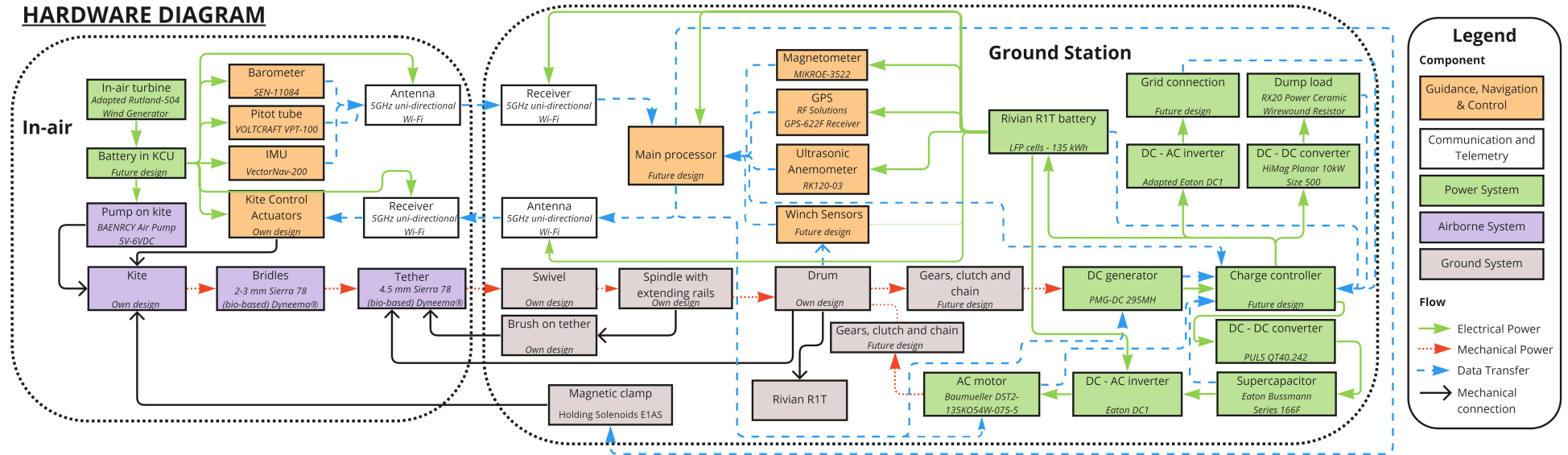


Figure 15.3: Hardware diagram

15.3. Budget breakdown

Figure 15.4 shows the total mass breakdown of the final design concept. The total mass of the system, now that all components have been sized, is 409.4 kg. Comparing this to the resource allocation that was performed in Chapter 7, where the total mass was estimated to be 426 kg, the final design is 3.9% lighter. How this total mass is broken down in several system aspects can also be seen in Figure 15.4.

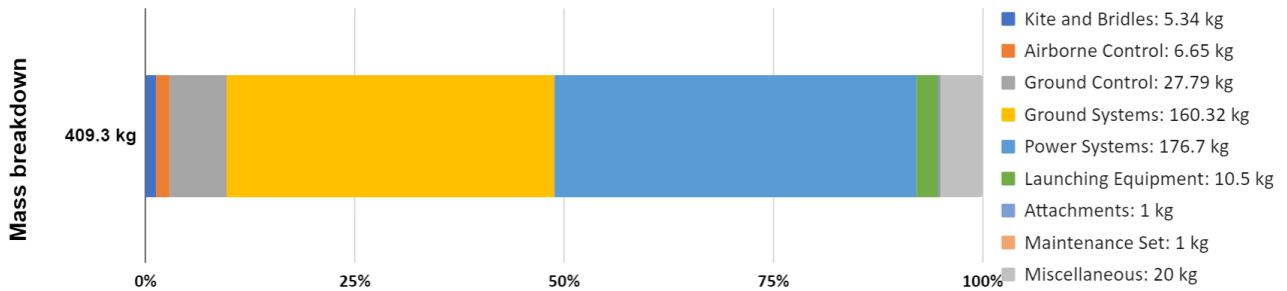


Figure 15.4: Optimised design mass breakdown

15.4. Sensitivity Analysis

In this section, a sensitivity analysis is performed. This analysis aims to clarify how the design interactions that were shown on the N2 chart in Section 9.2, influence each other, both qualitatively and quantitatively. This furthermore visualises the design space in which the team worked and check the code results consistency. The most significant interactions were plotted and discussed below.

Figure 15.5 and Figure 15.6 show how traction force, average power, and tether diameter are impacted by changing the kite area, while keeping all other input variables, such as the wind speed and the aerodynamic performance parameters, the same. Figure 15.5 shows that for an increase in the projected area of the kite, the average design reel-out traction force increases linearly, as does the average electric power. As discussed in Chapter 10, the reel-in and reel-out factors stay the same, which explains the linear behaviour of the graph. For clarity, the dots are not only coloured, but also increased in size with the same proportion as the values in the colour bar.

Figure 15.6 visualises how the tether diameter increases for an increase in the projected area, which is, as discussed for Figure 15.5, linearly related to the traction force. The tether diameter is not linearly related to the traction force, because the 4 mm tether has a relatively weaker fibre configuration than the 3, 5, and 6 mm have.

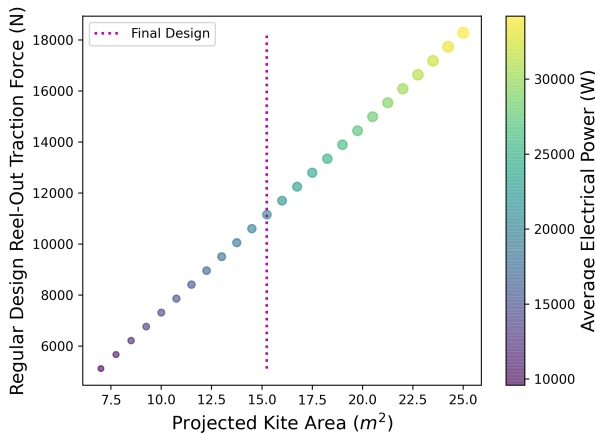


Figure 15.5: The traction force and average electrical power for different projected areas.

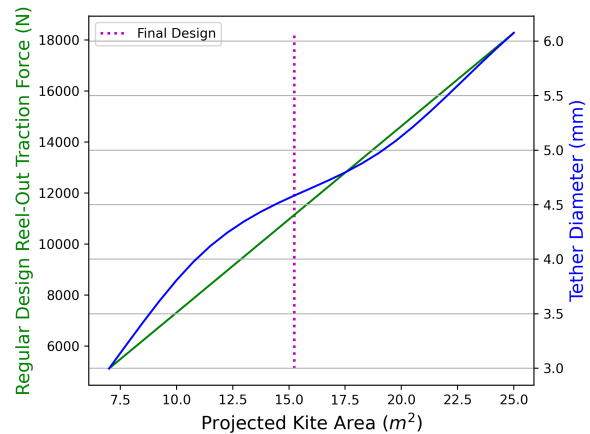


Figure 15.6: Tether diameter and projected area for different design loads during reel-out.

Because the drum length is constrained by the size of the truck bed, as discussed in Chapter 13, only the sensitivity of the required drum diameter will be analysed for this sensitivity. Figure 15.7 shows how the drum size increases for an increase in traction force. As explained in Chapter 13 the drum size is directly related to the tether diameter and tether length. For that reason, the shape of the curve makes sense; it matches the behaviour of the tether diameter for an increase in traction force.

Figure 15.8 shows a crucial relation, which was explained in depth in Section 13.2. This relation is between

the required friction coefficient of the ground, for the pickup truck to prevent sliding, and the design traction force. It is important to note that the required friction coefficient is calculated for the traction force with an additional safety factor of 1.2 to account for force peaks due to wind gusts. The maximum required coefficient was calculated for a range of -2° to 2° road angles, as specified by requirement AWE-TEC-OPS-03. From Figure 15.8, it can be concluded that for a traction force of 13500 N, the friction coefficient has to be higher than what they are estimated to be on some operational grounds. This is one of the main reasons traction force is constrained.

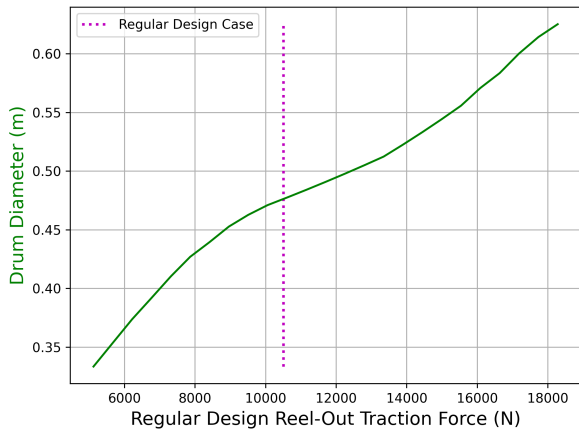


Figure 15.7: Drum diameter for different traction forces.

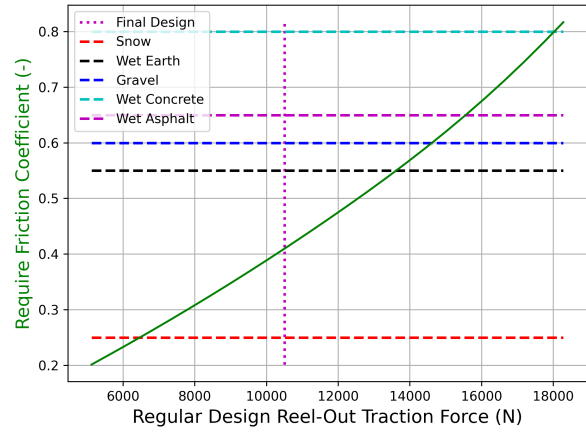


Figure 15.8: Required friction coefficients for different traction forces, including the friction coefficients of several operational surfaces.

Figure 15.9 shows the launching equipment mass needed for a varying ground wind speed. This relation was discussed in Section 13.5. As can be seen, the mass increases with quadratically. This is the case because the wind speed, and thus the wind force, as described in Section 13.5, is squared, and is thus quadratically linked to the necessary launching equipment weight.

A clear linear relation between the projected kite area and mass is visible in Figure 15.10. This matches expectations, because the mass of the kite is directly related to the kite area, which was explained in more detail in Section 12.6.

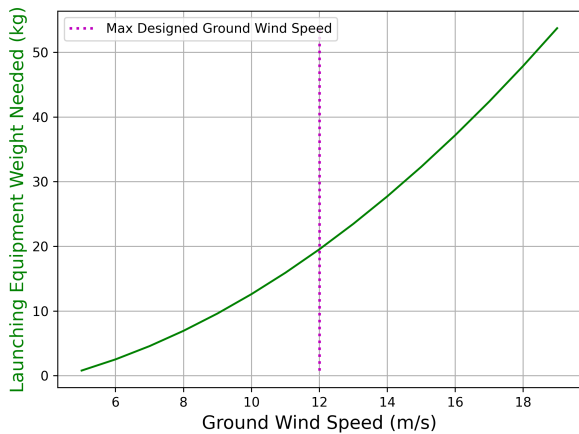


Figure 15.9: Launching equipment weight needed for different ground wind speeds.

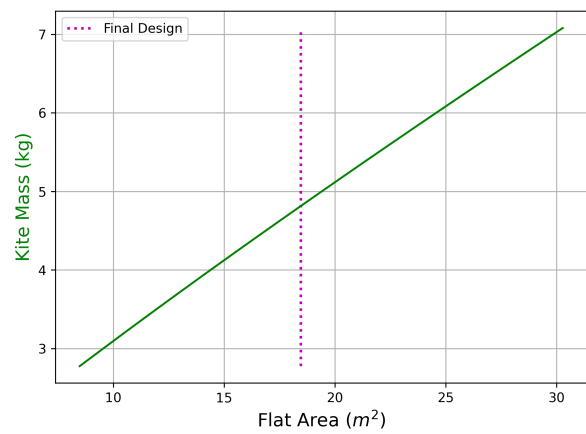


Figure 15.10: Kite mass for different projected areas and the same kite material thickness.

Next, Figure 15.11 shows what the average electrical output would be for different design wind speeds for which one could design, and how this would influence the reel-out speed that should be changed to remain under the tether force limit at higher wind speeds. One can see that the reel-out factor remains at its optimum of 0.25, until an average electrical power of 10 kW, after which it starts increasing. At the maximal evaluated wind speed of 20 m/s an output power of 40 kW could be reached.

Next, in Figure 15.12, the traction force during reel-out and average electrical output power is plotted for a range of C_L^3/C_D^2 . Again, the wind speed is constant, so improving the aerodynamic performance leads to an increase

in traction force. Therefore, this traction force levels out once the tether limit has been reached. The power, on the other hand, behaves like an inverse exponential function, rising quickly at first, but steadily flattens off afterwards.

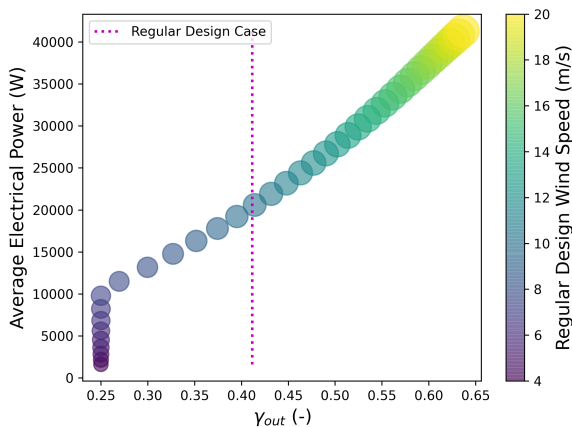


Figure 15.11: Average electrical power versus reel-out factor for a range of wind speeds.

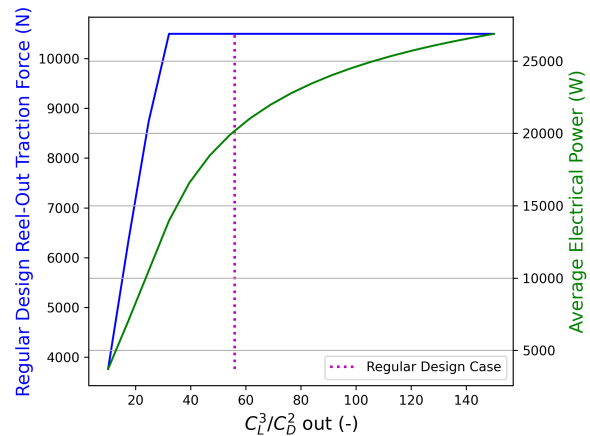


Figure 15.12: A range of C_L^3/C_D^2 values for reel-out versus reel-out traction force and average electric output power.

Furthermore, Figure 15.13 shows how the traction force during reel-out relates to the total cycle time at different wind speeds. First, it shows that the cycle times go down for higher wind speeds. This is due to the fact that for higher wind speeds, a higher reel-out velocity is needed, shortening the total cycle. Next, it can also be noted that from a certain wind speed onwards, the traction force does not increase any further, as it has reached the limit. At that point, the tether is reeled out even faster.

On Figure 15.14, the same trend can be observed, but the range of wind speeds is replaced here by a range of C_L^3/C_D^2 values for reel-out. The higher this value, the better the aerodynamic performance. When the wind speed is kept constant, the traction force will therefore increase, until it reaches its limit. Then the tether will be reeled out faster, shortening the cycle time.

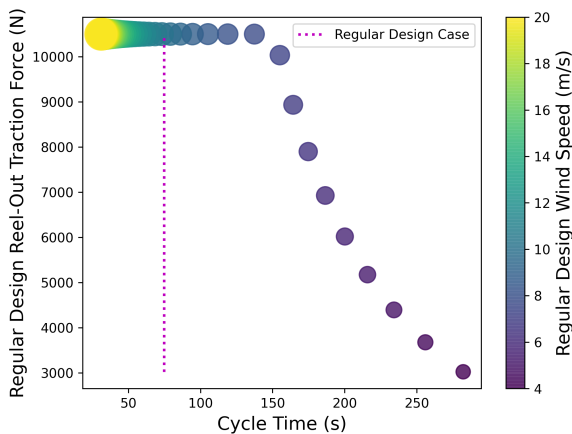


Figure 15.13: Reel-out traction force versus cycle time for a range of wind speeds.

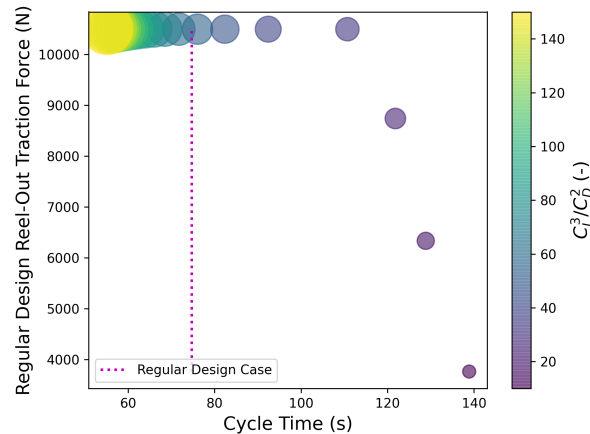


Figure 15.14: Reel-out traction force versus cycle time for a range of C_L^3/C_D^2 values for reel-out.

In Figure 15.15, where the reel-in and out factors are plotted versus a range of C_L^3/C_D^2 values. First for the reel-out factor, as mentioned before, the traction force increases with better aerodynamic performance, this causes the reel-out factor to increase faster once the tether limit has been reached in order to keep the traction force at this limit. In order to keep the pumping efficiency optimal, the reel-in factor should also go up in order not to spend too much time reeling in. Besides, a better aerodynamic performance also means less drag, allowing to reel in faster without needing more power for this.

Furthermore, Figure 15.16 shows the average electrical power versus reel-out factor for a range of C_L^3/C_D^2 values. It can be seen that better aerodynamic performance leads to a higher power output. Furthermore, as always, the reel-out factor increases in order to keep the traction force under the tether limit.

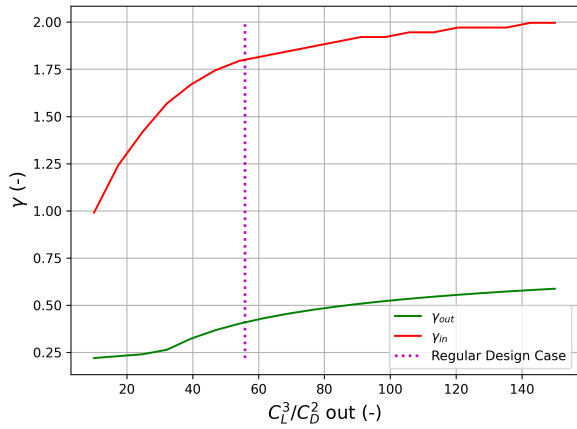


Figure 15.15: Reel-in and out factors versus a range of C_L^3/C_D^2 values for reel-out.

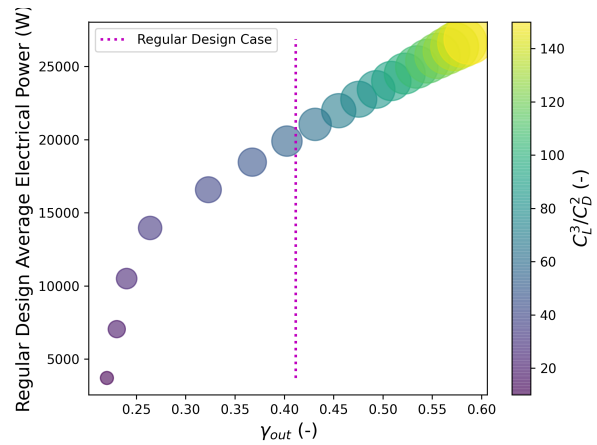


Figure 15.16: Average electrical power versus reel-out factor for a range of C_L^3/C_D^2 values.

In Figure 15.17 it can be seen how the supercapacitor storage scales with an increase in wind speed, for an optimised power cycle. The plot shows that the required storage increases for higher wind speeds, as more power, and thus energy, is needed to reel-in the kite when the wind pushes it harder. The same is thus true for the required motor power at higher wind speeds. Both lines do not reach the design ed value at the design wind speed, as a safety factor was included in the design.

Lastly, on Figure 15.18, it can be seen how the generated power during reel-out increases for higher wind speeds. The maximal power for which the generator is designed, is however higher to get the full potential of the system at all operating areas, as explained in Section 10.4.

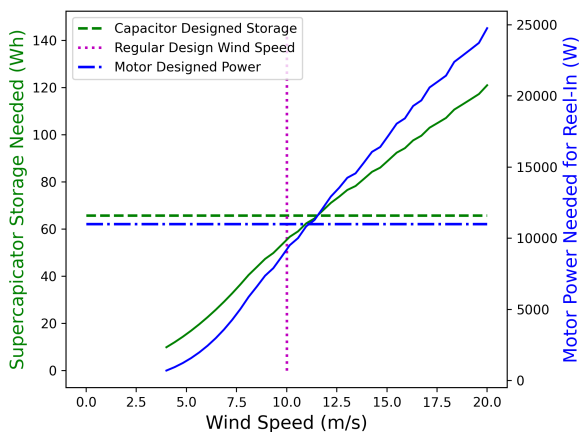


Figure 15.17: Required supercapacitor storage and motor power

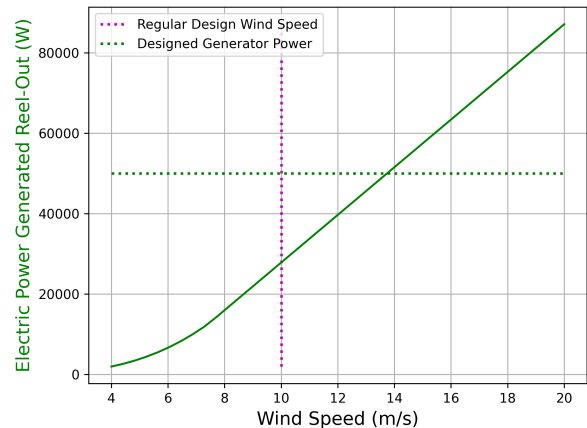


Figure 15.18: Electrical power generated during reel-out versus wind speed.

From this sensitivity analysis, it can be concluded that all parameters and subsystem characteristics were related as expected. No anomalies were found in connections, meaning the design results are expected to be reliable. A further analysis of the design result reliability is done in Chapter 16.

Verification and Validation

Verification and validation are a very important step in every design process. It should be performed on both a small and large scale. Therefore, in this chapter, all different models that were used will be verified and validated. First, in Section 16.1, the requirements are validated. Secondly, in Section 16.2, the aerodynamic models are verified and validated. Next, in Section 16.3, the Luchsinger model is verified, followed by Section 16.4, where all the structural calculations are verified and validated. Furthermore, Section 16.5 explains the verification and validation done for guidance, navigation and control. This is followed by Section 16.6, which ensures that for the design optimisation all the calculations models were brought together correctly. Finally, in Section 16.7 and Section 16.8, the final product is verified, using a compliance matrix, and validated respectively.

16.1. Requirement Validation

The quality of the requirements should be assessed, to ensure that the convergence to a final design is executed correctly. The best way to check whether the requirements are correct is by using the VALID approach. VALID stands for Verifiable, Achievable, Logical, Integral and Definitive. Each of the requirements needs to adhere to these five characteristics. Checking this is a continuously recurring process as requirements get updated, and new requirements rise during the design process.

Some requirements were found to be formulated in an unverifiable way. These have been adjusted to make sure all requirements are verifiable, following the VALID approach. Furthermore, since no killer requirements were identified, all requirements are achievable. To make sure all requirements are logical, identifiers are assigned to each subgroup. Compared to the requirements that were presented in the midterm report [10], a lot of new requirements arose, which were also given identifiers to ensure that all requirements are logical. Moreover, all requirements have been checked for completeness to ensure that they are integral. Lastly, it is made sure that the requirements are only interpretable in one way, meaning they are definitive.

16.2. Aerodynamic Model Verification and Validation

This section focuses on the verification and validation of the used aerodynamic model throughout this design. Section 16.2.1 discusses the model verification. This subsection provides unit tests and a result verification based on XFLR5 simulation data. The validation procedure is explained in Section 16.2.2 where the obtained VSM results are compared to wind tunnel test data for a simple wing.

16.2.1. Model Verification

In this subsection, the performed unit tests and result verification of the used aerodynamic model are presented. The main purpose of this verification is to check if the program correctly runs and produces sensible results.

Unit Testing

The geometry coordinate transformation and implementation in the main file is verified by plotting the originally generated kite shape and comparing it with the plotted transferred coordinates. As observed in Figure 16.1, the ellipsoid LE is correctly generated with a straight TE. Additionally, the taper ratio of 0.4 is verified through unit testing. Because of the need for segmentation, the shown planform in Figure 16.1 is visually correctly separated based on 6 control points, creating 5 segments. As observed, these segments are evenly spaced, based on equal cut-off arc lengths in the yz-plane (see Figure 16.2). Because of the segmentation in the yz-plane, the planform in Figure 16.1 is displayed with the segmented y values that were generated for Figure 16.2. The approximated projected area by the segmented design was found to approach the desired surface area with increasing number of segments, as expected. Lastly, the MAC that is shown in Figure 16.1. The y_{MAC} coordinate was calculated based on the numerical integration of the ellipse's function, divided by the length spanned by the x values range. This value was verified by manual calculations.

This segmented planform needed to undergo a coordinate transformation to be compatible with the VSM code. Therefore, Figure 16.3 shows the generated planform in this code with 2 additional split points (used for mesh refinement) per panel. This indicates a correctly implemented kite planform geometry. A similar approach is taken for the kite's front view in the yz-plane, with the same result. Figure 16.3 also displays the essential c/4 and 3c/4 points for the vortex distribution initiation. These points have been manually verified to be correctly plotted.

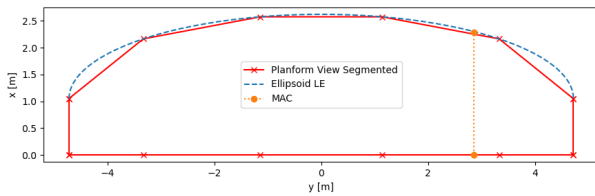


Figure 16.1: Kite planform and segmented planform approximation, with MAC indicated.

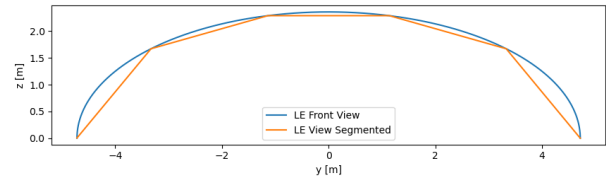


Figure 16.2: Kite front view with segmented approximation.

Lastly, Figure 16.4 shows the 3D implementation of the above described geometry. Since all of these geometry plots have shown to match the desired geometry generations, the geometry initialisation and implementation is verified.

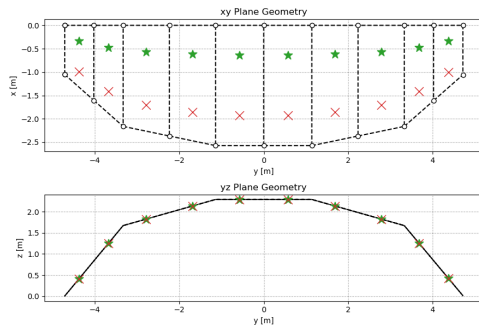


Figure 16.3: Kite top and front view verification image. (Segments = 5, $N_{split} = 2$)

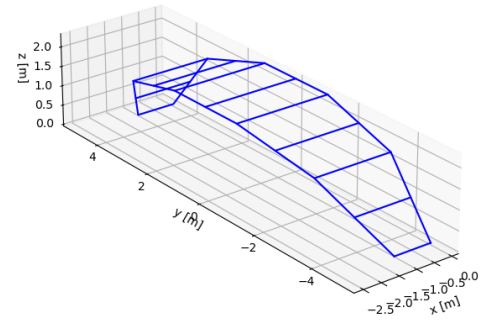


Figure 16.4: 3D kite coordinate implementation. (Segments = 5, $N_{split} = 3$)

Result Verification

The simulated camber influence shown by Figure 11.12 until Figure 11.14 shows coherence to the theoretic and observed camber effects in Section 11.4.4. The main outcomes of both analyses are increased drag, higher stall angles and higher lift coefficients for higher cambered wings. The results from the VSM program are therefore found to be consistent and verified with these observations. Hence, the camber is correctly processed by the code.

A similar verification approach is used for the thickness implementation. As described in Section 11.4.5, an increased thickness generates higher lift and drag coefficients and leads to higher stalling angles. This behaviour is observed for the kites with constant thickness. For the varying thickness along the wingspan configurations (constant t/c), this behaviour is not observed. The reason for this is the fact that the tips are stalling at lower angles of attack, when compared to the root stalling angles. This is explained by the smaller effect of vortex downwash to decrease the effective angle of attack, whereas the constant t/MAC configurations show a larger t/c at the tip compared to root t/c , leading to a delay of the general stall. Hence, this is in congruence with the mentioned literature observations in Section 11.4.5, additionally, this varying thickness distribution shows a similar trend as the Kitepower V3 kite [82].

For the remainder of the result verification, the VSM results are compared to the results of an XFLR5 VLM analysis. The main reason for a verification process using XFLR5 is the similarity in simulation method and limitations, as explained in Chapter 11. In order for these results to be compared with each other, a similar geometry at a similar Reynolds number was modelled. The simulated geometry is shown by Figure 16.5 and Figure 16.6 for XFLR5 and the Python VSM respectively, where further detail on the geometry is provided, while the Reynolds number formula is displayed by Equation (16.1).

In Equation (16.1), L is the object's length (MAC for a wing) in m, μ is the air bulk viscosity ($1.81 \text{ e-}5$), ρ is the air density and v_{true} is the true airspeed (m/s). Using sea-level standard values for the air density, bulk viscosity and combined with the MAC from Figure 16.5 with an air speed of 50 m/s, this resulted in a Reynolds number (Re) of 8.1×10^5 .

Note that because of the current unavailability of public LEI kite flow simulations, the VSM code can not be verified for the kite's aerodynamic shape. The verification method in this section can, however, verify that the model description is correctly implemented by simulating other geometries. The results for the VSM and XFLR5 simulations are shown in Figure 16.7. Before analysing the result plots, it is important to be aware that the VSM code uses the XFLR5 generated 2D polars as an input for its simulation, similar to how the XFLR5 VSM introduces polars to a 3D geometry.

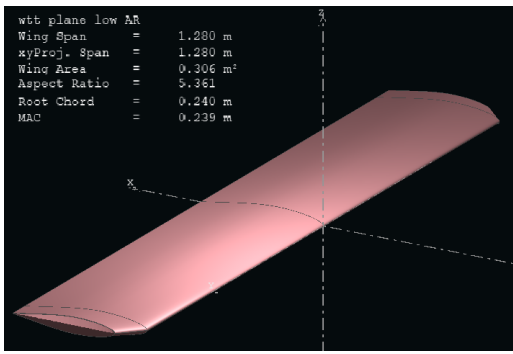


Figure 16.5: XFLR5 generated wing for verification analysis.

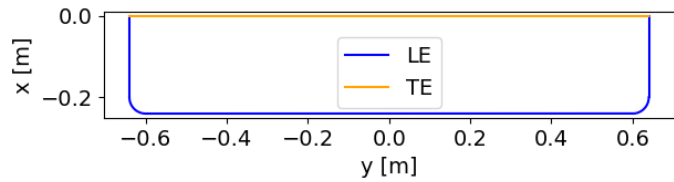


Figure 16.6: Python generated wing for verification analysis.

$$Re = \frac{\rho VL}{\mu} \quad (16.1)$$

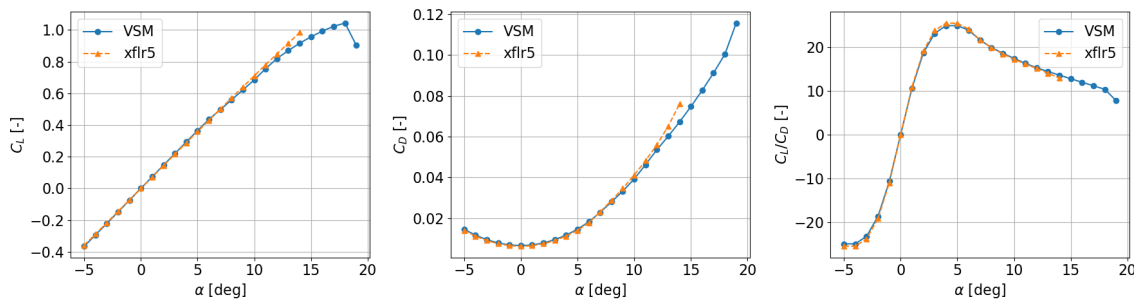


Figure 16.7: VSM and xflr5 results comparison for a rectangular wing. Simulation specifications: Airfoil = NACA 64₂A-015, $Re = 8.1 \times 10^5$, $M = 0.15$. $b = 1.28$ m, $AR = 5.36$, chord = 0.24 m.

Direct observation of Figure 16.7 leads to the conclusion that the VSM and XFLR5 VLM show very similar results. Especially in the linear region (up to $\pm 10^\circ$), the results almost match identically. For larger angles of attack, viscous and turbulent effects have greater impacts on the aerodynamic flow characteristics, leading to simulation inaccuracies. A major difference between the VSM simulation and XFLR5 VLM simulation is the stall angle. The VLM did not reach convergence at angles of attack larger than 15° , whereas the VSM was able to run until stall occurred (simulated to be 18°). In order to have a better overview of these result differences, Figure 16.8 shows a relative percentage error for the plotted polars per angle of attack.

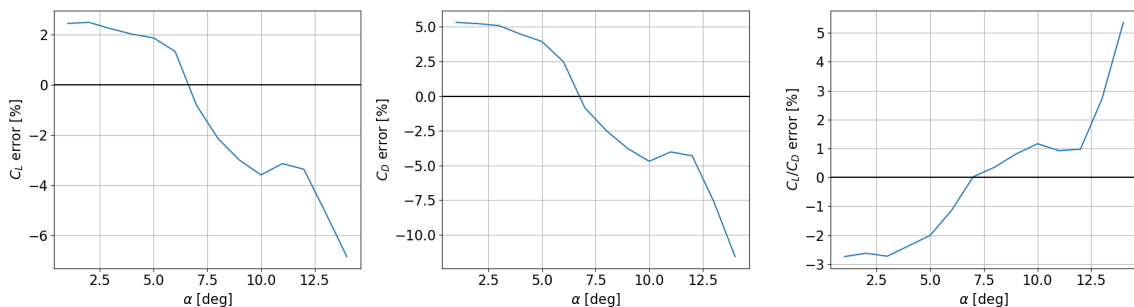


Figure 16.8: VSM and xflr5 relative error plots for a rectangular wing. Simulation specifications: Airfoil = NACA 64₂A-015, $Re = 8.1 \times 10^5$, $M = 0.15$. $b = 1.28$ m, $AR = 5.36$, chord = 0.24 m.

The relative error of the VSM program, compared to the XFLR5 VLM, stays below $|5\%|$ for all polar plots for angles of attack up to 12° . The drag results show the largest discrepancies with the XFLR5 results, with the largest relative difference of 11.73% for a 14° angle of attack. The main conclusion from this verification execution is that the VSM program shows very similar performance to XFLR5's VLM, especially in the linear flow regime. This is highlighted by both the absolute and relative errors between the analyses.

Because of the observed small differences, the VSM is shown to be correctly implemented in general. One aspect of this correct implementation is the initialisation of 2D polar data, which enables the VSM program's user to implement experimental 2D polar data for higher modelling accuracy. Therefore, this method can be used for aerodynamic simulations at a similar performance and reliability level as the well-established and researched XFLR5 VSM.

16.2.2. Model Validation

To ensure a fully validated program, a prototype of this project's kite system should be tested in a real world application. Ideally, this test would be performed in a controlled environment, where accurate measurements can be obtained. This would allow for crucial data gathering to be used for analysis and comparison with the numeric LEI kite simulation from this report.

Because of the project's limited resources, gathering real world data on a LEI kite system was not possible. Therefore, the validation procedure is run for available historical wind tunnel data from the AE2130-II course. The experimental test set-up, tested wing geometry and wing airfoil are discussed in the following paragraphs and shown by Figure 16.9 to Figure 16.11 respectively.

The used experimental data for the validation procedure is gathered in TU Delft's low speed, low turbulence wind tunnel [182]. 2D data is gathered using pressure sensors connected to a manometer to calculate 2D polars. For 3D data gathering, force data is gathered by a six-component balance, and made non-dimensional in data processing to obtain 3D polars. This wind tunnel is able to achieve low turbulence levels, more specifically around 0.02% at 25 m/s and around 0.07% at 75 m/s. The maximum achievable air speed is 120 m/s.

The 3D experimental set-up is shown by Figure 16.10. The test section consists of a simple half wing and a reflection plate. Specifications on the wing geometry are shown by Figure 16.9. The experiment was carried out using mechanically actuated turntables for angle of attack adjustments and an air speed of 50 m/s. Using the Reynolds number equation in Equation (16.1), led to a Re of 8.1×10^5 for the wind tunnel experiment. When modelling 2D polars for this set-up, the removable tip is replaced by a table to eliminate the wing tip effects. In this 2D set-up, essentially an infinite wing is recreated, and the data gathering process is switched from the force balance to the pressure sensors.

As mentioned already in Section 16.2.1, the simple rectangular wing concept does not have a continuously present separation bubble and this phenomenon's related flow complexity at low angles of attack. It does show a laminar separation bubble at higher angles of attack. Therefore, the simulated results are expected to show decreased performance at these higher angle of attack ranges.

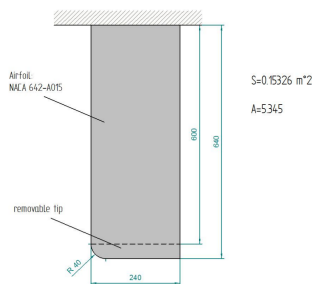


Figure 16.9: Experimental wing geometry [182].

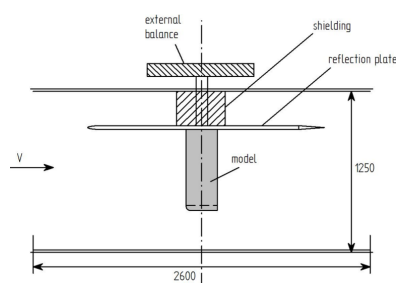


Figure 16.10: Set-up 3D experiment [182].

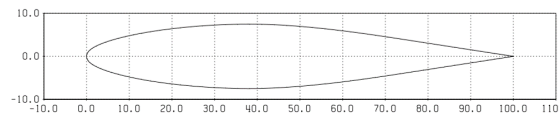


Figure 16.11: NACA 64₂A-015 airfoil geometry [182].

Because of the verified implementation of numerical 2D airfoil data in Section 16.2.1, the validation model used wind tunnel gathered data about the airfoil's polars for the VSM simulation. This choice was made to limit error propagation based on numerical polar approaching methods. This is visualised by Figure 16.12, where polars for the NACA 64₂015 airfoil are plotted for both measured data from wind tunnel tests (WTT) and simulated XFLR5 data (both for $Re = 8.1 \times 10^5$). This image clearly shows an overestimation of the C_l values for high angles of attack. Similarly, the C_d values are underestimated in this high α region. Implementation of this 2D polar data implicitly includes the 2D viscous effects, which XFLR5 does not succeed in modelling.

Based on the 3D experimental set-up and described VSM geometry implementation, Figure 16.13 show the C_L vs α , C_D vs α and C_L/C_D vs α result plots. These graphs show curves for the 3D wind tunnel data, XFLR5 simulation results and 2D experimental data implemented VSM results.

Based on Figure 16.13, both this project's experimental 2D polar implemented VSM and XFLR5's Vortex Lattice Method (VLM) show great potential for aerodynamic lift modelling. This is observed as the vortex step and lattice methods are known to have accurate lift approximations, and especially in the linear flow regime. The drag calculations for both of the simulation methods do not accurately approach experimental data. As expected by

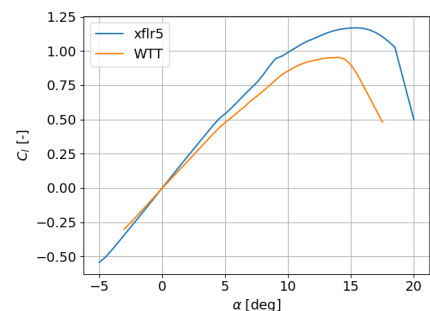


Figure 16.12: 2D XFLR5 vs WTT C_L polar comparison. $Re = 8.1 \times 10^5$, $v_{true} = 50$ m/s.

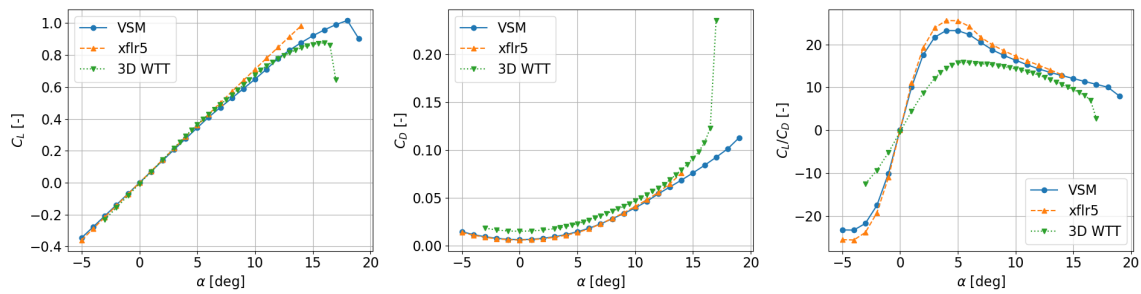


Figure 16.13: VSM, xflr5 and wind tunnel data results comparison for the experimental geometry from Figure 16.9. Simulation specifications: Airfoil = NACA 64₂A-015, $Re = 8.1 \times 10^5$, $v_{true} = 50$ m/s.

the documented limitations of the VSM and VLM theory in Chapter 11, the inability to accurately model viscous and viscoid effects leads to a significant and consistent drag underestimation. This also explains the higher observed stall angle and maximum lift coefficient as observed for the VSM simulation.

The inaccurate drag modelling directly affects the C_L/C_D vs α curve. In this graph, the numerical simulated results do not show accurate experiment approximations. The simulated aerodynamic efficiencies are consistently overestimated, the VSM simulates a 32% higher C_L/C_{Dmax} than what is observed from wind tunnel data analysis. Additionally, C_L/C_{Dmax} occurs at a lower angle of attack for the 3D measured curve.

The conclusion of this program validation is that the aerodynamic efficiency of the modelled geometry is overestimated. When using this program for an aerodynamic analysis, one should consider means of accounting for the program's limitations to accurately model the drag related viscous effects. However, the program does produce consistent and reliable results for lift modelling and can be used for lift estimations in the linear flow region.

Finally, the VSM program could not be validated for LEI kite-like structures. This validation process is considered to be a future recommendation when experiment measurements can be carried out on the to be modelled geometry. It would allow for a full validation procedure of the LEI kite structure geometries as were used in Chapter 11. Since the C_L , C_D and C_L/C_D are vital parameters in the kite's sizing process, the findings in this validation section should be taken into account for future design iterations when using the VSM program as a simulation tool.

16.3. Luchsinger Model Verification and Validation

In this section, the verification and validation of the Luchsinger model is presented. First, in Section 16.3.1 an overview of the calculation and result verification is given. Then, in Section 16.3.2 the performed model verification of the Luchsinger model is presented. Lastly, a short discussion on the Luchsinger model validation is presented in Section 16.3.3.

16.3.1. Calculation and Result Verification

In order to ensure the Luchsinger model was implemented correctly in the code, verification was performed. As the model only uses simple analytical formulas, those can be verified by recalculating the results by hand. In the code, those formulas were implemented per function. Unit tests were performed to verify each of these functions separately, knowing the in- and output, the programmed calculation was performed by hand with the same input. For every function, the output corresponded 100%, as expected.

At the end, the script returns a full power cycle with all its parameters. Entering these parameters into Equation (10.7), the Luchsinger based formula that gives the average electrical output power, should then return 20 kW, which was the required power, given as an initial input. The optimised power cycle parameters, calculated by the script, also gave a 100% match with this requirement. Furthermore, the results of the three-phase strategy were visually compared to the graphs shown in the chapter 3 in the airborne wind energy book [2]. This was done by inputting the values stated in the book into the code written. The values and most importantly the shape of the graph were very similar. The results were thus found to be verified and correct.

16.3.2. Luchsinger Model Verification

In order to verify if the Luchsinger model indeed gave the correct power cycle parameters, which are not only correct when returned to Equation (10.7), as described before, the team also came up with a way to verify these results with another equation. Taking Equation (10.3) and Equation (10.4), which evaluate the mechanical power generated during reel-out and reel-in, respectively and by using the reeling speeds, with which the time

ratio between the reel-out and -in phase can be defined, Equation (16.2) can be formed. In this equation also the efficiency during reel-in and -out is added, so that it also outputs the average electrical output power. Implementing the variables found using the Luchsinger model, this equation also exactly returned 20 kW as output power, verifying that the Luchsinger model is indeed correctly implemented.

$$P_{avg} = P_{out} \eta_{out} \frac{\gamma_{in}}{\gamma_{out} + \gamma_{in}} - \frac{P_{in}}{\eta_{in}} \frac{\gamma_{out}}{\gamma_{out} + \gamma_{in}} \quad (16.2)$$

16.3.3. Luchsinger Model Validation

The validation of the model is very limited. This is due to time constraint of the project, but mostly because experimental data is difficult to obtain. With more time and potentially testing, some data could be been acquired. This is then also a recommendation for the future. Furthermore, since the code is based on an already existing model, it was assumed that some form of validation had already been done. Which would make the model valid as long as it was verified to be correct.

16.4. Structural Calculations Verification and Validation

In this section, the verification and validation of the different structural models is presented. First, in Section 16.4.1 the verification and validation of the structural load analysis model is discussed. Then, the model that determines the required tether diameter is verified and validated in Section 16.4.2. Lastly, in Section 16.4.3 the model used to determine the kite mass is verified and validated.

16.4.1. Static Load Analysis

The code that is written to calculate the force in each of the bridle line has to be verified. This has been done by performing analytical calculations and comparing them to the numerical output values. From this, one small mistake was noticed in the code, which was immediately corrected. After changing the error, the code gave the correct force outputs per bridle line.

The wing loading distribution diagram is generated based on the aerodynamic VSM code. In this code, the spanwise lift and general load distributions are used as intermediate calculation results to provide values for the total system's coefficients. Since the VSM code is already verified in Figure 16.7, these data points only needed to be plotted. Visual inspection of Figure 12.5 and Figure 12.6 confirm this verification process.

16.4.2. Tether Diameter Verification and Validation

Verification of the calculation of the tether diameter can easily be done by comparing hand-calculated values to the outputs of the code. Using the datasheets of three different types of SK78 Dyneema® [131, 138, 183], the difference between code and reality could be assessed. The values are calculated using linear interpolation between the mean breaking loads for different tether diameter, for an applied load of 10 kN and a safety factor of 2. The results can be seen in Table 16.1.

Table 16.1: Tether diameter verification

Material	Unit	Diameter hand calculation	Diameter code output	Error
Sierra	mm	4.427	4.427	0.0
DX Core 78 HPS	mm	4.2939	4.2939	0.0
DX Core 78	mm	4.68421	4.68421	0.0

Using the characteristics of the Euroneema cable of Kitepower, the code that was written for the tether diameter can be validated [184]. Filling in the breaking load of 13.5 kN yields a diameter of 3.96 mm for uncoated SK78 Dyneema®, which has the same strength as uncoated SK75. Since this is only a 1% difference to the expected 4 mm, the exact data for Euroneema is unavailable, and the data on the Kitepower website is rounded, the code is validated.

16.4.3. Kite Mass Verification

The kite mass extrapolation is verified by performing calculations by hand. Using an Excel sheet, calculations by hand are performed. The output of the code for two different areas is compared to these hand-calculated values. This comparison is visualised in Table 16.2 and Table 16.3.

As can be seen, there is no difference between the output of the code and the hand-calculated values. This means the code is verified. One thing can be said about the inaccuracy of the estimation method. Since a second order polynomial behaves as a parabola for these data points, something which is illogical since the kite mass obviously goes up with increased surface, a power approximation is used to approximate the mass. This is not the best fit for the data, but results in a difference of 5% between the code and reality.

Validation for these mass estimations is challenging. Using the code for other kites can result in significant inaccuracies, since there are no other 7 strut kites with an aspect ratio of 5 and the same canopy shape, made

Table 16.2: Kite mass verification 15 m² kite.

Parameter	Unit	Mass Excel	Mass code	Error
Kite mass	kg	3.961	3.961	0.0
Airframe mass	kg	2.732	2.732	0.0
Canopy mass	kg	1.23	1.23	0.0
Valve and reinforcement mass	kg	0.682	0.682	0.0

Table 16.3: Kite mass verification 25 m² kite.

Parameter	Unit	Mass Excel	Mass code	Error
Kite mass	kg	5.756	5.756	0.0
Airframe mass	kg	3.706	3.706	0.0
Canopy mass	kg	2.05	2.05	0.0
Valve and reinforcement mass	kg	1.656	1.656	0.0

with an ALUULA airframe. To show this, it is assumed that to approximate the 3-strut Flite A-Series kite of Ocean Rodeo [185], 4 struts can be subtracted from the original code. For the 12 m² kite, this results in a mass of 2.36 kg. On the data sheet, a mass of 2.31 kg is given. This is a difference of 2%. For the 14.5 m² kite, the code gives a mass of 2.76 kg, while the given mass is 2.49 kg. This is a difference of 11%. For the 17 m² kite, the mass output by the code is 3.15 kg. On the data sheet, a mass of 2.58 kg is given, resulting in a difference of 22%. This clearly explains that even though the Flite A-Series has an aspect ratio around 5, the code does not work properly for kites of different configurations. This shows that future code improvement will be necessary to obtain more precise results.

16.5. Guidance, Navigation and Control Verification and Validation

The GNC system is vital for the reliability and efficiency of the system and should therefore be verified and validated. For this, the first important step is the creation or choice of an accurate model of the entire system. First, with this model, the different software blocks can be verified by simulating operational inputs and analysing the outputs on a software block level. Following this, the entire control system can be verified by testing it with the model of the kite system.

The validation is also performed in two steps. First, a form of validation has already been performed as the GNC system is very similar to systems already flown in practice, however not on a pickup truck. Therefore, the kite control is in concept validated, however not the entire GNC system. Therefore, the GNC system must also be validated when in use with the entire system and because of which real life testing must be performed to validate the GNC system.

16.6. Code Integration Verification

For the optimised design results, all calculation and model programs were integrated, as explained in Section 15.1. To ensure this integration is done correctly, it needs to be verified. The verification was done by first dividing the code into functions. Every function had certain inputs and outputs. The inputs were then also put into the original individual code from which the function originated. With the same inputs for both function and original individual code, the outputs have to be identical. This was tested, and is indeed the case for all functions. Furthermore, the code blocks were also run together to produce a set of output parameters (such as the kite area, weight, and drum diameter among others), with an initial set of parameters (the required power, wind speed, and operational altitude among others). Similarly, for the same set of individual parameters, the separate individual codes were used in succession to calculate the output parameters. This provided identical output parameters, thus verifying the code integration.

16.7. Product Verification by compliance matrix

Next to model verification, the entire product should be verified. Therefore, this section will discuss the compliance with requirements and constraints as a means of product verification. This is investigated by means of a compliance matrix. Table 16.4 and Table 16.5 give an overview of whether the requirements and constraints presented in Section 2.2 are met, together with an explanation. Under compliance in Table 16.4 and Table 16.5 there are three possible options: no, probably, and yes. No means that there is no compliance with the requirement or constraint, yes means that there is compliance with the requirement or constraint, and probably means that compliance is probably met but that a detailed analysis is still missing to be certain about the compliance. Furthermore, as specified in the Midterm Report, there are four methods to verify compliance with requirements [10]:

- **Demonstration:** The method of demonstration is showing that the product does what the product should do, according to a requirement.
- **Testing:** This method is based on testing the product in a controlled environment for a specific quality. This quality is specified by the requirement.
- **Analysis:** A mathematical model or analysis can be used to show that the product complies with the requirement. Analysis is performed when testing options are limited due to cost and / or time constraints.

- **Inspection:** This method of verification is used when the product can be inspected to comply with the requirements.

These methods are also added to the compliance matrix. Note that most of the requirement compliances have been shown using analytical and computational models, which falls under analysis. These models have been verified and validated as thorough as possible, nevertheless to ensure success of the system, more precise models will be used during the detailed design phase to further investigate the compliance of the design with the requirements. However, the analytical and computational models that are used have been verified and validated, leading to a good judgement on the compliance. Moreover, even though testing is always the preferred verification method, it has not been used a lot at this stage in the design process. However, most requirements will be tested in future steps of the development process to improve the verification accuracy.

Table 16.4: Compliance Matrix of Requirements.

Requirement ID	Compliance	Verification Method	Justification
General Requirements			
AWE-TEC-GEN-01	Yes	Analysis	This requirement is complied because of the independency of external electric energy when operating the system, as can be seen from the electrical block diagram presented in Figure 10.8 and power analysis presented in Chapter 10.
AWE-TEC-GEN-06	Yes	Inspection	No internal changes are made to the Rivian R1T, the AWES is only an add-on.
AWE-TEC-GEN-07	Yes	Inspection	The personal passenger space is not being used to store components of the AWES.
Aerodynamics Requirements			
AWE-TEC-AIR-06	Yes	Analysis	Compliance is shown in Section 11.6.
AWE-TEC-AIR-11	Yes	Analysis	Compliance is shown in Section 11.6.
Structures & Materials Requirements			
AWE-TEC-AIR-01	Yes	Inspection	The AWES uses a LEI kite, which is softkite based.
AWE-TEC-AIR-02	Yes	Analysis	The kite material that is used is able to carry the wing loading, applying a safety factor of 1.2. This has been discussed in Section 12.6.
AWE-TEC-AIR-03	Yes	Analysis	Compliance is shown in Section 12.2.1, by using a safety factor of 2 for the determination of the tether diameter.
AWE-TEC-AIR-07	Yes	Analysis	Compliance is shown in Section 12.5.1, by using a safety factor of 2 for the determination of the bridle diameter.
AWE-TEC-AIR-08	Yes	Analysis	Compliance is shown in Section 12.2.3.
AWE-TEC-AIR-09	Yes	Analysis	Compliance is shown in Section 12.2.3.
AWE-TEC-AIR-10	Probably	Analysis and Testing	Most of the materials and components of the airborne system can sustain the temperature range. However, a more detailed analysis and tests should be performed to verify the compliance with this requirement.
Operational Requirements			
AWE-TEC-OPS-01	Yes	Demonstration	This requirement has been taken into account during the design of the launching and landing system, as discussed in Section 6.3.2.
AWE-TEC-OPS-02	Probably	Testing	This is taken into account in the control and operations procedures, and works for similar AWES. However, testing should be performed to show compliance with this requirement.
AWE-TEC-OPS-03	Yes	Analysis	Compliance is shown in Section 13.2
AWE-TEC-OPS-04	Yes	Analysis	Compliance is shown in Section 13.4.
Power System Requirements			
AWE-TEC-PG-02	Yes	Analysis	The wiring will be designed to comply with this requirement.
AWE-TEC-PG-03	Yes	Analysis	The calculations and model in Chapter 10 provide evidence for this.
AWE-TEC-PG-04	Yes	Demonstration and Analysis	Most components are able to operate in this range, and where needed, heating and cooling is used. Tests should be performed to verify this further.
AWE-TEC-PG-05	Yes	Analysis	Compliance is shown in Section 12.5.2.
AWE-TEC-PG-06	Probably	Analysis and Testing	The drum material is chosen to ensure compliance with this requirement. However, a detailed analysis or tests have not been performed, but are necessary to ensure compliance with this requirement.
AWE-TEC-PG-07	Yes	Demonstration	Compliance is shown in Section 10.7.1.
AWE-TEC-PG-08	Yes	Demonstration	Compliance is shown in Section 10.7.1.
AWE-TEC-PG-09	Yes	Analysis	Compliance is shown in Section 10.6.
AWE-TEC-PG-10	Yes	Analysis	Compliance is shown in Section 10.6.
AWE-TEC-PS-02	Yes	Analysis	Compliance is shown in Section 10.7.2.
AWE-TEC-PS-06	Yes	Analysis	Compliance is shown in Section 10.7.4.
AWE-TEC-PS-07	Yes	Analysis	A wind turbine system is added onto the KCU to provide continuous power, as presented in Section 10.8.2
AWE-TEC-PS-08	Yes	Analysis	The power management system is completely automated, by the charge controller, as shown in Section 10.5.

Continued on next page

Table 16.4 – continued from previous page

Requirement ID	Compliance	Verification Method	Justification
AWE-TEC-PS-09	Yes	Demonstration and Analysis	Most components are able to operate in this range, and where needed heating and cooling is used. Tests should be performed to verify this further.
AWE-TEC-PS-10	Yes	Analysis	Compliance is shown in Section 10.7.4.
AWE-TEC-PS-11	Yes	Analysis	Compliance is shown in Section 10.7.3.
AWE-TEC-PS-12	Yes	Inspection	Compliance is shown in Section 10.7.4.
AWE-TEC-PS-13	Yes	Analysis	Compliance is shown in Section 10.7.4.
Guidance, Navigation and Control Requirements			
AWE-TEC-CS-01	Probably	Testing	Similar systems have a response time below 100 ms as specified in Section 14.5.
AWE-TEC-CS-04	Yes	Demonstration	Compliance is shown in Section 14.3.1.
AWE-TEC-CS-06	Yes	Demonstration	Compliance is shown in Section 14.2.2
AWE-TEC-CS-07	Yes	Demonstration	Compliance is shown in Section 14.3.1
AWE-TEC-CS-08	Yes	Demonstration	Compliance is shown in Section 14.2.2
AWE-TEC-CS-10	Yes	Demonstration	Compliance is shown in Section 14.2.2
AWE-TEC-CS-11	Yes	Demonstration	Compliance is shown in Section 14.2.2
AWE-TEC-CS-12	Probably	Analysis	Compliance is shown in Section 14.4.4
AWE-TEC-CS-13	Probably	Analysis	Compliance is shown in Section 14.4.4
AWE-TEC-CS-14	Yes	Analysis	Compliance is shown in Section 14.2.2

Table 16.5: Compliance Matrix of Constraints.

Constraint ID	Compliance	Verification Method	Justification
Cost			
AWE-CON-CO-01	Yes	Analysis	Compliance is shown in Section 17.1.
Scheduling			
AWE-CON-SCH-01	Yes	Demonstration	The preliminary design was handed in to the principle tutor on the 15th of June, which is within 10 weeks since the start of the DSE at the 19th of April.
AWE-CON-SCH-02	Yes	Inspection	All 10 students actively worked the project.
Safety			
AWE-CON-SAF-01	Yes	Analysis	Compliance is shown in Section 13.2.
AWE-CON-SAF-02	Probably	Demonstration and Testing	Operators will be educated on all the safety guidelines, measures, and operation procedures. However, human mistakes can always lead to accidents. Furthermore, all safety systems should get tested thoroughly.
Legislation			
AWE-CON-LEG-01	Probably	Demonstration	Compliance to airborne regulations is region dependent and should be proven according to local regulations. This airborne flight certification is discussed in Section 4.6.2.
AWE-CON-LEG-02	Yes	Inspection	There are no changes being made to the pickup truck, the AWES is only an add-on. Furthermore, all components of the AWES are completely contained within the cargo volume while driving on the road. Moreover, the AWES complies with the maximum payload capability of the pickup truck.
Sustainability			
AWE-CON-SUS-01	Yes	Analysis	Compliance is shown in Chapter 19.
AWE-CON-SUS-02	Yes	Inspection	No helium or other lifting gases are used by the AWES.
AWE-CON-SUS-03	Probably	Testing	This requirement could not be verified, since tests determining the noise levels of the different components need to be performed. However, AWES are expected to be less noisy than wind turbines, which have a noise level about 45 dB, as has been discussed in Section 4.6.2 and Chapter 19.
Reliability			
AWE-CON-REL-01	Yes	Analysis	Compliance is shown in Section 6.4.3.
AWE-CON-REL-02	Probably	Analysis and Testing	Most components are able to withstand this temperature range, and for other components cooling or heating will be implemented. However, some components still require a more detailed analysis and testing to ensure compliance with this requirement.
Design			
AWE-CON-DES-01	Yes	Inspection	Compliance is shown in Figure 15.1.
AWE-CON-DES-02	Yes	Analysis	Compliance is shown in Section 15.3.
AWE-CON-DES-03	Yes	Analysis	Compliance is shown in Section 10.7.4.

16.8. Product Validation

For product validation, the designed system is compared to a similar system AWE system, with a similar sub-system configuration. This was chosen to be the 20 kW system, using the Mutiny V2 kite described in [11]. The simulated performance factors of this system will be compared to the performance factor of the KITE-E system simulated by the team. It should be noted however that although both systems are described as '20 kW' systems, there is a big difference between the two. For the system with the V2 kite, the 20 kW is the mechanical power obtained during reel-out, whereas the KITE-E system reaches an average electrical output of 20 kW. Furthermore, the system with the V2 kite was developed almost ten years earlier than the KITE-E system. AWE being a brand-new technology, the system performance improved tremendously over the last years, as the interest in this revolutionary way to harvest the power of the wind and engineers are optimising the system. Table 16.6 shows how the simulation of the 20 kW V2 kite system compares to the simulation of the KITE-E system.

Table 16.6: Performance comparison for system validation.

Parameter	Unit	Simulated 20 kW V2 kite system	Simulated KITE-E system	Percentual difference
Projected Area	m ²	16.50	15.19	-7.94%
Flat Area	m ²	25.00	19.32	-26.44%
Projected to flat area ratio	-	0.66	0.83	-26.44%
Reel-out lift coefficient	-	1.00	1.07	7.00%
Reel-out drag coefficient	-	0.2	0.149	-25.50%
Reel-in lift coefficient	-	0.14	0.170	21.43%
Reel-in drag coefficient	-	0.07	0.103	47.14%
Lift-over-drag reel-out	-	5.0	7.14	42.80%
Lift-over-drag reel-in	-	2.00	1.03	-48.50%
Pumping efficiency	%	77.00	89.0	15.58%
Duty cycle	%	46.80	80.60	72.22%
Cycle efficiency	%	36.00	72.35	100.97%
Reel-out mechanical power	kW	21.6	42.62	97.31%
Average mechanical power	kW	7.90	33.02	317.97%
Average electrical output power	kW	4.00	20.00	400.00%
Nominal wind speed	m/s	12.00	10.00	-16.67%
Elevation angle	°	25.9	30.0	15.83%

First, looking at the projected areas, the area that actually generates the traction force, is a bit smaller. This is possible as the lift over drag during reel-out is 43% better than the one of the V2 kite, and 49% lower during reel-in, which is beneficial as a lower traction force is needed to reel the kite back in. Weight averaging those improvements based on the reel-in and -out times, the aerodynamic performance of the KITE-E kite is a factor 1.44 better. This results in an even bigger difference in flat area, as the planforms of new kites have optimised shapes, stepping away from the traditional surf kite shapes which generally have smaller projected to flat area ratios than the newly developed LEI kites for AWE purposes. Furthermore, it can be seen that the pumping efficiency, which shows how much of the generated energy remains after reel-in, and the duty cycle, which shows for how long during the power cycle energy is produced instead of used are higher compared to the system with the V2 kite. Multiplying those two results in the cycle efficiency, which is 101% better for the KITE-E system. This makes the power cycle a factor 2.01 better than the system with the V2 kite. Multiplying this with the superior aerodynamic performance, which was a factor 1.44 better, this already makes the KITE-E system a factor 2.90 better. This should lead to average mechanical power being a factor 2.90 better, as the improved electrical efficiencies are not accounted for. Looking at the average mechanical power in the table, which is 318% or actually a factor 4.18 better for KITE-E. There thus is a 30% difference between the estimated improvement factor and the real factor. However, this could be due to a different simulation model being used, and additionally, because some factors might not be included in this high-level comparison. However, as there are no major unexpected differences or inconsistencies, the product characteristics are validated.

Financial Analysis

In this chapter, an analysis of the finances is presented. This analysis has been done for the current state of the design, and is further expanded on for a timespan of eight years. The assumption is made that, at this point, production has been going on for a few years, and a product is being sold. In Section 17.1 a breakdown of the cost per system is presented. A return on investment is shown in Section 17.2. Lastly, Section 17.3 shows an operational profit analysis.

17.1. Cost Breakdown

In Table 17.1 presented below a detailed cost breakdown is shown, the costs are split up per subsystem and further into its components.

Table 17.1: Cost breakdown per subsystem

System	Component	Cost €
1. Airborne System	1.1 Kite and bridles	6590.53
	1.2 Tether	2029.96
	1.3 Wind turbine including batteries	247.93
		8868.42
2. Control System	2.1 KCU	1000.00
	2.2 Sensors	6713.26
	2.3 Main computer	1652.89
	2.4 Communication system	500.00
		9866.15
3. Ground Station	3.1 Generator	826.45
	3.2 Motor	3719.00
	3.3 Supercapacitor	1487.60
	3.4 Inverters	2709.00
	3.5 Converters	660.00
	3.6 Drum including gears and clutches	733.92
	3.7 Launching equipment	446.28
	3.8 Power overflow dump	24.82
	3.9 Spindle system	176.82
		10783.89
4. Miscellaneous	4.1 Kite repair set	19.83
	4.2 Tether splicing set	82.64
	4.3 Extra (wiring, bolts, etc) and unforeseen costs	2500.00
		2602.47
Total Subsystem Cost		32120.93
5. Labour	5.1 Development costs	4411.76
	5.2 Production	5000.00
		9411.76
Total		41532.69

The maximum total cost of this system has been set to be €45000.- as a stakeholder requirement (AWE-CON-CO-01). The choice has been made to take the limit on the total cost, excluding value-added tax (VAT). This is often done in the industry, and considering the system will also be targeted at governments and NGOs, which are assumed to have regulations on taxed, this seemed justified.

Most of the costs are based on specific components that are found to fulfil the needs of a subsystem, or research is done into comparable components if they need to be made specifically for this design.

For the cost of the kite, the different datasheets of Ocean Rodeo's A-Series kites are used to extrapolate the cost from the given kites [146, 185, 186]. Using a second order polynomial, the cost was determined at €5633.85 for a 20.16 m² Rise A-Series kite. Assuming that the kite needs to be specifically made according to the designed canopy planform, uses a more expensive canopy, and has one more strut, the cost is multiplied by a factor 1.4. This factor can be justified by the amount of kites that are produced, following from Section 4.9. This means the production process, even though it is for a specific kite shape, will not be a lot more expensive. This results in a total cost of €6518.21 excl. VAT for the kite.

The cost of further development is estimated by taking the same team of ten people, and seeing how much it would cost to maintain the team over the course of five years. Taking 45 weeks of working days of 40 hours in a year, with a cost per hour of €125,-, this comes down to €11.25 million. For production, testing and installation of the system, an estimate of €5000,- per system is used.

Lastly, something that should still be mentioned, is that since the estimated size of the market is 2550 units, it is possible that buying the components in bulk could mean a reduction in price for the components. This needs to be further evaluated, and discussed with suppliers.

17.2. Return On Investment

When developing a new product, an investment is needed for the design, development and production of the product before it can be sold. When such an investment is done, it is good to know what the estimation is on how much will be made on this investment. For this, calculating a return on investment (ROI) is standard practice. This is defined as follows:

$$ROI = \frac{\text{Total Revenue} - \text{Cost of investment}}{\text{Cost of investment}} \cdot 100\%. \quad (17.1)$$

To find a value for this ROI a selling price needs to be decided, for which an estimation is made, based on average profit margin in the industry of around 15%, this comes down to €47762.59 which has been rounded up to €47999,-, excluding VAT. This means that if the full costs are seen as investment, that the ROI will be 15.57%, over the time span of roughly 8 years. In Figure 17.1 a graphical representation is shown on the ROI estimation over the coming 8 years. This takes into account that an investment needs to be done before the production starts, and sales slowly start to ramp up. The break even point is seen at the point where the profit on investment crosses the x-axis.

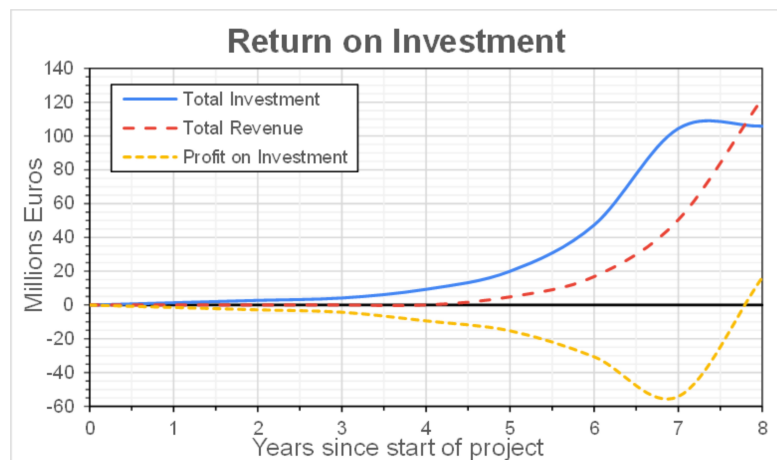


Figure 17.1: Estimation of the ROI

17.3. Operational Profit Analysis

With the purchase of a renewable energy system, it is always interesting to know how much money one can save by not having to buy the energy from the grid, and instead harvesting the free source of energy. This is opposed by the fact that the system needs to be initially bought and some parts experience wear, which need to then be replaced. To get a good estimate on this saving, and eventually even profit, during the operational lifetime, some aspects need to be evaluated.

First, the cost of running the system is of importance. The main source of cost is the replacement of parts in the system due to wear. The tether is a component that is under heavy load during operations, and therefore is a component that will need replacement a lot more than most other components. The designed for lifetime of the tether is 2526 hours of generating electricity, at a nominal power of 20kW, this means a total energy of 50520 kWh will be generated before the tether needs to be replaced. This does assume that the system will be able to generate the full 20 kW all the time, which is not feasible, but when the system generates less energy, the tether force is also less high, so it is assumed that the wear is also lower. To put a value on this, the cost per generated kWh is calculated, which comes down to 4.0 cents per kWh. Another component that needs to be taken into account is the kite. This has a lifetime of 4500 flight hours. The same is done here, and the cost per kWh is 7.3 cents for the kite. With the average cost per kWh of 60 cents when using the grid in the Netherlands, the profit the system makes over buying from the grid is 48.7 cents per kWh. With the selling price of the system being €47999,-, determined in Section 17.2, it will take a generated amount of energy of 98560 kWh, which is produced in 4928 hours. This is a bit over half a year of flight hours, which means that after this time the system starts making profit compared to charging through the grid.

Reliability, Availability, Maintainability, and Safety Analysis

In this chapter, the RAMS analysis of the AWES is presented. First, its reliability of is discussed in Section 18.1. This is followed by an assessment on the availability characteristics of the AWES system in Section 18.2. Then, maintainability of the different system components is presented in Section 18.3. Lastly, the safety precautions that need to be taken, are discussed in Section 18.4.

18.1. Reliability

The system's reliability is one of the crucial aspects for the successful commercialisation of AWE. AWES are a relatively new concept compared to the conventional static wind turbines. Only a few studies already addressed the reliability of these systems. Moreover, there are no recent studies that provide a complete methodology on improving the reliability of AWES [82]. However, to get an insight in the reliability of the system, the reliability of different subsystems of the AWES is assessed in the following subsections.

18.1.1. Kite system

First, the airborne system is analysed on reliability. For the kite, the ALUULA Vaepor composite is used. Since this is a fairly new composite, there is not much research and data available regarding the mean time before failure. From an employee of the kite company Ocean Rodeo, it has been estimated that the kite system can handle 4500 FH before a failure event occurs. The tether and bridle lines have a longer lifetime than estimated in [13], since a different material is used with an extra coating, increasing its life span to 2526 FH. Furthermore, the reliability of the kite holding its shape during operation has been estimated using the Weibull probability density function [13]. This results in an estimate of 200 FH until a failure event occurs. Since the kite is a self-made design, it is recommended to perform tests in, for example, a wind tunnel facility and verify the results mentioned above.

18.1.2. Ground system

The ground system of the KITE-E system differs from the system discussed in [13], so this will be analysed based on the mean time till failure (MTTF) of each component. Part of the anchoring are the car wheels which have a MTTF > 25000 hours [187]. The swivel rails, gears, clutches and launching clamp are all made of an aluminium alloy. Each part will constantly be used, but the movement is very monotone, as these parts will only rotate. According to the Weibull distribution a failure event will occur in one of these parts every 25000 hours. The truck bed is an important part of the system, however no pulling test or sheet fracturing tests have been performed on this yet. It is therefore recommended to do this in the future and determine whether the truck bed of the Rivian R1T can take on the forces.

18.1.3. Control system

A large part of the control system is the software implemented in all the sensors. The reliability of all the software programs has been determined using a constant probability density function. Every hour, there is a 0.001% chance that the software has a bug and does not function properly [13]. Regarding the hardware, there is a large range of differences. The IMU has an MTTF of approximately 150000 hours [86], the barometer 25000 hours [171], and the pitot tube 100000 hours [172]. Regarding the ground sensors, a Weibull distribution for the force sensors was found to be 100000 hours for the MTTF [13].

18.1.4. Power system

Again, the software MTTF for the power system is the same as the one provided in Section 18.1.3. The following MTTF has been established from several data sources: The Rivian has Lithium Iron Phosphate (LFP) cells with an MTTF of 90000 hours [188], the spindle motor a MTTF of 20000 hours [189], the supercapacitor a MTTF of 175000 hours [190], the converter a MTTF of 93000 hours [191], the inverter a MTTF of 1000000 hours [104], the generator a MTTF of 115000 hours [192], and the wind turbine on the KCU a MTTF of 50000 hours according to [13]. Only the dump load is unknown, so it is recommended to strictly track maintenance of the dump load.

18.2. Availability

Unfortunately, the only research performed on the availability of an AWES is the research from [13]. Here, a full analysis on the reliability, availability and safety of an AWES generating 100 kW of power is provided. Regardless of the fact that the system has to provide five times more power, some system aspects are closely related to the KITE-E system, thus the research can be assumed to be suitable for this RAMS analysis.

The availability of a system has been established and explained in terms of unavailability: "This is the probability that a specific cut set is in a failed state at time t ." [13] A cut set is a small group of events that could cause the whole system to fail, e.g. the ground station has an issue. Also, the Fussell-Vesely (FV) importance factor has been determined. This shows how much the failure of a specific cut set influences the failure of the whole system. The higher this value, the more influence it has on the whole system failing due to an issue in this specific cut set.

The results have shown that the unavailability of the kite system increases exponentially each day. This has been established based on the cut sets regarding ground system failure, kite damage, tether failure, control sensors and KCU failure, and power system failure. After one week of full operation, the unavailability of the whole system was determined to be 2.70%. The cut set "Kite damage due to ground control hardware problems" has the highest FV-factor with a value of 48.14%. This means that if this issue occurs, there is an approximate 50% chance of the whole system failing.

18.3. Maintainability

Maintenance is of utmost importance to improve the reliability and availability of the system and to ensure the safety and integrity of the AWES. Not being able to conduct maintenance can lead to a disastrous outcome, which are unpredictable as they can occur earlier than expected. This leads to a decrease of the reliability and availability of the system. Therefore, the accessibility and ease of maintenance is taken into account during the design phase. Furthermore, a predictive maintenance strategy is applied. This means that critical parts are actively monitored by sensors, such that initial failures can be detected early on, as heavy maintenance cannot be carried out at remote locations. Next to the implementation of a predictive maintenance strategy, also an in-depth maintenance plan for each subsystem is provided in Section 6.4.3. Before every flight, the control system performs a test run, during the flight sensors are monitoring the system actively, and after every flight visual inspections are performed and the components are cleaned. Furthermore, repair sets are provided, which can be used in case some damage to the kite or tether occurs. Moreover, lists of advised spare parts for specific operational sites will be provided, such that operators can bring them along and change them if needed. However, in order to avoid this, maintenance intervals are imposed, since heavy maintenance needs to be scheduled and needs to be executed by experts at a specialised facility. Lastly, also maintenance of the Rivian R1T needs to be carried out regularly, especially when it is operated in harsh environments. Maintenance is scheduled based on sensors within the car that keep track of the defects.

18.4. Safety

Safety should be taken into account throughout the complete life cycle of the AWES. Different safety precautions should be taken to ensure that no people are harmed during both production and operation of the AWES. Furthermore, during operations, no components should fail. This can cause a lot of damage to other components and can lead to a dangerous environment for the people operating the AWES. Moreover, the system should not be a treat to the environment. This is ensured by both adherence to the road and airspace regulations.

To ensure the safety of the employees at the workspace during manufacturing and assembly, a safety plan is implemented. Achieving this starts with providing all employees with an education on the safety standards and measures and providing them with the necessary safety equipment, such as safety shoes, glasses, masks and clothes. Even with these precautions, accidents can still occur. When this happens, first aid kits and a phone to call an ambulance should be available in the close vicinity. Lastly, all employees should have had a first aid training before they start working. These same procedures are also applied during the end-of-life phase.

Due to the fact that the AWES is a relative new concept, a lot of safety precautions are taken to ensure safe operations. Based on a failure mode and effect analysis, the main risks can be identified for which mitigation methods and safety precautions can be implemented, such as a safety line and a weak link. However, even when this is implemented, there is still a chance something goes wrong. Therefore, everyone that uses the system should be aware of the risks and the procedures that need to be performed in case of an emergency landing or failure of the system. To minimise harm being done by the system on the operator, emergency power buttons will be installed within reach of the operator. If something goes wrong, but the control system of the kite is still intact, the safe kite state will be initiated as explained in Chapter 8. This mitigates the danger of the kite crashing to the ground and harming the operator or surroundings.

Sustainability Compliance

In this chapter, a reflection is performed about the implementation of sustainability elements and the achievement of requirements. The chapter starts off with Section 19.1, which covers a reflection about the use of sustainable resources. The information in this mentioned section is used for the requirement compliance check in Section 19.2. Finally, a CO₂ equivalence emission estimation is assessed in Section 19.3.

19.1. Use of Sustainable Resources

Sustainability has had an important role throughout the entire KITE-E design process. The establishment of the sustainable development strategy in Chapter 3 introduced the main sustainability goals, approach methods and sustainability related requirements. These have been taken into account throughout the entire process and were woven into the functional analysis, trade-off decisions, operations and material selection.

The KITE-E design uses bio-based materials for its most failure susceptible and replacement demanding components. Since the kite, bridle and tether are the components that will suffer the most and the fastest from degradation, these components will have to be replaced regularly, as specified throughout the report. Therefore, it was of vital importance to choose bio-based and recyclable/reusable materials for these elements. This has been achieved through the selection of Sierra 78 bio-based Dyneema® and by selection of the recently developed ALUULA composite for the kite canopy and inflatable tube material. This material selection enables the assumption that the kite, tether and bridle system are 100% recyclable.

The motor, generator, drum, rails, spindle and swivel systems mainly consist of metallic alloys. At the AWES' end-of-life, these components can most likely be reused in other applications. In case these components will be ending their service lives, the majority of their individual components can be recycled. Since these items mainly consist of metal alloys, these can be molten and used in new components. A similar reasoning is taken for the electrical wiring, where the rubber wire casing will most likely be discarded.

The sensors and supercapacitor also mainly consist of metal components and can be decomposed. The supercapacitor is assumed to consist of 40% aluminium components, 30% of activated carbon, 25% of acetonitrile and 5% miscellaneous [88]. In this configuration, an estimated 50% of the supercapacitor is recyclable. This percentage is based on the aluminium parts and limited active carbon recyclability, but is expected to grow with increasing research in the field of activated carbon recycling.

Lastly, a component that can not be recycled nor reused is the KCU's foam protection. This does not greatly contribute to the system's mass and cost budgets, and is hence considered to be of less importance in this analysis.

19.2. Requirement Compliance Check

This section aims at investigating the sustainability related requirements and constraints. Therefore, a requirement compliance investigation is performed similar to those on a subsystem level. Results of this analysis are listed below:

- **AWE-CON-SUS-01:** Based on the material and component choices, almost no items will be discarded after their operational lifetime. Therefore, 70% recyclability will surely be obtained.
- **AWE-CON-SUS-02:** KITE-E does not use any lifting gases for its lift generation, hence it also does not use helium. This ensures compliance to this requirement.
- **AWE-CON-SUS-03:** This constraint could not entirely be verified. The kite itself will not generate a 45 dB ground noise level. The system does not only consist of the airborne kite and should be evaluated including the ground station. There is no data about the motor, generator or drum noise generation. Since these components can be quite noisy, no decision on compliance could be taken. This should be tested by means of testing / demonstration. In case of no compliance, noise shielding should be added to prevent excessive noise propagation.
- **AWE-CON-SAF-02:** This constraint could not entirely be verified. It is expected that no people should get injured by the prescribed operational measures, e.g. magnetic clamps for launching, get inside the truck

for launch and landing and the kite safety depowering manoeuvre. These measures need to be tested and demonstrated in real life applications to ensure that this requirement is met.

19.3. CO₂ Emission Estimates

This section provides an estimate for the KITE-E's CO₂ equivalence emissions. Based on the mass and lifetime breakdown in Chapter 15, the system's life cycle CO₂ emissions are estimated. This CO₂ estimation should be regarded as a preliminary estimation and should be used as an indication of the most critical aspects concerning environmental impact. Information about the actual CO₂ will be more accurate and detailed throughout the further design steps. Therefore, this estimation includes large assumptions to be eliminated in later design stages.

the first element of this estimation is the manufacturing of raw materials to the desired component for this project. Except for the kite, tether and bridles, the masses of raw materials are estimated based on the subsystem mass breakdowns in Chapter 15. From these, material composition assumptions are made on component level, based on the component function and general knowledge. Note that in Table 19.1, miscellaneous items contain foams, paints and other small items are combined. In order to obtain the material CO₂ equivalence contributions, the established masses are multiplied with a literature obtained specific emission factor [193]. As an estimate, 10% of the system's mass budget is produced as additional waste. The manufacturing process is concluded by an assembly and integration procedure, this stage is assumed to emit 50% of the total raw material processing emissions.

For the operations and maintenance stage, the CO₂ equivalence emissions are calculated for an operational time of 2628 FH, corresponding to an operation of 30% of a year. For this operational time, a consumption of 50 kg synthetic oil is estimated. The remainder of operations and maintenance CO₂ equivalence emissions are estimated based on the need for regular replacement of the kite and tether. As shown by the component lifetimes in Table 6.5, the kite has an operational lifetime of 4500 FH, with a tether lifetime of 2526 FH. For this analysis, one replacement of each of these components is considered. Finally, the AWES does not produce CO₂ when harvesting wind energy.

Assembly and integration CO₂ emissions are estimated based on literature obtained information [194]. It is important to realise that the manufacturing process can be optimised by applying lean manufacturing principles for large scale production, which are not taken into account in this analysis. Finally, the transportation emissions are estimated based on the need for raw material, (sub)-assembly and waste transportation. A raw material travel distance of 5500 km is assumed (transatlantic Amsterdam to New York distance) and is a combined road-waterway operation. For the (sub)-assemblies, this distance is increased to 7500 km to account for product delivery to further destinations. The waste disposal can remain within a range of 250 km. An overview of the CO₂ equivalence per design element is tabulated in Table 19.1. A summarising percentage-wise CO₂ breakdown is given by Figure 19.1.

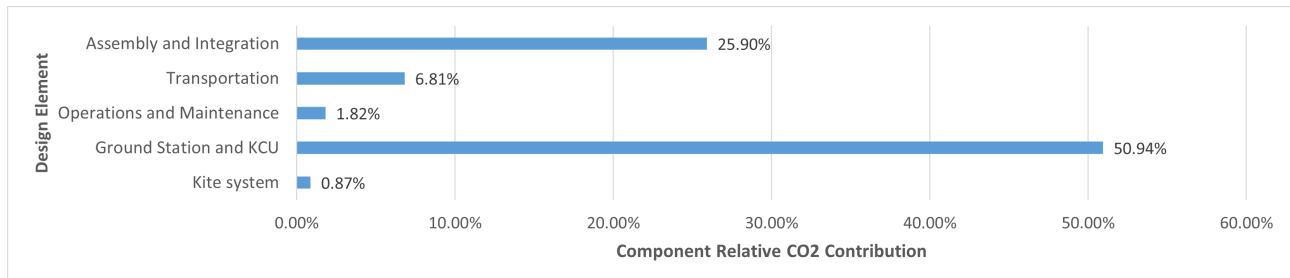
The KITE-E production and operation for 2628 FH emits a total of 9007 kg of CO₂ equivalence. From Figure 19.1, it is clear that the combined ground system and KCU system is the AWES' main contributor to CO₂ emissions. With a 50.94% contribution to the system's total emission, it emits almost double the amount of CO₂ when compared to the second-worst design element. The second and third most CO₂ emitting elements are the assembly and integration stage (25.90%) and transportation phase (6.81%). The kite system and operational and maintenance are found to have the least contributions to the global system's CO₂ emissions.

For later iterations of this emission assessment, the use of a dedicated life cycle assessment (LCA) tool should be considered. For the scope of this project, no commercially available LCA tool within the cost budget was found. For subsequent LCA's, the use of a market available LCA tool is recommended. Secondly, the system's development emissions should be taken into account for future iterations. Since sustainability is a vital aspect throughout this design, future development should take these recommendations into account for a more accurate emission assessment.

Finally, KITE-E's production and operation is compared to the CO₂ equivalence emission of a similar 20kW diesel generator. For this analysis, an equal operational time of 2628 hr is considered, leading to a total generated energy of 52560 kWh. The diesel generator is found to consume 6.06 l/hr [195]. With a specific emission of 2.606 kg CO₂/l [196], the diesel generator is found to emit 41502 kg of CO₂ over this operational time. This is more than quadruple the KITE-E's production and operational CO₂ emission. For an equal emission, a series of KITE-E systems could provide 4.6 times as much energy when compared to a diesel generator.

Table 19.1: Overview CO₂ equivalence emission for of KITE-E's production and an operational time of 2628 FH.

Component	Material	Quantity kg	CO ₂ Eq./kg	CO ₂ Eq. kg
Materials [193, 197]				
Kite System	ALUULA	5.00	10.60	53.00
	Polyurethane coating	0.10	3.61	0.36
	Sierra 78 bio-based Dyneema®	7.03	3.50	24.59
	XBO coating	0.20	3.50	0.70
Ground Station and KCU	Copper	2.00	1.25	2.50
	Rubber	0.50	4.00	2.00
	Aluminium Alloys	150.00	1.60	240.00
	Cast Iron	75.00	1.50	112.50
	Electrical Steel	75.00	49.00	3675.00
	Insulation	5.00	1.86	9.30
	Low Alloyed Steel	65.00	2.00	130.00
	Polyethylene Plastic	5.00	3.33	16.65
	Miscellaneous	20.00	20.00	400.00
Material Total		410.00		4666.60
	Scrap Material Production	61.50	20.00	1230.00
Assembly and Integration [194]				
Emissions				2333.30
Operations and Maintenance [193, 197]				
Lubrication Oil	Castrol Braycote 601 EF	50	1.7	85
Kite Replacement	ALUULA + Coating	5.1	10.46	53.361
Tether and Bridle Replacement	Sierra 78 bio-based Dyneema® + Coating	7.225	3.5	25.2875
Transportation [198]				
Component	Volume tonne	Distance km	gCO ₂ /tonne-km	CO ₂ Eq. kg
Raw Materials	2.5	5500	40	550
(Sub-) Assemblies	1.5	7500	5	56.25
Waste Disposal	0.5	250	60	7.5
Total				9007.30

**Figure 19.1:** Production and 2628 FH KITE-E operation relative CO₂ equivalence breakdown.

Project Future Outline

This chapter comprises KITE-E's projected future steps. Therefore, the general design and development logic with a Gantt chart is presented in Section 20.1. This is followed by a production plan in Section 20.2.

20.1. Design and Development Logic

The design and development logic diagram shown in Figure 20.1 is used to provide a general overview of the project's flow. It is used as an extension of the presented work flow and breakdown diagrams in the Project Planning Report [1]. Whereas these diagrams focussed on the conceptual design phase until the detailed design, the design and development logic diagram shows how this fits in the larger project scope. Additionally, it is used as the baseline information for the Gantt chart in Figure 20.2. As observed in Figure 20.1, the general flow is chronological, meaning that subsequent blocks are performed in a similar time sequence. This also includes that parallel blocks are simultaneously executed.

The project's future outline is split into five phases, from the design phase until end-of-life. As observed in Figure 20.1, the design performed within the DSE is considered to be the preliminary design. This decision is taken based on the missing worked out design aspects and the established recommendations in this report. Therefore, the obtained design at this stage is not yet ready to be considered as a final design and should be further evaluated in a detailed design continuation. This detail design process will focus on more exact design tools such as CFD, finite element analysis and more detailed power cycle models to further optimise at subsystem level. Additionally, this detailed design should also look into the AWES fixation to the Rivian R1T and the inter component rigid connections. Similarly to the already performed preliminary design, an iteration and optimisation process will be carried out at system integration level to provide an optimal and converged design. Throughout this detailed design stage, it is vital to perform continuous verification and validation for the models, results and requirements. Non-compliance might lead to the need for re-iteration of the existing design until compliance is met.

After this detailed design, the final design is established with the obtained mass, volume, cost and power breakdowns after the iteration process. At that point, the specific part designs will be analysed to determine the detailed drawings and assess the production possibilities and reliability. This analysis is then extended to the assembly level. From these analyses, the testing phase can be entered.

The testing phase will test whether the system complies with the required performance standards. First, product validation shall be provided by end-to-end information testing, mission scenario testing, operational readiness testing and stress testing. These tests will be performed on part, subsystem and full assembly level. Next, prototype testing will be performed to check the general system's integration and performance. After prototyping, a market campaign is launched in co-operation with Rivian to raise interest and introduce KITE-E to potential clients. The market campaign will be initiated with a grand product reveal event and continuously monitored with a social media and advertising strategy. Meanwhile, the testing phase is continued by qualification model testing, in which the AWES's ultimate load capabilities will be tested. Since these tests will test the design to its limits, the models will be discarded but can be disintegrated to enable reusage and recycling. Finally, a flight model is built for acceptance testing and verifies the system's capabilities to operate in operational design conditions. When non-compliance is observed during testing, the design should be re-iterated to make sure that compliance can be shown by testing. After certification and licensing, full scale commercial production will be started. This will bring the design phase to an end. Therefore, phases following certification will not be further explained in the design and development logic diagram.

Finally, the time scheduled projection of this design and development logic description is shown by the Gantt chart in Figure 20.2. This Gantt chart is generated for five years after the initial design steps of KITE-E. The team believes that full scale commercial production can be achieved, especially when co-operation with Kitepower and Rivian is established. The reasoning for this co-operation are the similarity of AWES concept with Kitepower and the market possibilities that this integrated system provides.

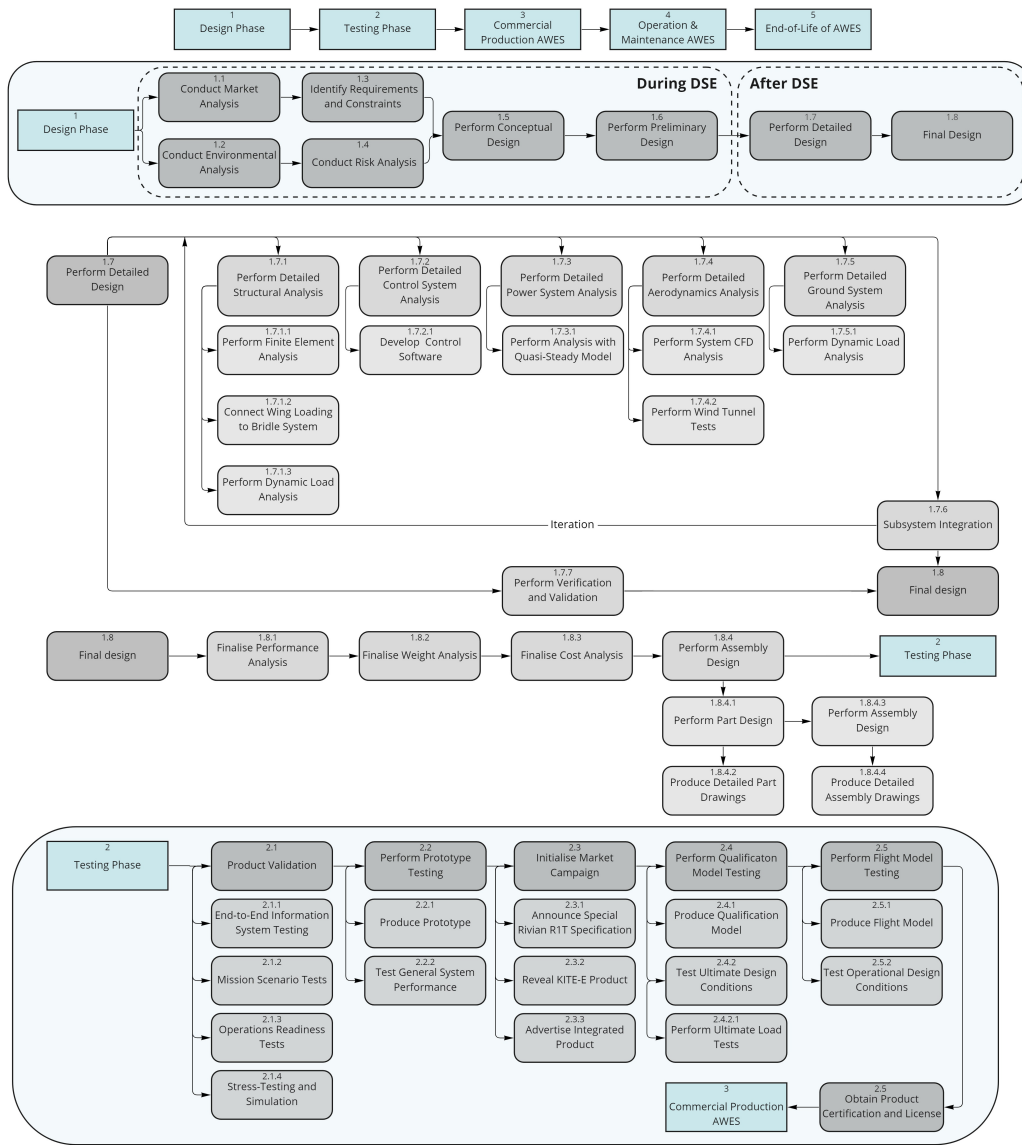


Figure 20.1: Project Design and Development Logic Diagram.

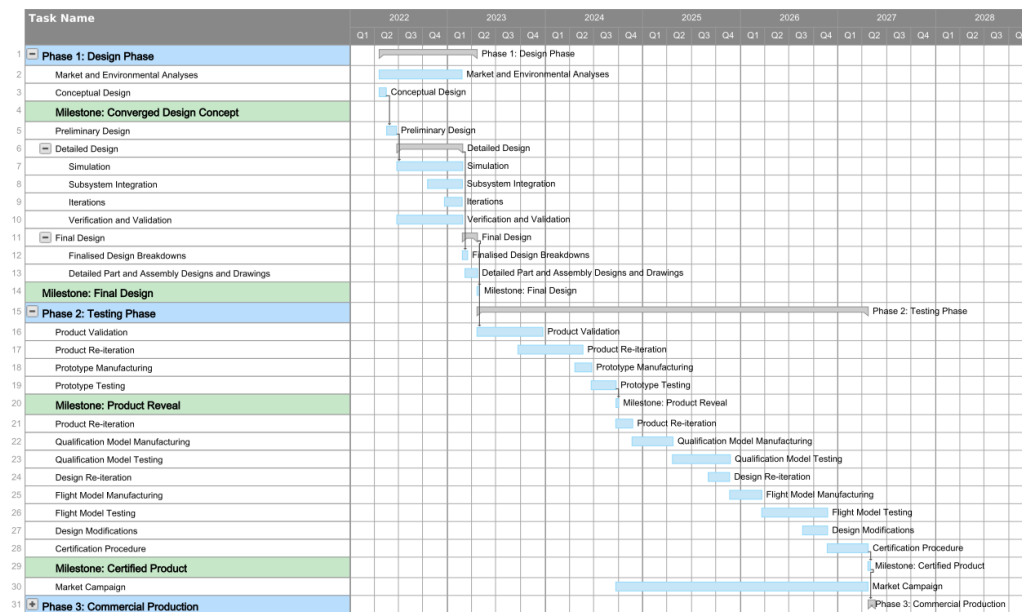


Figure 20.2: KITE-E future planning layout until commercial production.

20.2. Production Plan (F.1 & F.2)

In this section, the forecasted manufacturing, assembly, and integration procedures are explained. These processes are important to facilitate the transition from the prototyping phase to series production. During the production of the system, the principle of lean manufacturing will be used. Lean manufacturing maximises productivity of manufacturing processes due to the focus on minimizing waste. There will be minimum waste in terms of material, energy, time and human resource [199].

The system needs to be integrated on the truck bed of the Rivian R1T or potentially a similar pickup truck. The waiting time during installation for the customer has to be minimised, which can be done in multiple ways. The whole system should be ready for installation before the truck arrives in the factory. The methods that will be used are explained in the coming paragraphs.

The first method is the manufacturing system used in the factory. All the subsystems can be manufactured in parallel to avoid big storage spaces. To simultaneously finish all subsystem assemblies, the logistics plan must be extremely well-designed. Furthermore, a small stock of certain subsystems should be maintained. These minimise the risk of increased waiting times if a subsystem's production is delayed. This method is a blend of the just-in-time and just-in-case inventory philosophy spectra [200]. The KCU and ground station control systems can be used as examples. The production of these systems can take longer due to the high complexity of the subsystem. The subsystem comprises a high number of electrical components and many lines of code. To produce the subsystem and afterwards check the integrity of the component, extra time should be reserved for unforeseen circumstances.

Secondly, the assembly of the system is investigated. In the factory, several mock-ups of the Rivian R1T will be present. This mock-up of the truck will be used as a test bed for the sub-assemblies to merge into one integrated system. The mock-up can also be used for complete system testing of random production samples. The reel-in and reel-out of the tether can be tested for each fabricated system, when it is integrated on the mock-up. The same can be done for every build KCU. This way of operation prevents hiccups when each fabricated system is integrated on the truck.

Finally, to minimise the waiting time for the customer, the integration time of the system on the truck is investigated. The system is already fully tested on the mock-up truck and completely finished. The largest share of the integration time will be put into the preparing the truck for receiving the system. The whole truck should be adapted for the system, like drilling holes for the connection of the system or preparing the electrical connections and data ports. This time can be minimised by making overlay templates for the truck. For example, a mould with the correct positions for the holes of the connection bolts. Furthermore, the amount of electrical connection and data port for the system to the truck will be minimised by using plugs. All the wires can be connected to the plugs before installation, and only the plugs have to be connected to finish the system. This results in less preparation and integration time, as only the plug needs to be connected to the truck and plugged into the system for installation. As the last step in this process, the system can be integrated on the truck by moving subsystems immediately from the mock-up to the truck. This will minimise the time needed to check the integrated system.

Conclusions and Recommendations

The final chapter of this report contains the main conclusions and recommendations of KITE-E's design process. This chapter functions as a critical reflection on the established design choices and modelling methods. Therefore, Section 21.1 comprises the design conclusions, both on a subsystem and general level. This is followed-up by the recommendations' discussion in Section 21.2 where the team's advice for future design iterations is discussed.

21.1. Conclusions

The aim of this project was to design a softkite based, 20 kW rated AWES integrated in a pickup truck within ten weeks. With little to no prior knowledge about this operational procedure, the team was immersed in a new topic. After initial research and design planning, a Project Plan was established [1]. This was followed by a Baseline Report [18] where an initial sustainability strategy, market analysis and functional analysis were established. Additionally, this Baseline Report investigated an initial set of requirements and concluded with a design space exploration that was realised through a design option tree. The Midterm Report expanded on these initial analyses and showed the design concept convergence through design trade-offs on subsystem level, based on the design option tree [10]. From these decisions, a conceptual characteristics estimation was carried out, accompanied by a risk analysis. These three reports functioned as the foundation for this more detailed design evaluation. Therefore, the goal of this report in specific, was to present an updated and more detailed product version through detailed analysis methods. Therefore, the conclusions and reflections about this process are laid out in this section.

The first step in product design is to explore potential market gaps. A market exploration showed that the system fits both within the electric pickup truck market and the mobile energy generation market. Since no systems currently exist that combine the electric pickup truck and mobile energy generation markets, new opportunities for a market intrusion are found. It can thus be concluded that the MAWES provides an opening into a niche market, enabling unlimited range to electric pickup trucks while being energy-autarkic. Furthermore, it was concluded that there are three main operational regions, which are related to their respective fields of application. Firstly, the system can be used by well-off adventurers, in North-America and Patagonia. Secondly, the system provides a way to deliver energy in disaster struck regions, such as the Caribbean. Lastly, the system can be used in the Middle East for peace missions. The market analysis concluded with an estimated demand of 2550 units for the KITE-E.

In the identified operational regions, airborne regulations were found to greatly vary. With a rapidly changing regulatory philosophy about drones and other unmanned aerial vehicles, it is required to stay in touch with these updates. Therefore, KITE-E will require regulatory approval for several procedures and should be designed to adhere to the local airborne requirements. Although the system is desired to show regulatory approval, the design should always focus on the system's reliability and safety of the operator, surrounding people and on the integrity of the system itself. Finally, the system's operator should obtain the required operational licences to utilise the system.

A well integrated design should account for technical risks. This includes implementing mitigation and prevention methods to decrease the probability of the occurrence and the severity of the risks. The emergence of new risks in this report shows that risk identification is a reoccurring process and should be continuously updated throughout the future design phases. Furthermore, new risks will automatically come to light as more design details will be unveiled. At this stage, the tether was concluded to be the most critical element. Out of all parts, it has the shortest operational life and comprises the most severe design risks, since it functions as the connection between the kite and ground system.

As a first step in the detailed design process, the power cycle and all its characteristics were determined. For this, the Luchsinger model was used. Adhering to a required average electrical output of 20 kW, it was found that at the design wind speed of 10 m/s, the traction force was already be too high for the ground station to remain static during operations. Therefore, a less optimal power cycle, with higher reel-out speed, was adjusted to prevent this ground station movement. Furthermore, the projected area required to generate 20 kW electrical output power at this wind speed was found to be 15.19 m². The resulting power cycle at this wind

speed demands that the tether is reeled out at 41% of the wind speed, and reeled in at 180% of the wind speed and has a total cycle duration of 75 seconds. The components of the power circuit were sized based on the resulting power generated or required during the different phases. The generator was over designed, to also get the full potential out of the system at higher wind speeds. However, the sensitivity analysis showed that the implications of this higher power output on the other power system components were not studied in enough detail. This will be elaborated on in the recommendations.

In this report, the GNC was mainly designed on a conceptual, describing level. The focus was to come up with a general system capable of autonomously deciding on the operational power generation procedure, flight path and control plan actuation. The GNC system is actuated by an airborne KCU and communicates with the ground system through Wi-Fi connection. With reliability being a critical aspect for this subsystem, it uses simple and well-researched concepts. This might not necessarily lead to the optimal GNC system for this application, but complies to the requirements within the scope of this project.

During this preliminary design phase, multiple highly influential components were designed in parallel. This generates the need for a design optimisation, by reiterating on all the design results and ensuring all the components are tuned to each other. After optimisation, a kite with a 15.19 m² projected area has come out of the iterative process. Optimisation also led to the establishment of a new reel-in angle of attack range (-1° to 3°), since the initial range resulted in negative angles of attack. The kite system uses a similar bridle configuration to previous systems, however no optimisation could be performed. This is a result from the kite and bridles decoupling. In order to determine the optimal bridle configuration, a detailed load path analysis should be performed.

To continue on this load analysis, even though the ground system components have been identified and either determined to be implemented as commercialised products or conceptually developed in CATIA, no interconnections are investigated. This means that the load transfer from the structural load carrying components into the ground system and the attachment points has not been investigated. For the current design stage, the assumption of non-failing component attachments and connections is valid, since the top level functionalities and interfaces were given priority to ensure a system that is capable of fulfilling the requirements. Whereas it was out of this project's scope, later design stages should investigate and design these connections and attachments to withstand the encountered loads due to the kite's operation.

After having established the optimised kite design, a sensitivity analysis was performed to get an insight into the design interactions on a quantitative and qualitative level. The sensitivity analysis showed expected results, from which could be concluded that the used models produce the desired outputs. Furthermore, these insights are used to further optimise the design during the detailed design phase, since this shows which parameters can be changed in order to obtain desirable results and which parameters are most crucial for the system's performance.

With a total selling price of €47999/unit, a return of investment study is performed. This study concluded that the KITE-E program will reach its break-even point in mid 2028, after beginning commercialised production in 2027. With the design phase reaching to an end and commercialised production coming up, the team has estimated a demand of 2550 KITE-E products, having a combined revenue of €122.4 million. Additionally, the customer will benefit from the autarkic truck's capability to generate electricity. After 5236 h of operating the AWES, corresponding to half of a year's total hours, the customer has already earned back the KITE-E cost, including tether and kite replacement costs, essentially functioning as an equivalent 'energy' cost. These results were obtained from a comparison to an equivalent energy purchase from national power grids. This ROI study is indicative of KITE-E's estimated profitability and should be regarded as the initial step of a full financial report. This should be expanded on in future developments.

The requirements from the Baseline Report have been adjusted to both eliminate the TBD items and improve the requirement formulation according to the VALID standards. These requirements have been implemented throughout the whole detailed preliminary design phase. KITE-E was found to comply with most of the pre-defined requirements. More importantly, no requirements were found where non-compliance was immediately observed. However, compliance could not be proven for all requirements and constraints. The two main reasons for this compliance uncertainty are that no sufficiently detailed analysis was achievable within the ten weeks period, and that some requirements' compliance can only be shown when a demonstration or test is performed. Because of the lack of failed compliance requirements, the identified requirements could be deemed to be not challenging enough. This aspect might have limited the need for innovative solutions, and therefore, potential new design approaches. Therefore, requirements should be continuously reviewed during later design stages. On the other hand, this compliance observation might also mean a correctly implemented design approach, fully integrating the system's functionalities and requirements throughout the design process.

Next to requirements, the used analysis tools and models should also be verified and validated. Although

this report presented several approaches to achieve verification and validation for the used aerodynamic and power system models, this should be further investigated in later design steps. The aerodynamic VSM model verification and validation was performed using a rectangular wing. This analysis led to the conclusion that the aerodynamic characteristics were observed to have an overestimated and hence better performance. Additionally, no VSM verification and validation for a kite implementation could be performed, leading to design inaccuracies and uncertainties. Similarly, no model validation could be performed for other subsystem parameter estimations. This resulted from the lack of test data, which the numerical results could be compared with. Recommendations for verification and validation are further elaborated on in Section 21.2.

In general, sustainability was a recurring topic throughout the design. With influences in almost every design aspect, ranging from requirement identification to trade-off criteria. This led to an estimated product recyclability of over 70%, while the production and operation of the KITE-E system was found to be more than 4.5 times less emissive than the operation of a similar 20 kW diesel generator. This was concluded by evaluating an operational period of 2628 hours (30% of a year's total hours) for an equal energy generation. This re-emphasizes the system's potential as a potential green replacement for traditional energy generation systems.

The established production plan is lacking the required level of detail for initialising commercial production. This production plan should be updated with more information about specific production methods and flows from raw materials all the way up to the full assembly. All production, integration and assembly methods should be included in the production plan, which should be updated in later design phases.

To conclude, this report presented a complete preliminary design of a movable airborne wind energy system. Although many design aspects have been investigated in detail, the team realises that still a lot of research and simulation is needed to deliver a fully designed and optimised product. Therefore, a future outline was created to define the following design steps in order to achieve commercialised production by 2027. This is accompanied by the team's recommendations for future work in Section 21.2.

21.2. Recommendations

To end the report and to add to the conclusions, this section lays out the main recommendations for future design extensions. These recommendations have resulted from limitations and observations made during this project's design.

Firstly, future design steps should investigate the canopy to bridle lines attachments in more detail. In this report, these two structural aspects have been decoupled. Therefore, further design steps should include a load transfer analysis from lift generation until the load absorption in the ground system. Especially for the bridle and kite system, this can be performed through a finite element analysis. This would allow an optimisation for the bridle configuration. This also includes that a dynamic load analysis should be performed, since the kite is a highly dynamic system. Adding to this, the applied safety factors should be revised, as the currently used load factors are too low. This was concluded from private communications with Bryan van Ostheim [201].

For aerodynamics, it is recommended to expand the numerical analysis to a CFD model. The currently used numerical aerodynamic approximation shows good performance for lift estimations and is accurate in the linear flow regime. However, for the drag analysis, it lacks the ability to accurately model viscous effects and therefore overestimates the aerodynamic performance. Additionally, the used VSM program could not be validated for the used LEI airfoil. Therefore, controlled experiments should be performed in order to compare the simulation data to real world measurements. This would enable to perform model matching on the simulation program to obtain more detailed future iterations.

In order to further optimise this aerodynamic analysis, a tool could be created to simulate the kite's in-air deformation. Since a soft kite using a single foil airfoil is used with an inflatable structure, it is known that the kite system will show significant deformation [118]. Because of these anticipated structural deformations, the modelled kite in this report does not coincide with the actual flying model. Therefore, the aerodynamic analysis should be integrated with an aeroelasticity model to simulate the kite in flying circumstances.

Next, in the Luchsinger model, one important phase of the flight cycle is not modelled, namely the transition phase. However, the Luchsinger does not ignore this phase, and takes it into account via the transition efficiency. Contrary to the Luchsinger model, the quasi-steady model, does contain the transition phase, as can be seen in Figure 21.1. For a more accurate analysis and determination of the flight path, it is thus recommended to investigate and incorporate the quasi-steady model. Furthermore, as an addition

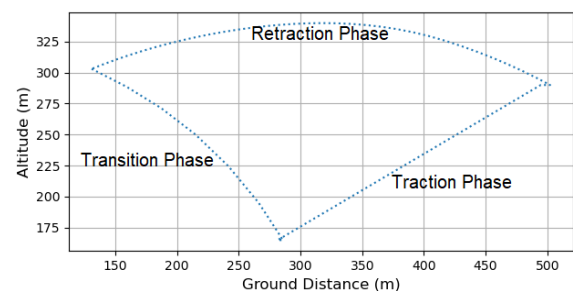


Figure 21.1: Flight path for operational height of the KITE-E system, generated with the Quasi-Static Model (QSM) [176].

to the Luchsinger model, it could be investigated how the kite's angle of attack should change during the flight cycle. When the kite encounters a wind gust, it could be that the power limit is reached, which means that the tether can not be reeled out any faster. When this happens, there are two other options to limit the tether force. Firstly, one could increase the elevation angle, which has already been discussed in Section 10.4. Secondly, as just mentioned, the kite's angle of attack could be changed. For this, the aerodynamic model, which gives the aerodynamic coefficients for a range of angles of attack, should be implemented, so that it can be calculated which angle is required to keep the force in the tether constant.

Both the implemented aerodynamic and power models (VSM and Luchsinger) should be validated using experimental data. By comparing with measured data during controlled test set-ups, the model's simulating accuracy and deficiencies can be determined. This would allow for model tweaking to create a better simulation model for future design iterations or even new designs. Similarly, the kite's mass estimation code should be validated by evaluating more data points about kite structural masses.

In addition to validating the aerodynamic and power characteristics with experimental data, physical experiments also need to be done to further investigate the other subsystems' characteristics. For example, the minimal operational ground wind speed that is needed for launching of the kite can be tested in real life. Furthermore, the minimum operational wind speed is dependent on the minimum control force. This minimal control force could be determined via experimental testing. Another case is that for the high level control loop, some assumptions have been made on the gusts and their magnitudes, which could be reassessed in real life conditions for efficiency. The system also depowers 10 seconds before the expected arrival of a large wind gust, these 10 seconds could be optimised, i.e. be shortened.

The KCU is a critical component and should be further investigated in later design phases. Since there is not much openly available information about this system, more detailed analysis should be invested in this crucial element. Firstly, the KCU should be investigated to not fail in critical kite failure conditions. This relates to an impact analysis and with an update of the KCU's structure according to the analysis' outcomes. This affects both the metal casing and the foam protection thickness. A more detailed investigation also leads to more accurate mass, size and cost estimations for this element. As for this design stage, only raw estimates for these budgets were obtained.

The concept of reverse pumping and, by a larger extent, the whole GCN system needs to be reviewed and extended. This project only looked into reverse pumping on a high level. Similarly, the GCN system has been described and analysed and designed on a conceptual basis. Therefore, in order to provide a commercial control system, software development needs to be considered in future design steps. After the software establishment, the correct implementation of the system's decision-making, operational modes and flight path planning capabilities can be tested.

Finally, the risk of a truck bed tear-out should be investigated. As discussed in Section 21.1, the interconnections between the components are not analysed, neither is the connection to the truck bed. Therefore, the potential risk of failure for this Rivian R1T related element should be researched, prevented and mitigated in future design stages.

The team believes that the establishment of these recommendations within future project phases could greatly increase the design's level of detail and model accuracies. This set of suggestions, in combination with the findings from this report, can be used as a baseline for more profound design analyses to finalise the design of this project and fulfil the promising application possibilities that it carries along.

References

- [1] DSE Group 15. *DSE Project Plan: Kite Powered Electric Pickup Truck*. 2022.
- [2] R. H. Luchsinger. "Pumping Cycle Kite Power". In: *Airborne Wind Energy*. Ed. by U. Ahrens, M. Diehl, and R. Schmehl. Berlin, Heidelberg: Springer Berlin Heidelberg, 2013, pp. 47–64. ISBN: 978-3-642-39965-7. DOI: 10.1007/978-3-642-39965-7_3. URL: https://doi.org/10.1007/978-3-642-39965-7_3.
- [3] R. van der Vlugt et al. "Quasi-steady model of a pumping kite power system". In: *Renewable Energy* 131 (2019), pp. 83–99. DOI: 10.1016/j.renene.2018.07.023.
- [4] U. Fechner. "A Methodology for the Design of Kite-Power Control Systems". PhD thesis. Delft University of Technology, 2016.
- [5] Catherine Clifford. *Paris climate accord leaders: What we do between now and 2030 will impact life on earth for hundreds of years*. May 2021. URL: <https://www.cnbc.com/2021/05/03/paris-climate-accord-leaders-behavior-will-impact-life-for-centuries.html>.
- [6] *About airborne wind energy*. URL: <https://airbornewindeur.ope.org/about-airborne-wind-energy/>.
- [7] *CO2 emissions from cars: Facts and figures (infographics): News: European parliament*. June 2022. URL: <https://www.europa.rl.europa.eu/news/en/headlines/society/20190313ST031218/co2-emissions-from-cars-facts-and-figures-infographics>.
- [8] Eionet. *New registrations of electric vehicles in Europe*. 2021. URL: <https://www.eea.europa.eu/ims/new-registrations-of-electric-vehicles>.
- [9] *Hydrogen production and distribution*. URL: https://afdc.energy.gov/fuels/hydrogen_production.html.
- [10] DSE Group 15. *DSE Midterm Report: Kite Powered Electric Pickup Truck*. 2022.
- [11] U. Fechner and R. Schmehl. "Model-Based Efficiency Analysis of Wind Power Conversion by a Pumping Kite Power System". In: *Airborne Wind Energy*. Ed. by U. Ahrens, M. Diehl, and R. Schmehl. Berlin, Heidelberg: Springer Berlin Heidelberg, 2013, pp. 249–269. ISBN: 978-3-642-39965-7. DOI: 10.1007/978-3-642-39965-7_14. URL: https://doi.org/10.1007/978-3-642-39965-7_14.
- [12] J. Oehler and R. Schmehl. "Aerodynamic characterization of a soft kite by in situ flow measurement". In: *Wind Energy Science* 4.1 (2019), pp. 1–21. DOI: 10.5194/wes-4-1-2019. URL: <https://wes.copernicus.org/articles/4/1/2019/>.
- [13] V. Salma, F. Friedl, and R. Schmehl. "Improving Reliability and Safety of Airborne Wind Energy Systems". In: *Wind Energy* 23.2 (2020), pp. 340–356. DOI: 10.1002/we.2433.
- [14] F. Girrbach et al. "Optimization-based sensor fusion of GNSS and IMU using a moving horizon approach". In: *Sensors* 17.5 (2017), p. 1159.
- [15] I. Oehlmann. "The Sustainable Footprint Methodology: Including sustainability in the project management of the Bergemeer Gas Storage project". MA thesis. Delft University of Technology, 2010.
- [16] R. Čiarnienė and M. Vienažindienė. "Lean manufacturing: theory and practice". In: *Economics and management* 17.2 (2012), pp. 726–732.
- [17] P. Olla. *Space Technologies for the Benefit of Human Society and Earth*. Springer, 2009.
- [18] DSE Group 15. *DSE Baseline Report: Kite Powered Electric Pickup Truck*. 2022.
- [19] T. Cain. *Who's winning the Electric Pickup Truck Sales Race?* Feb. 2022. URL: <https://driving.ca/column/driving-by-numbers/whos-winning-the-electric-pickup-truck-sales-race>.
- [20] D. Block, P. Brooker, et al. *Prediction of electric vehicle penetration*. Tech. rep. University of Central Florida. Electric Vehicle Transportation Center (EVTC), 2017.
- [21] *Airborne Wind Energy*. URL: <https://www.nrel.gov/docs/fy21osti/79992.pdf>.
- [22] *electricity generation - energy information administration*. URL: https://www.eia.gov/outlooks/aeo/pdf/electricity_generation.pdf.
- [23] URL: <https://www.energy.gov/sites/prod/files/2015/08/f25/LCOE.pdf>.
- [24] *Portable generator market*. URL: <https://www.marketsandmarkets.com/Market-Reports/portable-generator-market-195875841.html>.
- [25] *Airborne Wind Energy*. URL: <https://www.enerkite.de/en/>.
- [26] B. Richards and A. Schaefer. "Renewable Energy Powered Water Treatment Systems". In: Jan. 2009, pp. 353–374.
- [27] *Climate change*. URL: <https://www.un.org/en/global-issues/climate-change>.
- [28] M.E. Porter. *How competitive forces shape strategy*. Harvard Business School Press, 1991.
- [29] *Long Range Solar Electric Vehicle - Lightyear one*. URL: <https://lightyear.one/lightyear-one>.
- [30] *EF1-T pickup truck*. URL: <https://edisonfuture.com/pages/ef1-t-pickup-truck>.
- [31] *An overview of the last 20 years natural disasters*. URL: <https://www.undrr.org/media/48008/download>.
- [32] S. Edelstein. *GM reportedly to produce Electric Hummers for US military*. Nov. 2021. URL: https://www.motoraauthority.com/news/1134155_gm-reportedly-to-produce-electric-hummers-for-us-military#:~:text=GM.
- [33] A. Costall, B. Harris, and J. Pigois. "Electrical Resistivity Imaging and the Saline Water Interface in High-Quality Coastal Aquifers". In: *Surveys in Geophysics* 39 (July 2018). DOI: 10.1007/s10712-018-9468-0.
- [34] D. Berhane. "Determination of Losing and Gaining Reaches in Arid and Semi-Arid Environments of NSW". PhD thesis. Oct. 2015.
- [35] M. Schirber. *Global disaster hotspots: Who gets pummeled*. Dec. 2004. URL: <https://www.livescience.com/3783-global-disaster-hotspots-pummeled.html>.
- [36] *Which countries are becoming less peaceful?* URL: <https://www.economist.com/graphic-detail/2021/06/24/which-countries-are-becoming-less-peaceful>.
- [37] H. Schmidt et al. "The Social Acceptance of Airborne Wind Energy: A Literature Review". In: *Energies* 15.4 (2022). ISSN: 1996-1073. DOI: 10.3390/en15041384. URL: <https://www.mdpi.com/1996-1073/15/4/1384>.
- [38] J. Weber et al. *Airborne Wind Energy*. 2021. URL: <https://www.nrel.gov/docs/fy21osti/79992.pdf>.
- [39] EASA. *Easy Access Rules for Unmanned Aircraft Systems*. Sept. 2021. URL: <https://www.easa.europa.eu/document-library/easy-access-rules/online-publications/easy-access-rules-unmanned-aircraft-systems?page=5>.
- [40] EASA. *Certified Category - Civil Drones*. 2022. URL: <https://www.easa.europa.eu/domains/civil-drones/drones-regulatory-framework-background/certified-category-civil-drones>.
- [41] EASA. *Specific Category - Civil Drones*. 2022. URL: <https://www.easa.europa.eu/domains/civil-drones/drones-regulatory-framework-background/specific-category-civil-drones>.
- [42] B. Peeters and R. Nusselder. *Overview of critical noise values in the European Region*. URL: https://mp.nl/sites/default/files/publications/IG%5C%20Noise_Critical%5C%20noise%5C%20values%5C%20in%5C%20EU.pdf.
- [43] *Global Wind Atlas*. URL: <https://globalwindatlas.info/>.
- [44] *Global Solar Atlas*. URL: <https://globalsolaratlas.info/>.
- [45] E. Bournay. *UV index worldmap: Grid-Arendal*. URL: <https://www.grida.no/resources/7130>.
- [46] S. Pernreiter et al. "Landscape evolution in the south Yilgarn Craton and Albany-Fraser Orogen, Western Australia". In: (May 2018). DOI: 10.4225/08/5b22bb3b9f4af.
- [47] *How much wind does a kiteboarder need to fly a kite?* URL: <https://www.surfertoday.com/kiteboarding/how-much-wind-does-a-kiteboarder-need-to-fly-a-kite>.
- [48] D. Agwu et al. "Review Of Comparative Battery Energy Storage Systems (Bess) For Energy Storage Applications In Tropical Environments". In: (Sept. 2018).
- [49] S. Ma et al. "Temperature effect and thermal impact in lithium-ion batteries: A review". In: *Progress in Natural Science: Materials International* 28.6 (2018), pp. 653–666. ISSN: 1002-0071. DOI: <https://doi.org/10.1016/j.pnsc.2018.11.002>. URL: <https://www.sciencedirect.com/science/article/pii/S1002007118307536>.
- [50] *UN World Food Programme (WFP)*. URL: <https://www.wfp.org/>.
- [51] *The disaster relief organizations you need to know about*. URL: <https://www.galaxydigital.com/blog/disaster-relief-organizations>.
- [52] *Humvee*. URL: <https://military-history.fandom.com/wiki/Humvee>.
- [53] F. Bu et al. "Recent developments of advanced micro-supercapacitors: Design, fabrication and applications". In: *Npj Flexible Electronics* 4.1 (2020), pp. 1–16.
- [54] E. Mooij. *AE3200 - DSE-PM_SE Workshop 2 (Q4 2021-2022)*. Apr. 2022.
- [55] *How does cold weather affect wind speed?* URL: <https://www.windlogger.com/blogs/news/how-does-cold-weather-affect-wind-speed>.

- [56] H. Heath. *How is humidity related to wind speed?* Nov. 2019. URL: <https://www.rampfesthudson.com/how-is-humidity-related-to-wind-speed/#what-is-the-relationship-between-temperature-and-wind-speed>.
- [57] National Weather Service. *Air Pressure and Wind*. URL: https://www.weather.gov/media/zhu/ZHU_Training_Page/winds/pressure_winds/pressure_winds.pdf.
- [58] K. Xie, Q. Liao, H. Tai, B. Hu. *Non-Homogeneous Markov Wind Speed Time Series Model Considering Daily and Seasonal Variation Characteristics*. Feb. 2017. URL: <https://ieeexplore.ieee.org/abstract/document/7865960>.
- [59] North Carolina Climate Office. *Sea and land breezes*. URL: <https://legacy.climate.ncsu.edu/edu/Breezes>.
- [60] S. Rios-Marcuellob F. Bañuelos-Ruedasa C. Angeles-Camachoa. *Characteristics of a Dry Climate*. May 2010. URL: <https://www.sciencedirect.com/science/article/pii/S1364032110001309>.
- [61] D. Vallerio. "The physics of the atmosphere". In: 2014, pp. 23–42. DOI: 10.1016/b978-0-12-401733-7.00002-5.
- [62] NOAA US Department of Commerce. *The sea breeze*. Aug. 2019. URL: <https://www.weather.gov/jetstream/seabreeze>.
- [63] E. Crosman and J. Horel. "Sea and lake breezes: A Review of Numerical Studies". In: *Boundary-Layer Meteorology* 137.1 (2010), pp. 1–29. DOI: 10.1007/s10546-010-9517-9.
- [64] M. Thornton. *Forces governing the wind*. URL: <https://www.lakeeriewx.com/CaseStudies/MesoscaleWind/ForcesGoverningWind.html>.
- [65] Kitepower. May 2021. URL: <https://thekitepower.com/>.
- [66] Windfinder.com. *Windfinder - Wind, wave & Weather Reports, Forecasts & Statistics Worldwide*. URL: https://www.windfinder.com/?utm_source=nl.windfinder.com&utm_medium=web&utm_campaign=redirect#11/52.8722/5.2700/2022-05-21T21:00Z.
- [67] SE Windydy. *Windy as forecasted*. URL: <https://www.windy.com/52.448/4.543?52.065%5C%2C4.543%5C%2C8>.
- [68] *Windforecast: Netherlands - Delft*. URL: <https://www.windgu.ru.cz/237926>.
- [69] *Four maintenance-friendly designs to consider in New Machines*. July 2020. URL: <https://www.biomasengineeringequipment.com/four-maintenance-friendly-designs-to-consider-in-new-machines/>.
- [70] B. van den Corput. *Maximise profit with predictive maintenance of critical equipment*. URL: <https://www.ixon.cloud/knowledge-hub/predictive-maintenance-critical-equipment>.
- [71] B. Richards. *The Kiteboarder Magazine*. TbK, 2007.
- [72] *Kite repair kit*. URL: <https://www.drtuba.eu/products/kite-repair-kit>.
- [73] *IP ratings explained: IP Rating Chart*. Nov. 2021. URL: <https://rainfordsolutions.com/products/ingress-protection-ip-rated-enclosures/ip-enclosure-ratings-standards-explained/>.
- [74] *Splitsset: Pro*. URL: <https://www lijnenspecialist.nl/splitsset-pro>.
- [75] *DC Motors: Common Problems and Maintenance of Brushes*. URL: <https://dreisilker.com/blog/dc-motors-common-problems-and-maintenance-of-brushes>.
- [76] E. DeRose, B. Knopsnyder, and B. Rawal. *Reliability of SuperCapacitors: Paper 1*. 2019. URL: <https://www.avx.com/docs/techinfo/whitepapers/AVX-Whitepaper-Reliability-of-SuperCapacitors-Paper1.pdf>.
- [77] Rivian. *How do over the air updates work?* URL: <https://rivian.com/support/article/how-do-over-the-air-ota-updates-work>.
- [78] Jill Linde. Personal communication. June 10, 2022.
- [79] J. Evans. *AC Motors Part 5: AC Motor Life*. Dec. 2011. URL: <https://www.pumpsandsystems.com/ac-motors-part-5-ac-motor-life>.
- [80] *PMG lifetime*. URL: <https://qd-greef.en.made-in-china.com/product/nvbQEMNdCspU/China-20-Years-Lifetime-Low-Torque-Permanent-Magnet-Generator-Pmg.html>.
- [81] C.N. Rasmussen, A. Altiparmakis, and M. Däumling. "Electromagnetic and electrostatic storage". English. In: *DTU International Energy Report 2013*. Ed. by H. Hvidfeldt Larsen and L. Sønderberg Petersen. Technical University of Denmark, 2013, pp. 37–41. ISBN: 978-87-550-3968-1.
- [82] V. Salma, F. Friedl, and R. Schmehl. "Improving reliability and safety of airborne wind energy systems". In: *Wind Energy* 23.2 (2020), pp. 340–356.
- [83] KitePower. *The Kitepower Falcon 100kW*. 2020. URL: <https://thekitepower.com/product/>.
- [84] M.A. Rushdi et al. "Towing Test Data Set of the Kyushu University Kite System". In: *Data* 5.3 (2020). ISSN: 2306-5729. DOI: 10.3390/data5030069. URL: <https://www.mdpi.com/2306-5729/5/3/69>.
- [85] Lorenzo Fagiano and Trevor Marks. "Design of a Small-Scale Prototype for Research in Airborne Wind Energy". In: *Mechanics, IEEE/ASME Transactions on* 20 (July 2013). DOI: 10.1109/TMECH.2014.2322761.
- [86] *VN-200 GNSS/INS - world's first single packaged SMD GNSS/INS*. URL: <https://www.vectornav.com/products/detail/vn-200>.
- [87] Sogaenergyteam. *Electric motors and Alternators*. Mar. 2022. URL: <http://www.sogaenergyteam.com/wp-content/uploads/2018/05>.
- [88] FutureBridge. *Supercapacitors – A Viable Alternative to Lithium-Ion Battery Technology?* 2020. URL: <https://www.futurebridge.com/industry/perspectives-mobility/supercapacitors-a-viable-alternative-to-lithium-ion-battery-technology/>.
- [89] *Kite power: towards affordable, clean energy*. URL: <https://www.tudelft.nl/en/ae/current/spotlight/kite-power-towards-affordable-clean-energy>.
- [90] *What is the warranty coverage on a new Rivian?* URL: <https://rivian.com/support/article/what-is-the-warranty-coverage-on-a-new-rivian>.
- [91] Xavier Olive. "FDI(R) for satellites: How to deal with high availability and robustness in the space domain?" In: *International Journal of Applied Mathematics and Computer Science* 22 (Mar. 2012). DOI: 10.2478/v10006-012-0007-8.
- [92] *Benefits of a brushless DC motor over a brushed motor*. URL: <https://www.telcointercon.com/article/bldc-motor>.
- [93] D. Laskay. *BLDC Motor Controllers for Maximum Performance & Efficiency*. URL: https://www.jdtechsales.com/wp-content/uploads/2017/08/BLDC_Motor_Controllers_Perf_Efficiency_wp.pdf.
- [94] Y. Zhong et al. "Research on Energy Efficiency of Supercapacitor Energy Storage System". In: Nov. 2006, pp. 1–4. DOI: 10.1109/ICPST.2006.321547.
- [95] *Frictional coefficient (reference): Basic bearing knowledge*. URL: <https://koyo.jtekt.co.jp/en/support/bearing-knowledge/8-4000.html>.
- [96] URL: <https://www.skf.com/group/products/rolling-bearings/principles-of-rolling-bearing-selection/bearing-selection-process/operating-temperature-and-speed/bearing-friction-power-loss-and-starting-torque>.
- [97] M. De Lellis et al. "The Betz limit applied to Airborne Wind Energy". In: *Renewable Energy* 127 (2018), pp. 32–40. ISSN: 0960-1481. DOI: <https://doi.org/10.1016/j.renene.2018.04.034>. URL: <https://www.sciencedirect.com/science/article/pii/S0960148118304427>.
- [98] Y. Chen and J. Wang. "Energy-Efficient Control Allocation for Over-Actuated Systems With Electric Vehicle Applications". In: vol. 1. Jan. 2010. DOI: 10.1115/DSCC2010-4012.
- [99] *Permanent Magnet DC Generator data sheet - nsm*. URL: https://www.nsmr1.it/sites/default/files/2019-07/permanent-magnet-dc-generator-data-sheet-2019-nsm_0.pdf.
- [100] *DST2 135-400 AC synchronous high-torque motor*. URL: <https://www.baumueller-services.com/nl/downloads/motors/download/3-doc-motors/168-dst2-135-400-en>.
- [101] *Eaton Bussmann series 166F supercapacitor*. URL: <https://nl.rs-online.com/web/p/supercapacitors/1351073>.
- [102] windandsolar. *Diversion Dump Loads*. 2022. URL: <https://windandsolar.com/diversion-dump-loads/>.
- [103] TongYueXin. *RX20 Power Ceramic 5KW Wirewound Resistor*. 2022. URL: https://www.alibaba.com/product-detail/RX20-Power-Ceramic-5KW-Wirewound-Resistor_62075236963.html.
- [104] *Eaton-DC1-11kw*. URL: <https://inverterdrive.com/group/AC-Inverter-Drives-400V/Eaton-DC1-11kw-34024FB/>.
- [105] P. Harmon. *230V vs 110V, what about 208V and 240V and sockets*. URL: <https://phillihp.com/2013/05/26/230v-vs-110v-what-about-208v-and-240v-and-sockets/>.
- [106] *BAENRCY Air Pump 5V-6VDC Miniature Vacuum Pump Mini Air Pump 100KPa 370 Motor Air Pump*. URL: <https://www.amazon.com/NW-5V-6VDC-Miniature-Vacuum-100KPa/dp/B078H8V563>.
- [107] *WiFi power consumption calculator: How much power does a WiFi router use?* June 2020. URL: <https://letsaveelectricity.com/wifi-router-power-consumption-calculator/>.
- [108] S. Singh. *How much energy is your wi-fi router using?* May 2022. URL: <https://www.makeitcheaper.com.au/home-energy/how-much-energy-is-your-wi-fi-router-using/>.
- [109] KitePower. 2012. URL: <http://www.kitepower.eu>.
- [110] *Rutland - 504 Wind generator*. July 2019. URL: <https://www.oceanhandlery.com/rutland-504-wind-generator.html>.
- [111] H. Canet, P. Bortolotti, and C. Bottasso. "On the scaling of wind turbine rotors". In: *Wind Energy Science* 6.3 (May 2021), pp. 601–626. DOI: 10.5194/wes-6-601-2021.

- [112] *Lithium-Ion Battery*. Sept. 2020. URL: <https://www.cei.washington.edu/education/science-of-solar/battery-technology>.
- [113] M.D. Maughmer. "A comparison of the characteristics of eight sailing airfoil sections". In: 40 (1976), pp. 523–536.
- [114] M. Folkersma, R. Schmehl, and A. Viré. "Boundary layer transition modeling on leading edge inflatable kite airfoils". In: *Wind Energy* 22.7 (2019), pp. 908–921.
- [115] M. Diehl. "Airborne Wind Energy: Basic Concepts and Physical Foundations". In: *Airborne Wind Energy*. Ed. by U. Ahrens, M. Diehl, and R. Schmehl. Berlin, Heidelberg: Springer Berlin Heidelberg, 2013, pp. 3–22. ISBN: 978-3-642-39965-7. DOI: 10.1007/978-3-642-39965-7_1. URL: https://doi.org/10.1007/978-3-642-39965-7_1.
- [116] J. van den Heuvel. "Kitesailing: Improving system performance and safety". In: (2010).
- [117] R. Coenen. "Single Skin Kite Airfoil Optimization for AWES". In: (2018).
- [118] A. Viré et al. "Effect of Chordwise Struts and Misaligned Flow on the Aerodynamic Performance of a Leading-Edge Inflatable Wing". In: *Energies* 15.4 (2022), p. 1450.
- [119] D. Ma et al. "Effects of relative thickness on aerodynamic characteristics of airfoil at a low Reynolds number". In: *Chinese Journal of Aeronautics* 28.4 (2015), pp. 1003–1015.
- [120] J. Breukels, R. Schmehl, and W. Ockels. "Aeroelastic simulation of flexible membrane wings based on multibody system dynamics". In: *Airborne Wind Energy*. Springer, 2013, pp. 287–305.
- [121] İ.H. Güzelbey, Y. Eraslan, and M.H. Dođru. "Effects of Taper Ratio on Aircraft Wing Aerodynamic Parameters: A Comparative Study". In: *European Mechanical Science* 3.1 (2019), pp. 18–23.
- [122] X. Paulig, M. Bungart, and B. Specht. "Conceptual design of textile kites considering overall system performance". In: *Airborne wind energy*. Springer, 2013, pp. 547–562.
- [123] F. Gohl and Rolf H Luchsinger. "Simulation based wing design for kite power". In: *Airborne Wind Energy*. Springer, 2013, pp. 325–338.
- [124] C. Cone. *The theory of induced lift and minimum induced drag of nonplanar lifting systems*. National Aeronautics and Space Administration, 1962.
- [125] H Mason. "Aerodynamics of 3D Lifting Surfaces through Vortex Lattice Methods". In: *Applied Computational Aerodynamics. Department of Aerospace and Ocean Engineering Virginia Polytechnic Institute and State University, Blacksburg, Virginia* 24061 (1998), p. 72.
- [126] R. Damiani et al. "A vortex step method for nonlinear airfoil polar data as implemented in kiteaerodyn". In: *AIAA Scitech 2019 Forum*. 2019, p. 0804.
- [127] U. C. Domingo. *vortex_step_method*. 2022. URL: https://github.com/awegroup/vortex_step_method.
- [128] F. Trevisi, M. Gaunaa, and M. McWilliam. "The Influence of Tether Sag on Airborne Wind Energy Generation". In: *Journal of Physics: Conference Series* 1618.3 (Sept. 2020), p. 032006. DOI: 10.1088/1742-6596/1618/3/032006. URL: <https://doi.org/10.1088/1742-6596/1618/3/032006>.
- [129] Jan Hendrik Freter et al. "Motion Estimation for Tethered Airfoils with Tether Sag". In: *2020 IEEE International Conference on Multisensor Fusion and Integration for Intelligent Systems (MFIS)*. 2020, pp. 114–120. DOI: 10.1109/MFI49285.2020.9235235.
- [130] J. Oehler and R. Schmehl. "Aerodynamic characterization of a soft kite by in situ flow measurement". In: *Wind Energy Science* 4.1 (2019), pp. 1–21.
- [131] *Sierra 78: Custom and specialty ropes*. Apr. 2022. URL: <https://www.yalecordage.com/product/sierra-78/>.
- [132] Marlow Ropes. *Oceanus SK78*. URL: https://www.marlowropes.fr/system/files_force/downloads/OCEANUS.
- [133] B. Merry and J. Darwin. *The splicing handbook: Techniques for traditional and modern ropes and wires*. Bloomsbury Publishing, 2013.
- [134] K. A. Milne and A. J. McLaren. "An assessment of the strength of knots and splices used as eye terminations in a sailing environment". In: *Sports Engineering* 9.1 (2006), pp. 1–13. DOI: 10.1007/bf02844258.
- [135] H. Paul. *Splicebook: Tips and tricks for expert splicing and choosing the appropriate rope*. Geo. Gleistein, 2000.
- [136] *How to splice rope; Strength in splicing*. URL: <https://samsonrope.com/resources/how-to-splice-rope>.
- [137] *Splitsset: Yacht*. URL: <https://www lijnenspecialist.nl/splitsset-yacht>.
- [138] *DX Core 78 (bio-based) Dyneema®*. URL: <https://www.premiumropes.com/dx-core-78>.
- [139] H. Benavent. *Dyneema end to end Splice*. Mar. 2018. URL: <https://www.riggingdoctor.com/life-aboard/2016/3/27/dyneema-end-to-end-splice>.
- [140] I. Napper et al. "Potential microplastic release from the maritime industry: Abrasion of Rope". In: *Science of The Total Environment* 804 (2022), p. 150155. DOI: 10.1016/j.scitotenv.2021.150155.
- [141] R.P. Singh, M. Mallick, and M.K. Verma. "Studies on failure behaviour of wire rope used in underground coal mines". In: *Engineering Failure Analysis* 70 (2016), pp. 290–304. DOI: 10.1016/j.engfailanal.2016.09.002.
- [142] *Dyneema XBO Technology*. URL: https://www.dsm.com/dyneema/en_GB/our-products/dyneema-fiber/dyneema-xbo-technology.html.
- [143] R. Bosman et al. "Airborne Wind Energy Tethers with High-Modulus Polyethylene Fibers". In: *Airborne Wind Energy*. Ed. by U. Ahrens, M. Diehl, and R. Schmehl. Berlin, Heidelberg: Springer Berlin Heidelberg, 2013, pp. 563–585. ISBN: 978-3-642-39965-7. DOI: 10.1007/978-3-642-39965-7_33. URL: https://doi.org/10.1007/978-3-642-39965-7_33.
- [144] *Sierra 78 Data Sheet*. URL: https://www.yalecordage.com/wp-content/uploads/2021/03/Sierra_78_Data_Sheet.pdf.
- [145] R. Bosman. *Braided Rope Construction*. Dec. 2006.
- [146] *Rise A-series*. URL: <https://oceanrodeo.eu/products/rise-a-series?variant=37334000730274>.
- [147] K. Gemba. "Shape effects on drag". In: (May 2007).
- [148] R. Leuthold. "Multiple-Wake Vortex Lattice Method for Membrane-Wing Kites". PhD thesis. Dec. 2015. DOI: 10.13140/RG.2.2.30811.41765.
- [149] A. Solminihac et al. "Kite as a Beam: A Fast Method to get the Flying Shape". In: *Airborne Wind Energy: Advances in technology development and research*. Springer, 2018.
- [150] Kitemana. *Kite Design Basics*. URL: <https://www.kitemana.nl/info/blog/kite-design-basics-1218>.
- [151] A. Bosch et al. "Nonlinear Aeroelasticity, Flight Dynamics and Control of a Flexible Membrane Traction Kite". In: Sept. 2013, pp. 307–323. DOI: 10.1007/978-3-642-39965-7_17.
- [152] *Lijnenspecialist: Vakwerk in touwwerk en staalkabel*. URL: <https://www lijnenspecialist.nl/>.
- [153] *ALUULA TECHNOLOGY*. URL: <https://aluula.com/technology/#vaepor>.
- [154] *How strong is aluula*. URL: <https://hanglos.nl/news/350032/how-strong-is-aluula.html>.
- [155] *ALUULA VS. DACRON: WHY ALUULA ALWAYS WINS!* URL: <https://oceanrodeo.eu/blogs/news/aluula-vs-dacron>.
- [156] R. Chater. "Is This Sustainable". In: *International Kitesurf Magazine* 77 (Oct. 2019).
- [157] Brett Anderson. *Ocean Rodeo Flite: Dacron vs. aluula comparison*. May 2020. URL: <https://www.realwatersports.com/blogs/news/aluula-vs-dacron-comparison>.
- [158] Rivian. *R1t*. URL: <https://rivian.com/rit>.
- [159] J.Y. Wong. *Theory of Ground Vehicles*. Wiley, 2001. ISBN: 9780471354611. URL: <https://books.google.nl/books?id=LH8wd8im13AC>.
- [160] D. Edmunds. *How Good is the Rivian R1T Suspension? Watch Us Test It*. URL: <https://www.caranddriver.com/news/a39440064/rivian-rit-suspension-tested/>.
- [161] N. Rajeev. "Natural Frequency, Ride Frequency and their Influence in Suspension System Design". In: *International Journal of Engineering Research and Applications* 09.3 (2019), pp. 60–64. DOI: 10.9790/9622-0903036064. URL: <https://www.ijera.com/papers/vol19no3/Series-3/K0903036064%5C%20.pdf>.
- [162] M. Oduori, E. Musyoka, and T. Mbuya. "Material selection for a manual winch rope drum". In: *World Acad Sci Eng Technol Int J Chem Mol Nucl Mater Metall Eng* 10.1 (2016), pp. 129–135.
- [163] J. Shigley. *Shigley's mechanical engineering design*. Tata McGraw-Hill Education, 2011.
- [164] mechanicalc. URL: <https://mechanicalc.com/reference/beam-analysis>.
- [165] M. Shademan and A. Naghib-Lahouti. *Effects of aspect ratio and inclination angle on aerodynamic loads of a flat plate - advances in aerodynamics*. June 2020. URL: <https://aia.springeropen.com/articles/10.1186/s42774-020-00038-7>.
- [166] *5V electromagnet (20 kg holding force)*. URL: <https://www.difrobot.com/product-2230.html>.
- [167] CREATIVE shop. *Holding Solenoids e1as*. URL: <https://www.magnety.eu/holding-electromagnets/holding-solenoids-e1as/>.
- [168] U. Fechner. "A Methodology for the Design of Kite-Power Control Systems". PhD thesis. 2016. DOI: 10.4233/uuid:85efaf4c-9dce-4111-bc91-7171b9da4b77.
- [169] U. Fechner and R. Schmehl. "Design of a distributed Kite Power Control System". In: *2012 IEEE International Conference on Control Applications* (2012). DOI: 10.1109/cca.2012.6402695.
- [170] *Sen-11084*. URL: <https://www.digikey.nl/nl/products/detail/sparkfun-electronics/SEN-11084/5140765>.
- [171] *1782*. URL: <https://www.digikey.nl/nl/products/detail/adafuit-industries-llc/1782/4990781>.

- [172] *Conrad Electronic - Voltcraft VPT-100*. URL: <https://www.conrad.nl/nl/p/voltcraft-vpt-100-windmeter-5-tot-80-m-s-101719.html>.
- [173] *RK120-03 Ultrasonic Wind Speed & direction sensor: Rika Sensors*. URL: <https://www.rikasensor.com/rk120-03-ultrasonic-wind-speed-direction-sensor.html>.
- [174] *Mikroe-3522*. URL: <https://www.digikey.nl/nl/products/detail/mikroelektronika/MIKROE-3522/10187034>.
- [175] *RF Solutions GPS-622F GPS receiver*. URL: <https://nl.rs-online.com/web/p/gnss-gps-modules/7043300>.
- [176] M. Rodriguez. *Quasi Steady Model*. 2022. URL: <https://github.com/TUD-AE/DSE2021-22-Q4-project15>.
- [177] U. Fechner and R. Schmehl. *Flight Path Planning in a Turbulent Wind Environment*. 2019. URL: https://www.researchgate.net/publication/324135033_Flight_Path_Planning_in_a_Turbulent_Wind_Environment.
- [178] C. Jehle and R. Schmehl. "Applied Tracking Control for Kite Power Systems". In: *Journal of Guidance, Control, and Dynamics* 37.4 (2014), pp. 1211–1222. DOI: 10.2514/1.62380. URL: <https://doi.org/10.2514/1.62380>.
- [179] D. Nguyen and B. Widrow. "Neural Networks for Self-Learning Control Systems". In: *IEEE Control Systems Magazine* 10 (3 Apr. 1990).
- [180] A. Furey. "Evolutionary robotics in high altitude wind energy applications". In: 2012.
- [181] Bennie van den Hazel. *IMPACT MECHANICS OF HELMET COMPONENTS*. Jan. 2015. URL: https://essay.utwente.nl/69908/1/CONF-Report_internship%5C%20Bennie%5C%20van%5C%20den%5C%20Hazel.pdf.
- [182] L.L.M. Veldhuis. *Manual for Low Speed Windtunnel Test AE2130-II*. edition 1.4. Delft, The Netherlands: TUDelft, Sept. 2016.
- [183] *DX Core 78 HPS*. URL: <https://www.premiumropes.com/dx-core-78-hps>.
- [184] *Tether*. URL: <http://www.kitepower.eu/technology/3-sytem-components/49-tether.html>.
- [185] *Flite A-Series*. URL: <https://oceanrodeo.eu/products/flite-a-series>.
- [186] *Roam A-series*. URL: <https://oceanrodeo.eu/products/roam-a-series?variant=41511378157730>.
- [187] Goodyear. *How long do tires last?: Goodyear Tires*. Aug. 2021. URL: <https://www.goodyear.com/en-US/learn/tire-basics/how-long-do-tires-last>.
- [188] Farnaz Ganjezadeh, Thananan Tapananon, and Howard Lei. "Predicting Reliability of Lithium Ion Batteries". In: *International Journal of Engineering Research & Technology* 3.8 (Aug. 2014), pp. 1189–1192. DOI: ISSN:2278-0181.
- [189] *DST2 135-400 Englisch 01 13 en - BaumueLLer Services*. 2014. URL: <https://www.baumueLLer-services.com/de/downloads/motors/send/3-doc-motors/168-dst2-135-400-en>.
- [190] H. Pan, J. Li, and Y. Feng. "Carbon nanotubes for supercapacitor". In: *Nanoscale research letters* 5.3 (2010), pp. 654–668.
- [191] *QT40.242*. URL: <https://www.digikey.nl/nl/products/detail/puls-1p/QT40-242/6580613>.
- [192] J. Carroll, A. McDonald, and D. Mcmillan. "Reliability comparison of wind turbines with DFIG and PMG drive trains". In: *Energy Conversion, IEEE Transactions on* 30 (June 2015), pp. 663–670. DOI: 10.1109/TEC.2014.2367243.
- [193] *Emission factors in kg CO2-equivalent per unit*. URL: https://www.winnipeg.ca/finance/findata/matmgt/documents/2012/682-2012/682-2012_Appendix_H-WSTP_South_End_Plant_Process_Selection_Report/Appendix%5C%207.pdf.
- [194] Q. Qiao et al. "Comparative study on life cycle CO2 emissions from the production of electric and conventional vehicles in China". In: *Energy Procedia* 105 (2017), pp. 3584–3595.
- [195] *Diesel Generator Fuel Consumption Chart*. URL: <https://hardydiesel.com/resources/diesel-generator-fuel-consumption-chart/>.
- [196] *Alles over uitstoot*. Mar. 2020. URL: <https://www.anwb.nl/auto/nieuws-en-tips/alles-over-uitstoot>.
- [197] Dyneema. *sustainable solutions for fabrics and protective knitwear*. 2022. URL: https://www.dsm.com/dyneema/en_GB/about-us/latest-news/blog/dyneema-provides-innovative-and-sustainable-solutions-for-fabric-and-protective-knitwear.html.
- [198] ECTA. *Guidelines for Measuring and Managing CO2 Emission from Freight Transport Operations*. Mar. 2011. URL: <https://www.ecta.com/wp-content/uploads/2021/03/ECTA-CEFIC-GUIDELINE-FOR-MEASURING-AND-MANAGING-CO2-ISSUE-1.pdf>.
- [199] D Daniel. *What is lean manufacturing?* Apr. 2020. URL: <https://www.techtarget.com/searcherp/definition/lean-production>.
- [200] NetSuite.com. *Just-in-time vs just-in-case*. URL: <https://www.netsuite.com/portal/resource/articles/inventory-management/just-in-time-vs-just-in-case.shtml>.
- [201] Bryan van Ostheim. Personal communication. June 16, 2022.